Biochemical Regulation of
***Brassica napus* Diacylglycerol Acyltransferase 1**

by

Kristian Mark P. Caldo

A thesis submitted in partial fulfillment of the requirements for the degree of

Doctor of Philosophy

in

Plant Science

Department of Agricultural, Food and Nutritional Science
University of Alberta

ABSTRACT

Diacylglycerol acyltransferase 1 (DGAT1) is an integral membrane enzyme catalyzing the final and committed step in acyl-CoA-dependent triacylglycerol (TAG) biosynthesis. Previous metabolic control analysis showed that DGAT1 plays a substantial role in modulating the flow of carbon into seed oil in *Brassica napus*. In *B. napus* and many other organisms, DGAT1 has been used as a biotechnological tool to boost oil accumulation. Despite its key role in primary metabolism and biotechnological importance, no detailed structure-function information is available on the enzyme. This doctoral thesis aimed to shed light on the mechanism of action and regulation of DGAT1 by employing various techniques in molecular biology, and protein and lipid biochemistry.

The first part of this dissertation involved the development of a purification protocol for recombinant *B. napus* DGAT1 (BnaDGAT1) produced in *Saccharomyces cerevisiae*. The optimized protocol included solubilization of membrane-bound BnaDGAT1 in n-dodecyl-β-D-maltopyranoside micelles (DDM), cobalt affinity chromatography, and size-exclusion chromatography. BnaDGAT1 was eluted mainly as a dimer from the last chromatographic step. The purified enzyme was well-folded, intact, and active and utilized acyl-CoAs which represent the major fatty acids in canola-type *B. napus* seed oil.

In the second part of this dissertation, the hydrophilic N-terminal domain of BnaDGAT1 was identified as the enzyme's regulatory domain that is not essential for catalysis. This regulatory domain has an intrinsically disordered region (IDR) and a folded segment. The IDR exhibited an autoinhibitory function and appeared to facilitate

positive cooperativity through dimerization. The folded segment has an allosteric site for acyl-CoA/CoA. Acyl-CoA, a substrate of the enzyme, was found to serve as a homotropic allosteric activator. On the other hand, CoA was identified as a non-competitive feedback inhibitor through interaction with the same allosteric site. The three-dimensional solution structure of the allosteric site and the amino acid residues interacting with CoA were elucidated, revealing details on this important regulatory element for allosteric regulation.

In the third part of this dissertation, the purified enzyme in DDM micelles was lipidated and subjected to detailed kinetic analysis. Purified and lipidated BnaDGAT1 exhibited hyperbolic and sigmoidal responses to increasing concentrations of 1, 2-diacyl-*sn*-glycerol and acyl-CoA, respectively. Phosphatidate (PA) was identified as a feedforward activator of BnaDGAT1. The presence of PA may have facilitated the transition of the enzyme into the more active state that is also desensitized to substrate inhibition. PA may also relieve possible autoinhibition of BnaDGAT1 brought about by the N-terminal region. Furthermore, BnaDGAT1 was found to be a substrate of the sucrose non-fermenting kinase 1, which can phosphorylate the enzyme and convert it to a less active form. Based on these findings, an enzyme model is proposed illustrating the biochemical regulation of BnaDGAT1 through the aforementioned mechanisms.

PREFACE

The work presented in chapters 3-5 of this dissertation is based on the findings reported in the following papers. My contributions are summarized below each paper.

Chapter 3: Caldo KMP, Greer MS, Chen G, LemieuxMJ, Weselake RJ (2015). Purification and properties of *Brassica napus* diacylglycerol acyltransferase 1. FEBS Lett. 589: 773–778. Copyright (2017), with permission from John Wiley and Sons. License #4159460347317

Contributions: I designed and performed all the experiments under the guidance of my supervisors. I wrote the first draft of the manuscript and further revised the manuscript with the co-authors.

Chapter 4: Caldo KMP, Acedo JZ, Panigrahi R, Vederas JC, Weselake RJ, Lemieux MJ (2017). Diacylglycerol acyltransferase 1 is regulated by its N-terminal domain in response to allosteric effectors. Plant Physiology 175: 667–680 www.plantphysiol.org Copyright (2017) American Society of Plant Biologists

Contributions: I designed and performed most of the experiments under the guidance of my supervisors. I performed the NMR experiments together with JZA. I wrote the first draft of the manuscript and further revised the manuscript with the co-authors.

Chapter 5: Caldo KMP, Shen W, Xu Y, Hanley-Bowdoin L, Chen G, Lemieux MJ, Weselake RJ. *Brassica napus* diacylglycerol acyltransferase 1 is feedforward activated by phosphatidate and inhibited by SnRK1-catalyzed phosphorylation. To be submitted.

Contributions: I designed and performed all the experiments under the guidance of my supervisors, except the phosphorylation assay, which was performed by WS. I

wrote the first draft of the manuscript and further revised the manuscript with the co-authors.

ACKNOWLEDGEMENTS

I acknowledge the following people who had been instrumental in the completion of this thesis. Firstly, I would like to extend my deepest gratitude and appreciation to my supervisor, Dr. Randall Weselake, for providing me with continuous guidance, wisdom and support throughout the course of my doctoral studies. Thank you for sharing your knowledge of and passion for plant biochemistry and biotechnology, for providing a very stimulating and well-equipped research environment, and for giving me many opportunities for professional development. I am also very grateful to my co-supervisor, Dr. Joanne Lemieux, for sharing her knowledge and expertise on membrane proteins, and for her guidance and encouragement during my graduate work. I am also thankful to my committee members, Dr. Nat Kav and Dr. Jianping Wu, for their valuable advice and suggestions on various parts of my research. I am also thankful to Dr. Rene Jacobs for his helpful counsel and, together with Dr. Lingyun Chen, for serving as my arm's length examiners. I would also like to thank Dr. Timothy Durrett and Dr. Michael Gänzle for serving as external examiner and chair of my final PhD examination, respectively.

I am very grateful to my collaborators namely Dr. Wei Shen from North Carolina State University for performing the phosphorylation assays involving ^{32}P, Jeella Acedo and Dr. John Vederas from the Department of Chemistry for their help with NMR analysis, and Dr. Rashmi Panigrahi from the Department of Biochemistry for her help in protein work. I would also like to thank Dr. Sten Stymne for providing yeast strain H1246, which had been very useful to my research. I am also thankful to Dr. Elena Arutyunova for sharing her knowledge on membrane protein work and enzyme kinetics, and Yang Xu for her help and valuable suggestions in some of my experiments. I also

thank Dr. Guanqun Chen and Dr. Elzbieta Mietkewska for helping me get started in the lab with the proper techniques in lipid biochemistry and molecular biology. I am also thankful to the rest of the members of the Weselake group and Lemieux group who supported me in my graduate studies.

I also acknowledge the financial support for my PhD work provided by the Natural Sciences and Engineering Research Council of Canada, Alberta Innovates Bio Solutions, Alberta Innovates Technology Futures, and Alberta Canola Producers Commission.

I am also thankful to my grandparents, parents and siblings for their steadfast love and encouragement. I am extremely grateful to my wonderful wife for her unwavering love and support, and for always pushing me to continuously persevere and move forward throughout my graduate studies. And lastly, I am thankful to the One above for giving me the opportunity to explore His wonderful molecular creations.

TABLE OF CONTENTS

LIST OF TABLES

LIST OF FIGURES

LIST OF ABBREVIATION

ΔF	change in fluorescence
ACAT	acyl-CoA:cholesterol acyltransferase
ACCase	acetyl-CoA carboxylase
ACP	acyl carrier protein
AMPK	AMP-activated protein kinase
Arabidopsis (At)	*Arabidopsis thaliana*
BCCP	biotin carboxyl carrier protein
B. napus (Bna)	*Brassica napus*
BnaDGAT1	*Brassica napus* DGAT1 isoform BnaC.DGAT1.a
CCT	CTP:phosphocholine cytidylyltransferase
CD	circular dichroism
cDNA	complementary DNA
Co TALON	cobalt talon
CoA	coenzyme A
COSY	correlation spectroscopy
CPT	choline phosphotransferase
CT	carboxyltransferase
DAG	1,2-diacyl-*sn*-glycerol
DDM	n-dodecyl-β-D-maltopyranoside
DGAT	diacylglycerol acyltransferase
DOPC	1,2-dioleoyl-*sn*-glycero-3-phosphatidylcholine
DPC	n-dodecylphosphocholine

DSPC	1,2-distearoyl-*sn*-glycero-3-phoshatidylcholine
E. coli	*Escherichia coli*
ER	endoplasmic reticulum
FA	fatty acid
FAD	fatty acid desaturase
FAS	fatty acid synthase
FAT	fatty acyl-ACP thioesterase
FPLC	fast protein liquid chromatography
GC/MS	gas chromatography/mass spectrometry
G3P	*sn*-glycerol-3-phosphate
GPAT	*sn*-glycerol-3-phosphate acyltransferase
h	Hill coefficient
HPLC	high-performance liquid chromatography
HSQC	heteronuclear single quantum coherence spectroscopy
IDR	intrinsically disordered region
IND	insertion deletion
IPTG	isopropyl-β-D-thiogalactopyranoside
KAS	3-ketoacyl-ACP synthase
K_M	Michaelis constant
LACS	long-chain acyl-CoA synthetase
LPA	lysophosphatidate
LPAAT	lysophosphatidate acyltransferase
LPC	lysophophatidylcholine

LPCAT	lysophosphatidylcholine acyltransferase
MALDI-TOF	matrix-assisted laser desorption/ionization time-of-flight
MEGA-8	octanoyl-N-methylglucamide
Ni-NTA	nickel nitrilo-acetic acid
NMR	nuclear magnetic resonance spectroscopy
NOESY	Nuclear Overhauser effect spectroscopy
OD	optical density
PA	phosphatidate
PAGE	polyacrylamide gel electrophoresis
PAP	phosphatidic acid phosphatase
PC	phosphatidylcholine
PDAT	phospholipid: diacylglycerol acyltransferase
PDCT	phosphatidylcholine: diacylglycerol cholinephosphotransferase
PDH	pyruvate dehydrogenase complex
PE	phosphatidylethanolamine
PL	phospholipid
POPC	1-palmitoyl-2-oleoyl-*sn*-glycero-3-PC
PUFA	polyunsaturated fatty acid
RMSD	root-mean square deviation
$S_{0.5}$	Hill affinity constant
S. cerevisiae	*Saccharomyces cerevisiae*
SD	standard deviation
SDS	sodium dodecyl sulfate

SEC	size-exclusion chromatography
SNF1	sucrose non-fermenting protein kinase 1
SnRK1	sucrose non-fermenting-related kinase 1
TAG	triacylglycerol
TEV	tobacco etch virus
TLC	thin layer chromatography
TOCSY	Total correlation spectroscopy
V_{max}	maximum velocity

CHAPTER 1

Introduction

Triacylglycerol (TAG) is a lipid composed of three fatty acyl chains esterified to a glycerol backbone. TAG serves as a reservoir of reduced carbon for energy supply, membrane biogenesis, and cell signaling. In oleaginous plants, TAG is mainly deposited in seeds where it is later mobilized to fuel germination and early seedling growth. Plant TAG is highly enriched in vegetable oil which is an essential agricultural commodity serving as a main source of dietary lipid for man. Over the past years, the global demand for vegetable oil has been increasing rapidly due to the growing population and the increased use of seed oil for food, feed and industrial applications such as biofuel (Metzger and Bornsheuer, 2006; Durrett et al., 2008).

Oilseed rape (mostly *Brassica napus*), accounts for about 12% of global vegetable oil production (Woodfield et al., 2015). Oilseed rape, which is low in erucic acid ($22{:}1\Delta^{13cis}$) and glucosinolates, was developed in Canada and is known as canola (McVetty et al., 2016). Canola constitutes a multi-billion dollar industry in Canada. Over the last several decades, the seed oil content of Canadian canola has been increased incrementally through breeding (Rahman et al., 2013; Weselake et al., 2009). It is estimated that a one percent absolute increase in canola seed oil content would add $90M annually to the seed oil extraction and processing industry in Canada (Canola Council of Canada). Within the last two decades, considerable research has been conducted on increasing seed oil content in canola and other oil crops using metabolic engineering (Weselake et al., 2009; Woodfield et al., 2015). In many cases, substantial

increases in seed oil content have been achieved by manipulating only one reaction in storage lipid biosynthesis.

Considerable investigation has focused on diacylglycerol acyltransferases (DGAT; EC 2.3.1.20), which catalyze the acyl-coenzyme A (CoA)-dependent acylation of 1,2-diacyl-*sn*-glycerol (DAG) to produce TAG (Lung and Weselake, 2006; Liu et al., 2012). DGAT1 and DGAT2 are membrane-bound isoenzymes that essentially share no homology (Liu et al., 2012). The DGAT-catalyzed reaction was shown to substantially influence the level of oil accumulation during seed maturation in *B. napus* (Weselake et al., 2008; Taylor et al., 2009). In addition to increasing seed oil content, seed-specific over-expression of *DGAT1* in *B. napus* resulted in increased transcript production and microsomal DGAT activity during seed development (Weselake et al., 2008; Taylor et al., 2009).

Although DGAT activity has been studied for several decades using microsomes prepared from various TAG-forming tissues, the mode of action and regulation of DGAT enzymes remains poorly understood. In general, membrane-bound DGAT enzymes have been recalcitrant to purification to homogeneity in active form due to their hydrophobic nature and possible low abundance in natural tissue sources. Although there are early reports on the solubilization and partial purification and characterization of DGAT activity from mammalian and plant sources, these studies were likely based on mixtures of different DGAT isoenzymes (e.g. Polokoff and Bell, 1980; Kwanyuen and Wilson, 1986; Kwanyuen and Wilson, 1990; Andersson et al., 1994; Little et al., 1994; Valencia-Turcotte and Rodríguez-Sotres, 2001). DGAT1 belongs to the membrane-bound-O-acyltransferase family (Liu et al., 2012). The complementary DNA (cDNA)

encoding murine (*Mus musculus*) DGAT1 was first identified based on its limited homology to the cDNA encoding acyl-CoA:cholesterol acyltransferase 1 (ACAT1) (Cases et al., 1998). Closely following the cloning of the first mammalian *DGAT1*, the first plant *DGAT1* genes were cloned and functionally characterized from *Arabidopsis thaliana* (hereafter Arabidopsis)*, Nicotiana tabacum* and *B. napus* (Hobbs et al., 1999, Routaboul et al., 1999; Zou et al., 1999b, Bouvier-Navé et al., 2000; Nykiforuk et al., 1999; 2002). Laridizabal et al. (2001) used various chromatographic procedures to partially purify two forms of fungal (*Mortierella ramanniana*) DGAT2. This fungus is now known as *Umbelopsis ramanniana* (Lardizabal et al., 2008). Two DGAT2 polypeptides were excised from SDS-PAGE gels based on the correlations of their staining intensity with DGAT activity in the column fractions. The two polypeptides were partially sequenced and used to develop non-degenerate DNA primers, which were in turn used to clone the encoding cDNAs. Eventually, numerous cDNAs encoding DGAT1 or DGAT2 were cloned from various sources using genetic methods and the cDNAs were routinely expressed in recombinant protein-producing systems such as yeast (Liu et al., 2012). Recently, Cao et al. (2011) described the partial purification of recombinant tung tree (*Vernicia fordii*) DGAT1 in inactive form. In this case, a bacterial expression system was used to produce the recombinant enzyme.

Since DGAT1 has been identified as a key enzyme influencing seed oil accumulation in *B. napus* (Weselake et al., 2008), understanding the mode of catalysis and regulation of this isoenzyme will provide important molecular insights on how seed oil accumulation is controlled. Previously, the hydrophilic N-terminal domain of *B. napus* DGAT1 was shown to self-associate and interact with acyl-CoA at a non-catalytic

site suggesting that the enzyme may have allosteric properties (Weselake et al., 2006). In addition, *Corylus americana* and *Zea mays* DGAT1s have recently been shown to exhibit a sigmoidal response of activity to increasing concentrations of acyl-CoA (Roesler et al., 2016). More in-depth structure-function information on *B. napus* DGAT1 will provide a basis for developing biotechnological strategies to enhance DGAT1 activity and seed oil accumulation. Moreover, the information obtained for plant DGAT1 may be applicable for understanding the mammalian homologue, which is under intensive investigation as a potential drug target for treatment of lipid-related metabolic disorders (Zammit et al., 2008). *Brassica napus* DGAT1 exhibited 34-35.2% sequence identity with *Mus musculus* and *Homo sapiens* DGAT1.

This doctoral dissertation involves the preparation of highly purified recombinant BnaC.DGAT1.a isoform (Genbank ID: JN224474; hereafter referred to as BnaDGAT1), and the biochemical and biophysical characterization of the recombinant enzyme. The project is based on the following hypotheses:

1. Endoplasmic reticulum-bound BnaDGAT1 produced in *Saccharomyces cerevisiae* can be solubilized and highly purified in active form.
2. Kinetic and structural analysis of BnaDGAT1 and truncations of the enzyme will reveal that the N-terminal hydrophilic domain is involved in allosteric regulation of the enzyme.
3. Lipidation of purified BnaDGAT1 with phosphatidylcholine (PC) can increase the activity of the enzyme.

4. The effect of phosphatidate (PA) on the activity of purified and lipidated BnaDGAT1 will provide insight into how this Kennedy pathway intermediate stimulates DGAT activity.
5. Purified BnaDGAT1 can also be phosphorylated and subsequently down-regulated through the catalytic action of sucrose non-fermenting-related kinase 1 (SnRK1).

Chapter 2 of this dissertation presents a Literature Review which covers plant storage lipid biosynthesis, different types of enzyme regulation, purification and reconstitution of eukaryotic membrane proteins, previous biochemical studies on DGAT enzymes, and metabolic engineering approaches involving manipulation of the DGAT-catalyzed reaction to increase the TAG content of biomass. Chapter 3 deals with the solubilization and preparation of highly purified recombinant BnaDGAT1 in active form. In Chapter 4 it is shown that BnaDGAT1 is modulated by the enzyme's hydrophilic N-terminal domain in response to CoA/acyl-CoA levels. Other possible modes of enzyme regulation are examined in Chapter 5. These include activation by lipidation with PC, feedforward stimulation by PA, and phosphorylation catalyzed by SnRK1 so as to down-regulate DGAT activity. Chapter 6 is a General Discussion, which develops further perspective and suggests future directions. Lastly, the Appendices include descriptions of relevant pilot studies on acyltransferase solubilization and other investigations requiring additional research. The final Appendix describes my contributions to other manuscripts and published papers.

CHAPTER 2

Literature Review

2.1. Glycerolipids, including triacylglycerol

Glycerolipids comprise a group of lipids having at least one acyl chain connected to a glycerol backbone via an ether or ester linkage (Fig. 2.1). They are found in all cell types in plants and provide important structural and functional roles. Neutral glycerolipids include mono-, di- and triacylglycerols, which are mainly stored in fruits and seeds, although they are also present in low amounts in vegetative organs such as stems and leaves (Stymne and Stobart, 1987). Glyceroglycolipids are derivatives containing carbohydrate moiety such as monogalactosyl diacylglycerol, digalactosyl diacylglycerol and sulfoglucolipids. Polar glycerolipids include phospholipids such as phosphatidylcholine (PC), phosphatidylethanolamine (PE), phosphatidylserine and betaine lipids. Glyceroglycolipids and polar glycerolipids are important components of the membrane bilayer (Browse and Somerville, 1991).

Triacylglycerol (TAG) is composed of three fatty acyl chains esterified onto a glycerol backbone. The three positions in the glycerol backbone are not equivalent and are distinguished by a stereospecific numbering (*sn*) system. The carbon atoms in an L-glycerol in the Fischer projection are designated as *sn*-1, *sn*-2, and *sn*-3 from top to bottom. TAG serves as an important source of energy having highly reduced acyl chains, which contain twice the energy density of carbohydrates and proteins and can be stored in compact form, free from water. In plants, TAGs are mainly stored in seeds and are later mobilized to provide the energy needed for germination and seedling growth. During germination and seedling development, TAG provides fatty acids for energy

production and formation of carbohydrates. TAG is also important for fully-grown plants for normal growth and development. In addition, TAG can also provide precursors for the biosynthesis membrane lipids and signaling lipids. Lastly, TAG is important in maintaining lipid homeostasis as it serves as neutralized form of fatty acids, which can have cytotoxic properties when present in high amounts (Fan et al., 2013; Fan et al., 2014).

Plant TAGs are important sources of dietary oil and feedstock for various industrial applications. Over the past several years, the global demand for vegetable oil has been increasing due to the ballooning population. In addition, plant TAG has been increasingly used for other non-food applications such as the production of biodiesel or fatty acid methyl ester, biolubricants, and biopolymers (Metzger and Bornsheuer, 2006; Durrett et al., 2008). The major sources of vegetable oil include palm (*Elaeis guineensis*), coconut (*Cocos nucifera*), canola (mostly *Brassica napus*), soybean (*Glycine max*) and sunflower (*Helianthus annuus*). In Canada, canola is the main oil crop that contributes about $26 billion to the economy (Canada Council of Canada, 2017). Due to the importance of TAG in the food, biofuel and bioproduct industries, plant TAG biosynthesis has been intensively studied over past several decades using various oleaginous crops. In addition, research efforts have been directed to understand the biochemistry of mammalian TAG metabolism, which also received considerable attention since this pathway is associated with various lipid-related diseases such as obesity and diabetes (Liu et al., 2012).

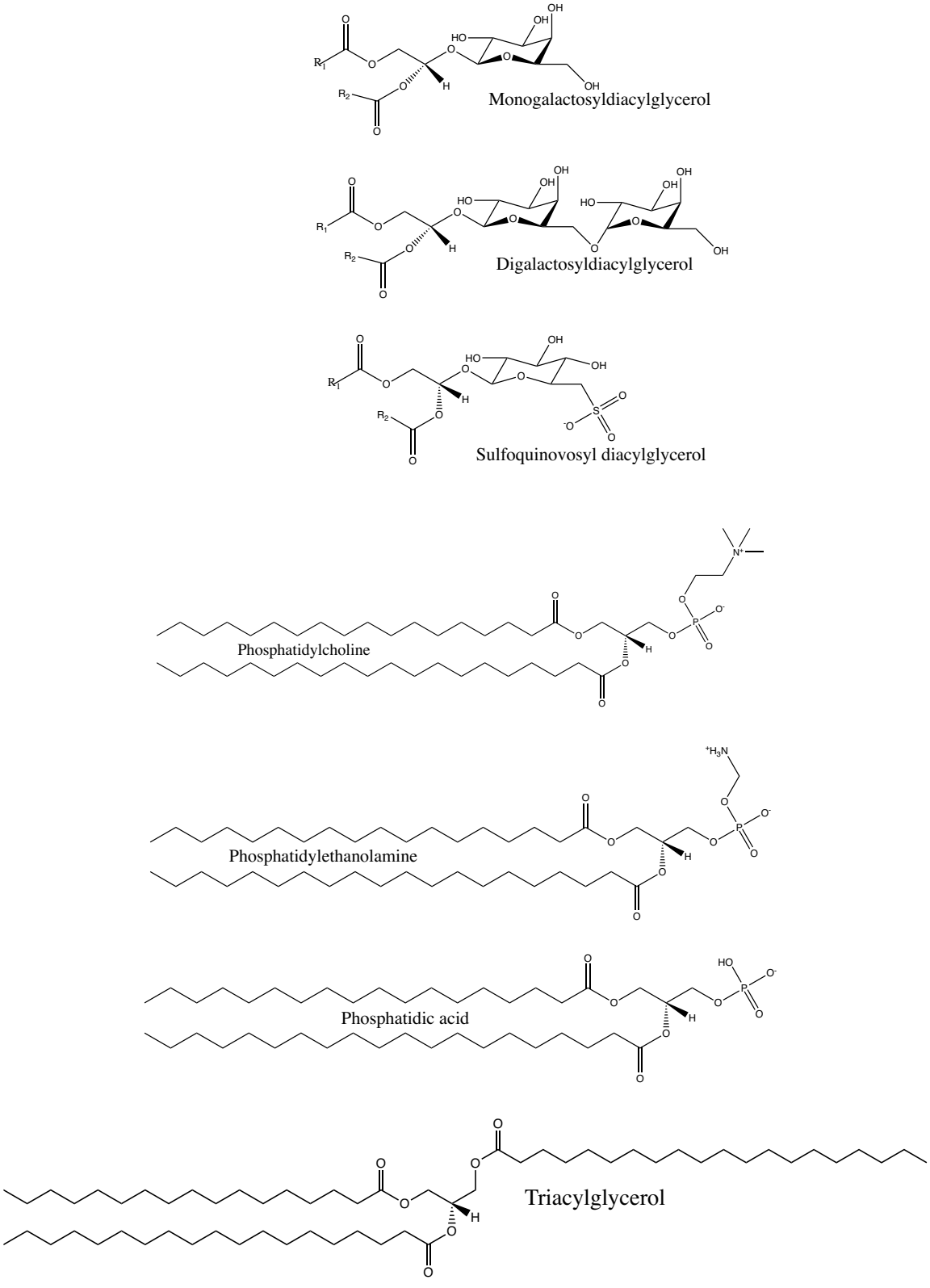

Figure 2.1. Structures of major glycerolipids in plants.

2.2. Plant fatty acid and triacyglycerol biosynthesis

2.2.1. Overview

The formation of storage lipid in oleaginous plants involves two major phases, specifically fatty acid biosynthesis and TAG assembly (Ohlrogge and Jaworski, 1997; Chapman and Ohlrogge, 2012; Chen et al., 2015). In fatty acid biosynthesis, sugars produced through photosynthesis are reduced into acyl chains, which are composed of hydrocarbons. This phase begins through the breakdown of sugars via glycolysis, which converts glucose into pyruvate. Pyruvate is converted into acetyl-Coenzyme A (CoA) by the plastidial pyruvate dehydrogenase (PDH) complex. Acetyl-CoA is then converted into acyl chains by the concerted action of the plastidial acetyl-CoA carboxylase (ACCase) and fatty acid synthase (FAS). The acyl chain can extend up to 16 or 18 carbons, which can undergo monounsaturation. After synthesis, acyl chains are released and transported out of the plastid and converted into acyl-CoA. In the acyl-CoA-dependent TAG assembly, three acyl chains from acyl-CoA are transferred onto a glycerol backbone. On the other hand, acyl-CoA-independent pathway forms TAG using acyl donors that do not have a thioester moeity such as PC. In seed oils enriched in polyunsaturated fatty acids (PUFAs) or unusual fatty acids, such as hydroxy fatty acids, monounsaturated fatty acids can undergo further desaturation or modification at the level of PC. Various acyl-editing processes facilitate the movement of modified acyl chains in PC into TAG.

2.2.2. Fatty acid biosynthesis

Fatty acids are produced in all plant cells and are used for a variety of biochemical reactions. The rate of fatty acid biosynthesis varies depending on factors such as the type

of plant cell, developmental stage, time of the day, and growth rate (Ohlrogge and Jaworski, 1997). In plants, fatty acids are synthesized in a separate organelle called plastids, in contrast to other organisms whereby the site of fatty acid biosynthesis is in the cytosol. Some fatty acids produced in the plastids are retained for the production of lipids within this organelle, in a process known as the prokaryotic pathway. Most fatty acids, however, are exported to the ER and other sites for glycerolipid assembly, which is a process referred to as the eukaryotic pathway (Roughan and Slack, 1982). Some glycerolipids produced in the eukaryotic pathway are transported back to the plastids (Browse et al., 1986).

2.2.2.1. Acetyl-CoA carboxylase

The first enzyme in fatty acid biosynthesis is ACCase, which converts and activates acetyl-CoA into malonyl-CoA. Malonyl-CoA serves as a two-carbon donor for the fatty acid synthase (FAS), which synthesizes the fatty acyl chain through a series of repetitive reactions. ACCase has four components namely biotin carboxylase (BC), biotin carboxyl carrier protein (BCCP), and α- and β-carboxyltransferases (CTs). ACCase exists in two forms that differ in their structure namely homomeric ACCase and heteromeric ACCase. Homomeric ACCase is composed of one large polypeptide (> 200 kDa) that folds to form different functional domains/subunits. This form is localized in the cytosol and is the predominant enzyme form for fatty acid biosynthesis in the cytosol of animals, fungi, and plastids of grasses. Homomeric ACCase is also present in the cytosol of plants and is involved in providing malonyl-CoA for fatty acid elongation, polyketide biosynthesis, and other specialized reactions (Fatland et al., 2005). On the other hand, heteromeric ACCase (htACCase) is an enzyme composed of four individual

proteins that can easily be dissociated (Alban et al., 1994) and is found in prokaryotes, algae, and plants (Huerlimann and Heimann, 2012). In plants, htACCase catalyzes the formation of malonyl-CoA for *de novo* fatty acid biosynthesis in the plastid.

The structural organization of the whole heteromeric ACCase is not yet fully understood although previous evidence suggests that it is composed of two different subcomplexes. The first subcomplex is composed of BC and BCCP. The crystal structures of each *Escherichia coli* ACCase subcomplex were previously determined. The *E. coil* BC-BCCP crystal structure showed a 1:1 stoichiometric ratio composed of two BC dimers and four BCCP monomers (Broussard et al., 2013). An earlier proteomics study, however, suggested that BC and BCCP, are present at 1:2 ratio (Lu et al., 2007 and Ishihama et al., 2008). Both findings indicate the presence of four active sites or biotinyl sites per BC-BCCP subcomplex. The other subcomplex is composed of the 2 α-CT and 2 β-CTs, as revealed in the crystal structure of the *E. coli* subcomplex (Bilder et al., 2006). The α-CT binds carboxybiotin while the β-CT binds acetyl-CoA, and the combination of these two components contributes to form one active site of the enzyme.

The regulation of ACCase has been intensively studied to reveal a myriad of regulatory mechanisms. Rat (*Rattus norvegicus*) and yeast (*Saccharomyces cerevisiae*) ACCases are feedback inhibited by palmitoyl-CoA, a final product in fatty acid biosynthesis (Ogiwaraet al., 1978). The gene expression level of yeast ACCase is also regulated in response to acyl-CoA concentration (Feddersen et al., 2007). In *E. coli*, ACCase is inhibited by acyl-ACP having 16-18 carbons (Davis and Cronan, 2001; Heath and Rock, 1995) and its gene expression is also modulated by long-chain acyl-ACP or

acyl-CoA (Zhang and Rock, 2009). In plants, the formation of malonyl-CoA and fatty acids is regulated by light (Nakamura and Yamada, 1979). This observation was later linked to the inhibition of ACCase by adenosine diphosphate (Eastwell and Stumpf, 1983) and the significant effect of various factors including pH, Mg^{++} and adenosine triphosphate (ATP) on ACCase activity (Nikolau and Hawke, 1983). A study on plastidial ACCase in *B. napus* microspore-derived cell suspension cultures reported that the plant enzyme is feedback inhibited by oleoyl-ACP (Andre et al., 2012). Plant htACCase is also negatively regulated by a homotrimeric PII protein, which acts as a sensor of various metabolites such as 2-oxoglutarate, pyruvate and ATP:ADP ratio (Feria Bourrellier et al., 2010). Plant htACCase is also inhibited by a newly identified family of proteins called biotin/lipoyl attachment domain containing proteins (Salie et al., 2016).

2.2.2.2. Fatty acid synthase

The product of the ACCase-catalyzed reaction is malonyl-CoA, which is subsequently used by the FAS complex as a 2-carbon donor to the growing acyl chain. FAS is composed of different subunits specifically β-ketoacyl-ACP synthase, β-ketoacyl-ACP reductase, β-hydroxyacyl dehydratase and enoyl-ACP reductase. Similar to *E. coli*, three β-ketoacyl-ACP synthases (KAS I-III) operate in the plastids. The first condensation reaction is carried out by KAS III, which uses acetyl-CoA and malonyl-ACP to form butyryl-ACP. The following series of condensation reactions is catalyzed by KAS I, which produces palmitoyl-ACP. Finally, the conversion of palmitoyl-ACP to stearoyl-ACP is catalyzed by KAS II (Jaworski et al., 1993; Tasy et al., 1992; Chen et al., 2015). The FAS-catalyzed reaction continues until either palmitoyl- and stearoyl-

ACPs are formed. Another plastidial enzyme, stearoyl-ACP desaturase, can catalyze the introduction of a *cis* double bond at position 9 of stearoyl-ACP forming oleoyl-ACP. Finally, the FAS reaction is terminated by two types of thioesterases, one of which prefers oleoyl-ACP [fatty acyl-ACP thioesterase A (FATA)] while the other one, FATB, prefers saturated acyl-ACPs (Dörmann et al., 1995 and Jones et al., 1995).

Although important in fatty acid biosynthesis, the over-production of individual components of the FAS complex including ACP, KAS III, KASI, FATA and FATB did not result in a change in the oil content of oil crops (Kinney, 1994). In addition, reduction (up to 50%) of BC and stearoyl-ACP desaturases through antisense gene expression did not affect seed oil content (Shintani et al., 1996 and Knutzon et al., 1992). These results suggest that the reactions catalyzed by FAS complex do not represent regulatory steps in seed oil accumulation, mainly because the components of the FAS are likely abundant in the cell (Ohlrogge and Jaworski, 1997).

2.2.2.3. Fatty acid export from the plastid and re-esterification

After synthesis, the acyl-ACPs are hydrolyzed releasing fatty acids, which are then transported out of the plastid by the fatty acid export 1 (Li et al., 2015). Fatty acid export 1 is localized in the inner plastidial membrane and is involved in transporting fatty acids into the intermembrane space. The free fatty acids are converted back into acyl-CoA just outside the plastids by the catalytic action of long chain acyl-CoA synthetases. Long chain acyl-CoA synthetases are bound to the cytosolic region of the plastid outer membrane (Andrews and Keegstra, 1983; Schnurr et al., 2002). In the ER, acyl-CoAs can be transported into the lumen by an ABC transporter (Kim et al., 2013).

2.2.3. The first three reactions of the Kennedy pathway

2.2.3.1. *sn*-Glycerol-3-phosphate acyltransferase

The Kennedy pathway (Weiss and Kennedy, 1956) leading to TAG and its association with membrane metabolism and acyl editing is shown in Figure 2.2. The first reaction in the Kennedy pathway is catalyzed by membrane-bound *sn*-glycerol-3-phosphate acyltransferase (GPAT). This enzyme catalyzes the addition of an acyl chain from acyl-CoA to *sn*-glycerol-3-phosphate (G3P) to form lysophosphatidate (LPA). Plastidial and soluble forms of GPAT use acyl-ACP as a substrate in the Kornberg-Pricer pathway (Kornberg and Pricer, 1953; Chen et al., 2011). On the other hand, *sn*-glycerol-3-phosphate (G3P) used in the Kennedy pathway, is formed from dihydroxy acetone phosphate via the catalytic action of *sn*-glycerol-3-phosphate dehydrogenase (Weselake et al., 2009). In Arabidopsis, 10 GPAT homologues have been identified and AtGPAT1 to 8 were found to be uninvolved in the Kennedy pathway (Chen et al., 2011). Rather, these AtGPAT isoforms represent a family of enzymes in land-plants that are needed for the biosynthesis of cutin and suberin (Beisson et al., 2007; Li et al., 2007; Shockey et al., 2015). AtGPAT9, on the other hand, was recently identified to be involved in production of LPA for use in the biosynthesis of membrane lipids and TAG (Shockey et al., 2015 and Singer et al., 2016).

2.2.3.2. Lysophosphatidate acyltransferase

The next acylation reaction is catalyzed by membrane-bound lysophosphatidate acyltransferase (LPAAT), which transfers an acyl chain from acyl-CoA to LPA forming phosphatidate (PA) (Fig. 2.2). In the Kornberg-Pricer pathway in the plastid, LPAAT activity utilizes acyl-ACP as the acyl donor (Chen et al., 2011). In certain oilseeds, ER

LPAAT exhibits substrate preference for specific fatty acids. Coconut LPAAT catalyzes the preferential addition of a lauryl chain (12:0) to the *sn*-2 position of the glycerol backbone (Knutzon et al., 1999). In addition, LPAATs from *B. napus* and flax (*Linum usitassimum*) prefer oleoyl and α-linoleoyl (18:2$\Delta^{9cis,12cis}$) acyl chains, respectively (Bourgis et al., 1999; Sorensen et al., 2005). Other plants producing unusual fatty acids have also been found to have LPAATs with high preferences for those fatty acids. LPAATs normally exhibit preference for unsaturated fatty acids allowing the enzyme to also play a key role in PC biosynthesis. The *sn*-2 position of PC is a site for further action of ER desaturases in the formation of PUFAs.

2.2.3.3. Phosphatidic acid phosphatase

Phosphatidic acid phosphatase (PAP) catalyzes the removal of the 3'-phosphate group from PA forming 1,2-diacyl-*sn*-glycerol (DAG) (Fig. 2.2). PAP homologues from Arabidopsis and *B. napus* were characterized in PAP-deficient yeast (Mietkewska et al., 2011). The enzyme was localized in the cytosol as well as in the nucleus upon supplementation of oleic acid. A plastidial form of PAP also catalyzes DAG formation (Chen et al., 2015). A double-knockout of the two Arabidopsis PAP genes led to ER proliferation and increased PC content (Eastmond et al., 2010). Mammalian and yeast PAP, also referred to as lipins, appear to modulate the flow of substrates between membrane lipids and TAG (Reue and Dwyer, 2009 and Carman and Han, 2009). Correspondingly, mammalian, yeast and plant PAP are found to regulate the biosynthesis of membrane lipids. A recent study in Arabidopsis showed that PAP modulates the level of PA, which activates CTP:phosphocholine cytidyltransferase (CCT), a key regulatory enzyme in PC biosynthesis (Craddock et al., 2015).

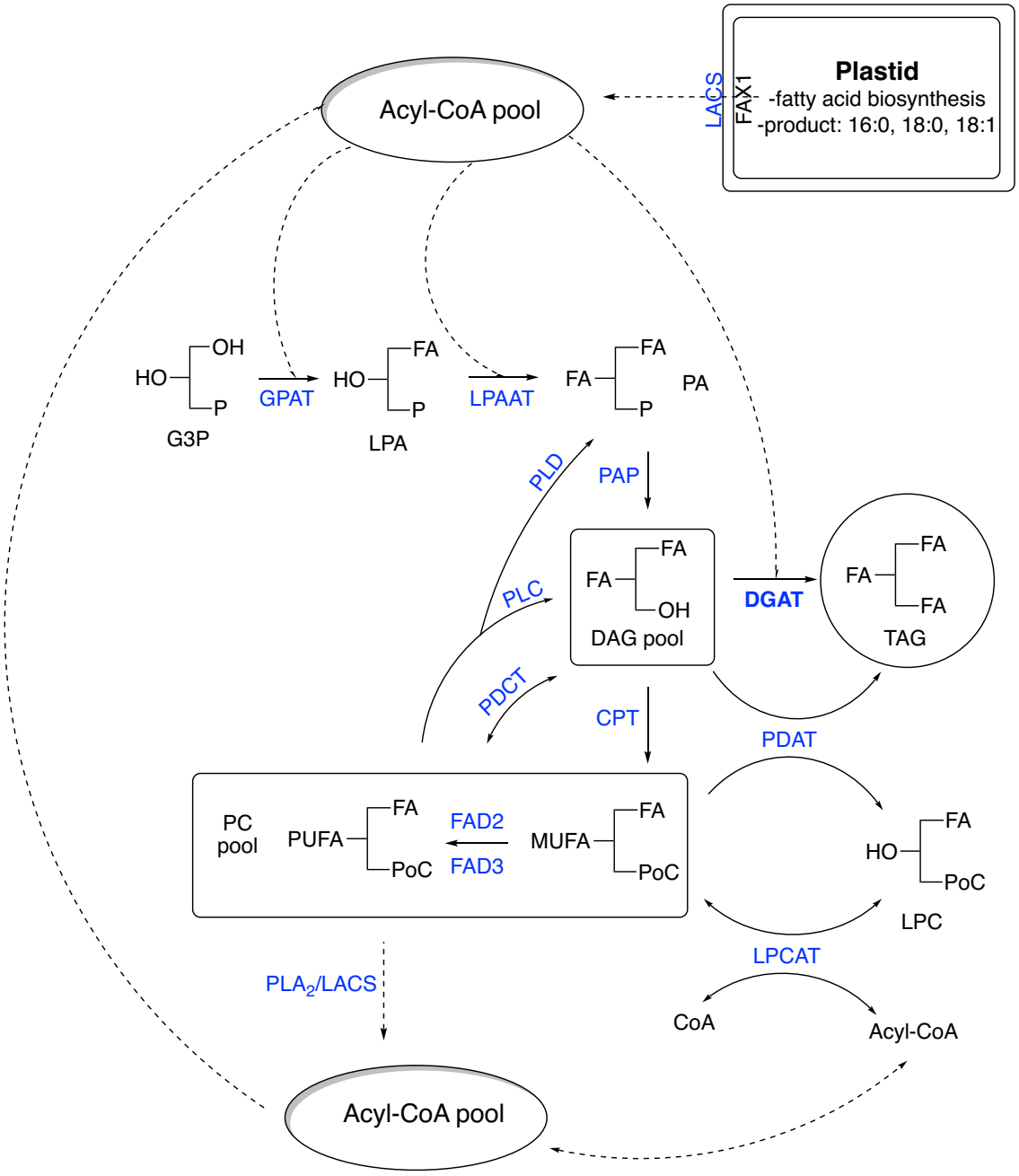

Figure 2.2. Triacylglycerol (TAG) biosynthesis is closely linked with phosphatidylcholine (PC) biosynthesis and acyl-editing pathways. In the plastids, fatty acids (16:0, 18:0, and 18:1) are produced *de novo* and are released by the inner plastidial membrane-bound fatty acid export 1 (FAX1). Outside the outer plastidial

membrane, long chain acyl-CoA synthetase (LACS) esterifies fatty acid into acyl-CoA, which eventually goes to the cytosolic acyl-CoA pool. In the acyl-CoA-dependent TAG biosynthesis, TAG is formed through the action of diacylglycerol acyltransferase (DGAT), which uses acyl-CoA to acylate 1,2-diacyl-*sn*-glycerol (DAG) forming TAG. DAG can arise either *de novo* from *sn*-glycerol-3-phosphate (G3P) or from the phosphatidylcholine pool (PC pool). In the acyl-CoA-independent TAG biosynthesis, phospholipid:diacylglycerol acyltransferase (PDAT) can transfer an acyl chain from the *sn*-2 of PC to DAG forming TAG and lysophosphatidylcholine (LPC). PC can be formed from DAG through the action of choline phosphotransferase (CPT). In PC, the *sn*-2 acyl chains can be further desaturated by fatty acid desaturases (FAD2 and FAD3). The acyl-CoA pool can be enriched in polyunsaturated fatty acids (PUFA) through acyl editing, where the modified acyl chains in PC are exchanged with the acyl-CoA pool. Acyl-editing can be facilitated by LPCAT and by the combined action of phospholipase A (PLA) and LACS. Headgroup exchange can also channel DAG backbone with PUFA from PC by phosphatidylcholine:diacylglycerol cholinephosphotransferase (PDCT), phospholipase C (PLC) and phospholipase D (PLD). Other abbreviations: FA, acyl chain; GPAT, *sn*-glycerol-3-phosphate acyltransferase; LPA, lysophosphatidate; LPAAT, lysophosphatidate acyltransferase; MUFA, monounsaturated fatty acids; PA, phosphatidate; PAP, phosphatidic acid phosphatase; PoC, phosphocholine. This figure is adapted from the AOCS Lipid Library® website.

2.2.4. Diacylglycerol acyltransferase

Diacylglycerol acyltransferases (DGATs) catalyze the final and committed step in the acyl-CoA-dependent biosynthesis of TAG biosynthesis via the Kennedy pathway (Fig. 2.2). These enzymes catalyze the addition of an acyl chain from acyl-CoA onto DAG to form TAG. To date, three non-homologous DGAT gene families have been identified and characterized. The first two gene families, DGAT1 and DGAT2, are embedded in the membrane lipid bilayer. The third gene family, DGAT3, is a soluble enzyme with DGAT activity (Lung and Weselake, 2006; Liu et al., 2012). Since DGAT is the main topic of this thesis, considerably more background information is provided for this enzyme than the other enzyme involved in TAG assembly.

Cases and colleagues (1998) reported the first *DGAT* cDNA, which was isolated from murine expressed sequence tag based on sequence similarity with cDNA encoding another acyltransferase, acyl-CoA:cholesterol acyltransferase 1 (ACAT1). Plant DGAT1 cDNAs were subsequently cloned from Arabidopsis (Hobbs et al. 1999; Zou et al., 1999b; Routaboul et al., 1999) and tobacco (*N. tabacum*) (Bouvier-Navé et al., 2000). The phenotype of *DGAT1* was first observed in Arabidopsis mutant, AS11, derived from plants treated with a chemical mutagen, ethyl methane sulfonate (Katavic et al., 1995). AS11 exhibited reduced TAG content in seeds leading to abnormally low TAG to DAG ratio. On the other hand, the study reported normal values for the ratio of DAG: LPA + PA, suggesting the inability of the mutant to convert DAG into TAG. This phenotype was later associated with an insertion in the *DGAT1* gene of AS11, thereby inactivating the enzyme (Zou et al., 1999b). The aforementioned study also noted that despite the inactivation of DGAT1, DGAT activity could still be detected suggesting the

existence of other enzymes with similar activity. This hypothesis was in agreement with studies involving *DGAT1* knockout mice (Smith et al., 2000). Later studies led to the identification of the other *DGAT* gene families. To date, many DGAT1 genes have been isolated and characterized from animal, plants and fungi (Turchetto-Zolet et al., 2011).

The second *DGAT* gene family, *DGAT2*, was first isolated, via protein purification approach, from the fungus *U. ramanniana* (Lardizabal et al., 2001). During partial purification of DGAT2 from *U. ramanniana*, a certain polypeptide observed during SDS-PAGE appeared to reflect DGAT activity in column fractions based on the relative intensity of the band. The polypeptide was excised from the gel, partially sequenced and the information used to develop degenerative primers for cloning the *DGAT2* gene. The study also reported the identification of homologous genes in *Caenorhabditis elegans* and *S. cerevisiae*. Subsequent studies identified *DGAT2* genes in humans (*Homo sapiens*) and mouse (Cases et al., 2001). Plant DGAT2 from plant species, tung tree *(Vernicia fordii*) and castor (*Ricinus communis*), was then identified and partially characterized (Shockey et al., 2006; Burgal et al., 2008). For several years, the function of DGAT2 in plants had been questionable, as deletion of the encoding gene in Arabidopsis did not affect seed oil content and a similar result was observed when *DGAT2* was knocked-out in AS11 lines (Zhang et al., 2009a). In addition, the expression of plant *DGAT2* in yeast H1246 was not able to rescue TAG biosynthesis (Zhang et l., 2009 and Weselake et al., 2009). Transient expression of Arabidopsis DGAT2 in tobacco (*Nicotiana benthamiana*) leaf, however, resulted to increased oil content (Zhou et al., 2013), and expression of codon-optimized AtDGAT2 in yeast H1246 restored

TAG biosynthesis (Ayme et al., 2014). The latter study showed that the inability of yeast to produce plant DGAT2 might be due to differences in codon preferences.

The third *DGAT* gene family, *DGAT3*, encodes a soluble enzyme localized in the cytosol. The first member of this family was isolated in *Arachis hypogea* through protein purification and gene isolation using degenerate primers based on initial amino acid sequence (Saha et al., 2006). Subsequent study in Arabidopsis led to the identification of a DGAT3 homologue, which was found to be involved in recycling 18:2 and 18:3 (α-linolenic acid; 18:3$\Delta^{9cis,12cis,15cis}$) fatty acids when TAG mobilization is halted (Hernández et al., 2012).

In addition to the aforementioned *DGAT* gene families, other enzymes were found to be exhibit DGAT activity. One example is the bifunctional wax synthase/DGAT, which was first isolated in *Acinetobacter* (Kalscheuer and Steinbuchel, 2003; Stoveken et al., 2005) and was also later characterized in Arabidopsis (Li et al., 2008). This enzyme predominantly catalyzes the formation of wax esters. Defective cuticle ridge is another soluble enzyme with DGAT activity, although it was reported to be mainly involved in cutin biosynthesis (Rani et al., 2010; Panikashvili et al., 2009). Another enzyme with putative DGAT activity is acyl-coenzyme A:monoacylglycerol acyltransferase 3, belonging to the a gene family which encode enzymes that catalyze the formation of DAG from MAG and acyl-CoA (Cao et al., 2007). These enzymes, however, are only present in animals and not in plants and are mainly associated with dietary fat absorption in the intestine. An unusual *Euonymus alatus* DGAT was also found to utilize acetyl-CoA rather than oleoyl-CoA as acyl donor to form 3-acetyl-1,2-diacyl-*sn*-glycerol, which has lower viscosity than normal oil (Durrett et al., 2010).

One major way of regulating enzyme activity is by controlling the spatial and temporal gene expression, and this can vary greatly depending on the organism. In mammals, *DGAT1* mRNA is highly expressed in the small intestine, liver, adipose tissue, and mammary gland, which all produce substantial amounts of TAG (Yen et al., 2008). In humans, the highest *DGAT1* expression is found in small intestine, testis and adipose tissues (Cases et al., 1998). Most tissues producing TAG were also found to express *DGAT2*, with the liver, adipose tissues and mammary gland producing the highest amounts in humans (Cases et al., 2001).

In Arabidopsis, *DGAT1* is expressed in leaves, roots, flowers, siliques, germinating seeds and seedlings (Zou et al., 1999b). Subsequent studies found that the highest expression is found in embryos at the cotyledonary stage (Hobbs et al., 1999; Lu et al., 2003). The expression level in the embryo was further shown to be dynamic, which increases continuously until late developmental stage and plummets at a late maturation stage (Li et al., 2010b). The latter study further found that the embryo expression level of Arabidopsis *DGAT2* increases during its development but at much lower level relative to *DGAT1*, but higher than the levels in roots, stems and leaves. The gene expression level of each *DGAT* gene family can differ depending on the species. For oilseeds, in general, *DGAT1* or *DGAT2* expression tends to correlate with the rate of oil accumulation during seed development, with *DGAT1* transcript being consistently present (Liu et al., 2012). In Arabidopsis and soybean, *DGAT2* seems to have low expression level compared to DGAT1, which seems to encode the major DGAT facilitating oil deposition (Li et al., 2010b). A different scenario is observed in tung tree

and castor, wherein *DGAT2* transcripts in developing seeds are present at higher levels than *DGAT1* (Kroon et al., 2006; Shockey et al., 2006).

Peanut *DGAT3* is predominantly expressed in seeds at early stages of development (8 to 24 days after flowering), and the level decreases at late stages (Saha et al., 2006). A more recent study reported that peanut DGAT3 has three isoforms and *AhDGAT3-3* is expressed in other plant tissues, with highest expression in leaf and flowers (Chi et al., 2014). Arabidopsis defective cuticle ridge is expressed in various tissues such as roots, cotyledons, stems, leaves, pollen grains and seeds (Panikashvili et al., 2009).

DGAT1 belongs to a superfamily of membrane-bound O-acyltransferases (MBOAT), which are polytopic membrane enzymes catalyzing the transfer of acyl group from acyl-CoA onto a hydroxyl or thiol functional group of lipids and proteins (Hofmann, 2000). MBOATs are predicted to have a pair of conserved histidine and asparagine/aspartic acid serving as active site residues (Chang et al., 2011). Human MBOATs can be grouped based on the acyl acceptor molecule. The first subgroup acylates the hydroxyl group of cholesterol or DAG and includes ACAT1, ACAT2 and DGAT1. The second group acylates a residue of a protein or peptide, which includes porcupine, sonic hedgehog, ghrelin and yeast Gup1. The third group acylates phospholipids such as GUP1 and the lysophopholipid acyltransferases (Chang et al., 2011).

ACAT, which transfers an acyl group from acyl-CoA to cholesterol, was the first MBOAT member discovered through kinetic analysis of rat liver lysate (Mukherjee et al., 1958). The *ACAT1* gene was identified in 1993 through expression in Chinese hamster cell devoid of ACAT activity (Chang et al., 1993). Based on ACAT1 sequence,

ACAT2 and *DGAT1* genes were subsequently isolated and characterized (Yu et al., 1996; Cases et al., 1998). ACAT1 is about 20% identical to DGAT1 and is the most well studied MBOAT member. It is found in most mammalian cells but not in plants. ACAT1 is a tetrameric enzyme having 9 transmembrane segments (Chang et al., 1998). The 7th transmembrane segment has the active site histidine while the active site asparagine is localized within a cytosolic loop. Furthermore, the acyl acceptor of ACAT1, cholesterol, is an allosteric activator of the enzyme (Liu et al., 2005).

2.2.5. Acyl-CoA-independent TAG biosynthesis and acyl-editing

The Kennedy pathway provides a straightforward route towards the formation of TAG using acyl-CoAs and G3P. In many species, however, TAG assembly is intricately associated with membrane metabolism (Fig. 2.2). Phospholipid:diacylglycerol acyltransferase (PDAT) catalyzes the transfer of an acyl chain from the *sn*-2 position of PC to DAG forming TAG (Dahlqvist et al., 2000) (Fig. 2.2). In Arabidopsis, six *PDAT* gene homologues were identified but only one gene (*PDAT1*) seems to be mainly responsible for the detected PDAT activity (Ståhl et al., 2004). When *PDAT1* was knocked out, the amount of TAG accumulation was not significantly affected suggesting that acyl-CoA-dependent TAG synthesis can compensate for the loss of PDAT activity (Ståhl et al., 2004 and Mhaske et al., 2005). The importance of this enzyme was realized when *PDAT1* was knocked out in a plant with inactivated *DGAT1*, which resulted to up to 80% reduction in TAG content and abnormal seed and pollen development (Zhang et al., 2009a). Furthermore, PDAT appears to be a key player in channeling fatty acids modified on PC (especially PUFAs) into TAG (Kim et al., 2011; van Erp et al., 2011; Pan et al., 2013).

Phosphatidylcholine:diacylglycerol cholinephosphotransferase (PDCT) is another enzyme that channels PUFAs or other PC-modified fatty acids into TAG (Fig. 2.2). Arabidopsis harboring inactivated PDCT did not exhibit any change in total TAG content but the level of PUFAs was reduced by 40% (Lu et al., 2009). PDCT transfers a phosphocholine headgroup from PC to the *sn*-3 position of DAG (Lu et al., 2009). This enzyme regulates the fatty acid composition by favoring the conversion of 18:1-containing DAG to PC, which is the substrate for further desaturation. DAG is a common intermediate in PC and TAG biosynthesis. Recently, Wickaramarthna et al. (2015) reported that flax PDCT may be involved in channeling 18:3 from PC into seed TAG.

CPT is another enzyme which catalyzes the conversion of DAG to PC (Fig. 2.2). The CPT-catalyzed reaction uses the phosphocholine derived from CDP-choline resulting in the formation of PC and CMP (Chen et al., 2015). An earlier study with developing flax seed cotyledons demonstrated the possible reversibility of the CPT-catalyzed reaction *in vivo* (Slack et al., 1983) but it should be noted that the reaction is thermodynamically unfavorable in the direction of DAG and CDP-choline formation (Chen et al., 2015).

The occurrence of two separate DAG pools was previously suggested by radiolabeling experiments (Bates et al., 2007; Bates et al., 2009). Newly formed fatty acids (often highly enriched in 18:1) are transported out of the plastids and converted to acyl-CoA that are utilized by GPAT and LPAAT of the Kennedy pathway to form a DAG pool enriched in 18:1. DAG enriched in 18:1 is then channeled into PC for further desaturation and acyl editing. PDCT then catalyzes the conversion of PUFA-enriched

PC into a second pool of PUFA-enriched DAG, which is now available for the Kennedy pathway to facilitate production of PUFA-enriched TAG (Bates et al., 2009).

Acyl editing mainly occurs in PC, which is the substrate for ER-bound desaturases. Various reactions can exchange acyl groups involving PC molecules. The main key players in these acyl exchanges are lysophosphatidylcholine acyltransferase (LPCAT) and phospholipase A_2. The forward reaction of LPCAT involves the transfer of acyl chain from acyl-CoA to lysophophatidylcholine (LPC) forming PC (Fig. 2.2). The reverse reaction, which is thermodynamically unfavorable, involves the release of acyl-CoA from PC though addition of CoA (Pan et al., 2015). Originally, it was proposed that PUFA chains on PUFA-enriched PC may be exchanged with new acyl-CoAs through the joint forward and reverse reactions of LPCAT (Stymne and Stobart, 1984). Recently, coupling of the flax LPCAT-catalyzed reverse reaction to the flax DGAT-catalyzed forward reaction was shown to represent a possible route for channeling PUFA into TAG (Pan et al., 2015). Utilization of PUFA-CoA by the DGAT-catalyzed reaction helped to drive the LPCAT-catalyzed reaction in reverse. In addition, the LPCAT-catalyzed reactions may differ in substrate preference for forward and reverse-catalyzed reactions (Lager et al., 2013).

Phospholipase A_2 can also release modified acyl chains from the *sn*-2 position of PC (Bayon et al., 2015) and the released modified fatty acid, can be converted to acyl-CoA through the catalytic action of long chain acyl-CoA synthetases (Fig. 2.2). Resulting lysophosphatidylcholine (LPC) can be reconverted to PC in the Land's cycle via LPCAT action (Lands, 1960; Wang et al., 2012). DAG with PUFA can also be released from PC through the action of phospholipases C and D and subsequently by

PAP. These PC-derived DAGs also provide as way for enriching TAG formation with PUFA (Bates et al., 2012).

2.2.6. Phosphatidylcholine biosynthesis

TAG accumulation is accompanied by PC biosynthesis in order to package the highly hydrophobic TAG molecules into oil bodies. Previously, it was proposed that TAG droplets formed in the outer leaflet of the ER pinch off from the ER surrounded by a monolayer of phospholipids (mainly PC) to form oil bodies (Huang, 1996). TAG biosynthesis and PC biosynthesis via the nucleotide route share common Kennedy pathway intermediates, branching out from DAG. In addition to DGAT, DAG can also be used by CPT, which adds a phosphocholine moiety from CDP-choline to DAG forming PC (Gibellini and Smith, 2010). The CDP-choline utilized by the CPT-catalyzed reaction is provided through the catalytic action of a key regulatory enzyme named CCT. CCT transfers phosphocholine produced by the choline kinase to CTP forming CDP-choline. PC can also be produced through the action of phosphatidylethanolamine *N*-methyltransferase, which transfers methyl groups from S-adenosylmethionine to PE forming PC (Vance et al., 2007).

2.2.7. Oil body formation

As indicated above, TAGs produced in the ER are package into organelles called lipid/oil bodies, which have a core of TAG molecules surrounded by one layer of phospholipids (Huang, 1996). Two models have been proposed for the formation of lipid bodies depending on the site of origin (Chapman et al., 2012). In both models, TAGs accumulate between the two leaflets of the ER. In seeds, the other phospholipid layer is coated and stabilized from coalescence by oleosins, which are small proteins having a

internal proline knot inserted into the lipid body and cytoplasmic N- and C-termini (Murphy, 1993 and Huang, 1992). Caleosin is another protein stabilizer associated with the lipid body that has a similar topology as oleosin having a hydrophobic centre containing a proline knot inserted into lipid body (Chen et al., 1999). The N- and C-terminal regions of caleosins are larger compared to oleosins, which have a helix-loop-helix EF motif binding calcium and a phosphorylation region, respectively. Aside from its structural importance in lipid bodies, caleosins also act as peroxygenases, which catalyze the formation of epoxy fatty acids by oxidizing unsaturated fatty acids (Hanano et al., 2006). This process is associated with the production of oxylipins, which are important in stress responses and immunity in plants (Mosblech et al., 2009). Stereoleosin is another protein associated with lipid bodies (Lin et al., 2002). Unlike oleosins and caleosins, stereoleosins only have a hydrophobic N-terminal region embedded in the lipid body and no proline knot motif. Stereoleosins have a cytosolic C-terminal region with a hydroxysteroid dehydrogenase domain that may be involved in brassinosteroid metabolism. Furthermore, other lipid-droplet associated proteins have been identified and found to be important for lipid body maintenance and regulation (Gidda et al., 2016). Recently, it was shown that TAG surrounded by PC buds off from the ER to form oil bodies through the assistance of molecules called SEIPINs, which are oil body machineries governing the size and quantities of oil bodies (Cai et al., 2015).

2.3. Biochemical regulation of metabolic enzymes

The regulation of enzyme activity can occur at different points from transcription to post-translation. Transcriptional regulation is mainly determined by *cis*-regulatory elements present in the gene sequence and *trans*-acting regulatory proteins such as transcription factors. Another important, direct and interesting mode of regulation occurs after the protein has been translated, and this includes allosteric regulation and covalent addition of various functional groups and moieties including phosphate, ubiquitin, SUMO and glycosyl group.

2.3.1. Allosteric regulation of enzymes

One major way by which an enzyme's activity is regulated is through allosteric regulation. This mode of regulation operates through the binding of a small molecule or biomolecule to a site other than the active site (referred to as an allosteric site). The binding at the allosteric site transmits a signal to other parts of the enzyme influencing the enzyme activity. Two models were proposed to illustrate allostery. Both models assume that multi-subunit enzymes can exist either in the tensed state or the relaxed state. The relaxed state is more responsive to ligand binding and corresponds to the more active state. The first model is called Monod, Wyman and Chaneux/MWC, concerted or symmetry model, and is based on the assumption that all subunits in a functional protein exist in the same state (Monod et al., 1965). In addition, the binding of ligand in one subunit favors the shift to the relaxed state, which is transmitted to the other subunits. Hemoglobin, which is a tetrameric enzyme having one oxygen-binding site per subunit, has been shown to follow this model (Eaton et al., 1999). The other model is known as Koshland, Nemethy and Filmer/KNF or sequential model, and is based on the

assumption that the subunits do not have to be in the same conformation at the same time (Koshland et al., 1966). Ligand binding occurs through induced fit, which facilitates the shift from the tense to the relaxed state. The other subunit may become more responsive to ligand, without a complete shift into the relaxed state. In recent years, these models have been re-evaluated to provide a combination of both models and accounting for conformational selection (Freiburger et al., 2014).

An allosteric effector may be a substrate, small molecule, or regulatory protein that can increase or decrease a protein's activity by binding to a site other than the active site. The binding of allosteric effector can bring about change in protein activity via different mechanisms. These mechanisms have been investigated in some enzymes through determination of the crystal structure of the protein in the presence and absence of bound ligand (Laskowski et al., 2009). One mechanism, as observed for the enzyme phosphoglycerate dehydrogenase, involves the change in accessibility of the active site. This enzyme is involved in the biosynthesis of serine, which serves as a feedback inhibitor. Serine can bind to an allosteric site in phosphoglycerate dehydrogenase causing a conformational change leading to blockage of the active site pocket (Thomson et al., 2005). A second mechanism of allosteric regulation involves changes in the affinity of the active site residues for the substrate. This is observed for 3-deoxy-D-arabinoheptulosonate-7-phosphate synthase, which is involved in the biosynthesis of aromatic amino acids. The feedback inhibitors of the enzyme are the end-product amino acids, which can bind to an allosteric site and initiate a distorted active site architecture with reduced affinity for substrates (Shumilin et al., 2002). A third possible mechanism of allosteric control involves changes in electrostatic properties of the active site upon

ligand binding. This is observed in chorismate mutase, wherein the binding of inhibitor leads to a movement of a glutamate side chain into the active site pocket. The substrate of this enzyme is anionic at physiological conditions and the presence of a similarly negatively charged glutamate side chain deters the substrate from binding (Lin et al., 1998). In some multimeric enzymes, one oligomeric state may be more functional than the other and ligand binding may facilitate the conversion between these states. An example of this is ATP phosphoribosyltransferase, which can exists as an inactive hexamer and as active dimers. The transition in oligomeric states of this enzyme is induced by the binding of a feedback inhibitor (Cho et al., 2003).

2.3.2. Regulation of enzyme activity through phosphorylation

Phosphorylation/dephosphorylation is an important regulatory mechanism that has been well-studied in many metabolic enzymes. Kinases are enzymes that transfer a phosphoryl group from ATP to a hydroxyl group of serine, threonine or tyrosine. Phosphorylation can be reversed through hydrolysis, which is catalyzed by phosphatases. Studies on proteins present in different plant organelles showed that phosphorylation is a very common phenomenon. Nuclei proteins are easily phosphorylated by endogenous protein kinases (Ranjeva et al., 1987), which are associated with regulation of gene expression (Kuehn et al., 1979; Wielgat et al., 1981). Plastidial proteins are also widely phosphorylated as well as proteins from mitochondria.

The addition of phosphoryl group can influence enzyme activity through different mechanisms. Phosphorylation has been found to induce conformational change leading to an enzyme form that can be more or less active than the unphosphorylated form. Other consequences of phosphorylation include altering the ability to form oligomers or

protein complexes and influencing the capacity to bind regulatory proteins among others. Plant mitochondrial PDH complex is an enzyme regulated through phosphorylation. This enzyme catalyzes the oxidative decarboxylation of pyruvate to form acetyl-CoA. This reaction links glycolysis to Krebs cycle whereas the plastidial PDH also provides substrates for the synthesis of fatty acids and several amino acids. Mitochondrial PDH can be phosphorylated or dephosphorylated at different sites (Luethy et al., 1996; Randall et al., 1996) by intrinsic PDH kinase and PDH phosphatase, respectively. In mammalian mitochondrial PDH complex, the addition of a phosphoryl group to PDH converts the enzyme into the inactive form (Korotchkina et al., 2001). Two out of the three phosphorylated serine residues in mammalian PDH were found to phosphorylated as well in plants (Tovar-Mendez et al., 2003). Interestingly, seed-specific down-regulation of the expression of the gene encoding mitochondrial PDH kinase during seed development in Arabidopsis was shown to result in increased seed weight and oil content (Zou et al., 1999a; Marillia et al., 2003). The results suggest that mitochondrial PDH action influences storage lipid biosynthesis.

Different families of kinases have been identified in plants. The calcium-dependent protein kinase is activated in the presence of calcium, which is a ubiquitous intracellular messenger elevated in response to various environmental, hormonal or stress stimuli (Poovaiah and Redyy, 1993). In plants, this kinase family act on various proteins such as aquaporins, nitrate reductase, and sucrose synthase (Lee et al., 1995; Johnson et al., 1992; Huber et al., 1996). The mitogen-activated kinase (MAPK) cascade is another interesting set of phosphorylation in cells involving three kinases operating sequentially wherein one kinase (MAPKKK) phosphorylates another enzyme

(MAPKK), which in turn acts on MAPK (Hardie, 1999). This cascade enables the amplification of a signal and is involved in controlling different developmental processes and facilitating stress, hormonal and immune responses (Rodriguez et al., 2010).

Cyclin-dependent kinase is another family of serine and threonine kinases that are involved in cell cycle regulation (Francis, 2007). CDKs are activated upon binding a family of proteins called cyclins. CDKs are also involved in other processes including transcriptional regulation, translational regulation and mRNA processing (Doonan and Kitsios, 2009). Another class of kinases is casein kinase, which are highly conserved proteins also involved in serine/threonine phosphorylation. Two plant casein kinases have been well-characterized. Casein kinase I has been shown to be involved in root development (Liu et al., 2003), flowering time (Dai and Xue, 2010), and sugar signaling regulation (Moriya and Johnston, 2004). On the other hand, casein kinase II is a component of the circadian clock system and is involved in regulating flowering time (Ogiso et al., 2009).

Sucrose non-fermenting-related kinase 1 (SnRK1) is a serine/threonine kinase that is involved in the regulation of carbon metabolism in plants. SnRK1 has three members in Arabidopsis and the number can vary from 2-20 depending on the species (Halford and Hardie, 1998). It has a catalytic domain comparable to sucrose non-fermenting-1 (SNF1) of yeast and AMP-activated protein kinase (AMPK) of animals (Hardie, 2000). When the level of glucose is low, SNF1 becomes activated and directly inhibits the anabolic enzymes such as ACCase and glycogen synthase (Woods et al., 1994; Hardie et al., 1994). AMPK is allosterically activated by AMP and inhibited by

ATP, acting as a sensor of the energy state of the cell (Hardie and Carling, 1997). AMPK inhibits ACCase and 3-hydroxy-3-methyl-glutaryl-CoA (HMG) reductase, which are ATP-consuming reactions, as means to conserve ATP (Davies et al., 1990; Gillespie and Hardie 1992). SnRK1 belongs to the SnRK gene family together with SnRK2 and SnRK3, the latter two of which are less homologous to SNF1 and AMPK1 and have been implicated in abscisic acid-related signaling and tolerance to salt, respectively (Gomez-Cadenas et al., 1999; Liu et al., 2000).

SnRK1 is composed of three subunits specifically α, β and γ subunits. The α subunit is the catalytic subunit having a kinase and a regulatory domain. This subunit has a conserved threonine residue within the activating T-loop, which is phosphorylated by the catalytic action of upstream kinases, GRIKs/geminivirus Rep-interacting kinases or also known as SnRK1 activating kinases/SnAK (Shen et al., 2009). SnRK1 is allosterically inhibited by trehalose-6-phosphate, which correlates with the level of sucrose in cells (Zhang et al., 2009b). Other identified inhibitors of SnRK1 include glucose, sucrose, glucose-6-phosphate, and glucose-1-phosphate (Toroser et al., 2000; Wu and Birch, 2010, Nunes et al., 2013). As for AMP, *in vitro* assay showed that SnRK1 is more resilient to dephosphorylation in the presence of AMP (Sugden et al., 1999). SnRK1 can be dephosphorylated by the catalytic action of clade A type 2C protein phosphatases (Rodrigues et al., 2013).

The key role of SnRK1 in carbon metabolism has been shown by the ability of this kinase to affect the activity of a number of key enzymes in primary metabolism. SnRK1 can catalyze the phosphorylation and subsequent inactivation of HMG-CoA reductase (Dale et al., 1995). HMG-CoA reductase catalyzes the production of mevalonate, which

is a key molecule for the biosynthesis of isoprenoids. Nitrate reductase, which is involved in absorption of exogenous nitrate, is also a substrate of SnRK1 (MacKintosh et al., 1995). This enzyme provides reduced nitrogen for the biosynthesis of amino acids. Sucrose phosphate synthase is another key enzyme phosphorylated by SnRK1 (McMichael et al., 1995). This enzyme is involved in the biosynthesis of sucrose. SnRK1 also acts on 6-phosphofructo-2-kinase/ fructose-2,6-bisphosphatase (F2KP), which is a bifunctional enzyme that controls the formation and dephosphorylation of fructose-2,6-bisphosphate (FBP) (Kulma et al., 2004). FBP is a regulatory molecule that inhibits fructose-1,6-bisphosphatase. Nonphosphorylating glyceraldehyde-3-phosphate dehydrogenase is also inactivated by SnRK1 phosphorylation (Piattoni et al., 2011). This enzyme provides NADPH for reductive biosynthesis by facilitating an alternative pathway in glycolysis. Proteins involved in photosynthesis are also found to be influenced by SnRK1 regulation although phosphorylation in this case, is likely to be a stimulatory signal (Nukarinen et al., 2016).

2.3.3. Intrinsically disordered domains as regulators of protein function

Prior to the mid-1990s, disordered proteins were underappreciated, as their prevalence was not well understood. The explosion in genome sequencing coupled with development of bioinformatic tools slowly shed light on the prevalence of disordered proteins in eukaryotes (Wright and Dyson, 2014). Disordered proteins are characterized by a low percentage of hydrophobic residues, which generally drive folding into a stable and defined three-dimensional structure. These proteins assume a variety of conformations ranging from extended coils to loose unstable globules (Dyson and Wright, 2005). Fully disordered proteins are called intrinsically disordered proteins

(IDPs), while other proteins have disordered portions referred to as intrinsically disordered regions (IDRs). One important characteristic of IDPs/IDRs is their ability to interact with multiple protein partners, enabling them to perform various roles in cellular signaling and regulation. IDPs/IDRs have been found to house small recognition elements, which are segments that fold upon interaction with protein partners. They bind to multiple interaction partners in a dynamic and transient manner. IDPs are usually identified through bioinformatics analysis using various available web servers such as DISOPRED, DisEMBL and IUPred, to name a few. Structural models are then obtained using nuclear magnetic resonance and small angle X-ray scattering experiments in combination with available data of ensembles in the Protein Ensemble Database (Sibille and Bernadó, 2012; Varadi et al., 2014).

IDPs have been found to regulate protein function in various ways. Due to their ability to bind multiple partners, and their susceptibility to post-translational modification, IDPs/IDRs exhibit allostery in a complex manner allowing the fine-tuning of signals (Motlagh et al., 2004). Their flexible nature allows them to be accessible to protein machineries that add post-translational modifications that tend to be in clusters (Pejaver et al., 2014). These post-translational modifications include acetylation, methylation, glycsolyation and phosphorylation, with the latter being the most predominant post-translational modifications in IDPs/IDRs (Iakoucheva et al., 2004). IDPs/IDRs have also been found to be enriched in autoinhibitory sequences, which are *cis* elements in protein that down-regulates the activity of the protein (Trudeau et al., 2013).

2.3.4. Biochemical regulation of key enzymes in carbon metabolism related to TAG biosynthesis

Extensive research has been directed towards the elucidation of the regulatory mechanisms of primary metabolic enzymes. Biochemical regulation allows an allosteric enzyme and/or enzyme subject to covalent modification to adjust directly to existing cellular conditions. The pathway for TAG biosynthesis starting from breakdown of sugar molecules to the Kennedy pathway is shown in Figure 2.3. Many metabolite effectors have been identified to modulate the activity of key soluble regulatory enzymes and these are indicated in gray boxes beside each enzyme. Prior to this thesis project, there was a huge gap in our knowledge of how specific enzymes involved in TAG assembly are regulated (Fig. 2.3) (Coleman and Lee, 2004).

The carbons used for TAG biosynthesis in plants can come from sucrose and starch. Glucose derived from these sources is first broken down into pyruvate through glycolysis. The major regulatory enzymes in plant glycolysis include phosphofructokinase (PFK), pyrophosphate: fructose-6-phosphate 1-phosphotransferase (PFP), and pyruvate kinase (PK), which are responsive to different activators and inhibitors (Fig. 2.3) (Plaxton, 1996). Pyruvate is then oxidatively decarboxylated into acetyl-CoA by the catalytic action of the pyruvate dehydrogenase complex (PDH), which is another tightly regulated enzyme responsive to various metabolites and signals (Fig. 2.3) (Tovar-Mendez et al., 2003). The resulting acetyl-CoA is then used by acetyl-CoA carboxylase (ACCase), which is a key regulatory enzyme in fatty acid biosynthesis (Fig. 2.3). The activity of ACCase is also modulated by different effectors and binding proteins (Sasaki and Nagano, 2014; Salie and Thelen, 2016).

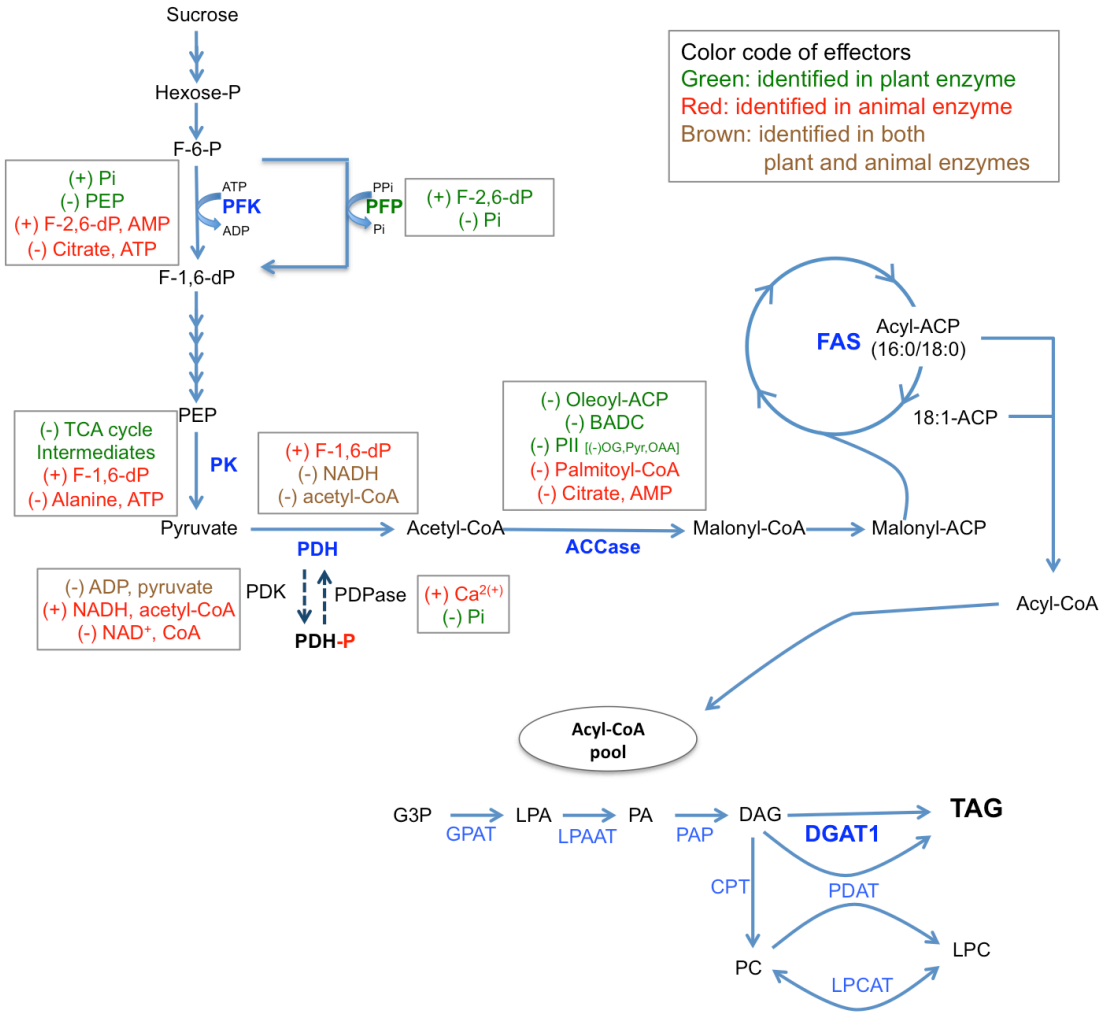

Figure 2.3. Metabolic pathways associated with the *sn*-glycerol-3-phosphate (G3P) pathway for triacylglycerol (TAG) biosynthesis. The carbons used for TAG biosynthesis are primarily derived from the breakdown of sugar molecules into pyruvate through the glycolytic pathway. The key regulatory enzymes of the glycolytic pathways include phosphofructokinase (PFK), pyrophosphate: fructose-6-phosphate 1-phosphotransferase (PFP), and pyruvate kinase (PK), which are all sensitive to various

metabolite effectors. Pyruvate is converted into acetyl-CoA through the action of the pyruvate dehydrogenase (PDH) complex, which is also tightly regulated by different effectors. PDH can be deactivated by pyruvate dehydrogenase kinase (PDK) and activated by pyruvate dehydrogenase phosphatase (PDPase). PDK and PDPase are also responsive to different effectors. Acetyl-CoA is used by acetyl-CoA carboxylase (ACCase) to catalyze the formation of malonyl-CoA, which is used by the fatty acid synthase (FAS) complex for *de novo* fatty acid synthesis. ACCase is also modulated by various effectors. Fatty acids are then transported to the cytosol for TAG assembly in the ER. In the Kennedy pathway, two fatty acyl chains from acyl-CoAs are esterified first onto a glycerol backbone through the action of *sn*-3-glycerol-phosphate acyltransferase (GPAT) and lysophosphatidate acyltransferase (LPAAT) catalyzes the formation of phosphatidate (PA). PA is then dephosphorylated to form 1,2-diacyl-*sn*-glycerol (DAG), which is a common intermediate for TAG and phosphatidylcholine (PC) biosynthesis. DAG can either be acylated by the action of DGATs (primarily DGAT1 in Arabidopsis and *B. napus*) to form TAG or be acted upon by choline phosphotransferase (CPT) to form PC. In plants, TAG can also be produced through the transfer of acyl chain from PC to DAG by phospholipid:diacylglycerol acyltransferase (PDAT). The newly established effectors of DGAT1 including CoA, acyl-CoA and PA are shown above the enzyme. Other abbreviations: AMP, Adenosine monophosphate; ATP, Adenosine triphosphate; BADC, Biotin/lipoyl attachment domain containing proteins; CoA, Coenzyme A; F-1,6-dP, Fructose-1,6-disphosphate; F-2,6-dP, Fructose-2,6-disphosphate; F-6-P, Fructose-6-phosphate; LPC, lysophosphatidylcholine; LPCAT, lysophosphatidylcholine acyltransferase; NADH, Nicotinamide adenine dinucleotide;

PAP, phosphatidic acid phosphatase; PEP, Phosphoenol pyruvate; Pi, Inorganic phosphate; Pyr, pyruvate; OAA, oxaloacetate, TCA, Tricarboxylic acid; 2-OG, 2-oxoglutarate. The information used to develop this figure are from Plaxton (1996), Tovar-Mendez et al. (2003), Coleman and Lee (2004), Sasaki and Nagano (2014), Salie and Thelen (2016).

2.4. Purification and reconstitution of eukaryotic membrane proteins

The biochemical characterization of eukaryotic membrane proteins may involve a number of challenges. In order to characterize a membrane protein, it must first be produced in recombinant form in a suitable system since membrane proteins usually exist in low amounts in biological membranes (Seddon et al., 2004). *E. coli* is a common system for recombinant production of prokaryotic membrane proteins and soluble prokaryotic and eukaryotic proteins. This system is generally not applicable to eukaryotic membrane proteins due to differences in the protein folding machineries and width of the lipid bilayer. *S. cerevisiae* is a very promising platform for recombinant production of eukaryotic membrane proteins (Hays et al., 2010). *S. cerevisiae* is a simple eukaryotic organism that has been well-studied. Different promoters have been used to produce recombinant proteins in *S. cerevisiae* and the widely used ones include the galactose-inducible GALACTOSE1/10 promoters, and the constitutive alcohol dehydrogenase 1/ADH1 and Translational elongation factor EF1 promoters (Hays et al., 2010). The inducible promoters are found to be effective for eukaryotic membrane proteins. In choosing the right yeast strain for expression, it is important to consider the strain with knocked out endogenous proteases especially vacoular Pep4p protease to obtain intact recombinant proteins (Jones, 2002). Other viable production systems for eukaryotic membrane proteins include *Pichia pastoris* (Brooks et al., 2013), human embryonic kidney cell lines (Gruswitz et al., 2010), *Lactococcus lactis* (Frelet-Barrand et al., 2010), and baculovirus-insect cells (Jarvis, 2009). Each system has its benefits. Yeast systems are generally cheaper compared with insect cells. Human embryonic kidney cell lines are easy to deal with but typically give low yield.

Once an efficient recombinant protein production platform has been identified and optimized, the next challenge involves finding a suitable detergent for solubilization. The detergent micelles will provide a suitable hydrophobic environment that mimics the lipid bilayer and make it amenable to separation from the rest of the bilayer components for purification. The right detergents must be screened based on their ability to extract the target membrane proteins from the membranes and their ability to preserve a functional protein. Another factor that can be considered is the critical micelle concentration of the detergent, which is the minimum concentration needed for detergent molecules to come together and form micelles. The most commonly used detergents include n-dodecyl-β-D-maltopyranoside, dodecyloctaethylene, octyltetraoxyethylene, dodecylnonaethylene, n-octyl-ß-Dglucopyranoside, n-dodecyl-N,N-dimethylamine-N-oxide, and n-dodecylphosphocholine, and dohexylphosphocholine choline-16 (Hays et al., 2010; Clark et al., 2010). For purification, affinity tags such as IgG, polyhistidine and FLAG® are added in the construct for affinity purification. Multiple chromatographic steps are usually employed to purify detergent-solubilized membrane proteins and may include size-exclusion chromatography and ion-exchange chromatography. Once the protein is purified in detergent micelles, reconstitution can be performed through addition of phospholipids, which are the actual components of the lipid bilayer. A solution of lipids forming liposomes can be added directly into protein-detergent complexes. The detergent can be removed using different methods such as dialysis, column chromatography, and /or through the use of detergent-adsorbing beads/Bio-beads® (Seddon et al., 2004).

2.5. Biochemical studies on diacylgycerol acyltransferase 1

Although the first *DGAT1* gene was identified more than 15 years ago and despite its importance in plant biotechnology and even in medical biochemistry, no DGAT1 from any species has been subjected to intensive structure-function studies due to difficulties in purifying the membrane-bound enzyme. Most membrane proteins are naturally low in abundance, making purification challenging. Advances in recombinant protein technology have increased the study of various membrane proteins, but their hydrophobic nature and propensity to aggregate/precipitate upon extraction from the lipid bilayer serve as barrier which must be overcome to generate sufficient protein for biochemical studies (Clark et al., 2010). To be amenable to purification, membrane proteins must first be extracted from the lipid bilayer and solubilized in detergents. Detergents, however, can denature proteins and remove cofactors needed for biological function. Previous solubilization and purification studies on plant DGAT1 have been met with limited success. Microsomal DGAT from germinating soybean was previously solubilized with 3-[(3-cholamidopropyl)dimethylammonio]-1-propanesulfonate and highly purified using a Sepharose CL-4B chromatography and agarose gel electrophoresis (Kwanyuen and Wilson, 1986). A follow-up study, however showed that the enzyme preparation was contaminated with oil body proteins (Wilson *et al*., 1993). DGAT activity from microspore-derived culture of *B. napus* was also solubilized using octanoyl-N-methylglucamide with 2M NaCl and analyzed using Sepharose 6 chromatography. The void volume, however, exhibited the highest DGAT activity indicating that the enzyme formed aggregates during chromatography (Little *et al*., 1994). The early purification studies of Kwanuen and Wilson (1986) and Little et al.

(1994), however, were conducted before it was discovered that there was more than one form of DGAT. Thus, the possible relative contributions of DGAT1 and DGAT2 to these earlier enzyme preparations is uncertain. Recently, tung tree DGAT1 was expressed in *E. coli*, solubilized with SDS and triton X-100 and purified with Ni-NTA affinity chromatography. The partially purified DGAT1, however, was reported to be degraded and inactive (Cao *et al*., 2011).

Without a purified protein, structure-function studies on DGAT1 were mainly accomplished through the following: a) bioinformatics analysis of published sequences, b) mutational analysis of potentially important residues or domains, c) heterologous expression and analysis of the enzyme in the microsomes and d) analysis of purified recombinant DGAT1 N-terminal domain. *In silico* topology analysis of DGAT1 sequences showed that the enzyme contains 8 to 10 transmembrane segments (Liu *et al*., 2012). In contrast, experimental analysis of murine DGAT1 using protease protection assays and indirect fluorescence showed that the enzyme only has three transmembrane regions (McFie *et al*., 2010). Furthermore, the study showed that murine DGAT1 has a cytosolic N-terminal domain while the remainder of the enzyme is embedded in the membrane. The remainder of the enzyme accounts for more than 50% of the enzyme and contains the conserved histidine implicated as one of the active site residues. Tung tree DGAT1, on the other hand, was reported to have two cytosolic termini, although the detailed topology was not reported (Shockey *et al*., 2006). Another study showed that human DGAT1 has dual topologies based on the presence of DGAT1 activity on both the cytosolic and luminal sides of the ER (Wurie *et al*., 2011). The oligomerization state of DGAT1 was also previously investigated through crosslinking studies. It was found

that the N-terminal domain of DGAT1 from mammalian or plant sources can associate to form dimers and tetramers (Weselake *et al*., 2006; McFie *et al.*, 2010). This domain also has the ability to bind acyl-CoAs (Weselake *et al*., 2006 and Siloto *et al*., 2008). The substrate binding sites of bovine (*Bos taurus*) DGAT1 were investigated using synchrotron circular dichroism analysis of peptide fragments corresponding to putative binding sites (Lopes et al., 2015). One peptide having the motif, FYxDWWN , which is also present in ACAT1, was found to interact with the acyl chain of acyl-CoA. On the other hand, the other peptide having a candidate DAG binding site (HKWCIRHFYKP), which is also present in protein kinase C and diacylglycerol kinase, interacts with DAG.

DGAT1 appears to be more promiscuous than DGAT2 in terms of substrate specificity. Murine DGAT2 only uses DAG as acyl acceptor (Yen et al., 2008). Murine DGAT1, on the other hand, can use different acyl acceptors including monoacylglycerol, long-chain alcohol and retinol in addition to DAG (Yen et al., 2005). As for the acyl donor, DGAT2 was initially found to be more specific for unusual acyl chains such as observed in *R. communis* DGAT2 and *Vernonia galamensis* DGAT2, which exhibit preference for ricinoleoyl-CoA and vernoleoyl-CoA, respectively (Kroon et al., 2006; Li et al., 2010a). Similar observations were found in fungal DGAT2s from *U. ramanniana* and *Claviceps purpurea*, which exhibit preference for medium chain acyl-CoA and ricinoleoyl-CoA, respectively (Lardizabal et al., 2001; Mavraganis et al. 2010). Recent studies, however, have identified DGAT1s in *E. guineensis* (Ayme et al., 2015) and *Cuphea avigera* var. *pulcherrima* (Iskandarov et al., 2017) with preference for medium-chain acyl-CoAs. It may thus be possible that acyl donor specificity for unusual fatty

acids cannot be directly attributed to neither DGAT1 nor DGAT2, but may differ on a case to case bases depending on the species.

The activity of microsomal DGATs, which likely contain both DGAT1 and DGAT2, was shown to be responsive to various ions, compounds and proteins. DGAT ion activators include Mg^{2+} and Mn^{2+} (Byers et al., 1999; Martin and Wilson, 1983), whereas ions that have a negative effect on DGAT activity include Zn^{2+}, Ca^{2+} and Hg^{2+} (Hobbs et al., 2000; Ichihara and Noda, 1982). Kennedy pathway intermediates such as G3P and PA were also found to activate DGAT activity, although it was hypothesized that addition of these metabolites may increase the available substrates for TAG formation leading to increased DGAT activity (Taylor et al., 1991; Byers et al., 1998; Byers et al., 1999). The same effect was exerted ATP on microsomal DGAT activity (Byers et al., 1999). Various proteins have also been found to activate DGAT activity including bovine serum albumin, acyl-CoA binding protein and an acylation-stimulating protein (Hobbs et al., 2000; Little et al., 1994; Yurchenko and Weselake, 2009; Weselake et al., 2000). Acyl-CoA binding protein may activate the enzyme by interacting with acyl-CoA, thereby preventing micelle formation and increasing the availability of substrate for DGAT enzymes (Yurchenko et al., 2009) and this may also be the reason for the positive effect of bovine serum albumin and acylating-stimulating protein on DGAT activity. Niacin was found to inhibit microsomal DGAT activity in Arabidopsis (Hobbs and Hills, 2000) and later studies showed that this cofactor is a non-competitive inhibitor of murine DGAT2 (Ganji et al., 2004).

As for possible regulatory mechanisms, murine DGAT1 has several predicted phosphorylation sites for protein kinase A, protein kinase C and tyrosine kinase (Yen et

al., 2008). Earlier studies suggested that DGAT activity in liver can be regulated by phosphorylation in response to glucagon (Haagsman et al., 1981). Other studies, however, showed that some of the putative phosphorylation sites did not seem to influence DGAT1 activity (Han, 2011; Humphrey et al., 2013). More recently, a study used previous findings coupled with bioinformatics analysis to identify 24 putative phosphorylation sites within the murine polypeptide, several of which were confirmed through mass spectrometry (Yu et al., 2015). The study further showed that the mutation of three putative serine phosphorylation sites at the N-terminus (S83, S86 and S89) to glutamate residues, which mimic phosphorylation, led to enzyme variants with higher activities. As for plant DGAT1, a study on *Tropaeolum majus* DGAT1 identified a putative SnRK1 phosphorylation site (Xu et al., 2008). Mutation of this residue resulted to an enzyme variant with increased activity. Overexpression of the mutated *DGAT1* in Arabidopsis also resulted in higher seed oil content relative to overexpression of the cDNA encoding the wild-type enzyme. The increased activity of AMPK, the animal counterpart of SnRK1, was found to inhibit TAG biosynthesis (Yin et al., 2015). This increased AMPK activity was achieved by treatment with nesfatin-1, which reduced the expression of genes involved in lipogenesis including *DGAT1*. It remains to be explored whether AMPK also acts directly with DGAT1 since AMPK belongs to a family of kinases that can influence the enzymes both at the transcriptional and post-translational levels (Ghilleber et al., 2011). These lines of evidence showed that DGAT1 could be regulated by phosphorylation and dephosphorylation, although direct biochemical experiments to support these are still lacking.

2.6. Metabolic engineering strategies involving DGAT1

To meet the world's increasing demand for vegetable oil, there have been increasing efforts to boost oil production in seeds as well as vegetative tissues through biotechnological approaches (Durrett et al., 2008; Weselake et al., 2009). In line with this endeavor, various strategies and genes have been explored to increase the flow to substrates into TAG. Based on studies enhancing the oil content of vegetative tissues, Vanhercke et al. (2014) categorized the approaches for increasing TAG accumulation as 'push', 'pull' and 'protect'.

Push strategies involve increasing the rate of fatty acid biosynthesis. One example is the overexpression of ACCase in potato, which resulted in increased fatty acid biosynthesis and a 5-fold increase in TAG content (Klaus et al., 2004). Recently, down-regulation of a negative protein regulator of ACCase also resulted to increase oil level in Arabidopsis seeds (Salie et al., 2016). The overexpression of cDNAs encoding transcription factors such as LEAFY COTYLEDON1 , LEAFY COTYLEDON2 and WRINKLED1 increased the expression of genes involved in lipid biosynthesis, which also translated to enhanced seed oil accumulation (Mu et al., 2008, Stone et al., 2008; Cernac and Benning, 2004). Push strategies also involve the down-regulation of pathways that uses fatty acid precursors. One example is the inhibition of starch biosynthesis through RNAi targeting of gene encoding adenosine diphosphate-glucose pyrophosphorylase. Coupled with co-expression of *WRINKLED1*, the aforementioned push strategy resulted in vegetative tissue with increased TAG content (Sanjaya et al., 2011).

Pull strategies involve increasing the flow of acyl chains into TAG assembly, which can be accomplished by the overexpression of acyltransferase genes. DGAT1 is the most widely used molecular tool for increasing the rate of TAG assembly. In addition to DGAT1, other acyltransferases such as LPAAT and monoacylglycerol acyltransferase have been used to pull acyl chains towards TAG accumulation (Maisonneuve et al., 2010; Petrie et al., 2012; El Tahchy et al., 2015).

Protect strategies are aimed at increasing the stability of oil bodies against degradation; these include the over-production of oleosins and down-regulation of TAG lipase. As indicated in section 2.2.9, oleosins are proteins embedded into oil bodies which prevent them from coalescing. The introduction of modified oleosins into Arabidopsis led to increased TAG content in leaves (Winichayakul et al., 2013). In addition, the down-regulation of a TAG lipase also led to higher oil levels in Arabidopsis vegetative tissue (Kelly et al., 2013).

DGAT1 has been a target for manipulation in lipid biotechnology to modify oil deposition in a variety of organisms considering that a number of studies have shown that the level of oil accumulation is correlated with the activity and expression level of this enzyme. Jako et al. (2001) first demonstrated that overexpression of a native *DGAT1* cDNA in Arabidopsis can increase seed oil content, while an Arabidopsis mutant having inactivated *DGAT1* exhibited low TAG levels (Katavic et al., 1995). In addition, previous metabolic control analysis showed that DGAT1 plays an important role in affecting the control of carbon flux towards oil formation in *B. napus* developing zygotic embryos (Weselake et al., 2008). Overexpression of Arabidopsis or *B. napus DGAT1* cDNAs in canola-type *B. napus* lines led to higher seed oil content when the transgenic

plant was grown under either greenhouse or field conditions (Weselake et al., 2008; Taylor et al., 2009). To date, numerous metabolic engineering approaches have used *DGAT1* cDNAs alone or in combination with other cDNAs to boost oil content in higher plants and other organisms. Most of these genetic interventions are summarized in Table 2.1.

Protein engineering of DGAT1 for increasing seed oil content has also been pursued. Protein engineering involves the introduction of amino acid residue substitutions in the enzyme and selection of more active variants. A number of desired enzymatic properties have been realized through directed evolution including higher catalytic efficiency, improved thermal stability, modified substrate specificity and even novel functionalities (Tao and Cornish, 2002). Random modifications of amino acid sequences can now easily be obtained using several available methods. The bottleneck in directed evolution is the screening and selection of variants that demonstrate the desired characteristics.

Previous researchers in our lab developed a high-throughput system for screening BnaDGAT1 with higher catalytic efficiency (Siloto *et al.*, 2009a). Using this platform, several improved BnaDGAT1 variants have already been identified (Chen et al., 2017). The combination of previously identified beneficial mutations may result in synergies that further increase seed oil content. Previously, mutation of a putative SnRK1 phosphorylation site in *T. majus* DGAT1 led to an enzyme form with higher activity, which was able to drive seed oil accumulation to higher levels than the wild-type enzyme (Xu et al., 2008). In addition, Zheng et al. (2008) have described a variant of *Z. mays* DGAT1-2 with a phenylalanine residue insertion at position 469 resulting in a

variant with increased DGAT activity and specificity for oleoyl moieties. The addition of an N-terminal tag in BnaDGAT1 also increased its activity in yeast through increased polypeptide accumulation (Greer et al., 2015). Previous mutation of putative serine residues to glutamate residues (mimics the negatively charged phosphate groups) in murine DGAT1 N-terminal region also resulted to enzyme variants with increased activity (Yu et al., 2015). More recently, a yeast-based high-throughput platform was able to identify a multi-site *G. max* DGAT1 mutant with 14 substitutions and the expression of the mutant was able to increase the TAG content in soybean seeds to higher levels compared to wild-type enzyme (Roesler et al., 2016). Numerous lines of experimental evidences have corroborated the effectiveness of DGAT1 as a molecular tool for boosting oil accumulation in various organisms. Future work on the structure and function of this enzyme may enable the exploitation of the full potential of DGAT1 in metabolic engineering strategies to increase the TAG content of various organisms.

Table 2.1. Metabolic engineering approaches implementing DGAT1 to increase/modify triacylglycerol (TAG) content in higher plants and other organisms.

Host species	Source of cDNA encoding DGAT1	Other interventions combined with DGAT1	Phenotype	Reference
Arabidopsis thaliana	Arabidopsis	-	Increased seed TAG content and seed weight	Jako et al. (1998)
Nicotiana tabacum, Saccharomyces cerevisiae	Arabidopsis	-	Increased seed TAG content and seed weight; increased TAG content in yeast	Bouvier-Nave et al. (2000)
Brassica napus	*B. napus,* Arabidopsis	-	Increased seed TAG content	Weselake et al. (2008) Taylor et al. (2009)
Arabidopsis, *B. napus*	*Tropaeolum majus*	mutated SnRK1 site (Ser to Ala)	Increased seed TAG content	Xu et al. (2008)
N. tabacum	Arabidopsis	-	Increased leaf TAG content	Andrianov et al. (2010)
Glycine max	*Vernonia galamensis*	DGAT1 DGAT2, Epoxygenase	Increased epoxy FA	Li et al. (2012)
Nicotiana benthamiana	Arabidopsis	MGAT2	Increased leaf TAG content	Petrie et al. (2012)
Arabidopsis, *S. cerevisiae*	Arabidopsis	cysteine-oleosin)	Increased leaf and root TAG content; increased yeast TAG content	Winichayakul et al. (2013)
N. tabacum	Arabidopsis	-	Increased leaf TAG content	Wu et al. (2013)
Arabidopsis sdp1 (lipase) mutant	Arabidopsis	WRI	Increased root, stem and leaf TAG content	Kelly et al. (2013)
N. benthamiana	Arabidopsis	WRI	Increased leaf TAG content	Vanhercke et al. (2013)
N. tabacum	Arabidopsis	WRI, oleosin	Increased leaf TAG content	Vanhercke et al. (2014)

Table 2.1. continued…

Yarrowia lipolytica	*Elaeis guineensis*	-	Increased content of medium-chain fatty acids in TAG	Aymé et al. (2015)
B. juncea	Arabidopsis	-	Increased seed TAG content and seed weight	Savadi et al. (2015)
N. benthamiana	Arabidopsis	Medium-chain FAT, CnLPAAT, WRI	Increased medium-chain fatty acid content and increased leaf TAG content	Reynolds et al. (2015)
Zea mays	*Z. mays*	-	Increased seed TAG content	Lan et al. (2015)
S. cerevisiae	*B. napus*	N-terminally modified DGAT1	Increased yeast TAG content	Greer et al. (2015)
Saccharum spp. hybrids	*Z. mays*	WRI, oleosin, ADP-glucose pyrophosphorylase (-)*, peroxisomal ABC transporter1 (-)	Increased leaf and stem TAG content	Zale et al. (2016)
G. max, S. cerevisiae	*Corylus americana, G. max*	Engineered DGAT1 variants	Higher seed TAG content; higher yeast TAG content	Roesler et al. (2016)
B. napus	*Sapium sebiferum*	-	Increased seed TAG content and lower oleic acid/higher linoleic acid	Peng et al. (2016)
C. sativa	*C. sativa*	-	Increased seed TAG content	Kim et al. (2016)
Jatropha curcas	Arabidopsis	-	Increased seed and leaf TAG content	Maravi et al. (2016)
N. benthamiana	*E. guineensis*	Thioesterase, CnGPAT9, CnLPAAT	Increased medium chain fatty acids in leaf TAG and increased leaf TAG content	Reynolds et al. (2017)
Z. mays	Arabidopsis	WR1, oleosin	Increased seed TAG content	Alameldin et al. (2017)
N. benthamiana	Arabidopsis	WRI, oleosin, FATA1, FATA2 and FATB	Increased leaf TAG content	El Tahchy et al. (2017)

Table 2.1. continued…

Solanum tuberosum L	Arabidopsis	WR1, oleosin	Increased tuber TAG content	Liu et al. (2017)
Tetraselmis chui	*Echium plantagineum*	-	Increased microalgal TAG content	Úbeda-Mínguez et al. (2017)
C. sativa	*Cuphea sp.*	CvFatB1, CvLPAAT	Increased capric acid (10:0) at *sn*-2 position of TAG	Iskandarov et al. (2017)
Chlorella ellipsoidea	Arabidopsis, *B. napus, S. cerevisiae*	-	Increased seed TAG content, increased seed weight and increased yeast TAG content	Guo et al. (2017)
S. cerevisiae N. benthamiana	*B. napus*	Single-site variants	Increased yeast TAG content and increased leaf TAG content	Chen et al. (2017)

*The (-) symbol denotes downregulation of expression.
Abbreviations: FA, fatty acid; FAT, fatty acyl-ACP thioesterase; MGAT, monoacylglycerol acyltransferase; CnLPAAT, *Cocos nucifera* lysophosphatidate acyltransferase; CnGPAT9, *Cocos nucifera sn*-glycerol-3-phosphate acyltransferase; Cv, *Cuphea viscosissima*; RNAi, RNA interference; WRI, WRI

CHAPTER 3

Purification and Properties of Recombinant *Brassica napus* Diacylglycerol Acyltransferase 1

3.1. Introduction

Diacylglycerol acyltransferases (DGATs) catalyze the acyl-Coenzyme A (CoA)-dependent acylation of 1,2-diacyl-*sn*-glycerol (DAG) to produce triacylglycerol (TAG) and CoA (Liu et al., 2012). Two non-homologous endoplasmic reticulum (ER)-bound DGAT families, with gene orthologs in a wide range of organisms, have been identified, namely DGAT1 and DGAT2 (Liu et al., 2012). An ER-bound bifunctional wax ester synthase/DGAT has also been reported in Arabidopsis and it appears to mainly function in wax ester biosynthesis in the stem epidermis (Li et al., 2008). This enzyme is related to the bifunctional wax ester synthase/DGAT previously identified in *Acinetobacter calcoaceticus* (Kalscheuer et al., 2003). Soluble DGATs have also been identified and characterized in the oleaginous yeast, *Rhodotorula glutinis* (Gangar et al., 2001), peanut (*A. hypogaea*) (Saha et al., 2006; Chi et al., 2014) and Arabidopsis (Rani et al., 2010). From a biotechnological perspective, *DGAT1* or *DGAT2* has been over-expressed in oleaginous plants (Jako et al., 2001; Lardizabal et al., 2008; Weselake et al., 2008; Weselake et al., 2009) and microorganisms (Chen and Smith, 2012; Liang and Jiang, 2013) including yeast and microalgae, as means of increasing TAG content. In contrast, drugs have been under development for the purpose of inhibiting DGAT activity in humans to combat obesity and related metabolic disorders (Liu et al., 2012).

The first *DGAT1* gene was identified over 15 years ago (Cases et al., 1998) and homologous genes have been identified in more than 50 organisms. Despite the

importance of DGAT1 in plant, microbial and algal biotechnology, and medicine, there are no reports on the purification of an active DGAT1 to apparent homogeneity from any species. As for many other membrane-bound enzymes, DGAT1 has been recalcitrant to effective purification, presumably due to its hydrophobic properties and low abundance in tissues (Liu et al., 2012). Microsomal DGAT activity from germinating soybean (*Glycine max)* was previously solubilized with 3-[(3-cholamidopropyl)dimethylammonio]-1-propanesulfonate (CHAPS), followed by gel filtration but only produced a partially purified enzyme preparation containing oleosin (Kwanyuen and Wilson, 1986; Kwanyuen and Wilson, 1990). In addition, DGAT from microspore-derived cultures of *Brassica napus* L. cv Jet Neuf was solubilized using octanoyl-*N*-methylglucamide (MEGA-8) in the presence of 2M NaCl and partially purified using gel-filtration chromatography with Sepharose CL-4B as the sieving matrix (Little et al., 1994). The void volume, however, exhibited the highest DGAT activity indicating the enzyme aggregated during chromatography. One of four forms of *B. napus* DGAT1 (Greer et al., 2014), known as BnaA.DGAT1.b (Genbank ID: JN224475), was first cloned by Nykiforuk et al. (1999) and the recombinant enzyme produced in *Pichia pastoris* was partially characterized (Nykiforuk et al., 2002). Recently, recombinant tung tree (*Vernicia fordii*) DGAT1 was produced in *Escherichia coli*, solubilized with SDS and Triton X-100, and subjected to immobilized nickel ion affinity chromatography (Cao et al., 2011). The partially purified DGAT1, however, was reported to be degraded and inactive.

In the current study, recombinant BnaDGAT1 produced in *Saccharomyces cerevisiae,* was solubilized with 1 % n-dodecyl-β-D-maltopyranoside (DDM).

Solubilized BnaDGAT1 was then highly purified in active form for the first time using immobilized cobalt ion affinity chromatography followed by gel filtration chromatography. BnaDGAT1 self-associated to form dimers and tetramers, and the purified enzyme effectively utilized a range of acyl-CoAs as fatty acyl donors.

3.2. Materials and methods

3.2.1. Construct preparation, expression in yeast and microsome isolation

BnaDGAT1 was cloned into pYES2.1/V5-His TOPO yeast expression vector (Invitrogen), which was subsequently modified using PCR, restriction enzyme digestion and ligation to introduce a tobacco etch virus (TEV) cleavage site before the C-terminal tags and to replace the His6 tag with His10 tag. The primers used for construct modification are listed in Table 3.1. The construct was then used for the transformation of *S. cerevisiae* INVSc1 (Invitrogen) with an S.c. EasyComp^{TM} Transformation Kit (Invitrogen) according to the manufacturer's instruction. Transformed yeast was inoculated in 10 mL 2% (w/v) raffinose synthetic liquid media lacking uracil (0.67% (w/v) yeast nitrogen base and 0.2% (w/v) synthetic complete dropout mix (SC synthetic minimal media)) and grown for 24 h at 30°C with shaking at 220 rpm and transferred into 250 mL of the same media for another 24 h. The yeast cells were then used to inoculate synthetic media containing 2% (w/v) galactose and 1% (w/v) raffinose at a starting OD value of 0.40. Once the OD value reached 8, the cells were harvested through centrifugation at 6000 x g for 10 min. The cell pellets were resuspended in Buffer A (50 mM Tris-HCl buffer at pH 8.0 containing 300 mM NaCl, 10% (v/v)

glycerol, 10 mM imidazole, 2 µg/mL pepstatin, 2 µg/mL leupeptin and 2 mM phenylmethylsulfonyl fluoride) and lysed by 2 passes at 35 kpsi through Benchtop homogenizer (Constant Systems). The lysate was spun at 10,000 x g for 20 min and the supernatant was subjected to ultracentrifugation at 105,000 x g for 1 h to recover the microsomal fraction. All centrifugation steps were carried out at 4 °C. Protein content was determined using Bradford protein assay (Bio-Rad) with BSA as a standard for most protein samples (Bradford et al., 1976). For samples containing 1% detergent, Pierce™ BCA Protein Assay Kit was used due to detergent interference with the Bradford protein assay.

3.2.2. Solubilization of DGAT1

CHAPS, n-lauroylsarcosine, Triton X-100 and Tween-20 were purchased from Sigma. DDM, n-dodecylphosphocholine (DPC), octyl-β-D-glucopyranoside and hexaethyleneglycol monooctyl ether were obtained from Anatrace. MEGA-8 was obtained from Soltec Ventures. BnaDGAT1 in yeast microsomes was solubilized using 1% (w/v) of the above-mentioned detergents in Buffer A at a detergent to protein ratio of 4:1. The mixture was then subjected to ultracentrifugation at 105,000 x g for 1 h. The solubilized fractions were incubated with 5X SDS loading buffer at 50°C for 5 min and resolved using SDS-PAGE followed by blotting onto polyvinylidene fluoride membrane. The recombinant enzyme was detected using anti-V5-HRP antibody (Invitrogen) coupled with ECL Advance Western Blotting Detection Kit (Amersham) using a variable mode imager (Typhoon Trio+, GE Healthcare). The BnaDGAT1 bands were semi-quantified using ImageJ software (Schneider et al., 2012).

Table 3.1. Primers used for cloning *BnaDGAT1* into pYES2.1/V5-His TOPO yeast expression vector (Invitrogen) and subsequent construct modification to introduce a TEV site before the V5 epitope and replace His6 tag with His10 tag.

Primer name	Sequence
BnaDGAT5endF	ATGGAGATTTTGGATTCTGGAG
BnaDGAT3endR	TGACATCTTTCCTTTGCGGT
BnaDGATIntSacIF	CTCTAGAGCTCCTCTGCTTCGG
pYES2.1H10XbaIR	AGAGTCTAGAAACTCAATGATGATGATGATGGTGATGGTGATGATGACC
pYES2.1TEVBstXIR	AGAGTGGGTGACCACCTTGAAAATACAAATTCTCGCCCTTTGACATCTTTC

3.2.3. Purification of DGAT1

Detergent-solubilized BnaDGAT1 was incubated with 3 mL TALON® Metal Affinity Resin (Clontech) for 2 h with rocking at room temperature. After packing the resin into Econo-Column® Chromatography Columns, 1.5 x 20 cm (Bio-Rad), it was washed twice with 20 column volumes of wash buffers (Buffer A and Buffer A with additional 5 mM imidazole) and BnaDGAT1 was then eluted in Buffer A, stepwise, with increasing concentrations of imidazole (50 to 500 mM). SDS-PAGE analysis was conducted to analyze purified fractions. The identity of the band corresponding to BnaDGAT1 was determined through in-gel tryptic digestion coupled with liquid chromatography-tandem mass spectrometry (Institute of Biomolecular Design, University of Alberta). The tag was removed through digestion with TEV protease (Sigma) at an optimized protein-TEV ratio of 0.1 mg of TEV per mg of BnaDGAT1. Finally, BnaDGAT1 was concentrated using Amicon Ultra-4 centrifugal filter units 50,000 NMWL (EMD Millipore) and loaded onto an FPLC-Superdex 200 13/30 (GE Healthcare Life Sciences) size-exclusion column pre-equilibrated with three column volumes of size-exclusion buffer (25 mM Tris-HCl at pH 8 containing 150 mM NaCl, 5% (v/v) glycerol, 1 mM EDTA and 0.05% DDM). Size-exclusion standards (Bio-Rad) were used to calibrate the column for the purpose of estimating the apparent molecular mass of the peaks. Protein samples at different stages of purification were analyzed using SDS-PAGE and stained with GelCode® Blue Stain Reagent (Thermo Scientific).

3.2.4. DGAT1 activity assays

Protein samples at different stages of purification were assayed for DGAT activity in a similar fashion to what was described previously (Byers et al., 1999). Enzyme

assays were performed at 30°C for 4 min in a 60-µL reaction mixture containing 333 µM *sn*-1,2-diolein (pre-dispersed in 0.2% Tween 20), 15 µM [^{14}C] oleoyl-CoA, 20 mM HEPES-NaOH pH 7.4, 0.46 mM $MgCl_2$ and 0.33 to 10 µg of protein sample. The exact amount of enzyme used was pre-determined so as not to consume more than 10% of the provided substrates during the course of the reaction. The enzyme reaction was initiated by addition of the protein sample and quenched with 10 µL of 10% SDS. The resulting mixture was applied onto a preparative thin-layer chromatography (TLC) plate (0.25 mm Silica gel, DC-Fertigplatten) with a separate lane for [^{14}C]-triolein standard. The plate was developed with hexane: diethyl ether: acetic acid (80:20:1, v/v/v). The products were visualized by phosphorimaging (Typhoon Trio Variable Mode Imager, GE Healthcare, QC, Canada). Spots corresponding to TAG were scraped and analyzed for radioactivity by Beckman-Coulter LS6500. Under these conditions, no apparent radiolabeled TAG was produced due to the action of endogenous DGAT activity. For the substrate specificity assay, [^{14}C] palmitic acid (16:0), [^{14}C] stearic acid (18:0), [^{14}C] oleic acid (18:1Δ^{cis9}), [^{14}C] linoleic acid (18:2$\Delta^{cis9,12}$) and [^{14}C] α-linolenic acid (18:3$\Delta^{cis9,12,15}$) were purchased from Perkin Elmer while CoA was obtained from Invitrogen. Thioesters of the abovementioned fatty acids were synthesized as described previously using a bacterial acyl-CoA synthetase (Invitrogen) (Taylor et al., 1990). Fifteen micromolar of the following [^{14}C] acyl-CoAs were used in the experiment: palmitoyl-CoA (60 Ci/mol), stearoyl-CoA (58.9 Ci/mol), oleoyl-CoA (56.3 Ci/mol), linoleoyl-CoA (58.2 Ci/mol) and α-linolenoyl-CoA (51.7 Ci/mol).

3.3. Results and Discussion

3.3.1. Production and solubilization of recombinant BnaDGAT1

Although DGAT1 has already been studied for many years and has been produced in different expression systems, the mechanisms of action and regulation of this enzyme remain unknown. Detailed structure-function analysis requires purified proteins and previous purification studies on DGAT1 had met with limited success. *In silico* topology analysis of DGAT1 sequences showed that the enzyme appears to contain 8 to 10 transmembrane segments (Liu et al., 2012) while experimental analysis of murine DGAT1 using protease protection assays and indirect fluorescence showed that the enzyme has three transmembrane regions (McFie et al., 2010). The presence of transmembrane domains poses a challenge to DGAT1 purification since the enzyme must be first solubilized with detergents that maintain enzyme activity.

In the current study, *BnaDGAT1* (isoform BnaC.DGAT1.a) was expressed in *S. cerevisiae* using a modified pYES2.1 vector to produce a microsomal fusion protein having a C-terminal V5 epitope-His10 tag linked by a TEV cleavage site. Nine detergents were then tested for their ability to solubilize the microsomal enzyme (Fig. 3.1). The expressed protein was detected through Western blotting using antibodies against the V5 epitope. BnaDGAT1 was maximally solubilized with n-laurylsarcosine, Triton X-100, DDM and DPC, all of which solubilized more than 80% of the total enzyme polypeptide. The remaining detergents evaluated solubilized less than 50% of the microsomal enzyme. No apparent formation of SDS-resistant multimer of BnaDGAT1 was detected following analysis of the solubilized fractions. In addition, less than 10% of total enzyme activity could be recovered using n-laurylsarcosine, Triton X-

100, DDM or DPC. Purification of DGAT1 was then pursued using DPC and DDM due to their non-denaturing properties and compatibility for structural studies.

3.3.2. Purification and molecular mass analysis of BnaDGAT1

Initial attempts at purification showed that BnaDGAT1 was less prone to aggregation and inactivation when solubilized in DDM than in DPC. Therefore, large-scale purification studies used DDM for solubilization of the enzyme. Preliminary optimization of DDM concentration showed that higher total enzyme activity can be recovered using detergent concentration less than 0.5% (w/v) in the presence of 2M NaCl. The high concentration of NaCl, however, interfered with cobalt affinity chromatography. Higher yield could still be obtained after immobilized metal ion affinity chromatography when the recombinant enzyme was initially solubilized with 1% (w/v) DDM in the presence of 0.3M NaCl (as in Fig. 3.1, lane 7). Although known to be a mild detergent, DGAT activity dropped by 16-fold following solubilization with 1% (w/v) DDM (Table 3.2). The reduced enzyme activity may be attributable to the high aggregation number of DDM and the low stability of the active DGAT1 conformation in detergent micelles. DDM molecules may have prevented the entry of hydrophobic substrates into the active site of the BnaDGAT1. It can be noted, however, that the specific activity of BnaDGAT1 increased as purification progressed.

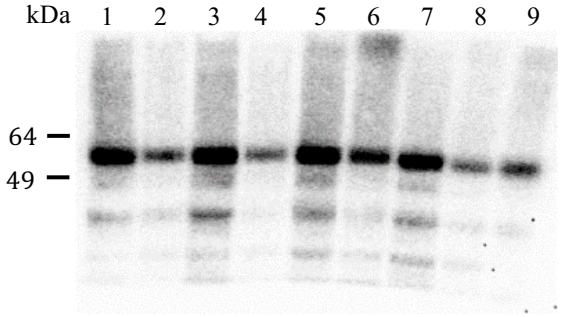

Figure 3.1. Western blot profile of solubilized BnaDGAT1 using different detergents. Microsomal proteins (250 µg) were solubilized in 100 µL buffer with different detergents for 2 h at 4°C, at a detergent concentration of 1% (w/v) and detergent to protein ration of 4:1. Solubilized enzyme recovered in supernatants obtained following centrifugation at 105,000 x g for 1h were resolved by SDS-PAGE, blotted onto polyvinylidene fluoride membrane and detected using anti-V5-HRP antibody coupled with enhanced chemiluminescence detection system. Ten µL of supernatant were applied per lane of the SDS gel. Detergents used: 1) n-lauroylsarcosine; 2) 3-[(3-cholamidopropyl)dimethylammonio]-1-propanesulfonate; 3) n-dodecylphosphochline; 4) Tween-20; 5) Triton X-100; 6) hexaethyleneglycol monooctyl ether; 7) n-dodecyl-β-D-maltopyranoside; 8) octyl-β-D-glucoside; 9) octanoyl-N-methylglucamide.

DDM-solubilized BnaDGAT1 was first partially purified using immobilized cobalt ion affinity chromatography. A His10 tag at the C-terminal was found to be effective for immobilized metal ion affinity chromatography after finding that the His6 tag was not effective in binding the recombinant enzyme efficiently in the presence of detergent. The eluted fractions were analyzed using SDS-PAGE and BnaDGAT1 was effectively eluted from the resin, stepwise, over a range of 150 to 300 mM imidazole (Fig. 3.2). The band corresponding to BnaDGAT1 had an apparent molecular mass of 58 kDa, which is slightly smaller than the theoretical mass of 64 kDa. This phenomenon has also been observed for other membrane proteins (Cortes and Perozo, 1997). In gel digestion coupled with LC MS/MS analysis verified the identity of the target polypeptide as BnaDGAT1 with the unique fragments identified in Table 3.3. The expression yield post-purification with cobalt ion affinity resin was 0.75 mg per liter of yeast culture.

The partially purified enzyme was subjected to TEV protease digestion to remove the purification tag. The enzyme solution was then concentrated and subjected to size-exclusion chromatography (SEC) to further purify the enzyme (Fig. 3.3A). Analysis of SEC fractions by SDS-PAGE indicated that BnaDGAT1 could be resolved into different oligomerization states (Fig. 3.3A and 3B). BnaDGAT1 polypeptide was present in the void volume and in two additional peaks that were resolved within the sieving range of the column. Regression analysis using a standard curve revealed that the major peak containing BnaDGAT1 exhibited an apparent

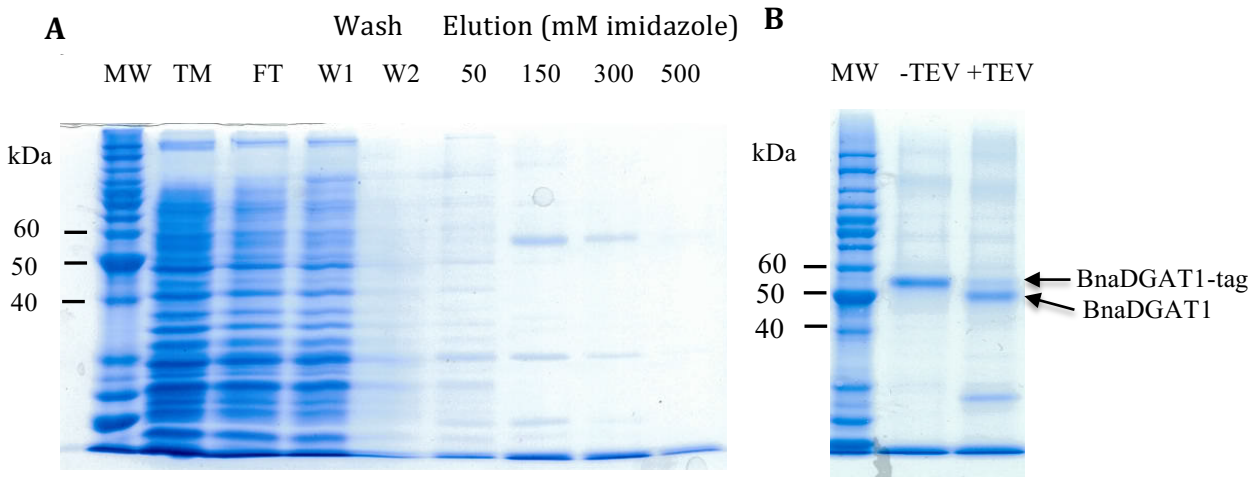

Figure 3.2. Partial purification of BnaDGAT1. by immobilized cobalt ion affinity chromatography followed by removal of the C-terminal tag. A, SDS-PAGE of column fractions. TM, total microsomal proteins; FT, flow-through. Ten µL of TM, FT and Wash1 and Wash 2 were loaded while 20 µL of eluents were used. B, SDS-PAGE of pooled fractions (elution with 150 mM and 300 mM imidazole) before and after treatment with tobacco etch virus (TEV). Twenty µL of sample were loaded per lane.

molecular mass of 214 kDa. If one DDM micelle with roughly a molecular mass of 45 kDa is associated with one BnaDGAT1 (with a molecular mass of 58.5 kDa after TEV cleavage), one BnaDGAT1-DDM micelle has a total molecular mass of about 103.5 kDa (Sampathkumar et al., 2012). It can then be inferred that the major peak is composed of a dimeric enzyme. Another peak containing BnaDGAT1, was eluted earlier and is roughly one-third the height of the major peak. This peak has an apparent molecular mass of 414 kDa, which is almost twice the size as the major peak, suggesting that the enzyme can also form tetramers. The current observations on self-association of BnaDGAT1 are consistent with previous crosslinking studies with a recombinant hydrophilic N-terminal fragment of BnaA.DGAT1.b and murine DGAT1, which were shown to form dimers and tetramers via the N-terminal region (McFie et al., 2010; Weselake et al., 2006). In addition, McFie and colleagues (2010) showed that murine DGAT1 lacking residues 2-84 can still form dimers but not tetramers and this truncated form has ~14-fold increased activity over the full-length enzyme. The oligomerization of DGAT1 may be an important phenomenon related to the mode of enzyme regulation that will need further investigation. In the current study, the symmetry of the prominent second peak in the size-exclusion profile (Fig. 3.3A) suggested that this enzyme fraction was suitable for use in crystallization trials. The specific activity of BnaDGAT1 in peak II was 26.0 nmol TAG/min/mg protein (Table 3.2) using [^{14}C] oleoyl-CoA and *sn*-1,2-diolein as substrates. Overall, the enzyme was purified about 7.6-fold over the microsomal fraction and 126-fold over the solubilized fraction (Table 3.2). The purified enzyme could be stored at 4°C for a week without any significant loss in activity.

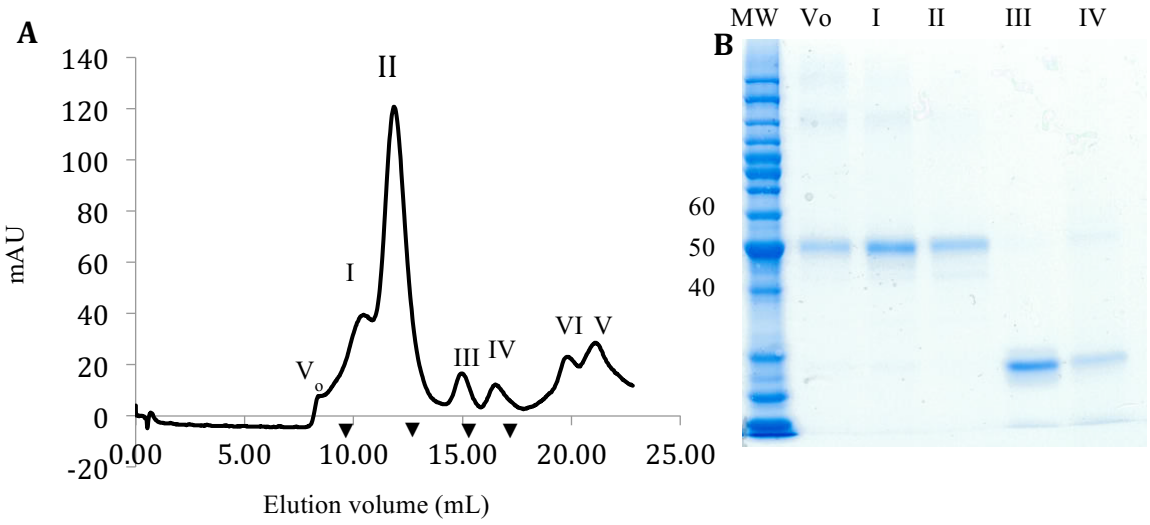

Figure 3.3. Purification of BnaDGAT1 by FPLC size-exclusion chromatography using a Superdex 200 10/30 column. A, Elution profile of proteins resolved by gel-filtration chromatography. The column calibration standards: bovine thyroglobulin (670 kDa, Stokes radius 86 Å), bovine γ-globulin (158 kDa, Stokes radius 51 Å), chicken ovalbumin (44 kDa, Stokes radius 28 Å), and horse myoglobin (17 kDa, Stokes radius 19 Å) were eluted at 9.73, 12.73, 15.26 and 17.06 mL (indicated by triangles), respectively. B, SDS-PAGE of fractions from size-exclusion chromatography. All peaks except peak II were concentrated five times prior to SDS-PAGE and 20 µL of each peak was loaded in the gel. This corresponds to 0.53, 2 and 1.28 µg protein for Vo, I and II, respectively.

Table 3.2. Purification of BnaDGAT1 from 3-L yeast culture.

Fractions	Volume (ml)	Total activity (nmol TAG/min)	Total protein (mg)	Recovery (%)	Specific activity (nmol TAG/ min/mg protein)	Purification fold
Microsome	60.0	787.46	231.24	100	3.41	1.0
Solubilized fraction	58.0	33.64	162.89	4.3 (100)[a]	0.21	0.06 (1.0)[a]
ICAC	4.0	45.97	2.26	5.8 (137)[a]	20.39	6.0 (98)[a]
Peak II of SEC	1.0	1.68	0.065	0.2 (5)[a]	26.00	7.6 (126)[a]

[a]Recovery (%) and purification fold relative to the solubilized fraction. ICAC, immobilized cobalt ion affinity chromatography; SEC, size-exclusion chromatography; TAG, triacylglycerol.

Table 3.3. Unique peptides identified for BnaDGAT1 derived from in gel trypsin digestion coupled with analysis by LC-MS/MS.

Sequences	
ANLAGENEIRESGGEAGGNVDVR	ANPEVSYYVSLK
SDSSnGLLPDSVTVSDADVR[a]	GDLLYGVER
VRESPLSSDAIFK	ANLAGENEIR
SDSSNGLLPDSVTVSDADVR	ESPLSSDAIFK
TLANSSDKANPEVSYYVSLK	

[a]n corresponds to deaminated asparagine

3.3.3. **Acyl-CoA substrate specificity of purified BnaDGAT1**

Acyl-CoA substrate specificity assays of purified BnaDGAT1, conducted using 15 μM acyl-CoA, indicated that the enzyme could effectively utilize a range of different substrates (Fig. 3.4), which represented the fatty acids typically found in the seed oil of *B. napus* DH12075 (Lock et al., 2009). BnaDGAT1 exhibited the highest activity with α-linolenoyl-CoA. Similar enzyme activities were obtained when oleoyl-CoA or palmitoyl-CoA were used as acyl donors, which were 85–86% of that obtained using α-linolenoyl-CoA. The enzyme exhibited the least preference for linoleoyl-CoA and stearoyl-CoA, which were 70 and 54% of the activity, respectively, with α-linolenoyl-CoA. These results are in general agreement with previous acyl-CoA specificity assays of a MEGA-8-solubilized DGAT activity from microsomes of microspore-derived embryos of *B. napus* L. cv Reston where the solubilized enzyme showed a greater preference for palmitoyl-CoA or oleoyl-CoA over stearoyl-CoA at substrate concentrations ranging from 5 to 20 μM (Little et al., 1994). The increased specificity for α-linolenoyl-CoA observed in the current study is interesting in the light of previous findings where antisense suppression of *BnaDGAT1* was shown to decrease the proportion of □-linolenic acid in the seed oil of transgenic *B. napus* DH12075 (Lock et al., 2009).

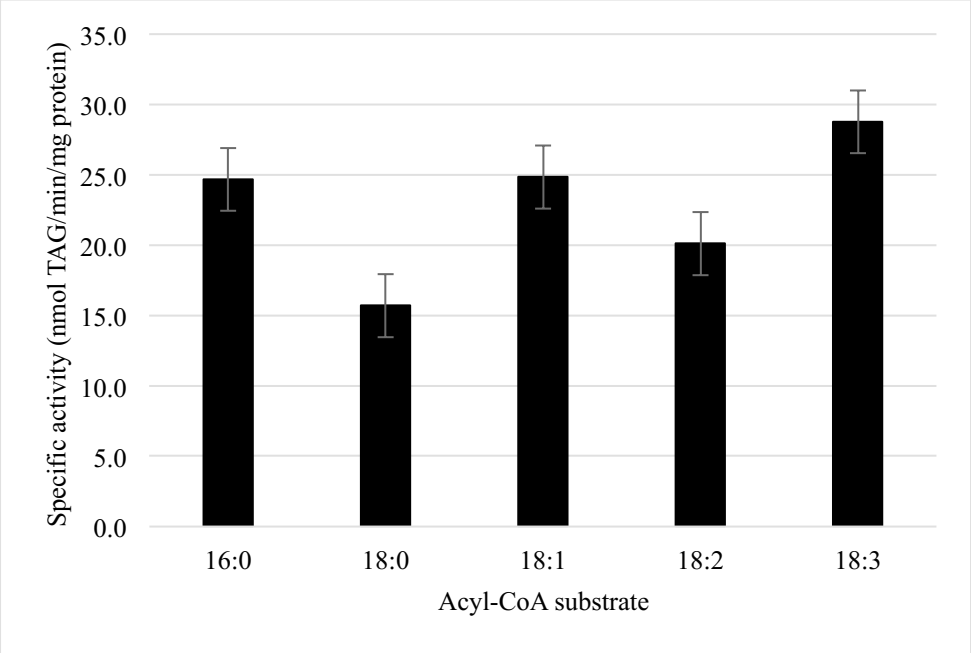

Figure 3.4. Acyl-CoA substrate specificity of purified BnaDGAT1 in n-dodecyl-β-D-maltopyranoside micelles. Three hundred-thirty nanograms of protein were used per reaction mixture with an acyl-CoA concentration of 15 μM. Enzyme reactions were allowed to proceed at 30°C for 4 min prior to quenching with SDS. All reactions were performed in triplicate and errors bars correspond to +/- standard deviation. Radiolabeled acyl-CoAs used: palmitoyl (16:0)-CoA; stearoyl (18:0)-CoA; oleoyl (18:1)-CoA; linoleoyl (18:2)-CoA; α-linolenoyl (18:3)-CoA.

3.4. Conclusions

In summary, this study reports the first successful purification of a DGAT1 in an active form. The selection of a suitable detergent was found to be crucial in purification along with the size of the poly-His tag used to facilitate immobilized cobalt ion affinity chromatography. Although solubilization with DDM reduced DGAT1 activity, the activity was recovered after column chromatography. The results of SEC confirmed previous findings that the enzyme can exist in different multimeric forms. Lastly, the substrate specificity study indicated that BnaDGAT1 could use a range of different acyl-CoAs, with the most effective substrate being □-linolenoyl-CoA. Overall, the successful purification of BnaDGAT1 in active form sets the foundation for the in-depth evaluation of structure-function in this biotechnologically important enzyme.

CHAPTER 4

Brassica napus Diacylglycerol Acyltransferase 1 is Regulated by Its Hydrophilic N-terminal Domain in Response to Allosteric Effectors

4.1. Introduction

Triacylglycerol (TAG) is the predominant component of the seed oil of oleaginous plants. Not only does TAG serve as an energy reserve to fuel germination and early seedling growth, but this highly reduced form of carbon is a nutritional source of dietary oil for humans and animals. Plant TAG can also serve as a feedstock for petrochemical alternatives such as biolubricants, biopolymers and biodiesel (Metzger and Bornsheuer, 2006). Diacylglycerol acyltransferases (DGATs) catalyze the acyl-coenzyme A (CoA)-dependent acylation of 1,2-diacyl-*sn*-glycerol (DAG) to generate TAG, and in some species such as *Brassica napus*, the level of enzyme activity appeared to have a substantial effect on the flow of carbon into TAG (Weselake et al., 2008; Liu et al., 2012). In developing seeds, two families of integral non-homologous membrane enzymes, DGAT1 and DGAT2, are known to contribute to catalyzing TAG formation. Because of the importance of the enzyme in carbon flow, over-expression of various plant *DGAT* cDNAs has been used to increase seed oil content in Arabidopsis (Jako et al., 2001) and oil crops such as canola-type *B. napus* (Weselake et al., 2008; Taylor et al., 2009) and soybean (*Glycine max*) (Lardizabal et al., 2008; Roesler et al., 2016). Increased DGAT production has also been used as a molecular strategy to boost the TAG content of algal species (Iwai et al., 2014). Mammalian DGAT1, on the other hand, is relevant in medicine, as it has been investigated as a drug target for a variety of lipid-related metabolic diseases including obesity and diabetes (Zammit et al., 2008; Birch et

al., 2010). Many DGAT1 inhibitors have already been designed, synthesized and tested (DeVita and Pinto, 2013). Bovine (*Bos taurus*) DGAT1 is also important in the cattle industry as it is used as a polymorphic genetic marker for the fat content of milk (Grisart et al., 2004; Winter et al., 2002). Despite the enzyme's key role in primary metabolism, and biotechnological and clinical relevance, little is known about the catalytic mechanism and regulation of DGAT1.

DGAT1 belongs to a family of enzymes named membrane-bound O-acyltransferases (MBOATs). Due to their hydrophobic nature, structural investigation to date of MBOATs has been limited to topological analysis. MBOAT members have highly conserved asparagine/aspartic acid and histidine residues that have been hypothesized to be involved in acyltransferase activity. There is little detailed structure-function information on any member of the MBOAT family and furthermore, no three-dimensional (3D) structure has been solved for any MBOAT. The DGAT1 family is highly conserved. DGAT1 possesses a very hydrophilic N-terminal region corresponding to about the first 100 residues, which is followed by 8-10 predicted transmembrane segments (Liu et al., 2012). The putative active site histidine residue of murine DGAT1 is predicted to be near the C-terminus of the enzyme (McFie et al., 2010). This study also demonstrated the importance of the N-terminal region in forming dimers and tetramers and hypothesized the role of this region in enzyme regulation. The active site region in bovine DGAT1 was characterized through secondary structure analysis and binding studies of short peptide fragments spanning the predicted substrate binding sites (Lopes et al., 2014). The N- and C-termini of tung tree (*Vernicia fordii*) DGAT1 were both localized in the cytosol and a C-terminal endoplasmic reticulum (ER)

retrieval motif was shown to target the plant enzyme to the ER (Shockey et al., 2006). Recently, four highly homologous isoforms of *B. napus* DGAT1, recombinantly produced in *Saccharomyces cerevisiae* H1246, were partially characterized (Aznar-Moreno et al., 2015; Greer et al., 2015; Greer et al., 2016) and recombinant isoform BnaDGAT1 was highly purified in active form (Caldo et al., 2015). A recombinant hydrophilic N-terminal fragment of isoform BnaA.DGAT1.b was previously shown to self-associate and interact with acyl-CoA through positive cooperativity based on the Lipidex-1000 assay (Weselake et al., 2006). The recombinant hydrophilic N-terminal fragment of murine DGAT1 was also shown to interact with acyl-CoA through positive cooperativity (Siloto et al., 2008). Recently, it was reported that *Coylus americana* DGAT1, several recombinant enzyme variants and *Zea mays* DGAT1 exhibited positive cooperativity through kinetic studies (Roesler et al., 2016). Thus, various lines of biochemical evidence suggest that DGAT1 enzymes may be regulated through allosteric interactions. The self-association properties of DGAT1 enzymes are consistent with the fact that most allosteric enzymes exhibit quaternary structure.

In the current study, the structure and function of the hydrophilic N-terminal domain of *B. napus* DGAT1 (BnaDGAT1/isoform BnaC.DGAT1.a) were examined. This domain was found to have an intrinsically disordered region (IDR) and a folded section. IDRs are recognized as important regions in proteins due to their role in cellular signaling and regulation (Wright and Dyson, 2015). The highly disordered segment was found to be involved in down-regulation of DGAT1 activity suggesting the presence of an autoinhibitory motif. BnaDGAT1 was also found to exhibit positive cooperativity, the extent of which diminished as more of N-terminus was removed. The involvement of the

N-terminal domain in self-association may therefore mediate positive cooperativity. The folded section, on the other hand, is important to maintain high acyl-CoA affinity at the active site and activity. In addition, CoA non-competitively inhibited BnaDGAT1, further confirming the presence of an allosteric site for CoA. The 3D nuclear magnetic resonance (NMR) solution structure of the folded segment containing the allosteric site was determined. The CoA/acyl-CoA binding site in the hydrophilic N-terminal domain and specific interactions involved in CoA recognition were also identified.

4.2. Materials and Methods

4.2.1. Production of recombinant full-length and truncated BnaDGAT1 in *S. cerevisiae* H1246 and *in vivo* assay for neutral lipid content

BnaDGAT.C.1a cDNA was codon-optimized and purchased from BioBasic (Ontario, Canada). The regions corresponding to amino acid residues 1-501 (full-length), 61-501, 81-501, and 114-501 were cloned into pYES2.1 vector (Invitrogen) and produced in *S. cerevisiae* H1246, which is devoid of TAG biosynthesis (Sandager et al., 2002). The clones were grown on solid synthetic media lacking uracil with 2% glucose ($^{w}/_{v}$). For recombinant protein production, a colony was picked and inoculated into a 3 mL synthetic media lacking uracil with 2% raffinose for overnight incubation at 30°C. The seed culture was transferred into 50 mL synthetic medium lacking uracil with 1% raffinose and 2% galactose, and grown again overnight at 30°C. The cultures were then analyzed after 24 h through the Nile red assay according to previously described methods (Siloto et al., 2009b). Briefly, 100 µL yeast culture was added with 5 µL of

0.1 mg/mL dye solution (Nile red dissolved in methanol). Fluorescence emission was measured before and after addition of dye solution, and the change in fluorescence unit over optical density (ΔF) was used as an indicator of neutral lipid content. Three technical replicates were performed for each BnaDGAT1 construct.

4.2.2. Yeast fatty acid analysis using Gas Chromatography-Mass Spectrometry

Fifty-mL cultures of induction media were harvested after 24 h, flash frozen, and freeze dried. Lipids were then extracted using the Folch method with minor modifications (Christie and Han, 2010). The lipid extracts were resolved on thin-layer chromatography (TLC) plates (silica G25) using 80:20:1 hexane/diethyl ether/acetic acid solvent system as mobile phase. The plates were sprayed with 0.5% primulin in 80:20 (v/v) acetone-water solution to visualize and identify the TAG spots under UV. The TAG isolates were derivatized by incubation in 2 mL methanolic-HCl for 1 h at 80°C. Reactions were quenched with addition of 2 mL saline, and methyl esters were isolated with two hexane extractions. Isolated fatty acid methyl esters were separated along a 30-m DB23 column (Agilent Technologies) using a 6896 N network GC system (Agilent Technologies), and quantified using a 5975 inert XL mass selection detector (Agilent Technologies). Triheptadecanoin and heneicosanoic methyl ester (Nu-Chek Prep.) were used as external and internal controls, respectively. Three biological replicates were analyzed for each construct.

4.2.3. Yeast microsome isolation, DGAT activity assay and Western blot analysis

Yeast cells grown using the above conditions were harvested at an OD of 6.0. The cell pellet was resuspended in lysis buffer (50 mM Tris–HCl buffer,pH 8.0, containing 300 mM NaCl, 10% (v/v) glycerol, 10 mM imidazole, 2 μg/mL pepstatin, 2 μg/mL leupeptin and 2 mM phenylmethylsulfonyl fluoride) and lysed through bead beating. The cell lysate was recovered after spinning at 10,000 x g for 30 min and then subjected to ultracentrifugation at 105,000 x g for 1 h. The 10,000-105,000 x g microsomal pellet was recovered, resuspended in lysis buffer, and stored at -80°C. The protein content of microsomes was determined using the Bradford assay using BSA as a standard (Bradford, 1976). For the DGAT assay, the reaction was performed at 30°C for 30 s to 1 min (10 min for BnaDGAT1$_{114\text{-}501}$) in a 60-μL reaction mixture containing 100 μM *sn*-1,2-diolein (pre-dispersed in 0.2% [v/v]) Tween 20), 0.1-15 μM [^{14}C] oleoyl-CoA (60 mCi/mmol) or [^{14}C] palmitoyl-CoA (60 mCi/mmol), 200 mM HEPES-NaOH pH 7.4, 4.6 mM $MgCl_2$ and 1–10 μg protein. The amount of protein was pre-determined so as not to consume greater than 10% of substrates during the course of the reaction. The enzyme reaction was initiated by addition of the acyl-CoA and quenched with 10 μL of 10% (w/v) sodium dodecylsulfate. For competition assays with Coenzyme A (CoA), CoA trilithium salt was dissolved in water and added into the reaction mixture at desired concentration. The resulting mixture was applied onto a preparative (TLC plate (0.25 mm Silica gel, DC-Fertigplatten) with a separate lane for [^{14}C]-triolein standard. The plate was developed with hexane:diethyl ether:acetic acid (80:20:1, v/v/v). The products were visualized by phosphorimaging (Typhoon Trio Variable Mode Imager, GE Healthcare, QC, Canada). Spots corresponding to TAG were scraped and analyzed for

radioactivity using Beckman-Coulter LS6500. Using GraphPad PRISM 7.0a, the data were fitted with Michaelis-Menten equation or Hill equation.

For quantification of recombinant protein production level, microsomes (containing 5-15 μg protein as indicated in the results) were incubated with 5× SDS loading buffer at room temperature for 15 min and the proteins were resolved through SDS–PAGE followed by electroblotting onto polyvinylidene fluoride membrane. The recombinant enzyme was probed with anti-V5-HRP conjugated antibody (Invitrogen) and detected through incubation with ECL Advance Western Blotting Detection Kit (Amersham) for 5 min. The blot was scanned using a variable mode imager (Typhoon Trio+, GE Healthcare) and the protein bands were semi-quantified using ImageJ software (Schneider et al., 2012).

4.2.4. Production and purification of recombinant BnaDGAT1$_{1\text{-}113}$

BnaDGAT1$_{1\text{-}113}$ was cloned into pET-16b vector between BamHI and XhoI restrictions sites. The plasmid was transformed into BL21(DE3) (NEB) and grown overnight in 200 mL Luria broth with 100 μg/mL ampicillin (LB-Amp). The seed culture was inoculated in 2 L LB-Amp and grown up to an OD600 of 0.8. After which, the production of recombinant proteins was induced through addition of 1 mM isopropyl-β-D-thiogalactopyranoside (IPTG) and subsequent incubation at 30°C for 6h. The cells were harvested, suspended in 100 mL lysis buffer consisting of 50 mM Tris-HCl pH 8.0 and 150 mM NaCl. The cells were lysed by sonication six times at 60% power with a 10 s on and 10 s off cycle. The cell lysate was recovered after spinning at 20,000 x g for 30 min and the resulting supernatant incubated with 2 mL Nickel-NTA resin (McLab). After transferring the resin to small disposable column, the resin was

washed with several volumes of lysis buffer. The fusion protein was eluted from the resin with 5 mL lysis buffer containing 500 mM imidazole. For the final purification step, the eluted proteins were subjected to FPLC-size exclusion chromatography (Superdex 200 16/40).

4.2.5. Production and purification of recombinant BnaDGAT1$_{1-80}$ and BnaDGAT1$_{81-113}$

BnaDGAT1$_{1-80}$ was cloned into pET-16b, expressed and purified using Ni-NTA as described above. BnaDGAT1$_{81-113}$ was cloned into the pET-SUMO vector (Invitrogen) according to the manufacturer's instructions. The plasmid was transformed into BL21(DE3) (NEB) and grown overnight in 50 mL LB with 50 μg/mL kanamycin. The seed culture was inoculated in 2 L LB-kanamycin and grown up to an OD600 of 0.8. After which, the expression of the SUMO- BnaDGAT1$_{81-113}$ was induced through addition of 1 mM IPTG and subsequently incubated at 30°C for 6 h. The cells were harvested, suspended in 100 mL lysis buffer consisting of 50 mM Tris-HCl pH 8.0 and 100 mM NaCl, and lysed through sonication. The cell lysate was recovered after spinning at 20,000 x g for 30 min and the resulting supernatant was incubated with 2 mL Nickel-NTA resin (Thermo Scientific) for 2 h and transferred into a small column. The fusion protein was eluted from the resin with 5 mL lysis buffer containing 500 mM imidazole. The SUMO tag was cleaved from the fusion protein using His-tagged SUMO protease (McLab, South San Francisco, CA) at 1 U protease per 20 μg fusion protein. The cleavage cocktail was composed of 50 mM Tris-HCl pH 8.0, 0.2% IGEPAL CA-360 (Sigma), 1 mM dithiothreitol, and 150 mM NaCl. Cleavage was complete after 20 h at 25°C. SDS-PAGE was run to confirm the completion of the cleavage. Partial

purification recombinant of the truncated BnaDGAT1 in the cleavage mixture was done with the use of 1 mL Ni-NTA agarose (Qiagen) resin, which removed the His-tagged SUMO and His-tagged SUMO protease. Further purification of $BnaDGAT1_{81\text{-}113}$ was accomplished by reverse phase high performance liquid chromatography (RP-HPLC) using a Phenomenex Luna C18(2) semi-preparative column (5 μm particle size, 100 Å pore size, 10 mm x 250 mm). The detector was set at 220 nm, while the flow rate was at 3 mL/min. Solvent A (water with 0.1% trifluoroacetic acid (TFA)) and solvent B (acetonitrile with 0.1% TFA) were used. Solvent B was set at 10% for 10 min, slowly increased to 20% for 10 min, 50% for another 15 min, and ramped up to 95% for 5 min. $BnaDGAT1_{81\text{-}113}$ eluted at 27 min, and was concentrated under vacuum, lyophilized, and stored at -20 °C.

4.2.6. Matrix-assisted laser desorption/ionization time-of-flight mass spectrometry

Matrix-assisted laser desorption ionization time-of-flight (MALDI-TOF) spectra were acquired using Perspective Biosystems Voyager Elite MALDI-TOF mass spectrometer in reflectron, delayed-extraction, positive ion mode. Sinapinic acid was used as the sample matrix.

4.2.7. Circular dichroism spectroscopy

Circular dichroism (CD) spectra of samples at 0.20 mg/mL were recorded on a Jasco J-810 spectropolarimeter. For far-UV measurement (190–260 nm), a 0.1 cm quartz cell was used in a nitrogen atmosphere. Ellipticity was recorded at scan speed of 50 nm/min, 0.5 nm resolution, 1.0 nm bandwidth, and 5 accumulations. The proteins were dissolved in 50 mM phosphate buffer pH 6.3, 50 mM NaCl (phosphate buffered saline [PBS]) for most experiments. For determination of the propensity of the protein to form

regular secondary structure, increasing amounts of trifluoroethanol in water (0-70%) were used. The solvent spectrum was also recorded as background, which was subtracted from the sample spectra.

4.2.8. NMR spectroscopy

BnaDGAT1$_{81\text{-}113}$ was dissolved in 600 μL 9:1 H_2O:D_2O that contained 30 mM sodium phosphate buffer (pH 6.3) and 25 mM NaCl. The sample was added with 4,4-dimethyl-4-silapentane-1-sulfonic acid (0.01% w/v) for referencing and loaded into a standard 5 mm NMR tube. One-dimensional ^{1}H NMR, and two-dimensional homonuclear ^{1}H–^{1}H -TOCSY, -gDQF-COSY, -NOESY, and heteronuclear natural abundance ^{1}H–^{15}N-HSQC spectra were acquired at 27 °C on a triple resonance HCN cryoprobe-equipped Varian VNMRS 700 MHz spectrometer with z-axis pulsed-field gradients and VNMRJ 4.2A as host control. The water signal was suppressed either by presaturation during the relaxation delay or water gradient tailored excitation. The experimental details are summarized in Table 4.1. NMRPipe and NMRView were used to process and analyze the data sets (Delaglio et al., 1995; Johnson, 2004). Chemical shifts were manually assigned based on precedent literature procedure (Wider et al., 1984; Wüthrich, 1986).

Table 4.1. NMR experimental parameters used for BnaDGAT1$_{81\text{-}113}$ spanning the allosteric site for CoA and acyl-CoA.

Experiment	Sweep width (Hz) (t2, t1)	ni	np	nt	Mix time
NOESY	8389, 8389	512	8192	32	175 ms
TOCSY	8389, 8389	512	8192	16	80 ms
gDQF-COSY	8389, 8389	512	8192	32	
NHSQC	8389, 3545	192	2098	128	

t2 = directly detected dimension

t1 = indirectly detected dimension

ni = number of complex points collected for the indirectly detected dimension

np = number of real + imaginary points for the directly detected dimension

nt = number of cumulative scans collected for each point of acquisition

4.2.9. Structure calculations

The structure of BnaDGAT1$_{81\text{-}113}$ was calculated using CYANA 2.1 (Güntert et al., 1997). Automatically and manually assigned NOE crosspeaks combined with angle restraints obtained from TALOS (Cornilescu et al., 1999) were utilized for the structural calculations that involved 7 cycles with 10000 steps per cycle. Simulated annealing calculated 100 conformers. The 20 conformers with the lowest energy were used for further analysis. The output data from CYANA included the root-mean-square deviation (rmsd) and Ramachandran plot. PyMOL was used to generate figures of the calculated structure. Coordinates of the structure were deposited in the Protein Data Bank (5UZL), while the chemical shift assignments were deposited in the Biological Magnetic Resonance Data Bank (30256).

4.2.10. HSQC binding experiments, phosphorus NMR, and docking studies

Binding of BnaDGAT1$_{81\text{-}113}$ (1.5 mM) to CoA in PBS (pH 6.3) was monitored using ^{15}N-HSQC with increasing amounts of CoA (0.75, 1.5 and 3 mM). Octanoyl-CoA or palmitoyl-CoA was also tested but drastic precipitation was encountered upon addition of the acyl-CoA. ^{31}P-NMR and ^{31}P-HSQC were performed to monitor chemical shift changes of phosphorus in CoA upon addition of the peptide. For the docking studies, AutoDockTools (v. 1.5.6) was used to convert the files of BnaDGAT1$_{81\text{-}113}$ and palmitoyl CoA from .pdb to .pdbqt extension. After which, AutoDock Vina (Vina, 2010) was used to dock CoA to BnaDGAT1$_{81\text{-}113}$. Figures were generated using PyMOL (Ward et al., 2004) and LigPlot (Wallace et al., 1995).

4.3. Results

4.3.1. The BnaDGAT1 N-terminal domain is not necessary for catalysis but contributes to modulating activity

BnaDGAT1 is predicted to have several membrane-spanning segments preceded by a relatively large hydrophilic N-terminal domain, that comprises more than 20% of the polypeptide (Fig. 4.1A). These features are conserved in all DGAT1 from various species. The BnaDGAT1 schematic shown in Fig. 4.1A is based on a topology prediction of 10 transmembrane domains but other predictions indicate 8 transmembrane domains. To probe the importance of the N-terminal domain in catalysis, the full-length enzyme and various truncated forms were recombinantly produced in *S. cerevisiae* H1246, which is devoid of the ability to synthesize TAG (Sandager et al., 2002). The specific activities were determined and normalized by the production level of each enzyme form relative to full-length BnaDGAT1 (Fig. 4.1B). Interestingly, BnaDGAT1$_{61\text{-}501}$ and BnaDGAT1$_{81\text{-}501}$ exhibited higher normalized specific activity compared to the full-length enzyme (Fig. 4.1C). These results suggest that the presence of amino acid residues 1-80 can down-regulate enzyme activity. Furthermore, despite the lower production level of BnaDGAT1$_{61\text{-}501}$ and BnaDGAT1$_{81\text{-}501}$, these enzyme forms were able to generate TAG amounting to about 60% of the total TAG produced by the full-length enzyme *in situ* (Fig. 4.2). On the other hand, BnaDGAT1$_{114\text{-}501}$, which is devoid of the entire N-terminal domain, was about 10-fold less active as the full-length enzyme (Fig. 4.1C). These results indicate that the N-terminal domain is not necessary to form an active enzyme but distinct segments of this domain contribute to modulating activity.

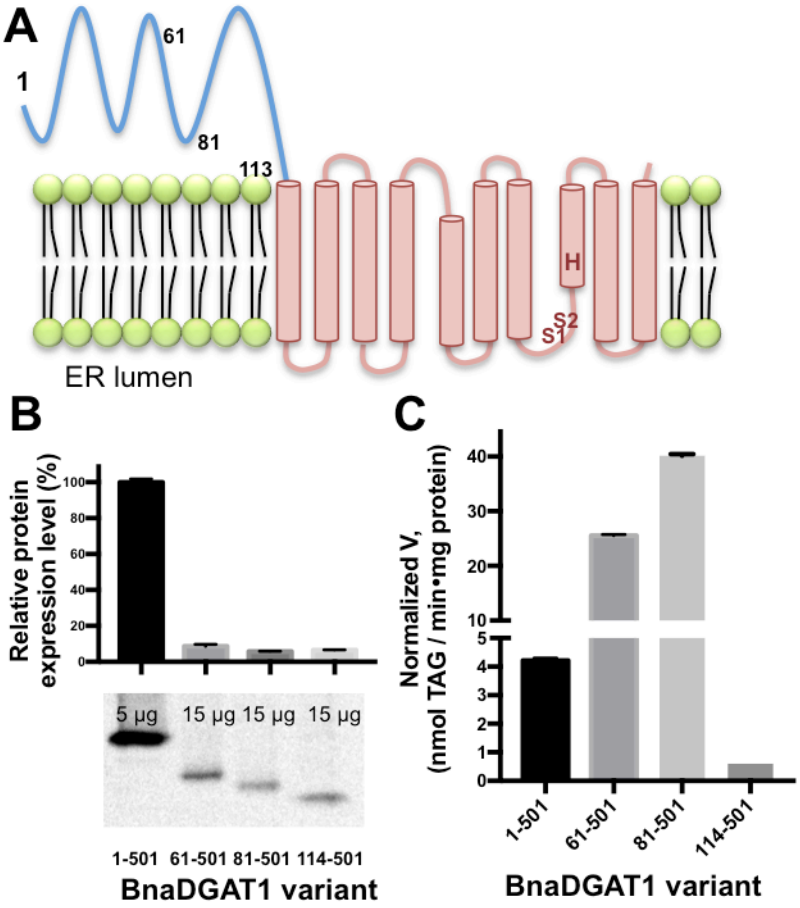

Figure 4.1. Truncation analysis of BnaDGAT1 N-terminal domain. A, BnaDGAT1 topology as predicted by TMHMM. BnaDGAT1 has a relatively large hydrophilic N-terminal domain (shown in blue) in the cytosolic face of the ER and 10 predicted transmembrane segments, housing the catalytic site, within the remainder of the enzyme. Numerals indicate the locations of the different enzyme truncation points. S1 and S2 correspond to the acyl-CoA and diacylglycerol binding regions in the active site, respectively, which were identified in bovine DGAT1 (Lopes et al., 2014). The putative catalytic histidine (bold H), identified in murine DGAT1, is also shown in the topology (Shockey et al., 2006). B, Protein expression level of BnaDGAT1 proteins with various

truncations. The amount of microsomal proteins used for blotting was indicated for each BnaDGAT1 construct. The amount of enzyme was semi-quantified using densitometric analysis using blots performed in duplicates. C, Normalized DGAT activity of $BnaDGAT1_{1\text{-}501}$, $BnaDGAT1_{61\text{-}501}$, $BnaDGAT1_{81\text{-}501}$ or $BnaDGAT1_{114\text{-}501}$. Specific activity was obtained at 2 μM oleoyl-CoA and the values were normalized by the protein expression level of each form. Reported values are means ± SD, n = 3.

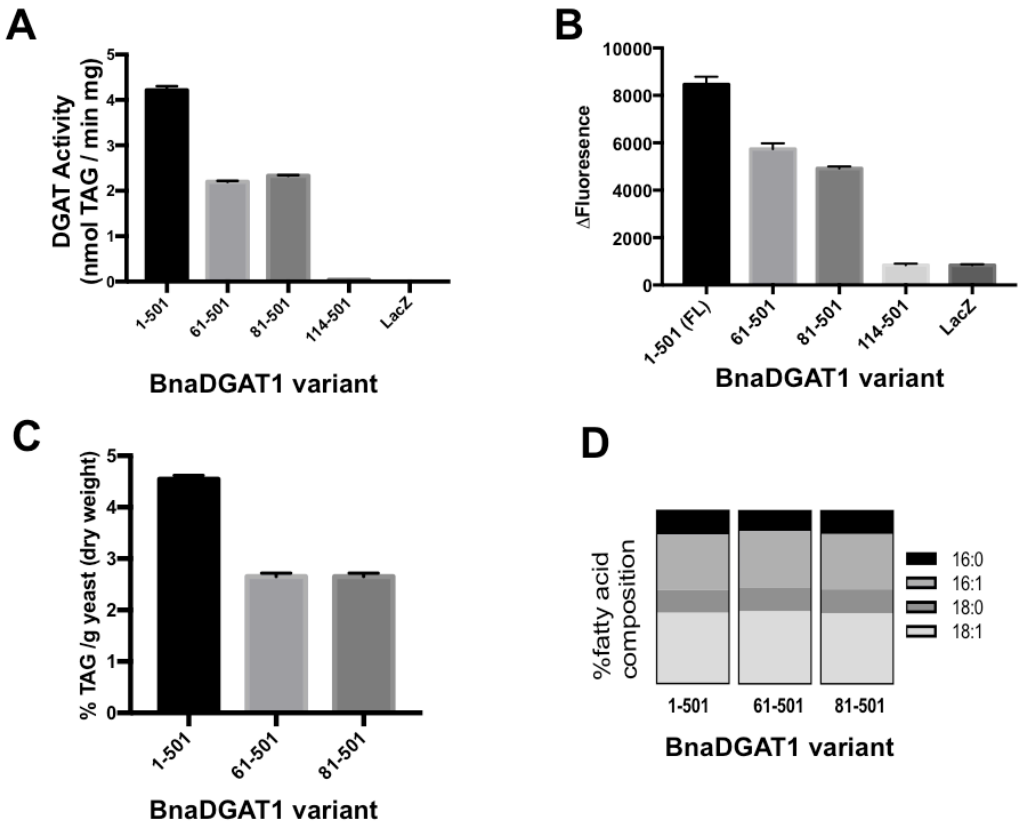

Figure 4.2. *In vivo* and *in vitro* activity of BnaDGAT1 variants. A, *In vitro* assay of BnaDGAT1 activity using ^{14}C-oleoyl-CoA and *sn*-1,2-dioeloylglycerol as substrates with microsomes, containing recombinant enzyme, prepared from yeast cultures. B, Nile red assay was used to monitor the activity of the BnaDGAT1 and truncated forms *in situ*, and the fluorescence intensity was measured and correlated with neutral lipid content (Siloto et al., 2009b). Yeast expressing vector with LacZ was used as control. C, The TAG produced by yeast producing recombinant BnaDGAT1, BnaDGAT1$_{61\text{-}501}$ or BnaDGAT1$_{81\text{-}501}$ was extracted, esterified and analyzed through gas chromatography-mass spectrometry (GC-MS). Yeast cells producing recombinant BnaDGAT1 produced 4.5 ± 0.1 % TAG/g yeast (dry weight) after 24 h incubation in induction media (early

stationary phase). BnaDGAT1$_{61-501}$ or BnaDGAT1$_{81-501}$ produced 2.7 ± 0.1 % TAG/ g yeast (dry weight) under the same conditions. D, GC-MS analysis showed that the fatty acid composition of TAG produced *in situ* by the three forms of recombinant BnaDGAT1 was essentially the same. Reported values are means ± SD, n = 3 technical replicates.

The activities of BnaDGAT1$_{1\text{-}501}$, BnaDGAT1$_{81\text{-}501}$ and BnaDGAT1$_{114\text{-}501}$ were assayed at increasing concentrations of acyl-CoA (Fig. 4.3A-C). Normalized DGAT activities are depicted on the Y-axes of each panel of Figure 4.3A-C. Maximum enzyme activity was observed at 1-2 μM acyl-CoA for BnaDGAT1$_{1\text{-}501}$ or BnaDGAT1$_{81\text{-}501}$. In contrast, maximum activity with BnaDGAT1$_{114\text{-}501}$ was not observed until about 5 μM acyl-CoA (Fig. 4.3C). This result suggests that the affinity of BnaDGAT1$_{114\text{-}501}$ for acyl-CoA was much lower than the full length BnaDGAT1 or BnaDGAT1$_{81\text{-}501}$ and residues 81-113 are important in maintaining high activity and affinity for the acyl donor at the active site.

The substrate saturation plots for BnaDGAT1 and the N-terminally truncated enzyme variants were found to be a better fit to the Hill equation over the Michaelis-Menten model based on R^2 values and residual analysis (Table 4.2). In the case of BnaDGAT1$_{114\text{-}501}$, the plot did not reach the asymptote due to substrate inhibition observed at higher concentrations of acyl-CoA (Fig. 4.3C). This plot did not fit any specific enzyme kinetic model. The Hill coefficients of BnaDGAT1 are 2.28 ± 0.13 and 2.65 ± 0.19 for oleoyl-CoA and palmitoyl-CoA, respectively, and are indicative of positive cooperativity. The Hill coefficient for N-terminally truncated enzyme BnaDGAT1$_{81\text{-}501}$ decreased to 1.26 ± 0.19 and 1.64 ± 0.11 for oleoyl-CoA and palmitoyl-CoA, respectively, suggesting that the N-terminal domain partially mediates positive cooperativity.

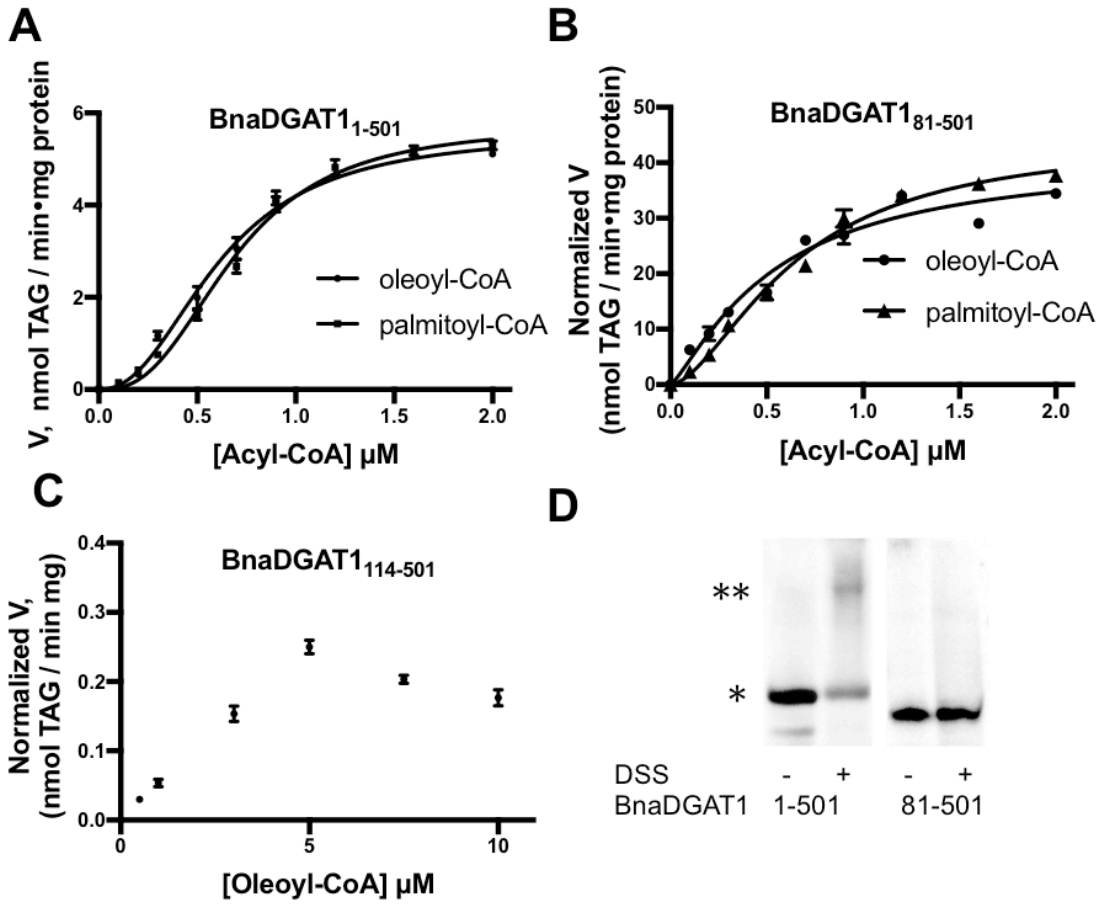

Figure 4.3. BnaDGAT1 N-terminal domain partially mediates positive cooperativity. Substrate saturation curves of A, full-length BnaDGAT1 B, $BnaDGAT1_{81\text{-}501}$ and C, $BnaDGAT1_{114\text{-}501}$.The data were fitted with Hill equation using Graphpad Prism 7.0a. The kinetic parameters are listed in Table 4.2. D, Cross-linking studies of BnaDGAT1 and truncated versions of the enzyme using disuccinimidyl suberate (DSS). The monomeric species is indicated by one asterisk (*), while the dimer is indicated by two asterisks (**). The BnaDGAT1 N-terminal region is required for interactions leading to dimeric enzyme form, which may allow it to partially mediate positive cooperativity through intermolecular interaction. Reported values are means ± SD, n = 3.

Table 4.2. Kinetic parameters of full-length and truncated BnaDGAT1 using palmitoyl-CoA and oleoyl-CoA as acyl donors. The data for the substrate saturation assays were fitted with Hill equation using Graphpad Prism 7.0a. The apparent V_{max} values were not normalized for DGAT abundance. Reported values are means ± SD, n = 3.

Enzyme	$BnaDGAT1_{1-501}$		$BnaDGAT1_{81-501}$	
Acyl donor	Oleoyl-CoA	Palmitoyl-CoA	Oleoyl-CoA	Palmitoyl-CoA
Apparent V_{max} (nmol TAG/min/mg protein)	5.58 ± 0.14	5.749 ± 0.16	2.27 ± 0.24	2.18 ± 0.09
Hill coefficient	2.28 ± 0.13	2.65 ± 0.19	1.26 ± 0.19	1.64 ± 0.11
Apparent $S_{0.5}$ (μM)	0.61 ± 0.02	0.69 ± 0.02	0.55 ± 0.11	0.67 ± 0.05
Goodness of Fit/R^2	0.9937	0.9916	0.961	0.992

In positive cooperativity, the binding of substrate at one site increases the affinity of substrate at another site. This effect is commonly achieved through inter-subunit communication in a quaternary structure situation (Laskowski et al., 2009). Taking this possibility into account, we investigated the ability of the N-terminal domain to facilitate the formation of a quaternary structure. The oligomeric states of BnaDGAT1 were determined using cross-linking experiments. Yeast microsomes containing recombinant variants of BnaDGAT1 were incubated with the membrane-permeable cross-linker, disuccinimidyl suberate (DSS). Treated or untreated protein samples were then subjected to SDS-PAGE and Western blot analysis (Fig. 4.3D). Untreated BnaDGAT1 showed one band with a molecular mass of about 50 kDa. For treated BnaDGAT1, two polypeptides were detected: the 50 kDa band and a second band with molecular mass twice the size of the 50 kDa band. This result suggested that the full-length enzyme is capable of forming a dimer. In contrast, treatment of BnaDGAT1$_{81\text{-}501}$with cross-linking agent did not result in any detectable polypeptide oligomerization (Fig. 4.3D), which suggested that dimer formation capability was associated with the first 80 amino acid residues of the enzyme. In addition, BnaDGAT1$_{81\text{-}501}$ still exhibited a certain degree of cooperativity, based on the Hill coefficients, shown in Table 4.2, in the absence of dimerization. This observation suggests that the binding of acyl-CoA to an allosteric site in the hydrophilic N-terminal domain increases the affinity of the active site for acyl-CoA, which is associated with the remainder of the same polypeptide.

4.3.2. CoA modulates activity of the active site acyltransferase

Previous Lipidex-1000 binding experiments showed that the N-terminal domain of isoform BnaA.DGAT1.b can interact with acyl-CoA at a possible allosteric site and that CoA could displace the thioester (Weselake et al., 2006). In the current study, the effect of CoA on BnaDGAT1 activity was investigated. The presence of increasing concentrations of CoA in the reaction mixture led to a corresponding decrease in acyltransferase activity (Fig. 4.4A). The activity was reduced by about 10% in the presence of 5 μM CoA and by as much as 70% when the CoA concentration was increased to 200 μM. The IC_{50} for CoA was found to be about 47 μM. To determine the mode of inhibition, the effect of increasing CoA concentration on the oleoyl-CoA saturation plot was evaluated (Fig. 4.4B, Table 4.3). In the presence of 10 μM CoA, the apparent V_{max} of the enzyme decreased from 5.55 ± 0.17 to 4.56 ± 0.25 nmol TAG/min/mg protein. The apparent V_{max} further decreased to 2.46 ± 0.16 nmol TAG/min/mg protein upon addition of 50 μM CoA. On the other hand, the apparent S0.5 of the enzyme remained essentially the same under the above conditions. These results indicate that CoA is a non-competitive BnaDGAT1 inhibitor that binds to an allosteric site, which may be within the N-terminal domain of the enzyme.

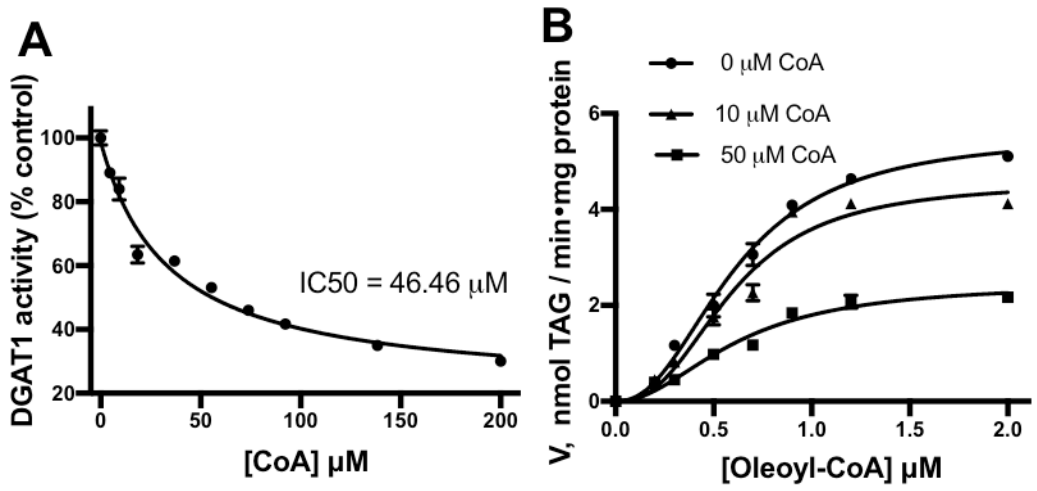

Figure 4.4. Activity assay of BnaDGAT1 in the presence of Coenzyme A. A, BnaDGAT1 activity in the presence of increasing concentrations of CoA. CoA was found to inhibit BnaDGAT1. B, Oleoyl-CoA saturation curve in the presence of different concentration of CoA. The apparent V_{max} decreased progressively upon addition of increasing amounts of CoA, while the apparent $S_{0.5}$ remained the same. These results indicate that CoA is a non-competitive inhibitor of the enzyme, and thereby inhibits BnaDGAT1 by binding to an allosteric site. Reported values are means ± SD, n = 3.

Table 4.3. Kinetic parameters of BnaDGAT1 using oleoyl-CoA as acyl donor and in the presence of varying amounts of CoA. The data for the substrate saturation assays were fitted with Hill equation using Graphpad Prism 7.0a. Reported values are means ± SD, n = 3. CoA was found to be a non-competitive inhibitor of BnaDGAT1.

[CoA]	Apparent V_{max} (nmol TAG/min/mg protein)	Apparent $S_{0.5}$ (μM)
Control	5.55 ± 0.17	0.61 ± 0.02
10 μM	4.56 ± 0.25	0.60 ± 0.04
50 μM	2.46 ± 0.16	0.62 ± 0.05

4.3.3. The BnaDGAT1 N-terminal domain is structurally flexible

The BnaDGAT1 N-terminal domain (amino residues 1-113) is not homologous to any structurally characterized protein domain. We first analyzed the amino acid sequence of BnaDGAT1$_{1\text{-}113}$ to obtain insights on its structure-function characteristics. The N-terminal domain is depleted of hydrophobic amino acid residues, which are important for promoting protein folding, and is composed predominantly of charged and polar residues. This combination has been correlated with intrinsic disorder in proteins (Uversky et al., 2000). This observation agrees with secondary structure analysis using DISOPRED (Ward et al., 2004), which showed that majority of the N-terminal hydrophilic region is likely in a disordered state, a characteristic that appears to be conserved among plant and animal DGAT1s (Fig. 4.5). The BnaDGAT1 N-terminal domain exhibits high sequence variability with prevalence of insertion/deletions in the primary structure, both of which are characteristics of IDRs (Brown et al., 2002; Light et al., 2013). In contrast, the remainder of BnaDGAT1 is relatively highly conserved, enriched in hydrophobic amino acid residues and expected to be well-folded based on DISOPRED analysis.

For structural investigation, full-length recombinant BnaDGAT1 was produced in *S. cerevisiae* H1246, solubilized in *n*-dodecyl-β-D-maltopyranoside (DDM), and purified as previously described (Fig. 4.6A) (Caldo et al., 2015). In addition, BnaDGAT1$_{1\text{-}113}$ was recombinantly produced in *E. coli* and purified (Fig. 4.6A, 4.7A). Far-UV CD spectroscopy was then used to analyze the secondary structure of purified BnaDGAT1 or BnaDGAT1$_{1\text{-}113}$ (Fig. 4.6B). The CD spectrum of full-length BnaDGAT1 in DDM micelles reveals a well-folded protein that is predominantly α-helical. In

contrast, the CD spectrum of BnaDGAT1$_{1\text{-}113}$ was indicative of a random coil polypeptide. This result confirmed that this region of the BnaDGAT1 polypeptide is mainly intrinsically disordered. Analysis of the CD spectra using K2D3 software (Louis-Jeune et al., 2012) showed that the full-length polypeptide is predominantly well-folded (about 68% α-helices/β-sheets) while the N-terminal domain only has about 29% α-helices/β-sheets.

Some IDRs have the ability to form specific stable conformations upon interacting with proteins/ligands (Wright and Dyson, 2015). The presence of trifluoroethanol (TFE) simulates the hydrophobic condition that can arise upon forming protein-protein interaction and has been used to assess the propensity of IDRs to undergo induced folding (Sun et al., 2010; Marín et al., 2012). The N-terminal domain of BnaDGAT1 was titrated with increasing amounts of TFE followed by CD analysis (Fig. 4.6C). Increasing amounts of TFE resulted to the appearance of distinct minima at 208 and 220 nm. This suggests that given the presence of the right binding partner or condition, specific segments of BnaDGAT1 N-terminal IDR can potentially form a defined structure. DISOPRED analysis identified the presence of possible protein ligand-binding sites within the disordered region (Fig. 4.5).

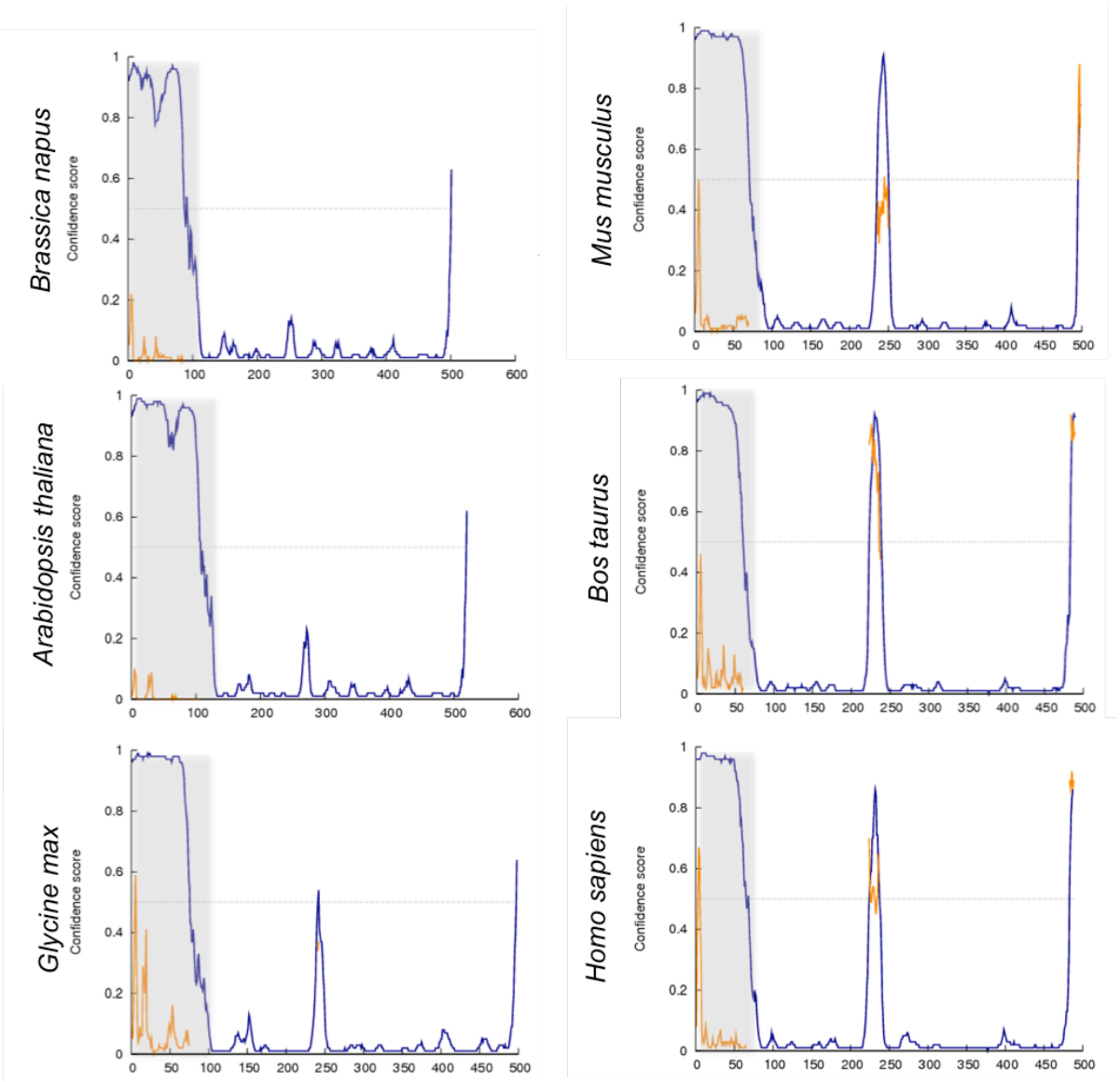

Figure 4.5. Intrinsic disorder profile of DGAT1 from different species and prediction for likelihood for protein binding sites. The figure was generated using DISOPRED analysis of primary protein sequences (Ward et al., 2004). The hydrophilic N-terminal regions are highlighted in gray. Blue lines correspond to probability of being disordered while yellow lines indicate the likelihood to participate in protein-protein interaction. The disordered nature of the N-terminal region appears conserved among DGAT1 proteins from various plant and animal species.

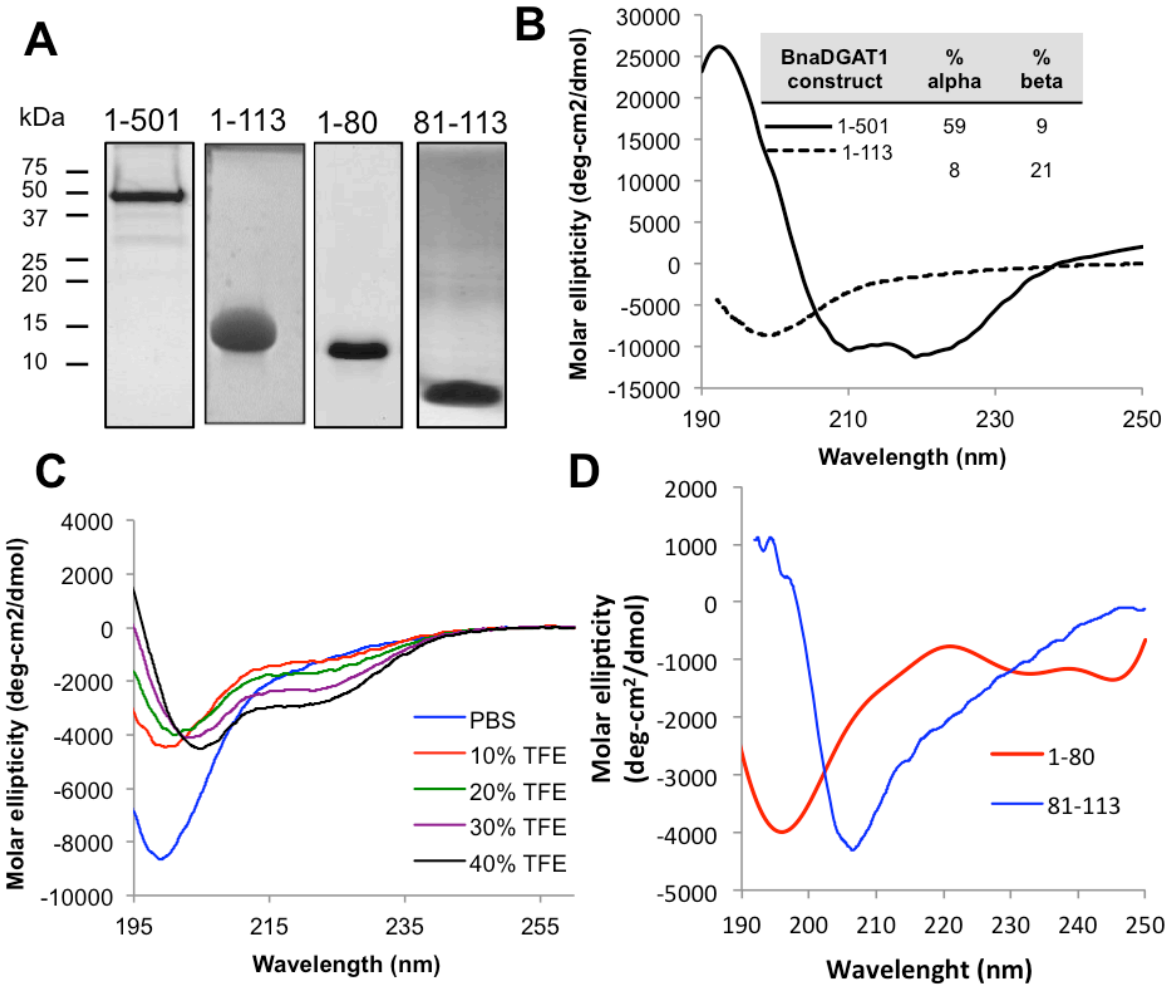

Figure 4.6. BnaDGAT1 N-terminal domain is composed of an intrinsically disordered region (IDR) and a folded segment, while full-length BnaDGAT1 is well-folded. A, SDS-PAGE of purified BnaDGAT1 in n-dodecyl-β-D-maltopyranoside (DDM) micelles, BnaDGAT1$_{1\text{-}113}$, BnaDGAT1$_{1\text{-}80}$ and BnaDGAT1$_{81\text{-}113}$. B, Far-UV circular dichroism spectra of BnaDGAT1 and BnaDGAT1$_{1\text{-}113}$ in DDM micelles and PBS, respectively. Percentage of secondary structure based on K2D3 analysis of CD spectra is indicated. Full-length BnaDGAT1 is predominantly α-helical, while BnaDGAT1$_{1\text{-}113}$ is mainly random coil. C, BnaDGAT1 N-terminal domain has propensity to form secondary structure upon titration with increasing amount of

trifluoroethanol. Some IDRs tend to form transient structure upon interaction with protein binding partners. D, CD spectra of BnaDGAT1$_{1\text{-}80}$ and BnaDGAT1$_{81\text{-}113}$. Residues 1-80 is highly disordered while 81-113 appears to form defined secondary structures.

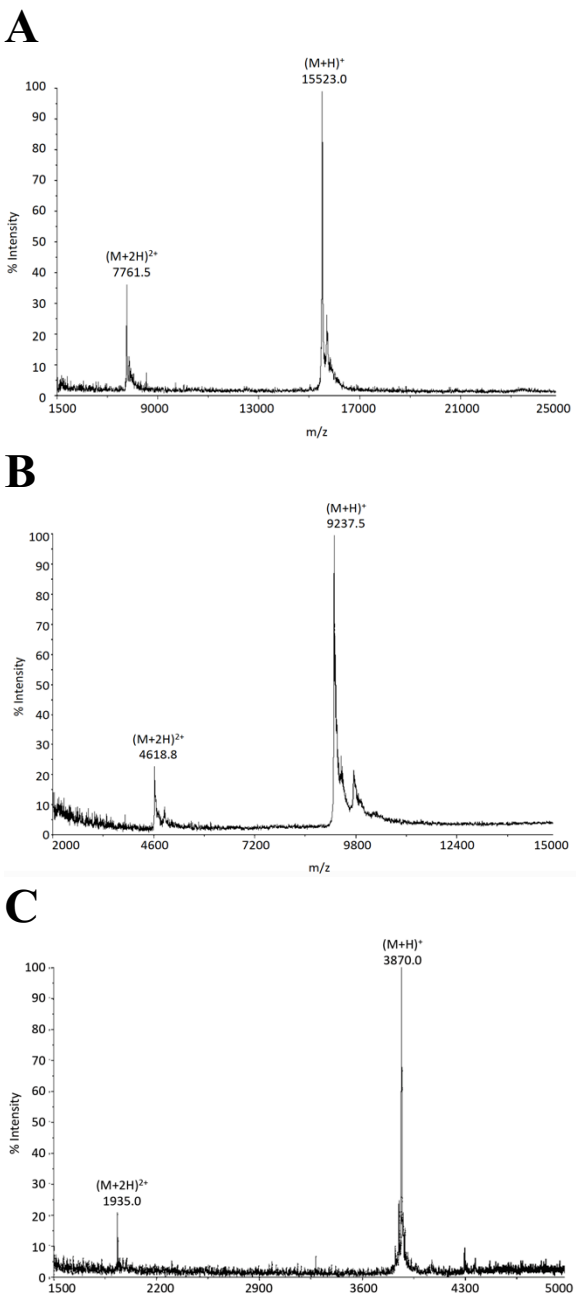

Figure 4.7. MALDI-TOF spectra of purified BnaDGAT1 N-terminal hydrophilic domain and the 2 distinct segments. A, BnaDGAT1$_{1\text{-}113}$, B, BnaDGAT1$_{1\text{-}80}$, and C, BnaDGAT1$_{81\text{-}113}$.

4.3.4. The BnaDGAT1 N-terminal domain is composed of an intrinsically disordered region and a folded portion

Truncation analysis showed that the removal of the first 80 amino acid residues did not decrease the responsiveness of the enzyme to increasing concentrations of acyl-CoA, while the opposite was observed upon deletion of amino acid residues 81-113 (Fig. 4.3). Our current results along with a previous study on the N-terminal domain of DGAT1 (Weselake et al., 2006) suggest that this binding site is localized along amino acid residues 81-113. DISOPRED analysis predicted that segment 1-80 of BnaDGAT1 is disordered, whereas the segment 81-113 has secondary structure (Fig. 4.5). Initial NMR structure elucidation of the entire N-terminal domain was not plausible due to lack of defined structure. We then recombinantly produced and purified BnaDGAT1$_{1-80}$ and BnaDGAT1$_{81-113}$ (Fig. 4.6A, 4.7B, 4.7C). Both polypeptide segments were subjected to far-UV CD analysis (Fig. 4.6D). The CD spectrum of BnaDGAT$_{1-80}$ is similar to that of BnaDGAT$_{1-113}$, indicating a random coil structure. The CD spectrum of BnaDGAT1$_{81-113}$, however, was indicative of a well-folded structure. These results suggested that BnaDGAT1$_{81-113}$, which may include an acyl-CoA/CoA binding site, would be suitable for structural elucidation using solution NMR spectroscopy. In turn, natural abundance ^{15}N-HSQC, ^{1}H-^{1}H TOCSY, NOESY and COSY datasets were acquired for BnaDGAT1$_{81-113}$ in 30 mM sodium phosphate buffer (pH 6.3) with 25 mM NaCl. The ^{15}N-HSQC spectrum (Fig. 4.8) showed a relatively good dispersion of the amide proton signals confirming that BnaDGAT1$_{81-113}$ exhibits a defined structure. The assignments are shown in Table 4.4. Peak lists of the chemical shift assignments and NOE constraints were then inputted into CYANA 2.1 for the structural calculations. The final calculation

utilized 356 NOE constraints with 300 short-range, 49 medium-range, and 7 long-range constraints (Table 4.5). The Ramachandran plot shows that no ϕ or ψ backbone angles are in the disallowed regions (Table 4.5).

The calculated structure of BnaDGAT1$_{81\text{-}113}$ showed that it is composed of an α-helix at the C-terminus spanning L103 to S112, a defined loop from A94 to P102 and an unstructured N-terminus (Fig. 4.9A). The root-mean-square deviation (rmsd) values for the structured regions were calculated to be 0.51 Å and 0.49 Å for the α-helix and loop backbone atoms, respectively. The low rmsd values indicate that the observed conformations are consistent throughout the 20 calculated structures (Fig. 4.9B). On the other hand, a higher rmsd of 1.58 Å for the backbone atoms was calculated for N81 to P93, which forms random coil. This coil is connected to the segment comprising amino acid residues 1 to 80 of the N-terminal domain, which is an IDR based on DISOPRED, CD and NMR analyses.

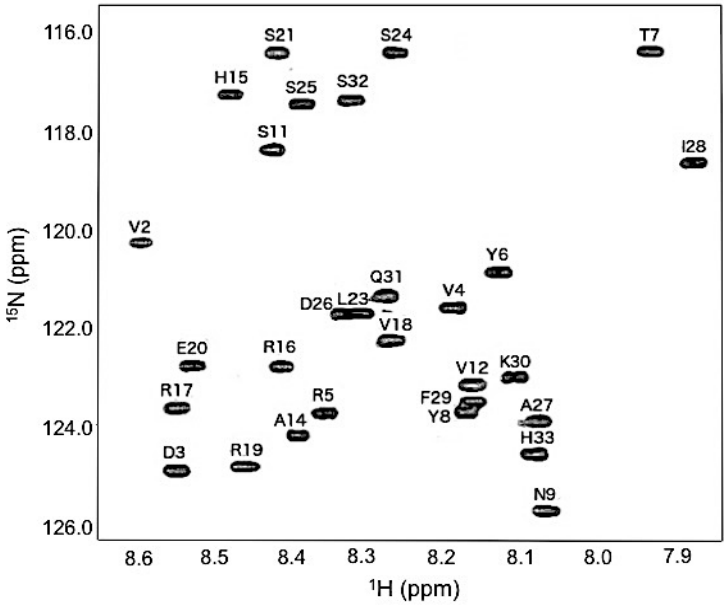

Figure 4.8. ^{15}N-HSQC spectrum of BnaDGAT1$_{81\text{-}113}$. All 29-backbone resonances are labeled using the one-letter notation of amino acids.

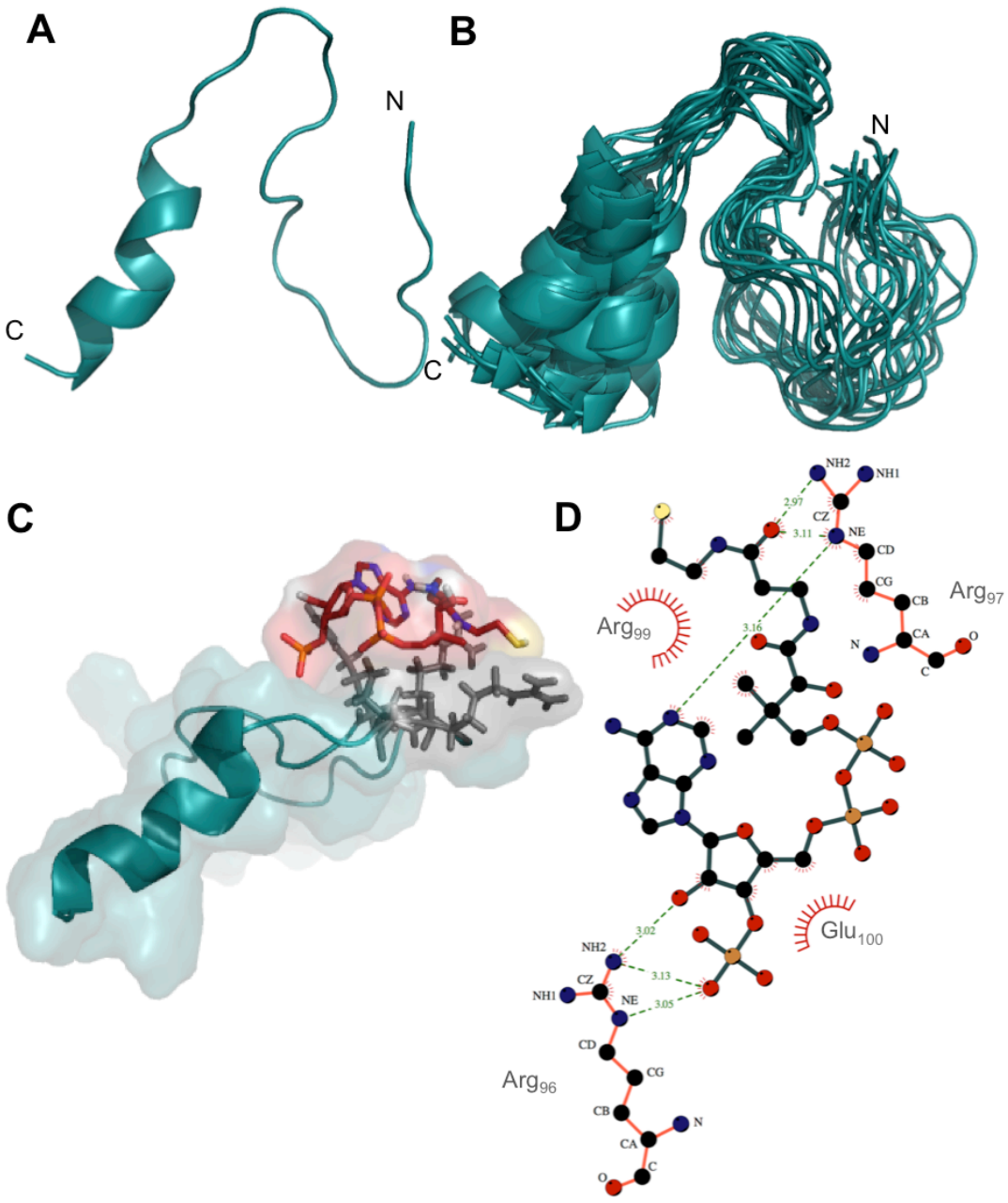

Figure 4.9. Three-dimensional structure of the allosteric site in BnaDGAT1 N-terminal domain, binding studies with CoA. A, NMR solution structure of BnaDGAT1$_{81\text{-}113}$ in 30 mM sodium phosphate buffer (pH 6.3) and 25 mM NaCl exhibiting an α-helix at the C-terminus. B, Overlay of 20 lowest energy conformers. C,

Docking of the allosteric site with CoA using AutoDock Vina (Vina, 2010). The interacting residues were identified using NMR titration experiments (Fig. 4.10). D, Layout of interacting residues obtained using LigPlot software (Wallace et al., 1995). Hydrogen bonds are shown by green dash lines while hydrophobic interactions are shown by red rays arranged in a circular fashion.

Table 4.4. BnaDGAT1$_{81-113}$ chemical shift assignments.

	N	HN	Hα	Hβ	Others
Asn-1			4.403	2.899, 2.981	δNH$_2$ 7.552, 6.866, δN 112.339
Val-2	120.236	8.551	4.179	2.079	γCH$_3$ 0.931
Asp-3	124.798	8.507	4.673	2.787, 2.626	
Val-4	121.549	8.165	4.079	2.087	γCH$_3$ 0.903, 0861
Arg-5	123.666	8.323	4.230	1.653	βCH$_2$ 1.520, 1.502, δCH$_2$ 3.115, 3.151, δNH 7.302,
Tyr-6	120.828	8.109	4.624	3.033, 2.895	δCH 7.090, εCH 6.801
Thr-7	116.413	7.922	4.235	4.062	γCH$_3$ 1.106
Tyr-8	123.632	8.148	4.511	2.937, 3.000	δCH 7.112, εCH 6.807
Arg-9	125.615	8.047	4.538	1.623, 1.734	βCH$_2$ 1.553, δCH$_2$ 3.145, δNH 7.123
Pro-10			4.354	2.296, 1.918	γCH$_2$ 1.984, δCH$_2$ 3.558, 3.510
Ser-11	118.382	8.382	4.429	3.840, 3.860	
Val-12	123.101	8.140	4.450	2.057	γCH$_3$ 0.914, 0.959
Pro-13			4.360	2.282, 1.837	γCH$_2$ 1.980, 2.024, δCH$_2$ 3.861, 3.664
Ala-14	124.098	8.355	4.218	1.327	
His-15	117.275	8.440	4.679	3.251, 3.162	δCH 7.279, εCH 8.591
Arg-16	122.720	8.376	4.323	1.906, 1.732	βCH$_2$ 1.619, 1.587, δCH$_2$ 3.183, δNH 7.196
Arg-17	123.554	8.505	4.361	1.822, 1.753	βCH$_2$ 1.658, 1.598, δCH$_2$ 3.198, δNH 7.218
Val-18	122.185	8.240	4.117	2.059	γCH$_3$ 0.927, 0.926
Arg-19	124.717	8.422	4.314	1.834, 1.757	βCH$_2$ 1.646, 1.606, δCH$_2$ 3.196, δNH 7.208
Glu-20	122.704	8.485	4.353	1.938, 2.072	γCH$_2$ 2.348
Ser-21	116.443	8.361	4.400	3.826, 3.828	
Pro-22			4.457	2.304, 1.940	γCH$_2$ 2.014, δCH$_2$ 3.811, 3.741
Leu-23	121.657	8.277	4.349	1.601, 1.632	γCH 1.637, δCH$_3$ 0.924, 0.876
Ser-24	116.439	8.236	4.440	3.947, 3.870	
Ser-25	117.467	8.351	4.428	3.951, 3.865	
Asp-26	121.678	8.300	4.624	2.763, 2.736	
Ala-27	123.825	8.058	4.237	1.367	
Ile-28	118.645	7.868	4.032	1.776	γCH$_2$ 1.113, 1.350, δCH$_3$ 0.806, γCH$_3$ 0.762
Phe-29	123.411	8.140	4.609	3.138, 3.044	δCH 7.244, εCH 7.2327, ζCH 7.274
Lys-30	122.937	8.087	4.254	1.799, 1.711	βCH$_2$ 1.409, 1.368, γCH$_2$ 1.657, δCH$_2$ 2.978
Gln-31	121.326	8.247	4.308	2.103, 1.988	γCH$_2$ 2.379, εNH$_2$ 7.711, 7.035, εN 112.399
Ser-32	117.383	8.290	4.424	3.843	
His-33	124.466	8.063	4.481	3.261, 3.079	δCH 7.239, εCH 8.528

Table 4.5. Structure calculation statistics for BnaDGAT1$_{81\text{-}113}$ spanning the allosteric site for CoA and acyl-CoA.

Total NOE peak assignments	359
short-range, |i-j|≤1	306
medium-range, 1<|i-j|<5	50
long-range, |i-j|≥5	3
average target function value (Å^2)	0.43 ± 0.14
RMSD for residues 1-14 (random coil)	
backbone atoms (Å)	2.59 ± 0.74
heavy atoms (Å)	3.38 ± 0.77
RMSD for residues 15-21 (loops)	
backbone atoms (Å)	0.58 ± 0.35
heavy atoms (Å)	1.57 ± 0.40
RMSD for residues 24-32 (α-helix)	
backbone atoms (Å)	0.34 ± 0.14
heavy atoms (Å)	0.98 ± 0.31
Ramachandran Plot	
Φ/Ψ in most favored regions	53.4 %
Φ/Ψ in additionally allowed regions	42.7 %
Φ/Ψ in generously allowed regions	3.9 %
Φ/Ψ in disallowed regions	0.0 %

4.3.5. The folded portion has the allosteric site for CoA

A previous study demonstrated that CoA alone could displace bound oleoyl-CoA from the N-terminal domain of BnaDGAT1, suggesting that the CoA moiety of acyl-CoA is critical to effective binding (Weselake et al., 2006). NMR titration of $BnaDGAT1_{81\text{-}113}$ with CoA was performed and binding was monitored through ^{15}N-HSQC (Fig. 4.10). Results showed that while most of the signals remained at exactly the same positions, movement of four amide protons was observed, signifying a change in chemical environment upon addition of CoA. No further chemical shift changes were observed beyond a 1:1 $BnaDGAT1_{81\text{-}113}$:CoA molar ratio, indicating saturation of binding and a stoichiometry of 1:1. The crosspeaks that moved were found to correspond to four polar amino acids (R96, R97, R99 and E100) that are located in the loop region (Fig. 4.10A). A closer examination of the structure of $BnaDGAT1_{81\text{-}113}$ revealed that all four residues are located on the same side of the loop (Fig. 4.9C). To examine the part of CoA that interacts with $BnaDGAT1_{81\text{-}113}$, ^{15}N-HSQC and ^{31}P-NMR were performed with CoA in the absence or presence of the peptide segment. ^{15}N-HSQC analysis of CoA, before and after binding, showed slight movement of the amide hydrogens near the diphosphate group (Fig. 4.10B). ^{31}P-NMR showed three major peaks corresponding to the phosphorus of the 3'-phosphate of ribose and two phosphorus atoms in the diphosphate moiety (Fig. 4.10C). Upon addition of the peptide, ^{31}P-HSQC revealed that the signal for ^{31}P of the phosphate group attached to ribose moved upfield from about 1 ppm to 0 ppm. On the other hand, the ^{31}P signals of the diphosphate moiety moved slightly downfield. These results suggest that the phosphate groups are involved in binding to the loop region of

BnaDGAT1$_{81\text{-}113}$. Taking into account these experimental results, a molecular model of the complex was derived by docking the calculated NMR solution structure of BnaDGAT1$_{81\text{-}113}$ with CoA using AutoDock Vina (Vina, 2010). The model suggests the formation of hydrogen bonds between the side chain of R96 and the 3'-phosphate and 2'-hydroxyl groups of CoA (Fig. 4.9D). Hydrogen bonds are also observed between CoA and R97, while hydrophobic interactions are present between CoA and all four amino acid residues (R96, R97, R99 and E100) that were earlier identified to be involved in binding through NMR titration experiments.

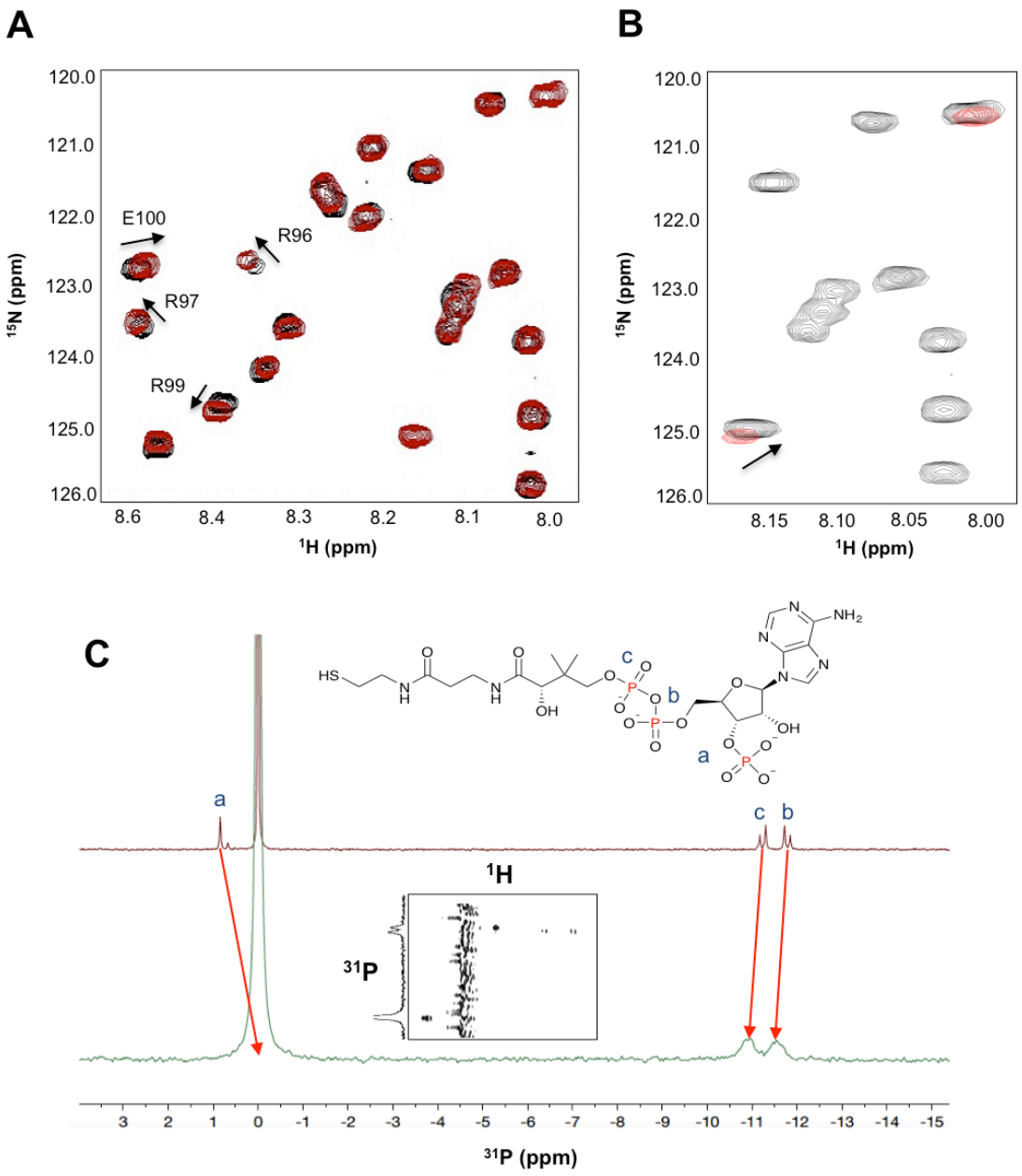

Figure 4.10. Ligand binding studies of BnaDGAT181-113 with Coenzyme A (CoA).

A, ^{15}N-HSQC spectrum of BnaDGAT1$_{81\text{-}113}$ with CoA at 1:1 molar ratio (red) and without CoA (black). B, ^{15}N-HSQC analysis of CoA with (black) and without (red) BnaDGAT1$_{81\text{-}113}$. C, CoA structure with the three phosphorus atoms labeled as a, b and

c. One-dimensional ^{31}P-NMR of CoA with (green) and without (red) BnaDGAT1$_{81\text{-}113}$. Two-dimensional ^{31}P-HSQC is also embedded to locate the peak of phosphorus a in the presence of the peptide.

4.3.6. The allosteric site is also needed for acyl-CoA-mediated homotropic allosteric activation

Mutational analysis of the loop amino acid residues implicated in CoA recognition was then performed to investigate their role in acyltransferase activity. A BnaDGAT1 variant having amino acid residue substitutions R96A, R97A, R99A and E100A was recombinantly produced in yeast H1246 and both *in vivo* DGAT activity and *in vitro* microsomal DGAT activity were assessed (Fig. 4.11A, 4.11B and 4.11C). The BnaDGAT1 mutant was found to exhibit low normalized *in vitro* microsomal activity having a normalized apparent V_{max} value of 1.60 ± 0.09 nmol TAG/min/mg protein, which is only about 29% as that of the wild-type enzyme (Fig. 4.11A). The BnaDGAT1 mutant also exhibited low activity *in vivo* compared to wild-type enzyme as shown by the results of TAG quantification using GC-MS analysis (Fig. 4.11C). These results demonstrate that the same allosteric site is also important for binding acyl-CoA, which allows the enzyme to form the more active state through homotropic allosteric activation. Furthermore, sequence alignment of DGAT1 from several plant and animal species indicated that the nature of the four amino acid residues implicated in CoA-binding and homotropic activation are highly conserved (Fig. 4.11D). NMR analysis of the interaction of BnaDGAT1$_{81\text{-}113}$ with various molecular species of acyl-CoA was also explored but this led to precipitation of the complex.

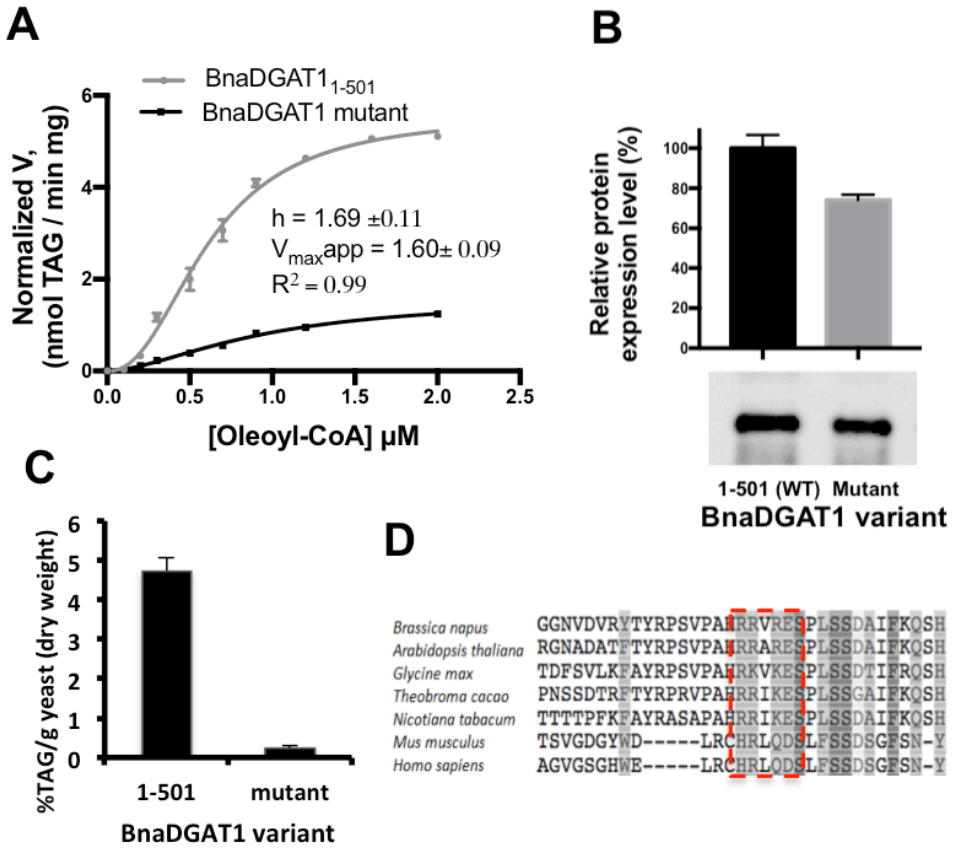

Figure 4.11. Mutational studies of the CoA binding site and its role for binding acyl-CoA for homotropic allosteric activation. A, Mutational analysis of CoA binding site through alanine mutation. Normalized activity of BnaDGAT1 mutant with R96A, R97A, R99A, and E100A mutations exhibited low activity *in vitro* compared to wild-type enzyme suggesting that these residues are needed for intramolecular homotropic allosteric activation with respect to acyl-CoA. B, Western blot and relative production level of recombinant BnaDGAT1 variant compared to wild-type (WT) enzyme. C, The TAG produced by yeast H1246 producing recombinant BnaDGAT1 variant (R96A, R97A, R99A, E100A) compared to WT enzyme analyzed through gas chromatography-mass spectrometry . The low *in vivo* activity in H1246 of the BnaDGAT1 mutant compared to the wild-type enzyme also supports the importance of the identified

residues for homotropic activation. D, Multiple sequence alignment of diacylglycerol acyltransferase 1 from plant and animal species showing the boxed highly conserved loop region implicated in CoA/acyl-CoA binding. Reported values are means ± SD, n = 3.

4.4. Discussion

Previous studies have demonstrated that N-terminally truncated forms of plant DGAT1 are capable of catalyzing TAG synthesis (Nykiforuk et al., 2002; Siloto et al., 2009b; Ahmad et al., 2015). Although the hydrophilic N-terminal domain of BnaDGAT1 does not participate in catalysis directly, our work demonstrates that this domain plays a key regulatory role in enzymatic function.

In the current study, CD and NMR experiments revealed that the regulatory N-terminal domain is composed of an IDR and a folded section. The presence of IDRs is common in higher organisms. Indeed, a recent study found that IDRs are found in 50% of membrane proteins, and are usually localized at the cytoplasmic face of the lipid bilayer (Bürgi et al., 2016). Computational studies also showed that multi-pass membrane proteins tend to have longer (~70 residues) IDRs facing the cytosol (Bürgi et al., 2016). This agrees with previous studies of plant DGAT1 indicating that the N-terminal region resides on the cytosolic face of the ER (Shockey et al., 2006; Weselake et al., 2006). Sequence analysis showed that the intrinsically disordered nature of the N-terminal domain is conserved in other plant DGAT1s as well as in non-plant DGAT1 from human, murine and bovine (Fig. 4.5). This suggests that the properties rendered by the N-terminal domain on DGAT1 might be conserved across different species.

IDRs are recognized as important regions of amino acid residues, as they have been found to perform a variety of roles in protein regulation and cellular signaling (Wright and Dyson, 2015). The IDR in the N-terminal domain of BnaDGAT1 has a down-regulatory effect on enzyme activity, which is due to the presence of an autoinhibitory sequence. Similarly, the increase in activity upon truncation of the N-

terminal domain was also observed in murine DGAT1 (McFie et al., 2010). A study on autoinhibited proteins revealed that inhibitory motifs are predominantly localized in disordered regions (Trudeau et al., 2013). In addition, the study suggested that disordered regions usually contain multiple phosphorylation sites and exhibit flexible structural conformations, which can operate combinatorially to enable the tight regulation of activity. Murine DGAT1 was found to have 12 putative phosphorylation sites within the N-terminal domain, 6 of which were confirmed through mass spectrometry analysis (Yu et al., 2015). BnaDGAT1 has 14 putative phosphorylation sites based on NetPhos 3.1 server (Blom et al., 1999). Interestingly, CCT, a key regulatory enzyme involved in the biosynthesis of another major lipid group (PC), was also found to have an autoinhibitory motif within a structurally flexible regulatory tail (Ding et al., 2012). The CCT regulatory tail has a number of putative phosphorylation sites similar to the DGAT1 N-terminal domain. The elucidated 3D structure of CCT demonstrated that the autoinhibitory motif within the regulatory tail interacts with the catalytic domain (Lee et al., 2014). This interaction blocks access into the active site and hinders dynamics of the key catalytic residue. The autoinhibitory motif was found to form an induced amphipathic helix upon binding while the rest of the regulatory tail remained disordered (Lee et al., 2014). Autoinhibitory motifs are known to inhibit the activity of other domains through intramolecular interactions (Pufall and Graves, 2002). DISOPRED analysis showed that the BnaDGAT1 IDR has a propensity to form protein-protein interactions (Fig. 4.5). The BnaDGAT1 autoinhibitory sequence may interact with cytosolic loops associated with the catalytic region of the enzyme, thereby down-regulating the activity of the enzyme. As mentioned earlier, the full-length BnaDGAT1

is well-folded and predominantly α-helical in DDM micelles while the IDR with autoinhibitory motif has a propensity to form structure (Fig. 4.6B and 4.6C). It remains to be determined whether the IDR of BnaDGAT1 forms a three-dimensional structure with the cytoplasmic loops of segment 114-501, which contains the catalytic site and numerous transmembrane domains (Fig. 4.1A).

The highly disordered region of BnaDGAT1, residues 1-80, was found to facilitate dimerization as evident from cross-linking studies (Fig. 4.3D). This agrees with our studies on purified full-length BnaDGAT1 in DDM micelles, which showed that the enzyme when subjected to gel filtration predominantly elutes with a retention time indicative of a dimer (Caldo et al., 2015). Previous studies on murine DGAT1 and BnaA.DGAT1.b N-terminal fragment also showed that the N-terminal domain plays a role in self-association (Weselake et al., 2006; McFie et al., 2010). The formation of quaternary structure could possibly facilitate intermolecular communication between subunits.

Our kinetic analysis of BnaDGAT1 showed that it exhibits positive cooperativity. This behavior for plant DGAT1 was also recently reported for both *C. americana* DGAT1 and *Z. mays* DGAT1 (Roesler et al., 2016). The study found that plant DGAT1s exhibited a sigmoidal response to increasing concentration of acyl-CoA, consistent with the findings on BnaDGAT1 in the current study. Furthermore, in the current study, deletion of the N-terminal domain led to a decrease in the Hill coefficient, suggesting that this region partially mediates positive cooperativity through intermolecular interactions. This observation agrees with the acyl-CoA binding characteristics of recombinant forms of the N-terminal region of *B. napus* DGAT1 or murine DGAT1

(Weselake et al., 2006; Siloto et al., 2008). Lipidex-1000 assays showed that the binding of the BnaA.DGAT1.b N-terminal fragment (amino acid residues 1-113) with various types of acyl-CoA followed a sigmoidal behavior, suggesting that the N-terminal domain can facilitate regulation through positive cooperativity. In addition, free CoA was shown to displace acyl-CoA from the N-terminal fragment suggesting that this non-catalytic site could interact with either thioester or CoA (Weselake et al., 2006). In the current study, *in vitro* enzyme assays showed that CoA is a non-competitive inhibitor of BnaDGAT1, which in turn suggested that CoA might be a physiological negative effector of the enzyme.

Kinetic analysis also showed that the first 80 amino acid residues of BnaDGAT1 do not play a significant role in binding acyl-CoA, while removal of amino acid residues 81-113, led to substantially reduced acyl-CoA affinity and enzyme activity. This finding showed that the acyl-CoA binding property, previously identified in BnaA.DGAT1.b (Weselake et al., 2006), specifically lies along amino acid residues 81-113 in the BnaDGAT1, under investigation in the current study. The 3D structure of the acyl-CoA/CoA binding site involving amino acid residues 81-113 was characterized. It is important to note that no 3D structure has been experimentally elucidated previously for any important motif of MBOATs. In contrast to the IDR in BnaDGAT1 N-terminal domain, the putative allosteric acyl-CoA binding site is a folded segment composed of loops and an α-helix. Subsequent structural and ligand binding analysis identified the specific amino acid residues involved in recognition of the CoA moiety. The amino acid residue substitutions R96A, R97A, R99A and E100A resulted in a substantial reduction in DGAT activity, which clearly demonstrated that this segment of the enzyme is

involved in regulating enzyme activity. Binding of acyl-CoA at the allosteric site in the N-terminus may enhance DGAT activity whereas binding of CoA may decrease enzyme activity.

Loops in proteins are common ligand binding sites. Importantly, the amino acid residues implicated in CoA binding are highly conserved among DGAT1 homologues including human and murine DGAT1s suggesting a common mechanism of binding (Fig. 4.9C). The motif identified is composed of [HR][RK]X[KRQ][DE]. The 3'-phosphate of the adenosine moiety of CoA was found to be a major point for interaction in this study. Previously, CoA was found to be a feedback inhibitor of phosphopantetheine adenylyltransferase (PPAT), which is a regulatory enzyme catalyzing the second last reaction involved in CoA biosynthesis (Rubio et al., 2008). The IC_{50} of CoA for PPAT is about 39 μM, which is close to the IC_{50} of about 47 μM for the CoA-BnaDGAT1 interaction based on our kinetic analysis.

An enzyme model is proposed wherein BnaDGAT1 activity is modulated by acyl-CoA and CoA (Fig. 4.12). Under conditions of high acyl-CoA levels, the level of free CoA is expected to decrease and vice-versa. The presence of at least two acyl-CoA binding sites (allosteric and catalytic sites) and positive cooperativity in BnaDGAT1 indicate that homotropic allosteric activation operates in BnaDGAT1 enabling its activity to adjust based on acyl-CoA levels. As observed in autoinhibited proteins, it is proposed that BnaDGAT1 initially exists in an inactive state with an autoinhibitor motif (*i*) bound to segment 114-501 (S114-501), which contains the numerous transmembrane domains and catalytic site. High levels of CoA stabilize the inactive state. CoA can be displaced by increasing concentration of acyl-CoA, which activates the enzyme due to a

conformational change induced by binding of thioester to the allosteric site. The binding of acyl-CoA in the N-terminal domain activates the catalytic domain within the remainder of the polypeptide (S114-501), and the activation signal is also transmitted to the other subunit through the dimerization segment (encircled) in the IDR. The process of regulation may also include other unidentified biochemical effectors, which may be involved in the release of the autoinhibitory region from S114-501. The proposed model, however, does not account for the apparent substrate inhibition observed for BnaDGAT1$_{114\text{-}501}$ at the two concentrations of acyl-CoA above 5 μM (see Fig. 4.3C), where the enzyme might have a second lower affinity non-catalytic acyl-CoA binding site, in S114-501, which results in down-regulation of the enzyme. Homotropic allosteric regulation in membrane proteins is not uncommon. Recently, another intramembrane enzyme, rhomboid protease, was found to be regulated through homotropic allosterism (Arutyunova et al., 2014).

It is interesting to consider the above model for BnaDGAT1 regulation in a physiological context. Acyl-CoAs are used in many other biochemical reactions (Ohlrogge and Jaworski, 1997) and the tight regulation of BnaDGAT1 activity may be needed to ensure that the enzyme is only highly active when there is a surplus of substrates for TAG biosynthesis. Long chain acyl-CoAs have been shown to have a regulatory role in mammalian lipid metabolism (Hu et al., 2005; Nagy et al., 2014). An early study implicated CoA and oleoyl-CoA as possible inhibitors of neutral lipase activity in the endosperm of 4 day old castor (*Ricinus communis*) seedlings (Hills et al., 1989). Acyl-CoAs were also shown to inhibit glucose-6-phosphate transporter and adenylate transporter in isolated plastids prepared from developing seeds of *B. napus*

(Fox et al., 2000). The inhibition of these transport proteins reduced the flux of carbon from glucose-6-phosphate or from acetate into long chain fatty acids. The rate of plant fatty acid biosynthesis, which determines the level of acyl-CoA, can vary greatly depending on various factors such as plant developmental stage, time of day and growth rate (Ohlrogge and Jaworski, 1997). The concentration of long chain acyl-CoA in developing *B. napus* seeds has been determined to be in the range of 3-6 μM (Larson and Graham, 2001). This is somewhat lower than the K_D of 17 μM determined for the binding of oleoyl-CoA to the recombinant N-terminal fragment of BnaA.DGAT1.b (Weselake et al., 2006). The availability of acyl-CoA under physiological conditions, however, has to be considered in terms the interaction of these thioesters with membranes and acyl-CoA binding proteins (Yurchenko and Weselake, 2011; Lung and Chye, 2016).

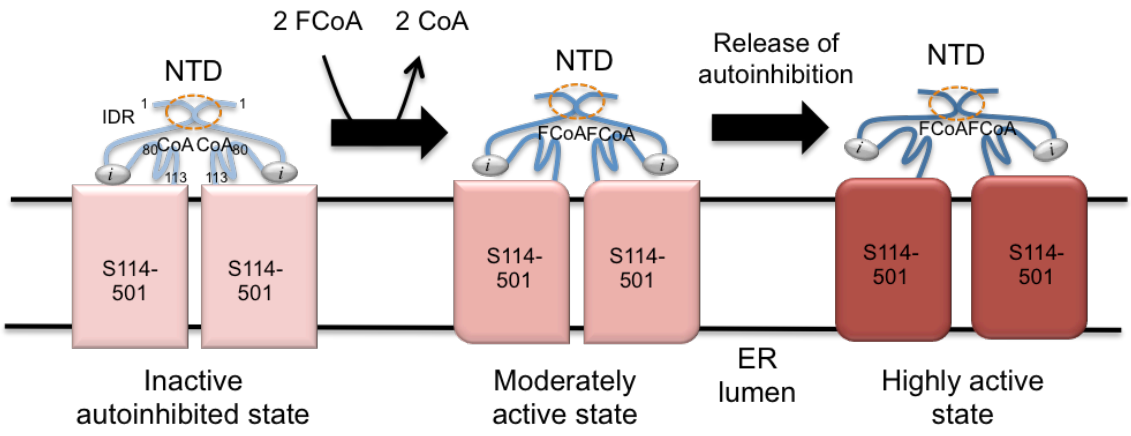

Figure 4.12. Proposed model for BnaDGAT1 regulation involving the hydrophilic N-terminal domain. The N-terminal domain (NTD) and the remainder of the enzyme (S114-501) are shown in blue and red, respectively. The enzyme initially exists in the inactive state with an autoinhibitor motif (*i*) in the N-terminal domain (amino acid residues 1-113) bound to S114-501, the latter of which houses the transmembrane segments and catalytic domain. High levels of Coenzyme A (CoA) stabilize the inactive state by binding to the allosteric site in the N-terminal domain. CoA can be displaced through increased availability of acyl-CoA (FCoA), which activates the enzyme by binding to the allosteric site. The binding of acyl-CoA activates the catalytic domain in S114-501 via a conformational change in the same polypeptide, and the signal is also transmitted to the other subunit through the dimerization segment (encircled) in the intrinsically disordered region (IDR) in the N-terminal domain. The release of the autoinhibitory region is hypothesized to lead to further conformational changes resulting to the highly active state.

Thus, it may be worthwhile to further explore activation of BnaDGAT1 in presence of acyl-CoA binding proteins or other acyl lipids. Given the absence of the acyl chain, free CoA concentrations are probably less affected by membranes and acyl-CoA binding proteins. In lyophilized developing Arabidopsis seeds, acyl-CoA content was determined to be over 10-fold greater than free CoA content (Gibon et al., 2002; Tumaney et al., 2004).

Physiologically, the situation may be more intricate *in vivo* due to different combinations of *B. napus* DGAT1 isoform monomers. Recently, it was reported that are four homologous *B. napus DGAT1* genes encoding four isoforms of the enzyme (Aznar-Moreno et al., 2015; Greer et al., 2015) referred to as BnaA.DGAT1.a, BnaA.DGAT1.b, BnaC.DGAT1.a (referred to as BnaDGAT1) and BnaC.DGAT1.b (Greer et al., 2015), with the main differences in amino acid sequence occurring in the IDR. The A and C genomes of *B. napus* each encode two isoforms of DGAT1 (Greer et al., 2015). Based on sequence identity, BnaA.DGAT1.a and BnaC.DGAT1.a belong to clade I whereas BnaA.DGAT1.b and BnaC.DGAT1.b belong to clade II (Greer et al., 2015; 2016). *In vitro* assays of DGAT activity with microsomes from yeast producing different recombinant isoforms of *B. napus* DGAT1 have shown that clade II enzymes exhibit a preference for linoleoyl-CoA as an acyl donor (Greer et al., 2016). Within the developing embryo of *B. napus* the possibility exists for the formation of dimers consisting of various combinations of the four BnaDGAT1 isoforms. Analysis of *B. napus DGAT1* transcripts has indicated that *BnaA.DGAT1.a* and *BnaC.DGAT1.a* are expressed at substantially higher levels than the two other transcripts (*BnaA.DGAT1.b* and *BnaC.DGAT1.b*), at all stages of seed development up to 35 days after flowering

(Aznar-Moreno et al., 2015). If it is assumed that the transcript levels are generally reflective of relative enzyme polypeptide levels, then the majority of *B. napus* DGAT1 dimers would be based on different combinations involving monomers BnaA.DGAT1.a and BnaC.DGAT1.a which are clade I enzymes that do not show a preference for linoleoyl-CoA.

4.5. Conclusion

This study sheds light on the regulatory function of the hydrophilic N-terminal domain of BnaDGAT1. This domain consists of an IDR and a folded allosteric site for binding of acyl-CoA and/or CoA. The regulatory roles of distinct portions of the N-terminal region were inferred through enzyme truncation and kinetic analysis. IDRs have been recently found to perform many functions than previously thought particularly in their role in cell signaling and regulation, and our results on the N-terminal domain agrees with the developing body of knowledge on IDRs. The 3D structure of the acyl-CoA/CoA binding site was also elucidated through solution NMR and the specific interactions with CoA were determined. BnaDGAT1 activity may be modulated based on the availability of acyl-CoA and CoA, and the ratio of the two metabolites.

CHAPTER 5

Brassica napus Diacylglycerol Acyltransferase 1 is Feedforward Activated by Phosphatidate and Inhibited by SnRK1-catalyzed Phosphorylation

5.1. Introduction

Triacylglycerol (TAG) is the main storage form of energy in oilseeds, which has served as a source of vegetable oil for food and industrial applications. TAG biosynthesis is composed of two phases, namely fatty acid biosynthesis and TAG assembly. Fatty acid biosynthesis occurs inside the plastid through the sequential action of acetyl-CoA carboxylase (ACCase) and the fatty acid synthase complex (Ohlrogge and Jaworski, 1997). ACCase catalyzes the carboxylation of acetyl-CoA to form malonyl-CoA, which serves as the 2-carbon donor to the growing acyl chain attached to the fatty acid synthase complex via the acyl carrier protein. In the second phase, the fatty acids formed in the plastids are transported into the endoplasmic reticulum for TAG assembly. TAG assembly involves acyl-CoA-dependent and acyl-CoA-independent pathways. The *sn*-glycerol-3-phosphate pathway, also known as the Kennedy pathway, involves the incorporation of three acyl chains from fatty acyl-CoA onto a glycerol backbone (Weiss et al., 1960; Chen et al., 2015). The first two acyl chains are added by the catalytic action of *sn*-glycerol-3-phosphate acyltransferase (GPAT) and lysophosphatidate acyltransferase (LPAAT) forming phosphatidate (PA). PA is then dephosphorylated to produce 1,2-diacyl-*sn*-glycerol (DAG) through the catalytic action of PA phosphatase. In oleaginous plants which form seed oils containing polyunsaturated fatty acids (PUFAs), the resulting DAG can be converted to phosphatidylcholine (PC) where further desaturation and acyl editing occur, with PUFA-enriched DAG eventually

returning to the Kennedy pathway (Chen et al., 2015). In addition, various processes, including acyl exchange, utilize polyunsaturated fatty acid (PUFA)-enriched PC as source of acyl chains to enrich the long chain acyl-CoA pool in PUFA thereby creating additional opportunities to enrich the PUFA content of TAG via the acyltransferases of the Kennedy pathway. The final reaction in the Kennedy pathway is driven by diacylglycerol acyltransferases (DGATs), which catalyze the acylation of DAG to produce TAG (Liu et al., 2012).

ACCase is a key regulatory enzyme in fatty acid biosynthesis. The regulation of animal, yeast and plant ACCases have been intensively investigated and found to operate under several layers of control. Plant plastidial ACCase is a heteromeric enzyme that is feedback inhibited by the level of oleoyl-ACP (Andre et al., 2012) and negatively regulated by a newly identified protein named biotin/lipoyl attachment domain containing proteins (Salie et al., 2016). In terms of TAG assembly, DGAT appears to substantially control the extent of oil accumulation in some oil crops, including canola (*Brassica napus* and *B. rapa*). The oil content of Arabidopsis and canola-type *B. napus* was found to correlate with the activity or expression level of DGAT (Jako et al., 2001; Weselake et al., 2008; Weselake et al., 2009). In addition, control analysis indicated that DGAT1 had a substantial effect on the flow of carbon into seed oil in *B. napus* (Weselake et al., 2008). In contrast to ACCase, the biochemical regulation of animal, plant or algal DGAT is not yet well-understood. DGATs can be grouped into three families. DGAT1 and DGAT2 are both membrane-bound enzymes but are non-homologous to one another, while DGAT3 is a soluble enzyme (Liu et al., 2012). Previously, various compounds including PA were found to stimulate the DGAT activity

in microsomes isolated from *B. napus* microspore-derived cell suspension cultures (Byers et al., 1999). In addition, *Tropaeolum majus* DGAT1 appeared to be more active upon mutation of a consensus site for sucrose non-fermenting-related kinase 1 (SnRK1) (Xu et al., 2008). The influence of PA and SnRK1 on plant DGAT activity, however, needs further investigation.

PA is an intermediate metabolite in both phospholipid and TAG biosynthesis. It is a minor component of the plant membrane lipids, accounting for less than 1% of phospholipids in most tissues (Welti et al., 2002). The cellular levels of PA, however, are dynamic and may increase dramatically under certain developmental and environmental conditions (Wang et al., 2006). PA has been shown to act as a secondary messenger in plant growth and development, as well as during stress (Testerink and Munnik, 2011). In addition, PA binds and influences the activity of various plant metabolic enzymes including phosphopenolpyruvate carboxylase (Monreal et al., 2010), phosphoethanolamine *N*-methyltransferase (Jost et al., 2009), monogalactosyldiacylglycerol synthase 1 (Dubots et al., 2010) and CTP:phosphocholine cytidylyltransferase (CCT) (Craddock et al., 2015).

Plant SnRK1 belongs to a subfamily of serine/threonine kinases that regulate metabolism in response to the energy state of the organism. It is homologous to yeast sucrose non-fermenting 1 (SNF1) protein kinase and mammalian AMP-activated protein kinase (AMPK). SnRK1, like SNF1 and AMPK, acts as energy sensor in metabolism and influences plant growth, development and the stress response (Broeckx et al., 2016). During metabolic stress or under depletion of glucose, these kinases activate catabolic pathways and inactivate anabolic processes either by altering gene expression or

phosphorylation of metabolic enzymes (Polge and Thomas, 2007). When the energy state of the plant is low or under stress, SnRK1 catalyzes the phosphorylation and subsequent inactivation of key enzymes involved in the biosynthesis of starch, amino acids and isoprenoids (Halford et al., 2003). It is also implicated in the regulation of transcription factors (e.g., bZIP) and regulatory proteins, which are a target of rapamycin kinase signaling (Hey et al., 2010). Recently, SnRK1-catalyzed phosphorylation was found to regulate the degradation of WRINKLED1, a transcription factor that positively regulates the expression of various lipid biosynthetic genes (Zhai et al., 2017). SnRK1 is responsive to sugar-phosphate levels when the energy state of the cell is high. Glucose-6-phosphate, trehalose-6-phosphate and glucose-1-phosphate were found to allosterically inhibit SnRK1 (Toroser et al., 2000; Zhang et al., 2009b; Nunes et al., 2013).

In this study, purified BnaDGAT1 (isoform BnaC.DGAT1.a) was lipidated through the addition of PC composed of different combinations of fatty acyl chains. The lipidated enzyme exhibited a hyperbolic response to increasing bulk concentrations of DAG whereas increasing acyl-CoA concentration resulted in a sigmoidal response. BnaDGAT1 activity was stimulated by PA and the enzyme was also a substrate of SnRK1, which catalyzes the phosphorylation of the enzyme converting it to a less active form.

5.2. Materials and Methods

5.2.1. Production and purification of recombinant BnaDGAT1

BnaDGAT1 cDNA was codon-optimized and synthesized by BioBasic Inc. (Ontario, Canada). The gene was cloned into pYES-NTA vector with His_{10} tag rather

than a His_6 for purification and enzymatic analysis. The vector was transformed into *Saccharomyces cerevisiae* B4744/H1246 and grown on agar plates with synthetic media lacking uracil. For recombinant protein production, a colony was picked and inoculated into a 10 mL synthetic media lacking uracil for overnight incubation at 30°C. The 10-mL seed culture was transferred into a 250 mL synthetic media and grown overnight at 30°C. The culture was transferred into induction media and grown overnight at 28°C and harvested after 24 h. The protein was then purified as previously described (Chapter 3; Caldo et al., 2015). Briefly, BnaDGAT1 in yeast microsomes was solubilized using 1% (w/v) n-dodecyl-β-D-maltopyranoside (DDM) for 2 h at 4°C. The mixture was then subjected to ultracentrifugation at 105,000 × *g* for 1 h. Detergent-solubilized BnaDGAT1 was incubated with 3 mL TALON® Metal Affinity Resin (Clontech) for 2 h with gentle rocking at 4°C. After packing the resin into Econo-Column® Chromatography Column, 1.5 × 20 cm (Bio-Rad), it was washed twice with 20 column volumes of 50 mM Tris HCL pH 8.0, 300 mM NaCl and 5% glycerol (Buffer A) with 5 mM imidazole and BnaDGAT1 was then eluted in Buffer A, stepwise, with increasing concentrations of imidazole (50–500 mM). SDS–PAGE was performed to analyze the purified fractions. The tag was removed through digestion with TEV protease (Sigma) at an optimized protein-TEV ratio of 0.1 mg of TEV per mg of BnaDGAT1. Finally, BnaDGAT1 was concentrated using Amicon Ultra-4 centrifugal filter units 100,000 NMWL (EMD Millipore) and loaded onto an FPLC-Superdex 200 13/30 (GE Healthcare Life Sciences) size-exclusion column pre-equilibrated with three column volumes of size-exclusion buffer (25 mM Tris–HCl, pH 8.0, containing 150 mM NaCl, 5% v/v glycerol, 1 mM EDTA and 0.05% w/v DDM). Size-exclusion standards (Bio-

Rad) were used to calibrate the column for the purpose of estimating the apparent molecular mass of the peaks. Protein samples at different stages of purification were analyzed using SDS–PAGE and stained with Coomassie Brilliant Blue.

5.2.2. Lipidation of purified BnaDGAT1

Purified BnaDGAT1 in DDM micelles was lipidated through the addition of PC to form mixed DDM-PC micelles. Initially, titration experiments with increasing amount of PC showed that 100 μM is needed to obtain maximum increase in activity. Different PCs with varying degree of unsaturation were used at 100 μM, including egg PC (, 1,2-dioleoyl-*sn*-glycero-3-PC, 1-palmitoyl-2-oleoyl-*sn*-glycero-3-PC, 1,2-disteroyl-*sn*-glycero-3-PC and soybean PC. All these PCs were obtained from Avanti Polar Lipids, Inc. These PCs were first resuspended in size-exclusion buffer without DDM (25 mM Tris–HCl, pH 8.0, containing 150 mM NaCl, 5% v/v glycerol, 1 mM EDTA) through sonication for 2 h at room temperature. They were then added with equal amount of BnaDGAT1 in size-exclusion buffer and the mixture was mixed at 20 rpm overnight at 4°C. The lipidated enzyme was found to have stable activity when stored at 4°C for a month.

5.2.3. DGAT1 activity assay

Purified protein samples were subjected to *in vitro* DGAT activity assay in a similar fashion to Byers et al. (1999). The assay was first optimized for purified BnaDGAT1 based on substrate saturation assay for each substrate. It was performed at 30°C for 1 min in a 60 μL reaction mixture containing 100 μM *sn*-1,2-diolein, 2 μM [^{14}C] oleoyl (18:1Δ^{9cis}; hereafter 18:1)-CoA, 200 mM HEPES-NaOH (pH 7.4) and 30 ng (purified) or 1 μg (microsomal) protein. Specifically, 100 μM *sn*-1,2-diolein and 2 μM

[^{14}C] 18:1-CoA were used based on the substrate saturation curve obtained for the purified enzyme. The reaction was quenched with 10 µL of 10% w/v SDS. The reaction mixture was applied onto a thin-layer chromatography plate with standards (0.25 mm Silica gel, DC-Fertigplatten). The plate was developed with hexane:diethyl ether:acetic acid (80:20:1, v/v/v). The products were visualized by phosphorimaging (Typhoon Trio Variable Mode Imager, GE Healthcare, QC, Canada). Spots corresponding to TAG were scraped and analyzed for radioactivity using Beckman-Coulter LS6500. For activity assays with PA, a reaction mixture cocktail without the enzyme was sonicated for 2 h prior the assay to ensure that PA is well-dispersed in solution.

5.2.4. Phosphorylation of BnaDGAT1 catalyzed by Arabidopsis SnRK1

The recombinant $(His)_6$-tagged SnRK1.1 kinase domain and GST-GRIK1 were expressed in *E. coli* and affinity-purified (Shen et al., 2009). SnRK1 was activated by GRIK1 and purified first with glutathione-Sepharose and then with NTA-Ni agarose, and stored in NTA-Ni elution buffer supplemented with 1 mM DTT in 50% glycerol (Greeley et al., unpublished). The DGAT1 substrates were first treated with cold ATP in a 45-µL reaction volume containing 10 µL 5x kinase buffer, 0.5 µL 10 mM ATP and 6.7 µL (1 µg) substrates at 30°C for 1 h. A mixture of 4.5 µL (0.5 µg) His-SnRK1(KD), or buffer only, and 0.5 µL 10 µCi/µL [γ-^{32}P]ATP was then added. The reactions were run for 30 min and stopped by addition of 50 µL 2x SDS-PAGE loading buffer and heat treatment at 50°C for 5 min. Forty microliters were loaded to a 9% gel for SDS-PAGE. After electrophoresis, the gel was stained in Coomassie Brilliant Blue, destained, and scanned in an Odyssey scanner (Licor) with 700-nm laser (84 µm resolution, high

quality, intensity 5) to obtain an image. The gel was dried and subjected to autoradiography.

5.3. Results

5.3.1. Purification and reconstitution of BnaDGAT1

Codon-optimized BnaDGAT1 was expressed in *S. cerevisiae* and purified as previously described (Chapter 3; Caldo et al., 2015). Briefly, yeast cells were harvested from a 2-L induction media, lysed and subjected to ultracentrifugation to recover the microsomal pellet. The membrane proteins were solubilized using DDM and the solubilized fraction was subjected to Co-TALON affinity purification and FPLC-size exclusion chromatography (Fig. 5.1A). Although the purified protein in DDM likely co-purified with yeast membrane lipids, the purified BnaDGAT1 was further lipidated through the addition of PCs with different fatty acyl chains to form mixed DDM-PC micelles. PC was chosen since it is the most abundant phospholipid in *B. napus* seeds (Katavic et al., 2006) and is commonly used in reconstituting membrane proteins (Maloney and Ambudkar, 1989). The various PCs were separately added into purified BnaDGAT1 in DDM micelles, and the activity of the enzyme was determined using an *in vitro* assay using [1-^{14}C]oleoyl-CoA as acyl-donor (Fig. 5.1B). Distearoyl-PC, having saturated acyl chains like DDM, did not change activity compared to BnaDGAT1 in DDM micelles. BnaDGAT1 exhibited highest activity in 16:0/18:1-PC (POPC) followed by egg PC having 1 and 1.6 average double bonds per PC molecule, respectively. A further increase in unsaturation was found to be unfavorable, with the enzyme becoming completely inactivated upon reconstitution with soybean (*Glycine max*) PC.

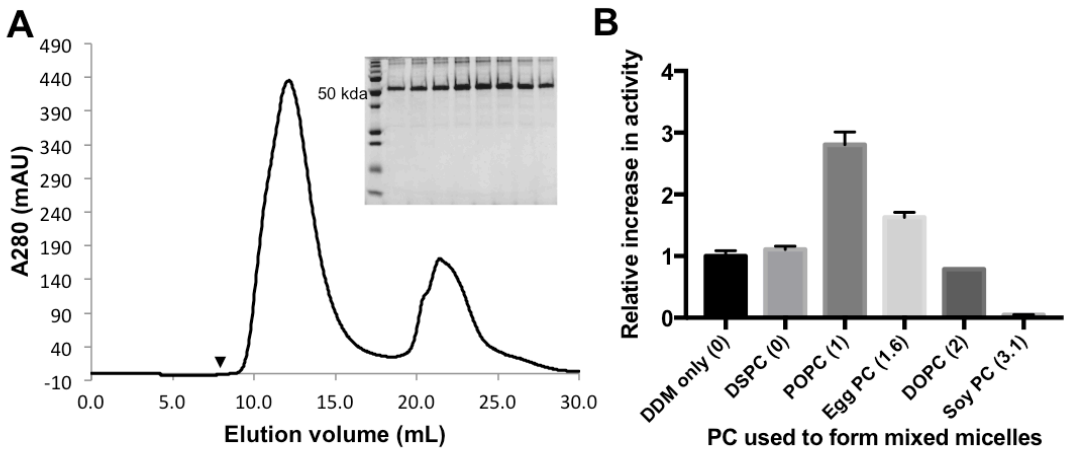

Figure 5.1. Purification and lipidation of BnaDGAT1. A, Size exclusion chromatography profile of BnaDGAT1 purification and SDS-PAGE of the fractions within the major peak corresponding to BnaDGAT1. An arrowhead indicates the position of the void volume. B, Relative increase in activity of purified BnaDGAT1 in DDM micelles after addition of different 1,2-diacyl-*sn*-glycero-3-phosphatidylcholine (PC). The abbreviations are as follows: DSPC, 1,2-distearoyl-*sn*-glycero-3-PC; POPC, 1-palmitoyl-2-oleoyl-*sn*-glycero-3-PC, DOPC: 1,2-dioleoyl-*sn*-glycero-3-PC. The average number of double bonds per PC molecule is indicated inside parenthesis. All lipids were purchased from Avanti Lipids, Inc. Reported values are means ± SD, n = 3.

Soybean PC is composed 63% linoleic acid (18:2$\Delta^{9cis,12cis}$; hereafter 18:2) , and has been used in the reconstitution of eukaryotic membrane proteins (Maloney and Ambudkar, 1989). We also tested the combination of PC with other phospholipids including phosphatidylserine, phosphatidylethanolamine and phosphatidylionositol, but no substantial effect on enzyme activity was observed (data not shown).

5.3.2. Kinetic properties of lipidated BnaDGAT1

The kinetic parameters of purified and lipidated BnaDGAT1 in mixed POPC-DDM micelles were evaluated. BnaDGAT1 has two substrates, a water-insoluble DAG and fatty acyl-CoA. The substrate saturation plot of BnaDGAT1 with respect to each substrate was determined. When DAG bulk concentration was increased at a constant oleoyl-CoA concentration, the activity response was hyperbolic reaching the asymptote at around 100 μM 1,2-dioleoyl-*sn*-glycerol (Fig. 5.2A). The plot was fitted with Michaelis-Menten equation and Hill equation but the former model was preferred based on R^2 values (Table 5.1). The maximal velocity and Michaelis constant were both reported as apparent values (apparent V_{max} and apparent K_m) since DAG and TAG are not truly soluble in the assay system thus bringing possible surface adsorption effects into play.

The substrate saturation plot for increasing oleoyl-CoA concentration at constant bulk DAG concentration exhibited a sigmoidal response (Fig. 5.2B). The plots of reaction velocity as a function of increasing oleoyl-CoA concentration were fitted with the Michaelis-Menten equation or the Hill model. Based on R^2 values, the Hill equation was the preferred model, suggesting that BnaDGAT1 exhibits cooperative substrate binding behavior with oleoyl-CoA (Table 5.1), as recently described for recombinant

BnaDGAT1 in yeast microsomes (Chapter 4; Xu et al., 2017). The microsomal preparation, however, is subject to possible interference with other proteins that interact with acyl-CoA, but the current results obtained with purified protein are similar to what was observed using microsomes containing recombinant enzyme. The Hill coefficient and $S_{0.5}$ of the plot was 2.74 and 1.6 μM, respectively. Interestingly, after the plot levels off near the maximum activity, a further increase in oleoyl-CoA concentration beyond 5 μM led to a substantial decrease in enzyme activity (Fig. 5.2C). The activity decreased steadily up to a concentration of 15 μM oleoyl-CoA. This suggests that BnaDGAT1 undergoes substrate inhibition. Once oleoyl-CoA concentrations beyond 5 μM are reached, the plot prefers a combined model for Hill equation and substrate inhibition, which was recently used to account for the effects of increasing oleoyl-CoA concentration on the activity of recombinant BnaDGAT1 in yeast microsomes (Xu et al., 2017). The combined model was previously proposed for another acyltransferase exhibiting the same kinetic behavior (Dovala et al., 2016).

The effect of bovine serum albumin (BSA) on the substrate saturation plot was also investigated (Fig. 5.2D) because BSA is used as an additive in *in vitro* DGAT assays (Little et al., 1994; Weselake, 2005a) although there is no general consensus on its use. BnaDGAT1 was less susceptible to substrate inhibition at 5-20 μM oleoyl-CoA in the presence of BSA at a concentration of 1 mg/mL. It can be noted, however, that the apparent V_{max} of the enzyme decreased from 123.1 ± 2.49 to 54.52 ± 2.23 nmol TAG/min/mg protein upon addition of BSA in the reaction mixture (Table 5.1). This may indicate that the effective concentration of acyl-CoA is reduced due to interaction with BSA.

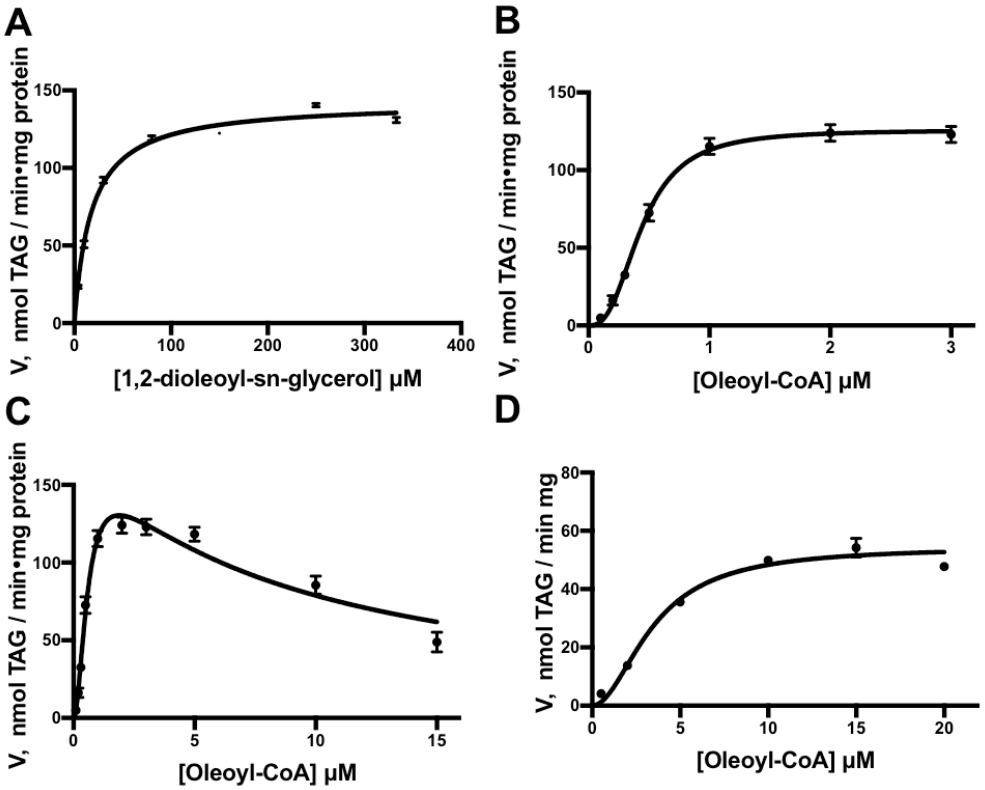

Figure 5.2. Substrate saturation assay of purified and lipidated BnaDGAT1.

Purified BnaDGAT1 in DDM micelles was lipidated through addition of 100 µM 1-palmitoyl-2-oleoyl-sn-glycero-3-phosphocholine and subjected to activity assays. A, Dependence of initial velocity on increasing bulk concentration of 1,2-dioleoyl-*sn*-glycerol. B, Dependence of initial velocity on increasing concentration of oleoyl-CoA (until no substrate inhibition observed) showing the sigmoidicity of the curve. C, Dependence of initial velocity on increasing concentration of oleoyl-CoA until 15 µM oleoyl-CoA. Substrate inhibition is observed beyond 5 µM oleoyl-CoA. D, Dependence of initial velocity on increasing concentration of oleoyl-CoA in the presence of 1 mg/mL bovine serum albumin (BSA). Previous studies conducted by us and others include BSA in DGAT1 activity assays (Aznar-Moreno et al., 2015, Siloto et al., 2009). Reported values are means ± SD, n = 3.

Table 5.1. Kinetic parameters of purified and lipidated BnaDGAT1. The plot of initial reaction velocity as a function of substrate concentration was fitted using the Michaelis-Menten equation or Hill equation using Graphpad Prism 7.0a. Values are means ± SD, n = 3.

	Diacylglycerol	**Oleoyl-CoA (low concentration)***	**Oleoyl-CoA (high concentration included)***	**Oleoyl-CoA (with 1 mg/mL BSA)**
Preferred model	Michaelis-Menten equation	Hill equation	Combined Hill equation and substrate inhibition (Dovala et al., 2016)	Hill equation
R^2	0.9971	0.9993	0.9723	0.9788
Apparent V_{max} (nmol TAG/ min/mg protein)	142.70 ± 2.49	123.1 ± 2.49	176.9 ± 13.6	54.52 ± 2.23
Apparent K_M or $S_{0.5}$** (μM)	17.50 ± 2.06	0.43 ± 0.02	0.62 ± 0.7	3.46 ± 0.26
Hill coefficient	1.09 ± 0.15	2.75 ± 0.24	1.90 ±0.21	1.94 ± 0.26

*Low concentration refers to a plot up to 3 micromolar where substrate inhibition is not yet observed. High concentration refers to a plot up to 15 micromolar where substrate inhibition is already observed. **The affinity constants for the Michaelis-Menten model and Hill equation are referredto as K_M and $S_{0.5}$, respectively.

5.3.3. Activation of BnaDGAT1 with phosphatidate

Enzymes are generally regulated by various physiological molecules that enable them to adjust to the metabolic state of the cell and the flux of metabolites in a pathway. PA is an intermediate in TAG and phospholipid biosynthesis (Chen et al., 2015). The effect of increasing concentration of 18:1/18:1-PA on the activity of purified and lipidated BnaDGAT1 (in DDM-POPC mixed micelles) was tested (Fig. 5.3A). The addition of PA was found to increase enzyme activity, with initial velocity doubling in the presence of only 10 μM PA. The enzyme activity increased by about 400% at the highest PA concentration considered. This result showed that 18:1/18:1-PA is a very potent activator of BnaDGAT1. When the effect of 100 μM 18:1/18:1-PA was evaluated at increasing oleoyl-CoA concentration, PA dramatically increased the apparent V_{max} of the enzyme from 123.1 ± 2.49 to 893.1 ± 29.01 nmol TAG/min/mg protein (Fig. 5.3B). In addition, the substrate saturation plot appeared more hyperbolic compared to one derived in the absence of PA. Detailed analysis revealed that the Hill coefficient of BnaDGAT1 decreased from 2.75 ± 0.24 to 1.61 ± 0.07 indicating that PA may have facilitated a conformational change to a more active state of BnaDGAT1 (Table 5.2). In addition, the enzyme was activated further at 10 μM oleoyl-CoA (Fig. 5.3C) where substrate inhibition was known to clearly occur in the absence of PA (Fig. 5.2C). This may indicate that the resulting conformational change upon PA binding desensitized the enzyme to substrate inhibition.

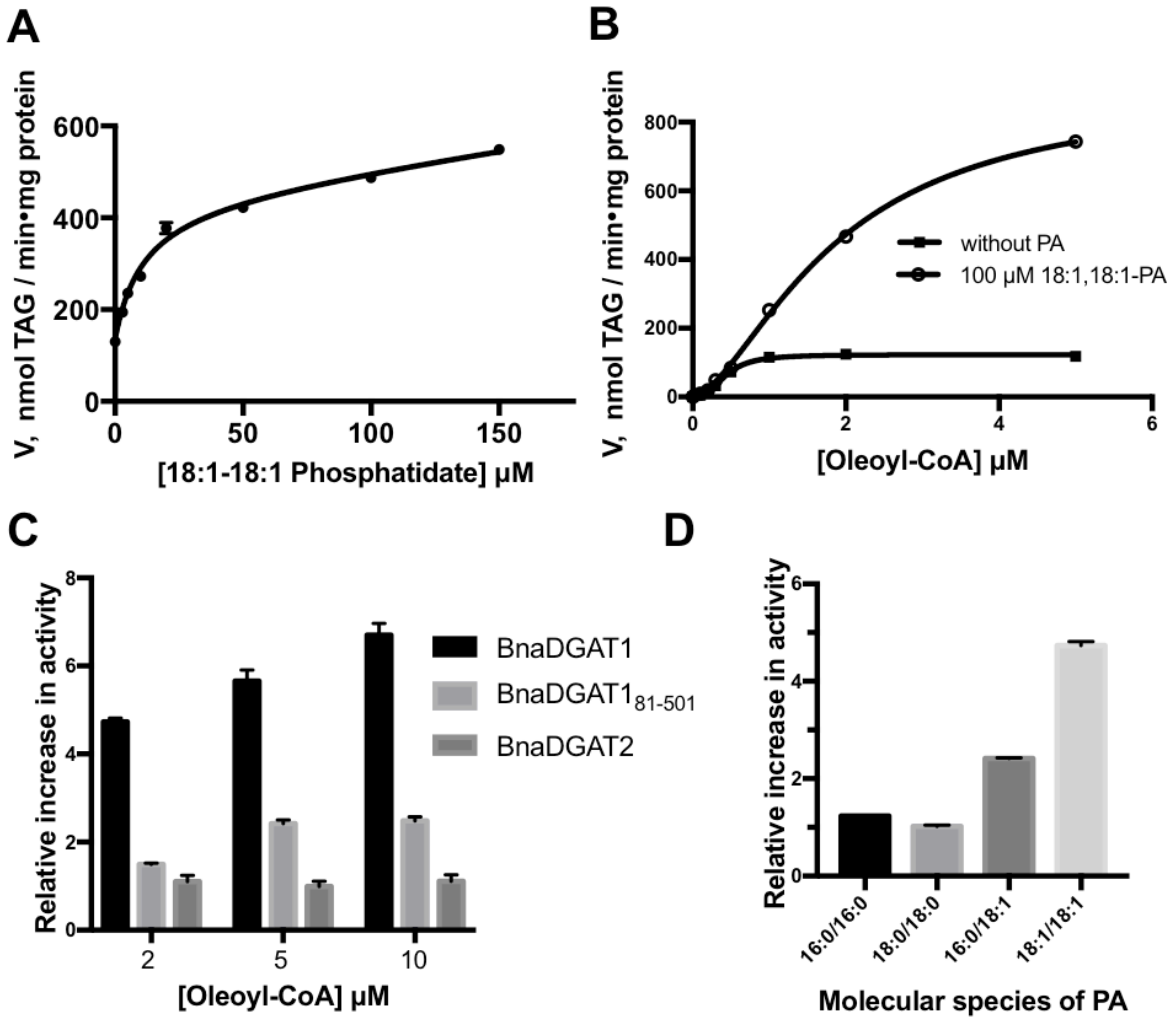

Figure 5.3. Feedforward activation of BnaDGAT1 by phosphatidate (PA).

A, Relative increase in purified and lipidated BnaDGAT1 activity upon addition of increasing concentration of 18:1/18:1-PA. B, Substrate saturation assay of purified and lipidated BnaDGAT1 in the presence of 100 µM 18:1/18:1-PA. The oleoyl-CoA saturation curve of BnaDGAT1 is also shown as reference. C, Relative increase in activity of microsomal BnaDGAT1, BnaDGAT1$_{81\text{-}501}$ and BnaDGAT2 at different concentrations of oleoyl-CoA upon addition of 100 µM 18:1/18:1-PA bulk concentration

in the reaction mixture. D, Relative increase in purified and lipidated BnaDGAT1 activity in the presence of different PAs at 100 μM bulk concentration. Reported values are means ± SD, n = 3.

Previously, we proposed the presence of an autoinhibitor motif within the BnaDGAT1 N-terminal domain, comprised by amino acid residues 1-80, since removal of this region appears to activate the enzyme (Chapter 4). The effect of PA on BnaDGAT1 devoid of the disordered segment (BnaDGAT1$_{81-501}$) was therefore evaluated. Due to the compromised recombinant production level of BnaDGAT1$_{81-501}$, purification of this enzyme form was unsuccessful. Microsomal BnaDGAT1 and BnaDGAT1$_{81-501}$ were then subjected to kinetic analysis in the presence or absence of PA (Fig. 5.3C). Microsomal BnaDGAT1 was activated by more than 4.7-fold in the presence of 2 μM oleoyl-CoA and 100 μM PA, similar to the purified and lipidated enzyme. On the other hand, BnaDGAT1$_{81-501}$, which is already more active than BnaDGAT1, was no longer as responsive to PA activation as full length BnaDGAT1. BnaDGAT1$_{81-501}$ was only activated by about 1.4-fold under the same conditions. Similar findings were observed at 5 and 10 μM oleoyl-CoA. This result suggests that PA activates BnaDGAT1 by influencing the autoinhibitor motif of the enzyme and as observed, PA no longer activates the truncated enzyme without the autoinhibitory motif to a great extent.

Recombinant BnaDGAT2 was also tested with PA. *BnaDGAT2* was codon-optimized and functionally expressed in H1246. As shown in Fig. 5.3C, microsomal recombinant BnaDGAT2 was not activated by PA. Therefore, PA-mediated feedforward activation seems to be specific to BnaDGAT1.

The effect of different molecular species of PA on activation of purified and lipidated BnaDGAT1 was also investigated (Fig. 5.3D). Unsaturated PAs were more

Table 5.2. Change in kinetic parameters of phosphatidate (PA)-activated BnaDGAT1. The plot of initial reaction velocity as a function of substrate concentration was fitted using the Michaelis-Menten equationor Hill equation using Graphpad Prism 7.0a. Values are means ± SD, n = 3

	Control	**With 100 µM bulk concentration PA**
R^2 for Michaelis-Menten equation	0.911	0.986
R^2 for Hill equation	0.9971	0.9993
V_{max} (nmol TAG/ min/mg protein)	123.1 ± 2.49	893.1 ± 29.01
Hill coefficient	2.75 ± 0.24	1.61 ± 0.07
$S_{0.5}$ (µM)	0.43 ± 0.02	1.86 ± 0.07

effective in activating BnaDGAT1. 18:1/18:1-PA and 16:0/18:1-PA activated BnaDGAT1 by about 4.7-fold and 2.4-fold, respectively (Fig. 5.3D). On the other hand, 16:0/16:0-PA only activated the enzyme by about 1.24 fold, while 18:0/18:0-PA had minimal effect on enzyme activity.

5.3.4. Inhibition of BnaDGAT1 through SnRK1 phosphorylation

BnaDGAT1 has a predicted SnRK1 phosphorylation site that appears to be conserved among plant DGAT1 (Fig. 5.4A). This site is localized in the cytosolic loop connecting the second and third predicted transmembrane segments, indicating that it is accessible to cytoplasmic kinases (Fig. 5.4B). Recombinant SnRK1 is first activated by geminivirus Rep interacting kinase-mediated phosphorylation (Shen et al., 2009). We tested if BnaDGAT1 is a substrate of SnRK1. BnaDGAT1 in DDM micelles and in PC-DDM micelles were incubated with activated SnRK1 using ^{32}P-ATP. The reactions were then subjected to SDS-PAGE and the gel with resolved proteins was dried. The dried gel was then exposed to a film revealing the location of BnaDGAT1. The corresponding positions in the autoradiogram showed that both BnaDGAT1 in DDM micelles and in PC-DDM micelles became radiolabeled with ^{32}P, indicating that BnaDGAT1 is phosphorylated by SnRK1 action (Fig. 5.4C). The negative control gave low signals on the blot, which may indicate the presence of BnaDGAT1 co-purified with a kinase. We then determined the specific activity of BnaDGAT1 before and after incubation with SnRK1. It was found that after 30 min incubation, the activity of BnaDGAT1 was reduced by about 40%, indicating that phosphorylation down-regulated the activity of the enzyme (Fig. 5.4D).

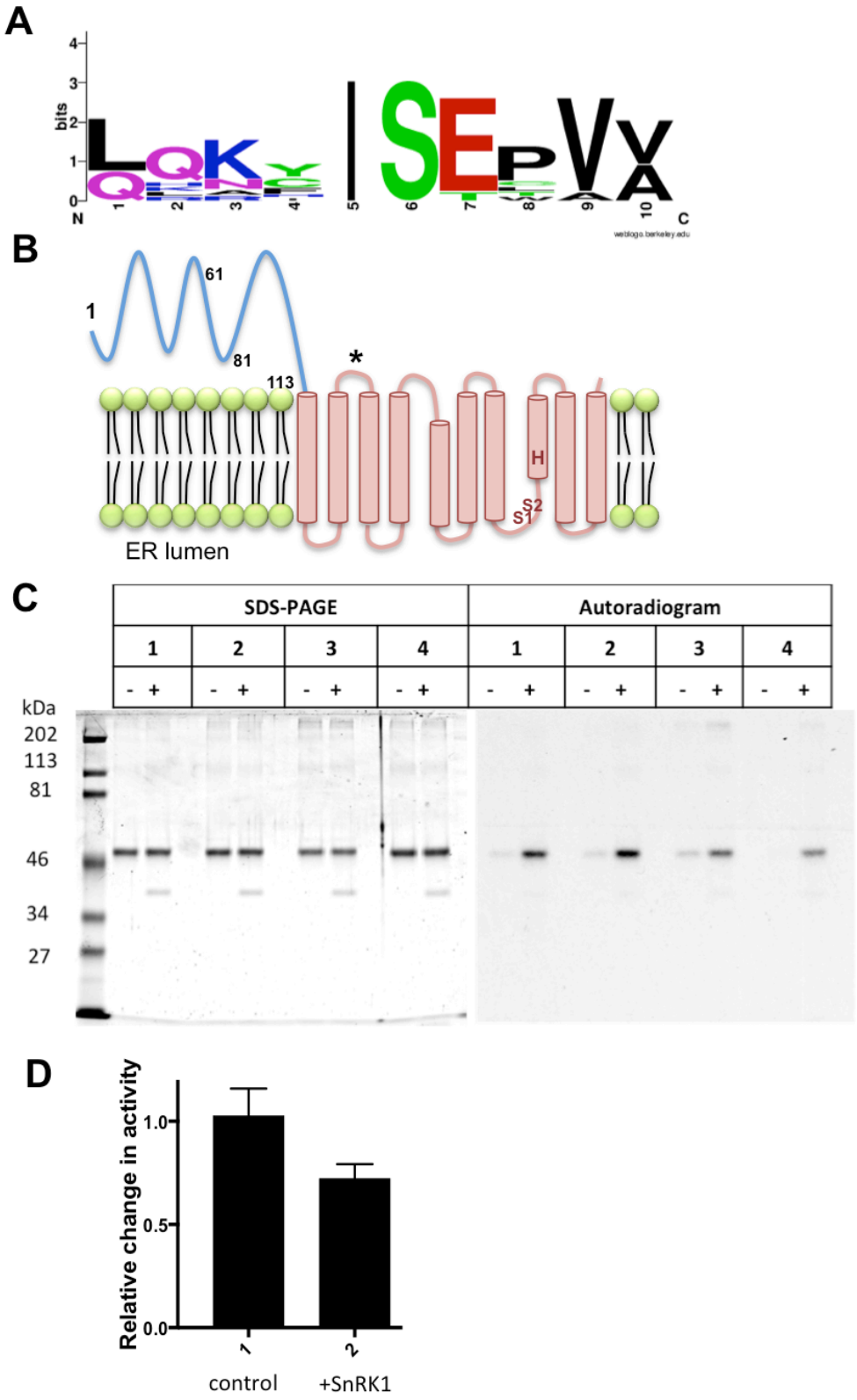
A
bits
N
C
B
1
61
81
113
*
H
S2
S1
ER lumen
C
SDS-PAGE
Autoradiogram
1
2
3
4
- +
kDa
202
113
81
46
34
27
D
Relative change in activity
1.0
0.5
0.0
control
+SnRK1

Figure 5.4. Inhibition of purified BnaDGAT1 via SnRK1-catalyzed phosphorylation. A, Sequence alignment of plant DGAT1 showing the highly conserved nature of the putative SnRK1 phosphorylation site. The SnRK1 consensus motif is indicated. B, Predicted topology of BnaDGAT1 showing the location of the putative SnRK1 phosphorylation site (indicated by an asterisk) in the cytoplasmic loop connecting the second and third transmembrane segment. C, SDS-PAGE and autoradiogram of resolved BnaDGAT1 before and after phosphorylation with SnRK1. Lanes 1 and 2 correspond to purified BnaDGAT1. Lanes 3 and 4 correspond to purified and lipidated BnaDGAT1. The plus (+) and minus (-) signs indicate the presence and absence of added SnRK1 kinase, respectively. D, DGAT1 activity before and after phosphorylation. Reported values are means ± SD, n = 3.

5.4. Discussion

In this study, the enzymatic activity of purified BnaDGAT1 was assessed after lipidation with different molecular species of PC. Results of the activity assays showed that the activity of the enzyme is greatly influenced by the nature of the PC side chains (Fig. 5.1B). The enzyme exhibited highest activity in 16:0/18:1-PC DDM mixed micelles. The PCs used have different numbers of double bonds per molecule, which can be correlated with membrane fluidity. The more double bonds present, the more dynamic is the bilayer. Membrane protein functions are regulated by lipid bilayer composition, mainly due to non-specific interactions that affect the deformation of the bilayer in response to protein conformational changes (Lundbaek et al., 2010). We then proceeded in using purified BnaDGAT1 in 16:0/18:1-PC DDM mixed micelles for the biochemical assays unless stated otherwise.

The lipidated BnaDGAT1 was subjected to substrate saturation assays with DAG and oleoyl-CoA (Fig. 5.2). It was found that BnaDGAT1 exhibits hyperbolic response to increasing concentration of bulk DAG. On the other hand, the lipidated enzyme exhibits sigmoidal response to increasing concentration of oleoyl-CoA (Fig.5.2). This agrees with previous reports on unpurified microsomal enzyme of *C. americana* DGAT1, *Z. mays* DGAT1 and BnaDGAT1 (Roesler et al., 2016; Chapter 4). Previous studies have shown that BnaDGAT1 can form oligomers, which indicate the existence of intermolecular communication between subunits (Caldo et al., 2015). This may enable the enzyme to adjust its activity based on acyl-CoA levels. DGAT1 was first identified due to its homology to ACAT 1. In contrast to DGAT1, the activity of ACAT1 exhibits sigmoidal response to increasing concentration of cholesterol (Chang et al., 1998). It was

also found to have two binding sites for cholesterol through competition studies with plant sterols, while DGAT1 was found to have two binding sites for acyl-CoA (Chapter 4).

At oleoyl-CoA concentrations above 5 μM, further increases in substrate concentration led to a decrease in enzyme activity (Fig. 5.2C). One plausible reason would be the formation of acyl-CoA micelles at higher concentration leading to decreased availability of acyl-CoA. The critical micelle concentration of acyl-CoA, however, is reported to be in the range of 33–67 μM (Constantinides and Steim, 1988; Wei et al., 2009). Other membrane-bound acyl transferases have been reported to exhibit increasing activity at high acyl-CoA concentration (greater than 5 to greater than 100 μM) (Chang et al., 1998; Kalscheuer and Steinbüchel, 2003; Stöveken et al., 2005).

If it is assumed that substrate inhibition is operative in the case of BnaDGAT1, then this may represent a mechanism to ensure that acyl-CoAs are not devoted entirely to TAG formation. It has been suggested that substrate inhibition can either be biologically relevant or just an artifact in the laboratory setting due to unusually high substrate concentration (Reed et al., 2010). Recently, Xu et al. (2017) identified a BnaDGAT1 variant, with single amino acid residue substitution, which is less susceptible to substrate inhibition. This study suggests that by changing specific amino acid residues, certain conformational changes may be observed in BnaDGAT1 that enable it to become less sensitive to substrate inhibition. It should be noted that substrate inhibition is also observed in other metabolic enzymes such as phosphofructokinase, which is a key glycolytic enzyme (Su and Storey, 1994). Phosphofructokinase uses ATP to catalyze the phosphorylation of fructose-6-phosphate but undergoes substrate

inhibition at high ATP concentration. This regulation ensures that the cell's carbon supply is not allocated mainly for ATP production when the energy state of the cell is already high (Reed et al., 2010).

The effect of PA on lipidated BnaDGAT1 was tested and it was found that PA acts as an activator of the enzyme (Fig. 5.3), consistent with an observation previously made using microsomes prepared from microspore-derived cell suspension cultures of *B. napus* (Byers et al., 1999). The previous study suggested that PA may be an allosteric activator of microsomal BnaDGAT or may serve as a substrate of microsomal PA phosphatase, which can channel endogenously-formed DAG more effectively into the subsequent DGAT-catalyzed reaction. The current study showed that purified BnaDGAT1 is activated by PA. Metabolite effectors generally bind to enzymes and initiate a conformational change. PA may bind to BnaDGAT1 causing a change to a more active conformation that is also more desensitized to substrate inhibition allowing the enzyme to operate efficiently under high local acyl-CoA levels. Although reported total acyl-CoA concentrations in the range of the range of 3-6 μM during seed development in *B. napus* (Larson and Graham, 2001), it is possible that higher localized concentrations may be prevalent *in vivo* at the site of TAG synthesis (Yurchenko et al., 2014). In addition, it was observed that molecular species of PA enriched in unsaturated acyl chains were more effective in activating the enzyme than PA containing saturated acyl chains. A previous study showed that newly produced fatty acids are targeted to undergo acyl editing (Bates et al., 2007). In this process, DAG enriched in 18:1 is initially converted to PC wherein 18:1 undergoes further desaturation to 18:2 and □-linolenic acid (18:3□^{9cis,12cis,15cis}). Movement of PUFAs from PC into the acyl-CoA pool

may involve acyl exchange and or the combined action of phospholipase A_2 and acyl-CoA synthetase (Chen et al., 2015). In essence, these processes would enrich the PUFA content of the acyl-CoA pool thus creating more opportunities to produce PA enriched in unsaturated fatty acids. Allowing BnaDGAT1 to be more responsive to unsaturated PA over saturated PA would ensure that sufficient editing of the acyl-CoA pool has occurred prior to stimulating TAG biosynthesis via the BnaDGAT1-catalyzed reaction.

The possible mechanism of activation by PA was investigated by determining the effect of PA on BnaDGAT1$_{81\text{-}501}$. Residues 1-80 correspond to a highly disordered segment, which appears to have an autoinhibitory motif that down-regulates enzyme activity. Without this motif, the enzyme is in a more active state (Chapter 4). Interestingly, it was found that the degree of activation of BnaDGAT$_{81\text{-}501}$ by PA is less compared to the full-length enzyme (Fig. 5.3C). Thus, the possible conformational change in BnaDGAT1 brought about by binding of PA may also result in displacement of the autoinhibitory motif. The effect of PA on BnaDGAT1 is incorporated into a model recently proposed which describes the regulation of BnaDGAT1 activity (Fig. 5.5) (Chapter 4). PA is proposed to cause a conformational change in the catalytic terminal domain of BnaDGAT1 and lead to displacement of the autohibitory motif. This results in the enzyme transitioning from a moderately active state to a highly active state. The proposed model shows that acyl-CoA or CoA can interact with the hydrophilic N-terminal domain of the BnaDGAT1 and allosterically regulate enzyme activity in the catalytic region which lies beyond the N-terminal domain. High acyl-CoA levels promote the moderately active state and high CoA levels promote the more inactive state.

PC biosynthesis, which includes the action of CCT and choline phosphotransferase (CPT), has been studied extensively in mammalian systems (Fagone and Jackowski, 2013). CCT catalyzes the formation of CDP-choline which in turn is transferred to DAG via the catalytic action of CPT. This pathway is shown in relation to the Kennedy pathway in plants in Figure 5.6 (Craddock et al., 2015). BnaDGAT1 is very similar to CCT1 in that this enzyme also has an autoinhibitory motif within a regulatory region that has a propensity to become disordered (Ding et al., 2012). In addition, a recent study in Arabidopsis has shown that PA activates CCT1 while CCT1 with truncated region encompassing the autoinhibitory motif could no longer be activated by PA (Craddock et al., 2015). CCT1 is a key enzyme in the nucleotide pathway for PC synthesis whereas DGAT1 activity has been shown to have a substantial effect on the flow of carbon into seed TAG in members of the Brassicaceae (Jako et al., 2001; Weselake et al., 2008; Weselake et al., 2009). Thus, the co- activation of CCT1 and DGAT1 may ensure that phospholipid synthesis keeps pace with TAG and oil body formation in the developing zygotic embryo of Brassicaceae members such as Arabidopsis and *B. napus* (Fig. 5.6). Previously, it was proposed that oil bodies pinch off of the ER surrounded by a monolayer of phospholipid molecules (Huang, 1996). In general, the activation of CCT1 would stimulate additional membrane synthesis to sustain oil body production. It is important to note that DAG is also converted to PC for formation of PUFA and acyl editing of both *de novo* formed DAG and the acyl-CoA pool (for reviews see Bates and Browse, 2012; Chen et al., 2015).

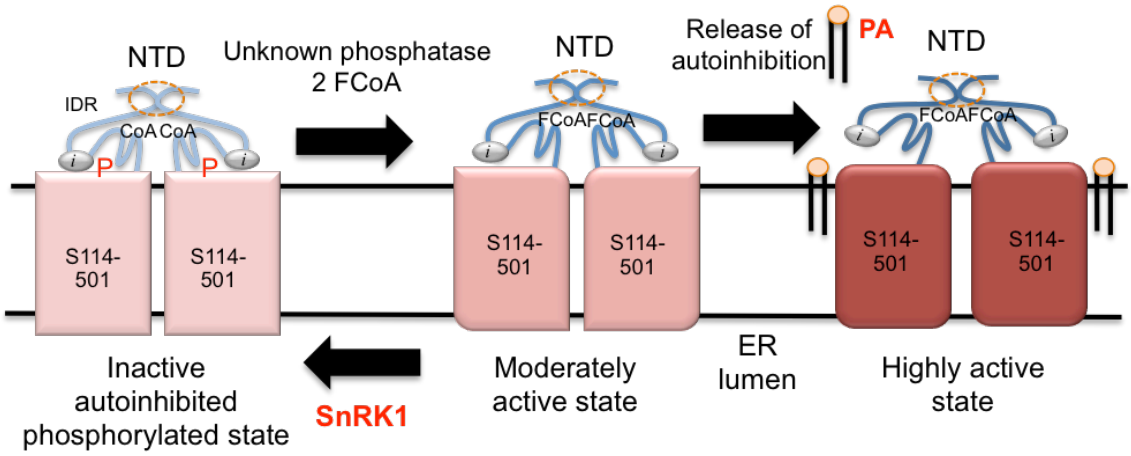

Figure 5.5. Proposed model for regulation of BnaDGAT1 activity incorporating feedforward activation and phosphorylation. Phosphatidate (PA) serves as a feedforward activator of BnaDGAT1, possibly by binding to and initiating a conformational change in the membrane-bound catalytic domain and displacing the proposed autoinhibitory motif. The proposed model shows that acyl-CoA or CoA can interact with the hydrophilic N-terminal domain of the BnaDGAT1 and allosterically regulate enzyme activity in the catalytic region which lies beyond the N-terminal domain (Caldo et al., under review). High acyl-CoA levels promote the moderately active state and high CoA levels promote the more inactive state. BnaDGAT1 is also a substrate of SnRK1, which can phosphorylate the enzyme and convert it to a less active form. An unknown protein phosphatase may be involved in the dephosphorylation and activation of the inactive enzyme.

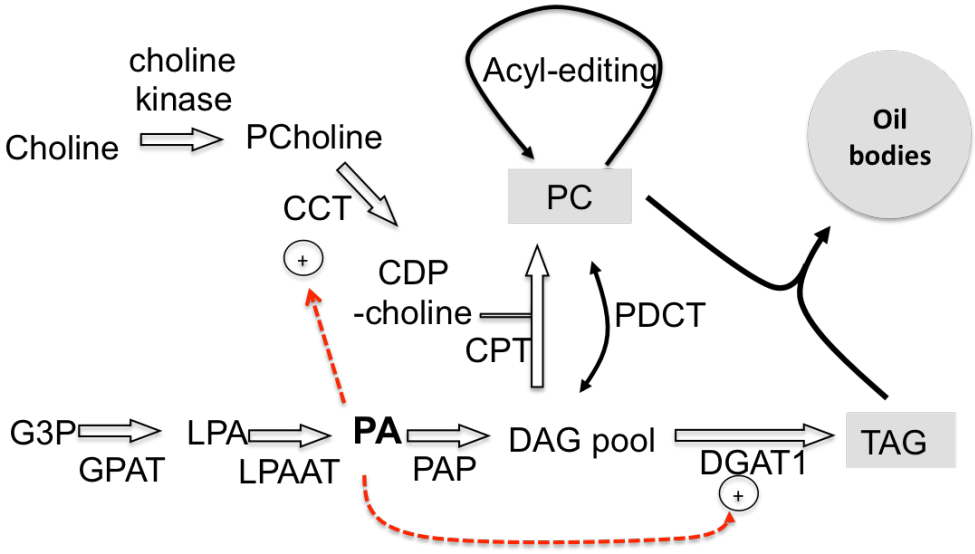

Figure 5.6. Phosphatidate (PA) allows the concomitant activation of phosphatidylcholine (PC) and triacylglycerol (TAG) biosynthesis through feedforward activation of CTP:Phosphocholine cytidyltransferase 1 (CCT1) and diacylglyerol acyltransferases 1 (DGAT1), respectively. PC is needed to package TAG into oil bodies. 1,2-diacyl-*sn*-glycerol (DAG) from the Kennedy pathway can also be converted to PC for formation of polyunsaturated fatty acids (PUFA) and acyl-editing to ultimately generate DAG and acyl-CoA enriched in PUFA. Other abbreviations: G3P, *sn*-glycerol-3-phosohate; LPA, lysophosphatidate; GPAT, *sn*-glycerol-3-phosphate acyltransferase; LPAAT, lysophosphatidate acyltransferase; PAP, phosphatidic acid phosphatase; PCholine, phosphocholine; CPT, choline phosphotransferase; PDCT, phosphatidylcholine:diacylglycerol cholinephosphotransferase. Image generated based on information from Weiss and Kennedy (1956), Bates and Browse (2012), Chen et al. (2015) and Craddock et al. (2015).

It is interesting to interpret early metabolic engineering results in the light of our newly discovered effect of PA on increasing BnaDGAT1 activity. Previously, Zou et al. (1997) reported that over-expression of a gene encoding a putative yeast *sn*-2 acyltransferase with LPAAT activity led to increased seed oil content when constitutively expressed in Arabidopsis or *B. napus* (Zou et al., 1997). Later, the same yeast gene was used to increase seed oil content in soybean via seed specific expression (Rao and Hildebrand, 2009). In addition, the overexpression of a cDNA encoding a *B. napus* LPAAT in Arabidopsis also increased seed oil content (Maisonneuve et al., 2010). Perhaps transformation of Arabidopsis or *B. napus* by genes or cDNAs encoding enzymes with LPAAT activity leads to elevated levels of PA which in turn stimulate DGAT1 activity, which has been clearly shown to be important in controlling the flow of carbon into seed TAG (Jako et al., 2001; Weselake et al., 2008; Weselake et al., 2009).

Phosphorylation of BnaDGAT1 represents another mode of regulation explored in the current study. Plants encode a large number of protein kinases that may enable them to adapt to the changing environmental conditions. Kinases are enzymes that catalyze the phosphorylation of metabolic enzymes, which may be activated or deactivated by this modification. Previous studies on *Tropaeolum majus* DGAT1 suggested that the presence of an SnRK1 phosphorylation motif in plant DGAT1 (Xu et al., 2008). Subsequent substitution of the amino acid residue undergoing phosphorylation with an alanine residue followed by production of recombinant enzyme in yeast or Arabidopsis led to enzymes with higher activity *in vitro*. In the current study, direct evidence is provided which shows that the phosphorylation of BnaDGAT1 is catalyzed by SnRK1

(Fig. 5.4). It has been previously established that SnRK1 catalyzes the phosphorylation and subsequent inactivation of sucrose-phosphate synthase, nitrate reductase and HMG-CoA reductase, which are key enzymes in the biosynthesis of starch, proteins, and isoprenoids, respectively (Halford et al., 2003; Broeckx et al., 2016). The current results show that SnRK1 also directly regulates TAG biosynthesis via down-regulation of DGAT1 activity. Recently, WRINKLED1, a positive regulator of lipid biosynthetic gene expression, was shown to be a substrate of SnRK1 (Zhai et al., 2017). The SnRK1-mediated phosphorylation of WRINKLED1 rendered this transcription factor more susceptible to ubiquitination and subsequent degradation, which can result in a reduced rate of lipid accumulation. SnRK1, therefore, can regulate TAG biosynthesis both at the transcriptional and post-translational levels. In a similar manner, SnRK1 has also been previously found to activate expression of genes encoding enzymes involved in sucrose catabolism, in addition to inactivating sucrose-phosphate synthase through post-translational phosphorylation (Halford et al., 2003). In the model for BnaDGAT1 regulation in Fig. 5.5, SnRK1 action is shown to contribute to transitioning the enzyme from the moderately active state to the inactive phosphorylated state. An unknown protein phosphatase may be involved in converting the down-regulated enzyme to a more active form. SnRK1 is known as the energy sensor of the cell and the current results suggest that it can also regulate the formation of highly reduced and energy-rich TAGs.

In conclusion, this study provides further insight into the regulation of BnaDGAT1 activity and the possible coordination of storage lipid biosynthesis and oil body formation with membrane biosynthesis in the developing zygotic embryo of Arabidopsis

or *B. napus*. The new information on regulation of BnaDGAT1 activity by PA and SnRK1-catalyzed phosphorylation may also serve as basis for developing biotechnological strategies for further increasing seed oil content in the *Brassicaceae* and other oleaginous species. For example, enhancing the expression of *LPAAT* in combination with *CCT1* and *DGAT1* during seed development would provide higher levels of PA (via increased LPAAT activity) to activate increased amounts of CCT1 and DGAT1 which would in turn lead to increased production of membrane and TAG, respectively, to in turn facilitate more extensive oil body formation. In addition, modification of the SnRK1 phosphorylation site in DGAT1, to prevent phosphorylation, using genome editing could result in increased DGAT 1 activity during seed development to fuel increased TAG accumulation.

CHAPTER 6

General Discussion

The first phase of the doctoral dissertation was to highly purify recombinant *Brasicca napus* diacylglycerol acyltransferase 1 (DGAT1) in active form for biochemical and biophysical characterization of the enzyme, and for crystallization trials. *B. napus* contains four DGAT1 isoforms (Greer et., 2015; 2016), which are highly homologous to the sole Arabidopsis DGAT1. More specifically, this doctoral dissertation focused on BnaC.DGAT1.a isoform (BnaDGAT1) for purification and subsequent characterization since this isoform was used for directed evolution and could be produced at high levels in yeast (*Saccharomyces cerevisiae*) (Siloto et al., 2009a; Greer et al., 2015; Chen et al., 2017). The purification procedure, illustrated in Figure 6.1, resulted in an active well-folded enzyme in n-dodecyl-β-D-maltopyranoside (DDM) micelles. This represents the first report of a purification procedure, implementing column chromatography, resulting in a highly purified and active enzyme for any membrane-bound DGAT. Previously, Lardizabal et al. (2001) partially purified DGAT2 in active form from a fungal source using column chromatography. The purified BnaDGAT1 in DDM micelles eluted mainly as a dimer with a minor tetrameric peak. This is in agreement with previous studies indicating the ability of DGAT1 enzymes from various sources to form dimers and tetramers (Cheng et al., 2001; Weselake et al., 2006; McFie et al., 2010). Purified BnaDGAT1 also exhibited high substrate specificity for α-linolenoyl-Coenzyme A (CoA), similar to that found for this microsomal BnaDGAT1 isoform (BnaC.DGAT1.a) (Greer et al., 2016), indicating that the folded structure in DDM

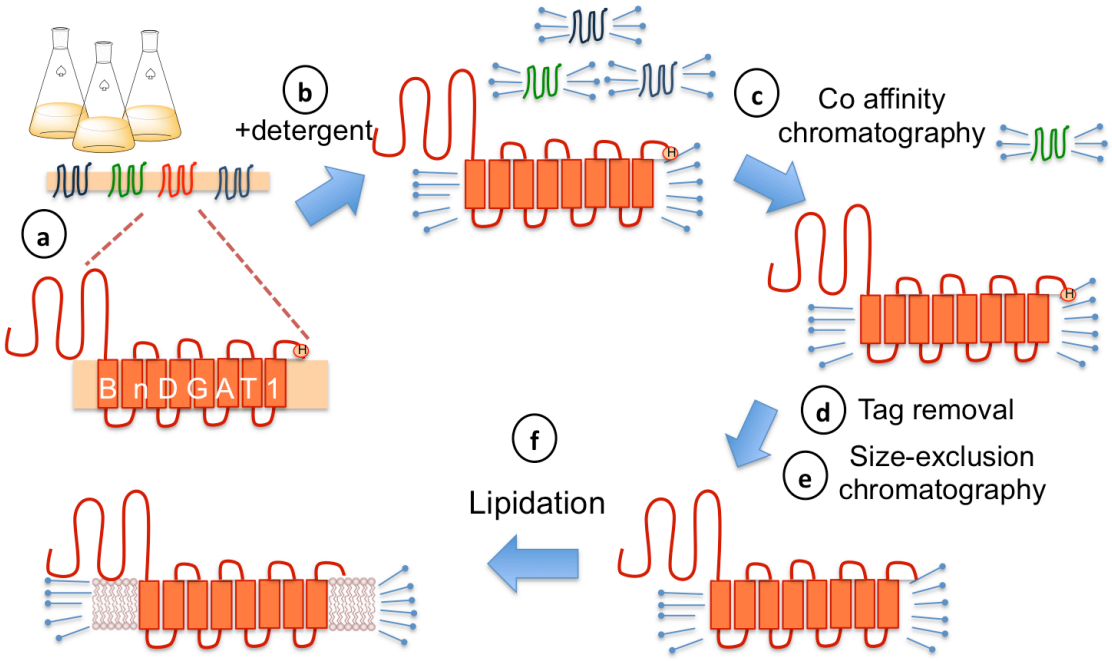

Figure 6.1. Purification scheme optimized for BnaDGAT1. a) Codon-optimized BnaDGAT1 is recombinantly produced in *S. cerevisiae* and the membrane fraction is isolated. b) Membrane-bound enzymes are solubilized in n-dodecyl-β-D-maltopyranoside (DDM) detergent. c) Solubilized BnaDGAT1 is partially purified using cobalt (Co) affinity chromatography. d) The poly-histidine tag is removed through protease treatment with tobacco etch virus protease. e) The partially purified enzyme is further purified using size-exclusion chromatography. f) Purified BnaDGAT1 in DDM micelles is lipidated with phosphatidylcholine.

likely resembles the native form. Having purified BnaDGAT1 opened up several possibilities to probe the structure-function in the enzyme and the possible mode of enzyme regulation. Future work with the purified protein may involve the elucidation of the three-dimensional enzyme structure either through X-ray crystallography or cryo-electron microscopy. It should be noted that several crystallization trials were attempted during this thesis project without success.

To further mimic the bilayer conditions, the purified protein was lipidated through addition of phosphatidylcholine (PC) (Chapter 5). The presence of different PCs, varying in the degree of unsaturation of the acyl chains, resulted in different degrees of enzyme activation (Fig. 5.1B). The most effective molecular species of PC was 1-palmitoyl-2-oleoyl-*sn*-glycero-PC, which increased BnaDGAT1 activity by three-fold. Therefore, purified BnaDGAT1 (Table 3.2) would exhibit a specific activity of about 80 nmol TAG/min/mg protein when treated with this molecular species of PC. Since BnaDGAT1 would naturally exist in the presence of PC in the ER, the enzyme would likely be in the lipidated and more active state.

An earlier study demonstrated that developing seeds of *B. napus* L. cv Westar, harvested at about 30 days after flowering, exhibit a DGAT activity of about 40 pmol TAG/min/seed (Weselake et al., 1993). Assuming that BnaDGAT1 is the major class of DGAT (rather than DGAT2) contributing to TAG biosynthesis in *B. napus* and that the enzyme was assayed under similar conditions (Chapter 3), it is estimated that 100 developing seeds would contain about 50 μg of BnaDGAT1. Microspore-derived cell suspension cultures of *B. napus* L. cv Jet Neuf have also been used to study storage lipid biosynthesis and DGAT activity (Weselake and Taylor, 1999; Weselake, 2000; 2005b).

In an earlier study by Weselake et al. (1993), it was shown that the cells, from the cell suspension culture, exhibited a DGAT activity of about 25 pmol TAG/min/gram of fresh weight. Therefore, it is estimated 100 g of sedimented cells (obtained at 7 days post-subculture) would contain about 30 μg of BnaDGAT1. These estimations suggest that BnaDGAT1 is present in relatively low abundance in both developing seeds and microspore-derived cell suspension cultures of *B. napus*. In contrast, the recombinant BnaDGAT1 content of a 60 mL of suspended yeast microsomes from a 3-L yeast culture is about 9.84 mg (Table 3.2). Thus, earlier attempts at purifying DGAT from natural sources, such as microspore-derived cell suspension cultures of *B. napus* (Little et al., 1994), were plagued by the low content of enzyme in the starting material.

Detailed kinetic analysis of purified and lipidated BnaDGAT1 revealed insights on how BnaDGAT1 operates in the membrane. Purified and lipidated BnaDGAT1 exhibited positive cooperativity with increasing concentrations of acyl-CoA in the reaction mixture. This behavior was also observed with recombinant BnaDGAT1 in yeast microsomes, which is in agreement with recent studies on *Corylus americana* and *Zea mays* DGAT1 (Roesler et al., 2016). BnaDGAT1 cooperativity appears to be influenced by dimerization (intermolecular) and the presence of an allosteric site for acyl-CoA/CoA (intramolecular). Consequently, when the enzyme was truncated at the N-terminus, which spans a possible oligomerization domain, the degree of cooperativity decreased. The intrinsically disordered region (IDR) of the hydrophilic N-terminal domain also contained an autoinhibitory motif. Future work may involve mutational analysis to probe the exact location of the autoinhibitory sequence in the IDR as well as the dimerization interface.

Top down control analysis of fatty acid biosynthesis and TAG assembly suggests that most of the control (70%) of TAG accumulation in *B. napus* is associated with TAG assembly rather than fatty acid biosynthesis (Weselake et al., 2008). Seed specific over-expression of *DGAT1*, however, has been shown to reduce the control exerted by the process of TAG assembly to about 50% with shared control of about 50% by fatty acid biosynthesis (Weselake et al., 2008). More specifically, the level of DGAT activity appears to have a substantial effect on the flow of carbon into TAG (Weselake et al., 2008; Weselake et al., 2009). Thus, given the influence of BnaDGAT1 activity on carbon flow towards TAG, it seems reasonable that this enzyme may have regulatory properties which allow it to respond to varying metabolic conditions. This doctoral dissertation identified three BnaDGAT1 allosteric effectors. CoA was found to serve as an inhibitor whereas acyl-CoA and phosphatidate (PA) were found to activate BnaDGAT. CoA is also the product of the DGAT-catalyzed reaction and acyl-CoA also serves as a substrate (or acyl donor) of DGAT. Prior to this study, there is little information available on the biochemical regulation of TAG assembly enzymes (Fig. 2.3) and the results of this study filled in gap in knowledge.

The mode of action of the identified BnaDGAT1 effectors was investigated in detail. Acyl-CoA was found to be an allosteric activator of BnaDGAT1, specifically binding to the folded segment of the hydrophilic N-terminal domain. The binding of acyl-CoA in this site may induce the conversion of the enzyme into the more active state in a process known as homotropic allosteric activation. Mutational analysis of this acyl-CoA binding site resulted in a BnaDGAT1 variant with lower apparent V_{max} and lower Hill coefficient than the native recombinant enzyme, suggesting the reduced ability of

the variant to transition into the more active state. Aside from being an important intermediate in TAG biosynthesis, acyl-CoA has also been found to modulate the activity of other enzymes. Palmitoyl-CoA is a feedback inhibitor of animal ACCase (Ogiwaraet al., 1978), while 18:1-ACP serves as the counterpart inhibitor of the plant plastidial ACCase (Andre et al., 2012). The same acyl-CoA binding motif site in the hydrophilic N-terminal domain of BnaDGAT1 also binds CoA, which was characterized as a non-competitive feedback inhibitor of BnaDGAT1. CoAs are normally esterified to acyl chains, and the high levels of CoA indicate that the acyl-CoAs have been depleted and that there is a need to slow down the use of acyl-CoAs in TAG biosynthesis. It is possible that other enzymes involved in acyl-CoA metabolism may be regulated by acyl-CoA:CoA ratio. As mentioned earlier, animal and plant ACCases are inhibited by palmitoyl-CoA and oleoyl-ACP, respectively, and previous reports indicate that spinach and rat liver ACCases are both activated by CoA (Laing and Roughan, 1982 and Yeh et al., 1981). Future studies on other acyltransferases may be pursued to determine their possible sensitivity to acyl-CoA:CoA ratio. Other enzymes have also been found to be sensitive to the ratio of different metabolite forms, as the predominance of one form over the other accurately gives an exact indication of the metabolic status of the cell. One good example is the adenylate pool, which serves as important enzyme effector in metabolism in addition to its role as energy carriers. Each adenylate form (ATP versus ADP/AMP) generally exerts opposing effects on the activity of enzymes that are responsive to at least two adenylates (Atkinson, 1966). As an example, ATP allosterically inhibits animal PFK while AMP activates the enzyme (Plaxton, 1996). Other enzymes regulated by the ATP:(AMP/ADP) ratio include isocitrate

dehydrogenase (Kornberg and Pricer, 1950; Lin et al., 2001), muscle glycogen phosphorylase (Barford et al., 1991), muscle 6-phosphofructo-1-kinase (Zancan et al., 2008) and liver fructose-1,6-bisphosphatase (Marcus and Hosey, 1980).

The hydrophilic N-terminal regulatory domain of BnaDGAT1 contains an allosteric site for CoA and acyl-CoA. The purified and lipidated BnaDGAT1 has a Hill coefficient of 2.75, which may indicate the presence of more than two acyl-CoA binding sites in one BnaDGAT1 dimer. Previous binding experiments with acyl-CoA and the hydrophilic N-terminal domain of BnaDGAT1 support the presence of an allosteric site in the N-terminal domain of BnaDGAT1 (Weselake et al., 2006), suggesting that a dimeric BnaDGAT1 may bind four acyl-CoAs. Interestingly, a truncated BnaDGAT1 with a deleted segment spanning the possible dimerization region still exhibited positive cooperativity. This suggests that monomeric BnaDGAT1 with an allosteric site for acyl-CoA undergoes homotropic allosteric activation. Homotropic activation achieved through the binding of acyl-CoA at an allosteric site subsequently leads to a conformational change in the catalytic domain causing an increase in activity. This process of conformational shift can be further understood once a structure of the full enzyme is available. It is possible that the ability of the hydrophilic N-terminal domain of BnaDGAT1 to adjust activity based on the acyl-CoA/CoA pool is also present in other enzymes which use acyl-CoA as substrate. This mode of regulation can be considered as way for membrane-embedded BnaDGAT1 to communicate with the metabolic status of the cytosol.

Phosphatidate (PA) is a very important signalling molecule in plants affecting many processes related to growth, development, and stress responses (Testerink and

Munnik, 2011). In addition to its role as signalling molecule, PA may also be an effector modulating lipid homeostasis (Fig. 6.2). In this doctoral dissertation, PA was identified as a feedforward activator of BnaDGAT1. The increased flux of substrates into the Kennedy pathway calls for a need to stimulate BnaDGAT1 as it catalyzes the final step in TAG biosynthesis, and PA may play an important role in this synchronization. Furthermore, PA has been found to activate cytidine triphosphate:phosphocholine cytidyltransferase (CCT) (Craddock et al., 2015) and inhibit phosphoethanolamine *N*-methyltransferase (PEAMT) (Jost et al., 2009), which are important regulatory steps in the biosynthesis of PC. Increasing levels of PA result in the activation of CCT, which provides phosphocholine for the formation of PC via the CCT pathway. This high PA level may also indicate that precursor levels for CCT pathway are sufficient and there is no need for additional PC biosynthesis via the PEAMT-catalyzed reaction. PA also activates monogalactosyldiacylglycerol synthase 1 (MDG1), which catalyzes a key step in galactolipid biosynthesis in the chloroplast (Dubots et al., 2010).

The mechanism by which PA affects protein function is still unknown, although there are studies that suggest that PA binding induces protein conformational changes (Testerink and Munnik, 2005; Raghu et al., 2009). The interaction is proposed to be mainly due to ionic/hydrogen bond interactions between the negatively charged phosphate of PA and positively charged side chains of lysine or arginine residues (Kooijman et al., 2007). The other proposed mechanism does not involve direct

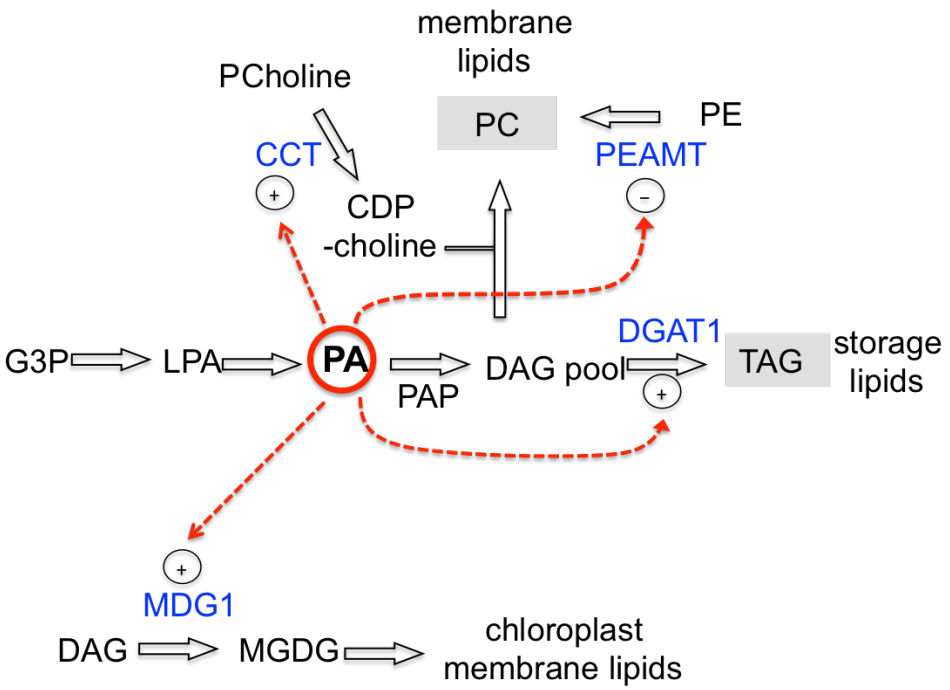

Figure 6.2. Phosphatidate (PA) is emerging as a key effector regulating lipid homeostasis, in addition to being an important precursor for major membrane and storage lipids. PA has been found to influence the activity of regulatory enzymes in lipid biosynthesis such as cytidine triphosphate:phosphocholine cytidyltransferase (CCT) and phosphoethanolamine *N*-methyltransferase (PEAMT) in PC biosynthesis, diacylglycerol acyltransferase 1 (DGAT1) in TAG biosynthesis and MDG1 in galactolipid biosynthesis. Other abbreviations: CDP-choline, cytidine diphosphate-choline; DAG, 1,2-diacyl-*sn*-glycerol; G3P, *sn*-glycerol-3-phosphate; LPA, lysophosphatidate; MDG1, monogalactosyldiacylglycerol synthase 1; MGDG, monogalactosyldiacylglycerol; PAP, phosphatidic acid phosphatase; PC, phosphatidylcholine; PE, phosphatidylethanolamine; PCholine, phosphocholine; TAG, triacylglycerol. The information used to develop this figure are from Jost et al. (2009), Dubots et al. (2010), Craddock et al. (2015), and the current findings.

interaction with PA, but is based on the ability of PA to affect the curvature and charge of the lipid bilayer. This may lead to altered membrane architecture, which may have a direct consequence on the function of target proteins (Kooijman and Burger, 2009). The presence of PA activated BnaDGAT1 by possibly interacting directly with the enzyme and favoring the transition into the more active state. The resulting conformational change may have rendered the enzyme more resilient to substrate inhibition as observed through kinetic analysis. Future characterization of the PA-binding site on BnaDGAT1 may reveal important insights on the specificity of PA binding and mechanism of activation.

It would be interesting to consider the influence of PA in TAG biosynthesis in the context of PC biosynthesis since this metabolite serves as feedforward activator of both CCT and DGAT1. The concomitant activation of these two enzymes may be needed to ensure that the increased accumulation of TAG is accompanied by increased PC biosynthesis, so as to efficiently package into oil bodies, which is composed of a TAG core surrounded by phospholipid monolayer. This coordination of CCT and DGAT1 activity may also ensure that the ER is not depleted of PC components used for oil body formation when the seed is actively synthesizing TAG.

Lysophosphatidate acyltransferase (LPAAT) catalyzes the formation of PA from LPA and acyl-CoA. The over-expression of a gene encoding a putative yeast *sn*-2 acyltransferase in Arabidopsis, *B. napus* or soybean has been shown to result in higher seed oil content (Zou et al., 1997; Rao and Hildebrand, 2009). The over-expression of *LPAAT* from *B. napus* also led to increased seed oil content in Arabidopsis (Maisonneuve et al., 2010). Recently, heterologous expression of peanut *LPAAT2* in

Arabidopsis increased seed oil content in transgenic lines (Chen et al., 2015). Thus, it is possible that the increased formation of PA due to increased *sn*-2 acyltransferase levels may have stimulated DGAT1 resulting in higher seed oil accumulation. The co-expression of *Cuphea LPAAT2* and *DGAT1* in developing seeds of *Camelina sativa* also led to higher medium chain fatty acids in the seed oil, indicating that LPAAT activity thus may influence on DGAT1 (Iskandarov et al., 2017). In future work, it would be interesting to check for a possible physical interaction between LPAAT2 and DGAT1 which may allow direct channeling of PA generated by the LPAAT-catalyzed reaction to the PA effector site on DGAT1.

This doctoral dissertation also confirmed that BnaDGAT1 is a substrate of sucrose non-fermenting-related kinase 1 (SnRK1). SnRK1 action has been shown to modulate the key enzymes in anabolic pathways such as those involved in the biosynthesis of sucrose, protein and isoprenoids (Fig. 6.3). In this doctoral dissertation, SnRK1 catalyzed the phosphorylation of BnaDGAT1 so as to down-regulate the activity of the enzyme. Previously, mutation of this putative SnRK1 phosphorylation site in *Tropaeolum majus* DGAT1 abolished its down-regulatory effect resulting in an enzyme variant with higher activity (Xu et al., 2008). This variant was able to increase seed oil content in Arabidopsis to higher levels relative to the wild-type enzyme. Recently, it was also shown that SnRK1 catalyzes the phosphorylation of WRINKLED1, a transcription factor that positively regulates lipid biosynthesis (Zhai et al., 2017). This post-translational modification of WRINKLED1 resulted in less lipid accumulation because SnRK1-mediated phosphorylation rendered the transcription factor more susceptible to ubiquitination and subsequent degradation.

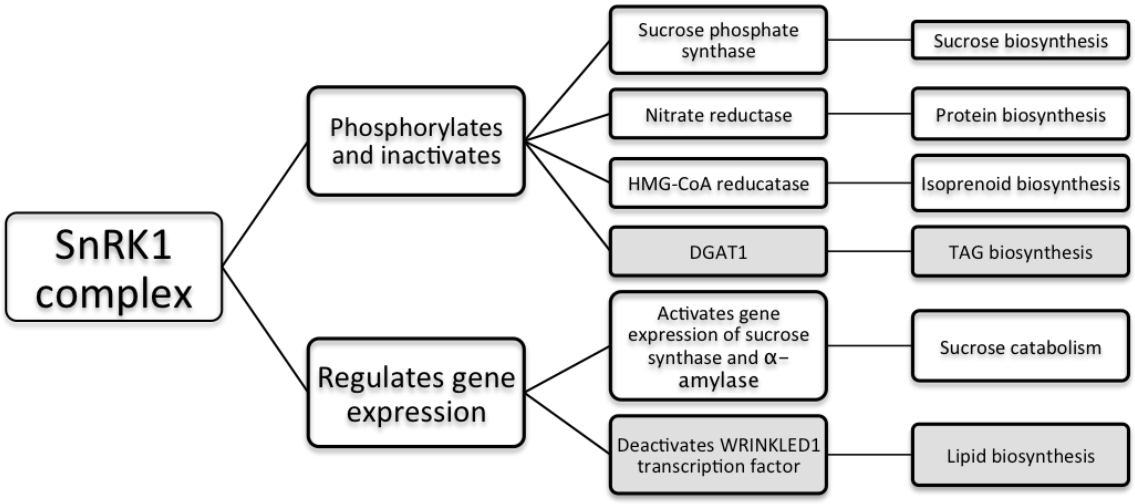

Figure 6.3. SnRK1 regulates key enzymes that are directly and indirectly involved in carbon metabolism. When the energy level is low, SnRK1 can directly catalyze the phosphorylation and inactivation of biosynthetic enzymes directly and indirectly involved in carbon anabolism. SnRK1 phosphorylation can also affect gene expression. It can activate the transcription of enzymes involved in sucrose catabolism and deactivates the transcription factor needed for gene expression of lipid biosynthetic enzymes. This figure was adapted from Halford et al. (2003) and updated based on a recent study by Zhai et al. (2017), and the current findings. Abbreviations: DGAT1, diacylglycerol acyltransferase 1; HMG-CoA, 3-hydroxy-3-methyl-glutaryl-coenzyme A; TAG, triacylglycerol.

In summary, the results of this doctoral dissertation shed light on the regulation of TAG assembly via DGAT1, which appears to have a relatively large influence on the extent of seed oil accumulation in canola-type *B. napus* and other oleaginous organisms. Structure-function studies to probe enzyme action and regulation were conducted using purified recombinant enzyme and recombinant enzyme in yeast microsomes. The hydrophilic N-terminal domain of BnaDGAT1 was shown to be the enzyme's regulatory domain, which includes two distinct segments, namely an IDR and folded segment. Dimeric BnaDGAT1 exhibited positive cooperativity with respect to increasing acyl-CoA concentration presumably allowing the enzyme subunits to finely adjust their activity based on acyl-CoA levels. The allosteric site for acyl-CoA was identified within the folded segment of the hydrophilic N-terminal domain indicating that cooperativity may also be partly accounted for by homotropic allosteric activation. In addition, the N-terminal domain interacted with CoA, which was identified as a non-competitive feedback inhibitor of the enzyme. CoA may accumulate under depleting acyl-CoA conditions. The N-terminal domain may possibly act as a sensor of acyl-CoA:CoA ratio, allowing the fine-tuning of the rate of intramembrane TAG formation in relation to prevailing cytosolic conditions. In addition, PA was shown to activate BnaDGAT1 through the feedforward activation. Since PA also activates CCT, PA mediated activation of DGAT1 may ensure that the final step of TAG biosynthesis is coordinated with effective oil body formation. Lastly, SnRK1-catalyzed phosphorylation was found to decrease BnaDGAT1 activity, thereby demonstrating that TAG biosynthesis is directly modulated by SnRK1, which appears to be key regulator of carbon metabolism in plants.

REFERENCES

Ahmad I, Sharma AK, Daniell H, Kumar S (2015) Altered lipid composition and enhanced lipid production in green microalga by introduction of brassica diacylglycerol acyltransferase 2. Plant Biotechnol J **13:** 540–550

Alameldin H, Izadi-Darbandi A, Smith SA, Balan V (2017) Metabolic engineering to increase the corn seed storage lipid quantity and change its compositional quality. Crop Sci **57:** 1–11

Alban C, Baldet P, Douce R (1994) Localization and characterization of two structurally different forms of acetyl-CoA carboxylase in young pea leaves, of which one is sensitive to aryloxyphenoxypropionate herbicides. Biochem J **300:** 557–565

Andersson M, Wettesten M, Borén J, Magnusson A, Sjöberg A, Rustaeus S, Olofsson SO (1994) Purification of diacylglycerol:acyltransferase from rat liver to near homogeneity. J Lipid Res **35:** 535–545

Andre C, Haslam RP, Shanklin J (2012) Feedback regulation of plastidic acetyl-CoA carboxylase by 18:1-acyl carrier protein in *Brassica napus*. Proc Natl Acad Sci U S A **109:** 10107–10112

Andrews J, Keegstra K (1983) Acyl-CoA synthetase is located in the outer membrane and acyl-CoA thioesterase in the inner membrane of pea chloroplast envelopes. Plant Physiol **72:** 735–740

Andrianov V, Borisjuk N, Pogrebnyak N, Brinker A, Dixon J, Spitsin S, Flynn J, Matyszczuk P, Andryszak K, Laurelli M, Golovkin M, Koprowski H (2010)

Tobacco as a production platform for biofuel: overexpression of *Arabidopsis* DGAT and LEC2 genes increases accumulation and shifts the composition of lipids in green biomass. Plant Biotechnol J **8:** 277–287

Anobom CD, Pinheiro AS, De-Andrade RA, Aguieiras EC, Andrade GC, Moura MV, Almeida RV, Freire DM (2014) From structure to catalysis: recent developments in the biotechnological applications of lipases. Biomed Res Int **2014:** 684506

Arutyunova E, Panwar P, Skiba PM, Gale N, Mak MW, Lemieux MJ (2014) Allosteric regulation of rhomboid intramembrane proteolysis. EMBO J **33:** 1869–1881

Atkinson DE (1968) The energy charge of the adenylate pool as a regulatory parameter. Interaction with feedback modifiers. Biochemistry **7:** 4030–4034

Aymé L, Baud S, Dubreucq B, Joffre F, Chardot T (2014) Function and localization of the *Arabidopsis thaliana* diacylglycerol acyltransferase DGAT2 expressed in yeast. PLoS One **9:** e92237

Aymé L, Jolivet P, Nicaud JM, Chardot T (2015) Molecular characterization of the *Elaeis guineensis* medium-chain fatty acid diacylglycerol acyltransferase DGAT1-1 by heterologous expression in *Yarrowia lipolytica*. PLoS One **10:** e0143113

Aznar-Moreno J, Denolf P, Van Audenhove K, De Bodt S, Engelen S, Fahy D, Wallis JG, Browse J (2015) Type 1 diacylglycerol acyltransferases of *Brassica napus* preferentially incorporate oleic acid into triacylglycerol. J Exp Bot **66:** 6497–6506

Barford D, Hu SH, Johnson LN (1991) Structural mechanism for glycogen

phosphorylase control by phosphorylation and AMP. J Mol Biol **218:** 233–260

Bates PD, Durrett TP, Ohlrogge JB, Pollard M (2009) Analysis of acyl fluxes through multiple pathways of triacylglycerol synthesis in developing soybean embryos. Plant Physiol **150:** 55–72

Bates PD, Ohlrogge JB, Pollard M (2007) Incorporation of newly synthesized fatty acids into cytosolic glycerolipids in pea leaves occurs via acyl editing. J Biol Chem **282:** 31206–31216

Bates PD, Browse J (2012) The significance of different diacylgycerol synthesis pathways on plant oil composition and bioengineering. Front Plant Sci **3:** 147

Bayon S, Chen G, Weselake RJ, Browse J (2015) A small phospholipase A2-α from castor catalyzes the removal of hydroxy fatty acids from phosphatidylcholine in transgenic *Arabidopsis* seeds. Plant Physiol **167:** 1259–1270

Beisson F, Li Y, Bonaventure G, Pollard M, Ohlrogge JB (2007) The acyltransferase GPAT5 is required for the synthesis of suberin in seed coat and root of *Arabidopsis*. Plant Cell **19:** 351–368

Bernerth R, Frentzen M (1990) Utilization of erucoyl-CoA by acyltransferases from developing seeds of *Brassica napus* (L.) involved in triacylglycerol biosynthesis. Plant Sci **67:** 21–28

Bilder P, Lightle S, Bainbridge G, Ohren J, Finzel B, Sun F, Holley S, Al-Kassim L, Spessard C, Melnick M, Newcomer M, Waldrop GL (2006) The structure of the carboxyltransferase component of acetyl-CoA carboxylase reveals a zinc-binding motif unique to the bacterial enzyme. Biochemistry **45:** 1712–1722

Birch AM, Buckett LK, Turnbull AV (2010) DGAT1 inhibitors as anti-obesity and

anti-diabetic agents. Curr Opin Drug Discov Devel **13:** 489–496

Blom N, Gammeltoft S, Brunak S (1999) Sequence and structure-based prediction of eukaryotic protein phosphorylation sites. J Mol Biol **294:** 1351–1362

Bourgis F, Kader JC, Barret P, Renard M, Robinson D, Robinson C, Delseny M, Roscoe TJ (1999) A plastidial lysophosphatidic acid acyltransferase from oilseed rape. Plant Physiol **120:** 913–922

Bouvier-Navé P, Benveniste P, Oelkers P, Sturley SL, Schaller H (2000) Expression in yeast and tobacco of plant cDNAs encoding acyl-CoA:diacylglycerol acyltransferase. Eur J Biochem **267:** 85–96

Bradford MM (1976) A rapid and sensitive method for the quantitation of microgram quantities of protein utilizing the principle of protein-dye binding. Anal Biochem **72:** 248–254

Broeckx T, Hulsmans S, Rolland F (2016) The plant energy sensor: evolutionary conservation and divergence of SnRK1 structure, regulation, and function. J Exp Bot **67:** 6215–6252

Brooks CL, Morrison M, Joanne Lemieux M (2013) Rapid expression screening of eukaryotic membrane proteins in *Pichia pastoris*. Protein Sci **22:** 425–433

Broussard TC, Kobe MJ, Pakhomova S, Neau DB, Price AE, Champion TS, Waldrop GL (2013) The three-dimensional structure of the biotin carboxylase-biotin carboxyl carrier protein complex of *E. coli* acetyl-CoA carboxylase. Structure **21:** 650–657

Brown CJ, Takayama S, Campen AM, Vise P, Marshall TW, Oldfield CJ, Williams CJ, Dunker AK (2002) Evolutionary rate heterogeneity in proteins with long

disordered regions. J Mol Evol **55:** 104–110

Browse J, Somerville CR (1991) Glycerolipid synthesis: biochemistry and regulation. Annu Rev Plant Physiol Plant Mol Bio **42:** 467–506

Browse J, Warwick N, Somerville CR, Slack CR (1986) Fluxes through the prokaryotic and eukaryotic pathways of lipid synthesis in the '16:3' plant *Arabidopsis thaliana*. Biochem J **235:** 25–31

Budde RJ, Fang TK, Randall DD (1988) Regulation of the phosphorylation of mitochondrial pyruvate dehydrogenase complex in situ: effects of respiratory substrates and calcium. Plant Physiol **88:** 1031–1036

Burgal J, Shockey J, Lu C, Dyer J, Larson T, Graham I, Browse J (2008) Metabolic engineering of hydroxy fatty acid production in plants: RcDGAT2 drives dramatic increases in ricinoleate levels in seed oil. Plant Biotechnol J **6:** 819–831

Bürgi J, Xue B, Uversky VN, van der Goot FG (2016) Intrinsic disorder in transmembrane proteins: roles in signaling and topology prediction. PLoS One **11:** e0158594

Byers SD, Laroche A, Smith KC, Weselake R (1998) Probing the regulation of diacylglycerol acyltransferase from microspore-derived cell suspension cultures cilseed rape. Adv in Plant Lipid Res 191–193

Byers SD, Laroche A, Smith KC, Weselake RJ (1999) Factors enhancing diacylglycerol acyltransferase activity in microsomes from cell-suspension cultures of oilseed rape. Lipids **34:** 1143–1149

Caldo KMP, Acedo JZ, Panigrahi R, Vederas JC, Weselake RJ, Lemieux MJ (2017) Diacylglycerol acyltransferase 1 is regulated by its N-terminal domain in

response to allosteric effectors. Plant Physiol **175:** 667–680

Caldo KM, Greer MS, Chen G, Lemieux MJ, Weselake RJ (2015) Purification and properties of recombinant *Brassica napus* diacylglycerol acyltransferase 1. FEBS Lett **589:** 773–778

Cai Y, Goodman JM, Pyc M, Mullen RT, Dyer JM, Chapman KD (2015) *Arabidopsis* SEIPIN proteins modulate triacylglycerol accumulation and influence lipid droplet proliferation. Plant Cell **27:** 2616–2636

Cao H, Chapital DC, Shockey JM, Klasson KT (2011) Expression of tung tree diacylglycerol acyltransferase 1 in *E. coli*. BMC Biotechnol **11:** 73

Cao J, Cheng L, Shi Y (2007) Catalytic properties of MGAT3, a putative triacylgycerol synthase. J Lipid Res **48:** 583–591

Cao YZ, Huang AH (1987) Acyl-coenzyme A preference of diacylglycerol acyltransferase from the maturing seeds of cuphea, maize, rapeseed, and canola. Plant Physiol **84:** 762–765

Carman GM, Han GS (2009) Phosphatidic acid phosphatase, a key enzyme in the regulation of lipid synthesis. J Biol Chem **284:** 2593–2597

Cases S, Smith SJ, Zheng YW, Myers HM, Lear SR, Sande E, Novak S, Collins C, Welch CB, Lusis AJ, Erickson SK, Farese RV (1998) Identification of a gene encoding an acyl-CoA:diacylglycerol acyltransferase, a key enzyme in triacylglycerol synthesis. Proc Natl Acad Sci U S A **95:** 13018–13023

Cases S, Stone SJ, Zhou P, Yen E, Tow B, Lardizabal KD, Voelker T, Farese RV (2001) Cloning of DGAT2, a second mammalian diacylglycerol acyltransferase, and related family members. J Biol Chem **276:** 38870–38876

Cernac A, Benning C (2004) WRINKLED1 encodes an AP2/EREB domain protein involved in the control of storage compound biosynthesis in *Arabidopsis*. Plant J **40:** 575–585

Chang CC, Huh HY, Cadigan KM, Chang TY (1993) Molecular cloning and functional expression of human acyl-coenzyme A:cholesterol acyltransferase cDNA in mutant Chinese hamster ovary cells. J Biol Chem **268:** 20747–20755

Chang CC, Lee CY, Chang ET, Cruz JC, Levesque MC, Chang TY (1998) Recombinant acyl-CoA:cholesterol acyltransferase-1 (ACAT-1) purified to essential homogeneity utilizes cholesterol in mixed micelles or in vesicles in a highly cooperative manner. J Biol Chem **273:** 35132–35141

Chang CCY, Sun J, Chang TY (2011) Membrane-bound O-acyltransferases (MBOATs). Frontiers in Biology **6:** 177

Chapman KD, Dyer JM, Mullen RT (2012) Biogenesis and functions of lipid droplets in plants: Thematic Review Series: Lipid Droplet Synthesis and Metabolism: from Yeast to Man. J Lipid Res **53:** 215–226

Chapman KD, Ohlrogge JB (2012) Compartmentation of triacylglycerol accumulation in plants. J Biol Chem **287:** 2288–2294

Chen G, Woodfield HK, Pan X, Harwood JL, Weselake RJ (2015) Acyl-trafficking during plant oil accumulation. Lipids **50:** 1057–1068

Chen G, Xu Y, Siloto R, Caldo KMP, Vanhercke T, El Tahchy A, Niesner N, Chen Y, Mietkiewska E, Weselake RJ (2017) High performance variants of plant diacylglycerol acyltransferase 1 generated by directed evolution provide insights into structure-function. Plant J *In press*

Chen JE, Smith AG (2012) A look at diacylglycerol acyltransferases (DGATs) in algae. J Biotechnol **162:** 28–39

Chen JC, Tsai CC, Tzen JT (1999) Cloning and secondary structure analysis of caleosin, a unique calcium-binding protein in oil bodies of plant seeds. Plant Cell Physiol **40:** 1079–1086

Chen S, Lei Y, Xu X, Huang J, Jiang H, Wang J, Cheng Z, Zhang J, Song Y, Liao B, Li Y (2015) The peanut (*Arachis hypogaea* L.) gene AhLPAT2 increases the lipid content of transgenic *Arabidopsis* seeds. PLoS One **10:** e0136170

Chen X, Snyder CL, Truksa M, Shah S, Weselake RJ (2011) *sn*-Glycerol-3-phosphate acyltransferases in plants. Plant Signal Behav **6:** 1695–1699

Cheng D, Meegalla RL, He B, Cromley DA, Billheimer JT, Young PR (2001) Human acyl-CoA:diacylglycerol acyltransferase is a tetrameric protein. Biochem J **359:** 707–714

Chi X, Hu R, Zhang X, Chen M, Chen N, Pan L, Wang T, Wang M, Yang Z, Wang Q, Yu S (2014) Cloning and functional analysis of three diacylglycerol acyltransferase genes from peanut (*Arachis hypogaea* L.). PLoS One **9:** e105834

Christie WW, Han X (2010) Lipid analysis-isolation, separation, identification and lipidomic analysis. Oily Press, Bridgwater, UK pp. 446.

Cho Y, Sharma V, Sacchettini JC (2003) Crystal structure of ATP phosphoribosyltransferase from *Mycobacterium tuberculosis*. J Biol Chem **278:** 8333–8339

Clark KM, Fedoriw N, Robinson K, Connelly SM, Randles J, Malkowski MG, DeTitta GT, Dumont ME (2010) Purification of transmembrane proteins from

Saccharomyces cerevisiae for X-ray crystallography. Protein Expr Purif **71:** 207–223

Coleman RA, Lee DP (2004) Enzymes of triacylglycerol synthesis and their regulation. Prog in Lipid Res **43:** 134–176

Constantinides PP, Steim JM (1988) Micellization of fatty acyl-CoA mixtures and its relevance to the fatty acyl selectivity of acyltransferases. Arch Biochem Biophys **261:** 430–436

Cornilescu G, Delaglio F, Bax A (1999) Protein backbone angle restraints from searching a database for chemical shift and sequence homology. J Biomol NMR **13:** 289–302

Cortes DM, Perozo E (1997) Structural dynamics of the *Streptomyces lividans* K^+ channel (SKC1): oligomeric stoichiometry and stability. Biochemistry **36:** 10343–10352

Craddock CP, Adams N, Bryant FM, Kurup S, Eastmond PJ (2015) Phosphatidic acid phosphohydrolase regulates phosphatidylcholine biosynthesis in *Arabidopsis* by phosphatidic acid-mediated activation of CTP:phosphocholine cytidylyltransferase activity. Plant Cell **27:** 1251–1264

Dahlqvist A, Stahl U, Lenman M, Banas A, Lee M, Sandager L, Ronne H, Stymne S (2000) Phospholipid:diacylglycerol acyltransferase: an enzyme that catalyzes the acyl-CoA-independent formation of triacylglycerol in yeast and plants. Proc Natl Acad Sci U S A **97:** 6487–6492

Dai C, Xue HW (2010) Rice early flowering1, a CKI, phosphorylates DELLA protein SLR1 to negatively regulate gibberellin signalling. EMBO J **29:** 1916–1927

Dale S, Wilson WA, Edelman AM, Hardie DG (1995) Similar substrate recognition motifs for mammalian AMP-activated protein kinase, higher plant HMG-CoA reductase kinase-A, yeast SNF1, and mammalian calmodulin-dependent protein kinase I. FEBS Lett **361:** 191–195

Davies SP, Sim AT, Hardie DG (1990) Location and function of three sites phosphorylated on rat acetyl-CoA carboxylase by the AMP-activated protein kinase. Eur J Biochem **187:** 183–190

Davis MS, Cronan JE (2001) Inhibition of *Escherichia coli* acetyl coenzyme A carboxylase by acyl-acyl carrier protein. J Bacteriol **183:** 1499–1503

Delaglio F, Grzesiek S, Vuister GW, Zhu G, Pfeifer J, Bax A (1995) NMRPipe: a multidimensional spectral processing system based on UNIX pipes. J Biomol NMR **6:** 277–293

DeVita RJ, Pinto S (2013) Current status of the research and development of diacylglycerol O-acyltransferase 1 (DGAT1) inhibitors. J Med Chem **56:** 9820–9825

Ding Z, Taneva SG, Huang HK, Campbell SA, Semenec L, Chen N, Cornell RB (2012) A 22-mer segment in the structurally pliable regulatory domain of metazoan CTP: phosphocholine cytidylyltransferase facilitates both silencing and activating functions. J Biol Chem **287:** 38980–38991

Doonan JH, Kitsios G (2009) Functional evolution of cyclin-dependent kinases. Mol Biotechnol **42:** 14–29

Dörmann P, Voelker TA, Ohlrogge JB (1995) Cloning and expression in *Escherichia coli* of a novel thioesterase from *Arabidopsis thaliana* specific for long-chain acyl-

acyl carrier proteins. Arch Biochem Biophys **316:** 612–618

Dovala D, Rath CM, Hu Q, Sawyer WS, Shia S, Elling RA, Knapp MS, Metzger LE (2016) Structure-guided enzymology of the lipid A acyltransferase LpxM reveals a dual activity mechanism. Proc Natl Acad Sci U S A **113:** E6064–E6071

Dubots E, Audry M, Yamaryo Y, Bastien O, Ohta H, Breton C, Maréchal E, Block MA (2010) Activation of the chloroplast monogalactosyldiacylglycerol synthase MGD1 by phosphatidic acid and phosphatidylglycerol. J Biol Chem **285:** 6003–6011

Durrett TP, Benning C, Ohlrogge J (2008) Plant triacylglycerols as feedstocks for the production of biofuels. Plant J **54:** 593–607

Durrett TP, McClosky DD, Tumaney AW, Elzinga DA, Ohlrogge J, Pollard M (2010) A distinct DGAT with *sn*-3 acetyltransferase activity that synthesizes unusual, reduced-viscosity oils in *Euonymus* and transgenic seeds. Proc Natl Acad Sci U S A **107:** 9464–9469

Dyson HJ, Wright PE (2005) Intrinsically unstructured proteins and their functions. Nat Rev Mol Cell Biol **6:** 197–208

Eastmond PJ, Quettier AL, Kroon JT, Craddock C, Adams N, Slabas AR (2010) Phosphatidic acid phosphohydrolase 1 and 2 regulate phospholipid synthesis at the endoplasmic reticulum in *Arabidopsis*. Plant Cell **22:** 2796–2811

Eastwell KC, Stumpf PK (1983) Regulation of plant acetyl-CoA carboxylase by adenylate nucleotides. Plant Physiol **72:** 50–55

Eaton WA, Henry ER, Hofrichter J, Mozzarelli A (1999) Is cooperative oxygen binding by hemoglobin really understood. Nat Struct Biol **6:** 351–358

El Tahchy A, Petrie JR, Shrestha P, Vanhercke T, Singh SP (2015) Expression of mouse MGAT in *Arabidopsis* results in increased lipid accumulation in seeds. Front Plant Sci **6:** 1180

El Tahchy A, Reynolds KB, Petrie JR, Singh SP, Vanhercke T (2017) Thioesterase overexpression in *Nicotiana benthamiana* leaf increases the fatty acid flux into triacylgycerol. FEBS Lett **591:** 448–456

Erp HV, Kelly AA, Menard G, Eastmond PJ (2014) Multigene engineering of triacylglycerol metabolism boosts seed oil content in *Arabidopsis*. Plant Physio **165:** 30–36

Fagone P, Jackowski S (2013) Phosphatidylcholine and the CDP-choline cycle. Biochim Biophys Acta **1831:** 523–532

Fan J, Yan C, Roston R, Shanklin J, Xu C (2014) *Arabidopsis* lipins, PDAT1 acyltransferase, and SDP1 triacylglycerol lipase synergistically direct fatty acids toward β-oxidation, thereby maintaining membrane lipid homeostasis. Plant Cell **26:** 4119–4134

Fan J, Yan C, Xu C (2013) Phospholipid:diacylglycerol acyltransferase-mediated triacylglycerol biosynthesis is crucial for protection against fatty acid-induced cell death in growing tissues of *Arabidopsis*. Plant J **76:** 930–942

Fatland BL, Nikolau BJ, Wurtele ES (2005) Reverse genetic characterization of cytosolic acetyl-CoA generation by ATP-citrate lyase in *Arabidopsis*. Plant Cell **17:** 182–203

Feddersen S, Neergaard TB, Knudsen J, Faergeman NJ (2007) Transcriptional regulation of phospholipid biosynthesis is linked to fatty acid metabolism by an

acyl-CoA-binding-protein-dependent mechanism in *Saccharomyces cerevisiae*. Biochem J **407:** 219–230

Feria Bourrellier AB, Valot B, Guillot A, Ambard-Bretteville F, Vidal J, Hodges M (2010) Chloroplast acetyl-CoA carboxylase activity is 2-oxoglutarate-regulated by interaction of PII with the biotin carboxyl carrier subunit. Proc Natl Acad Sci U S A **107:** 502–507

Francis D (2007) The plant cell cycle--15 years on. New Phytol **174:** 261–278

Freiburger L, Miletti T, Zhu S, Baettig O, Berghuis A, Auclair K, Mittermaier A (2014) Substrate-dependent switching of the allosteric binding mechanism of a dimeric enzyme. Nat Chem Biol **10:** 937–942

Frelet-Barrand A, Boutigny S, Kunji ER, N R (2010) Membrane protein expression in *Lactococcus lactis*. Methods Mol Bio **601:** 67–85

Fox SR, Rawsthorne S, Hills MJ (2000) Role of acyl-CoAs and acyl-CoA-binding protein in regulation of carbon supply for fatty acid biosynthesis. Biochem Soc Trans **28:** 672–674

Gangar A, Karande AA, Rajasekharan R (2001) Isolation and localization of a cytosolic 10S triacylglycerol biosynthetic multienzyme complex from oleaginous yeast. J Biol Chem **276:** 10290–10298

Ganji SH, Tavintharan S, Zhu D, Xing Y, Kamanna VS, Kashyap ML (2004) Niacin noncompetitively inhibits DGAT2 but not DGAT1 activity in HepG2 cells. J Lipid Res **45:** 1835–1845

Ghillebert R, Swinnen E, Wen J, Vandesteene L, Ramon M, Norga K, Rolland F, Winderickx J (2011) The AMPK/SNF1/SnRK1 fuel gauge and energy regulator:

structure, function and regulation. FEBS J **278:** 3978–3990

Gibellini F, Smith TK (2010) The Kennedy pathway-De novo synthesis of phosphatidylethanolamine and phosphatidylcholine. IUBMB Life **62:** 414–428

Gibon Y, Vigeolas H, Tiessen A, Geigenberger P, Stitt M (2002) Sensitive and high throughput metabolite assays for inorganic pyrophosphate, ADPGlc, nucleotide phosphates, and glycolytic intermediates based on a novel enzymic cycling system. Plant J **30:** 221–235

Gidda SK, Park S, Pyc M, Yurchenko O, Cai Y, Wu P, Andrews DW, Chapman KD, Dyer JM, Mullen RT (2016) Lipid droplet-associated Proteins (LDAPs) are required for the dynamic regulation of neutral lipid compartmentation in plant cells. Plant Physiol **170:** 2052–2071

Gietz RD, Schiestl RH (2007) Frozen competent yeast cells that can be transformed with high efficiency using the LiAc/SS carrier DNA/PEG method. Nat Protoc **2:** 1–4

Gillespie JG, Hardie DG (1992) Phosphorylation and inactivation of HMG-CoA reductase at the AMP-activated protein kinase site in response to fructose treatment of isolated rat hepatocytes. FEBS Lett **306:** 59–62

Gómez-Cadenas A, Verhey SD, Holappa LD, Shen Q, Ho TH, Walker-Simmons MK (1999) An abscisic acid-induced protein kinase, PKABA1, mediates abscisic acid-suppressed gene expression in barley aleurone layers. Proc Natl Acad Sci U S A **96:** 1767–1772

Greer MS, Pan X, Weselake RJ (2016) Two clades of type-1 *Brassica napus* diacylglycerol acyltransferase exhibit differences in acyl-CoA Preference. Lipids

51: 781–786

Greer MS, Truksa M, Deng W, Lung SC, Chen G, Weselake RJ (2015) Engineering increased triacylglycerol accumulation in *Saccharomyces cerevisiae* using a modified type 1 plant diacylglycerol acyltransferase. Appl Microbiol Biotechnol **99:** 2243–2253

Greer MS, Zhou T, Weselake RJ (2014) A novel assay of DGAT activity based on high temperature GC/MS of triacylglycerol. Lipids **49:** 831–838

Grisart B, Farnir F, Karim L, Cambisano N, Kim JJ, Kvasz A, Mni M, Simon P, Frère JM, Coppieters W, Georges M (2004) Genetic and functional confirmation of the causality of the DGAT1 K232A quantitative trait nucleotide in affecting milk yield and composition. Proc Natl Acad Sci U S A **101:** 2398–2403

Gruswitz F, Chaudhary S, Ho JD, Schlessinger A, Pezeshki B, Ho CM, Sali A, Westhoff CM, Stroud RM (2010) Function of human Rh based on structure of RhCG at 2.1 A. Proc Natl Acad Sci U S A **107:** 9638–9643

Güntert P, Mumenthaler C, Wüthrich K (1997) Torsion angle dynamics for NMR structure calculation with the new program DYANA. J Mol Biol **273:** 283–298

Guo X, Fan C, Chen Y, Wang J, Yin W, Wang RR, Hu Z (2017) Identification and characterization of an efficient acyl-CoA: diacylglycerol acyltransferase 1 (DGAT1) gene from the microalga *Chlorella ellipsoidea*. BMC Plant Biol **17:** 48

Haagsman HP, de Haas CG, Geelen MJ, van Golde LM (1981) Regulation of triacylglycerol synthesis in the liver: a decrease in diacylglycerol acyltransferase activity after treatment of isolated rat hepatocytes with glucagon. Biochim Biophys Acta **664:** 74–81

Halford NG, Hardie DG (1998) SNF1-related protein kinases: global regulators of carbon metabolism in plants. Plant Mol Biol **37:** 735–748

Halford NG, Hey S, Jhurreea D, Laurie S, McKibbin RS, Paul M, Zhang Y (2003) Metabolic signalling and carbon partitioning: role of Snf1-related (SnRK1) protein kinase. J Exp Bot **54:** 467–475

Han J (2011) Regulation of acyl-CoA:diacylglycerol acyltransferase-1 by protein phosphorylation. Doctoral dissertation, University of Saskatchewan, Saskatoon

Hanano A, Burcklen M, Flenet M, Ivancich A, Louwagie M, Garin J, Blée E (2006) Plant seed peroxygenase is an original heme-oxygenase with an EF-hand calcium binding motif. J Biol Chem **281:** 33140–33151

Hardie DG (1999) Plant protein serine/threonine kinases: classification and functions. Annu Rev Plant Physiol Plant Mol Biol **50:** 97–131

Hardie DG, Carling D (1997) The AMP-activated protein kinase: fuel gauge of the mammalian cell. Eur J Biochem **246:** 259–273

Hardy TA, Huang D, Roach PJ (1994) Interactions between cAMP-dependent and SNF1 protein kinases in the control of glycogen accumulation in *Saccharomyces cerevisiae*. J Biol Chem **269:** 27907–27913

Hays FA, Roe-Zurz Z, Stroud RM (2010) Overexpression and purification of integral membrane proteins in yeast. Methods Enzymol **470:** 695–707

He X, Turner C, Chen GQ, Lin JT, McKeon TA (2004) Cloning and characterization of a cDNA encoding diacylglycerol acyltransferase from castor bean. Lipids **39:** 311–318

Heath RJ, Rock CO (1995) Regulation of malonyl-CoA metabolism by acyl-acyl

carrier protein and beta-ketoacyl-acyl carrier protein synthases in *Escherichia coli*. J Biol Chem **270:** 15531–15538

Hernández ML, Whitehead L, He Z, Gazda V, Gilday A, Kozhevnikova E, Vaistij FE, Larson TR, Graham IA (2012) A cytosolic acyltransferase contributes to triacylglycerol synthesis in sucrose-rescued *Arabidopsis* seed oil catabolism mutants. Plant Physiol **160:** 215–225

Hey SJ, Byrne E, Halford NG (2010) The interface between metabolic and stress signalling. Ann Bot **105:** 197–203

Hills MJ, Murphy DJ, Beevers H (1989) Inhibition of neutral lipase from castor bean lipid bodies by coenzyme A (CoA) and oleoyl-CoA. Plant Physiol **89:** 1006–1010

Hobbs DH, Hills MJ (2000) Expression and characterization of diacylglycerol acyltransferase from *Arabidopsis thaliana* in insect cell cultures. Biochem Soc Trans **28:** 687–689

Hobbs DH, Lu C, Hills MJ (1999) Cloning of a cDNA encoding diacylglycerol acyltransferase from *Arabidopsis thaliana* and its functional expression. FEBS Lett **452:** 145–149

Hofmann K (2000) A superfamily of membrane-bound O-acyltransferases with implications for wnt signaling. Trends Biochem Sci **25:** 111–112

Hu L, Deeney JT, Nolan CJ, Peyot ML, Ao A, Richard AM, Luc E, Faergeman NJ, Knudsen J, Guo W, Sorhede-Winzell M, Prentki M, Corkey BE (2005) Regulation of lipolytic activity by long-chain acyl-coenzyme A in islets and adipocytes. Am J Physiol Endocrinol Metab **289:** E1085–92

Huang AH (1996) Oleosins and oil bodies in seeds and other organs. Plant Physiol **110:**

1055–1061

Huang AHC (1992) Oil bodies and oleosins in seeds. Ann Rev of Plant Physiol Plant Mol Bio **43:** 177–200

Huber SC, Huber JL, Liao PC, Gage DA, McMichael RW, Chourey PS, Hannah LC, Koch K (1996) Phosphorylation of serine-15 of maize leaf sucrose synthase. Occurrence *in vivo* and possible regulatory significance. Plant Physiol **112:** 793–802

Huerlimann R, Heimann K (2013) Comprehensive guide to acetyl-carboxylases in algae. Crit Rev Biotechnol **33:** 49–65

Humphrey SJ, Yang G, Yang P, Fazakerley DJ, Stöckli J, Yang JY, James DE (2013) Dynamic adipocyte phosphoproteome reveals that Akt directly regulates mTORC2. Cell Metab **17:** 1009–1020

Iakoucheva LM, Radivojac P, Brown CJ, O'Connor TR, Sikes JG, Obradovic Z, Dunker AK (2004) The importance of intrinsic disorder for protein phosphorylation. Nucleic Acids Res **32:** 1037–1049

Ichihara K, Noda M (1982) Some properties of diacylglycerol acyltransferase in a particulate fraction from maturing safflower seeds. Phytochemistry **21:** 1895–1901

Ishihama Y, Schmidt T, Rappsilber J, Mann M, Hartl FU, Kerner MJ, Frishman D (2008) Protein abundance profiling of the *Escherichia coli* cytosol. BMC Genomics **9:** 102

Iskandarov U, Silva JE, Kim HJ, Andersson M, Cahoon RE, Mockaitis K, Cahoon EB (2017) A specialized diacylglycerol acyltransferase contributes to the extreme medium-chain fatty acid content of *Cuphea* seed oil. Plant Physiol **174:** 97–109

Iwai M, Ikeda K, Shimojima M, Ohta H (2014) Enhancement of extraplastidic oil synthesis in *Chlamydomonas reinhardtii* using a type-2 diacylglycerol acyltransferase with a phosphorus starvation-inducible promoter. Plant Biotechnol J **12:** 808–819

Jako C, Kumar A, Wei Y, Zou J, Barton DL, al. E (2001) Seed-specific over-expression of an *Arabidopsis* cDNA encoding a diacylglycerol acyltransferase enhances seed oil content and seed weight. Plant Physio **126:** 861–874

Jarvis DL (2009) Baculovirus-insect cell expression systems. Methods Enzymol **463:** 191–222

Jaworski JG, Post-Beittenmiller D, Ohlrogge JB (1993) Acetyl-acyl carrier protein is not a major intermediate in fatty acid biosynthesis in spinach. Eur J Biochem **213:** 981–987

Johnson BA (2004) Using NMRView to visualize and analyze the NMR spectra of macromolecules. Methods Mol Biol **278:** 313–352

Johnson KD, Chrispeels MJ (1992) Tonoplast-bound protein kinase phosphorylates tonoplast intrinsic protein. Plant Physiol **100:** 1787–1795

Jones A, Davies HM, Voelker TA (1995) Palmitoyl-acyl carrier protein (ACP) thioesterase and the evolutionary origin of plant acyl-ACP thioesterases. Plant Cell **7:** 359–371

Jones EW (2002) Vacuolar proteases and proteolytic artifacts in *Saccharomyces cerevisiae*. Methods Enzymol **351:** 127–150

Jost R, Berkowitz O, Shaw J, Masle J (2009) Biochemical characterization of two wheat phosphoethanolamine N-methyltransferase isoforms with different

sensitivities to inhibition by phosphatidic acid. J Biol Chem **284:** 31962–31971

Kalscheuer R, Steinbüchel A (2003) A novel bifunctional wax ester synthase/acyl-CoA:diacylglycerol acyltransferase mediates wax ester and triacylglycerol biosynthesis in *Acinetobacter calcoaceticus* ADP1. J Biol Chem **278:** 8075–8082

Kashlan OB, Scott CP, Lear JD, Cooperman BS (2002) A comprehensive model for the allosteric regulation of mammalian ribonucleotide reductase. Functional consequences of ATP- and dATP-induced oligomerization of the large subunit. Biochemistry **41:** 462–474

Katavic V, Agrawal GK, Hajduch M, Harris SL, Thelen JJ (2006) Protein and lipid composition analysis of oil bodies from two *Brassica napus* cultivars. Proteomics **6:** 4586–4598

Katavic V, Mietkiewska E, Barton DL, Giblin EM, Reed DW, Taylor DC (2002) Restoring enzyme activity in nonfunctional low erucic acid *Brassica napus* fatty acid elongase 1 by a single amino acid substitution. Eur J Biochem **269:** 5625–5631

Katavic V, Reed DW, Taylor DC, Giblin EM, Barton DL, Zou J, Mackenzie SL, Covello PS, Kunst L (1995) Alteration of seed fatty acid composition by an ethyl methanesulfonate-induced mutation in *Arabidopsis thaliana* affecting diacylglycerol acyltransferase activity. Plant Physiol **108:** 399–409

Kelly AA, van Erp H, Quettier AL, Shaw E, Menard G, Kurup S, Eastmond PJ (2013) The sugar-dependent1 lipase limits triacylglycerol accumulation in vegetative tissues of *Arabidopsis*. Plant Physiol **162:** 1282–1289

Keogh MR, Courtney PD, Kinney AJ, Dewey RE (2009) Functional characterization

of phospholipid N-methyltransferases from *Arabidopsis* and soybean. J Biol Chem **284:** 15439–15447

Kim H, Park JH, Kim AY, Suh MC (2016) Functional analysis of diacylglycerol acyltransferase1 genes from *Camelina sativa* and effects of CsDGAT1B overexpression on seed mass and storage oil content in *C. sativa*. Plant Biotech Rep **10:** 141–153

Kim HU, Lee KR, Go YS, Jung JH, Suh MC, Kim JB (2011) Endoplasmic reticulum-located PDAT1-2 from castor bean enhances hydroxy fatty acid accumulation in transgenic plants. Plant Cell Physiol **52:** 983–993

Kim S, Yamaoka Y, Ono H, Kim H, Shim D, Maeshima M, Martinoia E, Cahoon EB, Nishida I, Lee Y (2013) AtABCA9 transporter supplies fatty acids for lipid synthesis to the endoplasmic reticulum. Proc Natl Acad Sci U S A **110:** 773–778

Kinney AJ, WD H (1995) Improved soybean oils by genetic engineering. Presented at Biochem Mol Biol Plant Fatty Acids Glycerolipids Symp, South Lake Tahoe, Calif

Klaus D, Ohlrogge JB, Neuhaus HE, Dörmann P (2004) Increased fatty acid production in potato by engineering of acetyl-CoA carboxylase. Planta **219:** 389–396

Knutzon, Hayes, Wyrick, Xiong, Maelor Davies H, Voelker (1999) Lysophosphatidic acid acyltransferase from coconut endosperm mediates the insertion of laurate at the *sn*-2 position of triacylglycerols in lauric rapeseed oil and can increase total laurate levels. Plant Physiol **120:** 739–746

Knutzon DS, Thompson GA, Radke SE, Johnson WB, Knauf VC, Kridl JC (1992) Modification of *Brassica* seed oil by antisense expression of a stearoyl-acyl carrier

protein desaturase gene. Proc Natl Acad Sci U S A **89:** 2624–2628

Kooijman EE, Burger KN (2009) Biophysics and function of phosphatidic acid: a molecular perspective. Biochim Biophys Acta **1791:** 881–888

Kooijman EE, Tieleman DP, Testerink C, Munnik T, Rijkers DT, Burger KN, de Kruijff B (2007) An electrostatic/hydrogen bond switch as the basis for the specific interaction of phosphatidic acid with proteins. J Biol Chem **282:** 11356–11364

Kornberg A, Pricer WE (1951) Di- and triphosphopyridine nucleotide isocitric dehydrogenases in yeast. J Biol Chem **189:** 123–136

Kornberg A, Pricer WE (1953) Enzymatic esterification of alpha-glycerophosphate by long chain fatty acids. J Biol Chem **204:** 345–357

Korotchkina LG, Patel MS (2001) Probing the mechanism of inactivation of human pyruvate dehydrogenase by phosphorylation of three sites. J Biol Chem **276:** 5731–5738

Koshland DE, Némethy G, Filmer D (1966) Comparison of experimental binding data and theoretical models in proteins containing subunits. Biochemistry **5:** 365–385

Kroon JT, Wei W, Simon WJ, Slabas AR (2006) Identification and functional expression of a type 2 acyl-CoA:diacylglycerol acyltransferase (DGAT2) in developing castor bean seeds which has high homology to the major triglyceride biosynthetic enzyme of fungi and animals. Phytochemistry **67:** 2541–2549

Kuehn GD, Affolter HU, Atmar VJ, Seebeck T, Gubler U, Braun R (1979) Polyamine-mediated phosphorylation of a nucleolar protein from *Physarum polycephalum* that stimulates rRNA synthesis. Proc Natl Acad Sci U S A **76:**

2541–2545

Kwanyuen P, Wilson RF (1986) Isolation and purification of diacylglycerol acyltransferase from germinating soybean cotyledons. Biochim Biophys Acta **877:** 238–245

Kwanyuen P, Wilson RF (1990) Subunit and amino acid composition of diacylglycerol acyltransferase from germinating soybean cotyledons. Biochim Biophys Acta **1039:** 67–72

Kulma A, Villadsen D, Campbell DG, Meek SE, Harthill JE, Nielsen TH, MacKintosh C (2004) Phosphorylation and 14-3-3 binding of *Arabidopsis* 6-phosphofructo-2-kinase/fructose-2,6-bisphosphatase. Plant J **37:** 654–667

Lager I, Yilmaz JL, Zhou XR, Jasieniecka K, Kazachkov M, Wang P, Zou J, Weselake R, Smith MA, Bayon S, Dyer JM, Shockey JM, Heinz E, Green A, Banas A, Stymne S (2013) Plant acyl-CoA:lysophosphatidylcholine acyltransferases (LPCATs) have different specificities in their forward and reverse reactions. J Biol Chem **288:** 36902–36914

Laing WA, Roughan PG (1982) Activation of spinach chloroplast acetyl-Coenzyme A carboxylase by coenzyme A. FEBS Lett **144:** 341–344

Lan BX, Wu ZK, Wang L, Yang LC, Yang LY, He YQ, Jiang B (2015) Transformation and expression of DGAT1-2 gene and its effect on the oil content of super-high oil corn. J of South China Ag U **5:** 43–47

Lands WE (1960) Metabolism of glycerolipids. 2. The enzymatic acylation of lysolecithin. J Biol Chem **235:** 2233–2237

Lardizabal K, Effertz R, Levering C, Mai J, Pedroso MC, Jury T, Aasen E, Gruys

K, Bennett K (2008) Expression of *Umbelopsis ramanniana* DGAT2A in seed increases oil in soybean. Plant Physiol **148:** 89–96

Lardizabal KD, Mai JT, Wagner NW, Wyrick A, Voelker T, Hawkins DJ (2001) DGAT2 is a new diacylglycerol acyltransferase gene family: purification, cloning, and expression in insect cells of two polypeptides from *Mortierella ramanniana* with diacylglycerol acyltransferase activity. J Biol Chem **276:** 38862–38869

Larson TR, Graham IA (2001) Technical advance: a novel technique for the sensitive quantification of acyl-CoA esters from plant tissues. Plant J **25:** 115–125

Laskowski RA, Gerick F, Thornton JM (2009) The structural basis of allosteric regulation in proteins. FEBS Lett **583:** 1692–1698

Lee J, Taneva SG, Holland BW, Tieleman DP, Cornell RB (2014) Structural basis for autoinhibition of CTP:phosphocholine cytidylyltransferase (CCT), the regulatory enzyme in phosphatidylcholine synthesis, by its membrane-binding amphipathic helix. J Biol Chem **289:** 1742–1755

Lee JW, Zhang Y, Weaver CD, Shomer NH, Louis CF, Roberts DM (1995) Phosphorylation of nodulin 26 on serine 262 affects its voltage-sensitive channel activity in planar lipid bilayers. J Biol Chem **270:** 27051–27057

Li F, Wu X, Lam P, Bird D, Zheng H, Samuels L, Jetter R, Kunst L (2008) Identification of the wax ester synthase/acyl-coenzyme A: diacylglycerol acyltransferase WSD1 required for stem wax ester biosynthesis in *Arabidopsis*. Plant Physiol **148:** 97–107

Li R, Yu K, Hatanaka T, Hildebrand DF (2010a) *Vernonia* DGATs increase accumulation of epoxy fatty acids in oil. Plant Biotechnol J **8:** 184–195

Li R, Yu K, Hildebrand DF (2010b) DGAT1, DGAT2 and PDAT expression in seeds and other tissues of epoxy and hydroxy fatty acid accumulating plants. Lipids **45:** 145–157

Li R, Yu K, Wu Y, Tateno M, Hatanaka T, Hildebrand DF (2012) *Vernonia* DGATs can complement the disrupted oil and protein metabolism in epoxygenase-expressing soybean seeds. Metab Eng **14:** 29–38

Li Y, Beisson F, Koo AJ, Molina I, Pollard M, Ohlrogge J (2007) Identification of acyltransferases required for cutin biosynthesis and production of cutin with suberin-like monomers. Proc Natl Acad Sci U S A **104:** 18339–18344

Liang MH, Jiang JG (2013) Advancing oleaginous microorganisms to produce lipid via metabolic engineering technology. Prog Lipid Res **52:** 395–408

Light S, Sagit R, Ekman D, Elofsson A (2013) Long indels are disordered: a study of disorder and indels in homologous eukaryotic proteins. Biochim Biophys Acta **1834:** 890–897

Lin AP, McCammon MT, McAlister-Henn L (2001) Kinetic and physiological effects of alterations in homologous isocitrate-binding sites of yeast NAD^+-specific isocitrate dehydrogenase. Biochemistry **40:** 14291–14301

Lin LJ, Tai SS, Peng CC, Tzen JT (2002) Steroleosin, a sterol-binding dehydrogenase in seed oil bodies. Plant Physiol **128:** 1200–1211

Lin SL, Xu D, Li A, Nussinov R (1998) Electrostatics, allostery, and activity of the yeast chorismate mutase. Proteins **31:** 445–452

Little D, Weselake R, Pomeroy K, Furukawa-Stoffer T, Bagu J (1994) Solubilization and characterization of diacylglycerol acyltransferase from microspore-derived

cultures of oilseed rape. Biochem J **304:** 951–958

Liu J, Chang CC, Westover EJ, Covey DF, Chang TY (2005) Investigating the allosterism of acyl-CoA:cholesterol acyltransferase (ACAT) by using various sterols: *in vitro* and intact cell studies. Biochem J **391:** 389–397

Liu J, Ishitani M, Halfter U, Kim CS, Zhu JK (2000) The *Arabidopsis thaliana* SOS2 gene encodes a protein kinase that is required for salt tolerance. Proc Natl Acad Sci U S A **97:** 3730–3734

Liu Q, Guo Q, Akbar S, Zhi Y, El Tahchy A, Mitchell M, Li Z, Shrestha P, Vanhercke T, Ral JP, Liang G, Wang MB, White R, Larkin P, Singh S, Petrie J (2017) Genetic enhancement of oil content in potato tuber (*Solanum tuberosum L.*) through an integrated metabolic engineering strategy. Plant Biotechnol J **15:** 56–67

Liu Q, Siloto RM, Lehner R, Stone SJ, Weselake RJ (2012) Acyl-CoA:diacylglycerol acyltransferase: molecular biology, biochemistry and biotechnology. Prog Lipid Res **51:** 350–377

Liu W, Xu ZH, Luo D, Xue HW (2003) Roles of OsCKI1, a rice casein kinase I, in root development and plant hormone sensitivity. Plant J **36:** 189–202

Lock YY, Snyder CL, Zhu W, Siloto RM, Weselake RJ, Shah S (2009) Antisense suppression of type 1 diacylglycerol acyltransferase adversely affects plant development in *Brassica napus*. Physiol Plant **137:** 61–71

Lopes JL, Nobre TM, Cilli EM, Beltramini LM, Araújo AP, Wallace BA (2014) Deconstructing the DGAT1 enzyme: Binding sites and substrate interactions. Biochim Biophys Acta **1838:** 3145–3152

Louis‐Jeune C, Andrade‐Navarro MA, Perez-Iratxeta C (2012) Prediction of protein secondary structure from circular dichroism using theoretically derived spectra. Proteins **80:** 374–381

Lu C, Xin Z, Ren Z, Miquel M, Browse J (2009) An enzyme regulating triacylglycerol composition is encoded by the ROD1 gene of *Arabidopsis*. Proc Natl Acad Sci U S A **106:** 18837–18842

Lu CL, de Noyer SB, Hobbs DH, Kang J, Wen Y, Krachtus D, Hills MJ (2003) Expression pattern of diacylglycerol acyltransferase-1, an enzyme involved in triacylglycerol biosynthesis, in *Arabidopsis thaliana*. Plant Mol Biol **52:** 31–41

Lu P, Vogel C, Wang R, Yao X, Marcotte EM (2007) Absolute protein expression profiling estimates the relative contributions of transcriptional and translational regulation. Nat Biotechnol **25:** 117–124

Lundbaek JA, Collingwood SA, Ingólfsson HI, Kapoor R, Andersen OS (2010) Lipid bilayer regulation of membrane protein function: gramicidin channels as molecular force probes. J R Soc Interface **7:** 373–395

Luethy MH, Miernyk JA, David NR, Randall DD (1996) Plant pyruvate dehydrogenase complexes. In Alpha-Keto Acid Dehydrogenase Complexes. MS Patel, TE Roche, Robert Harris. Birkhäuser pp. 71

Lung SC, Chye ML (2016) Deciphering the roles of acyl-CoA-binding proteins in plant cells. Protoplasma **253:** 1177–1195

Lung SC, Weselake RJ (2006) Diacylglycerol acyltransferase: a key mediator of plant triacylglycerol synthesis. Lipids **41:** 1073–1088

Mackintosh C, Douglas P, Lillo C (1995) Identification of a protein that inhibits the

phosphorylated form of nitrate reductase from spinach (*Spinacia oleracea*) leaves. Plant Physiol **107:** 451–457

Maisonneuve S, Bessoule JJ, Lessire R, Delseny M, Roscoe TJ (2010) Expression of rapeseed microsomal lysophosphatidic acid acyltransferase isozymes enhances seed oil content in *Arabidopsis*. Plant Physiol **152:** 670–684

Maloney PC, Ambudkar SV (1989) Functional reconstitution of prokaryote and eukaryote membrane proteins. Arch Biochem Biophys **269:** 1–10

Maravi DK, Kumar S, Sharma PK, Kobayashi Y, Goud VV, Sakurai N, Koyama H, Sahoo L (2016) Ectopic expression of AtDGAT1, encoding diacylglycerol O-acyltransferase exclusively committed to TAG biosynthesis, enhances oil accumulation in seeds and leaves of Jatropha. Biotechnol Biofuels **9:** 226

Marcus F, Hosey MM (1980) Purification and properties of liver fructose 1, 6-bisphosphatase from C57BL/KsJ normal and diabetic mice. J Biol Chem **255(6):** 2481–2486

Marillia EF, Micallef BJ, Micallef M, Weninger A, Pedersen KK, Zou J, Taylor DC (2003) Biochemical and physiological studies of *Arabidopsis thaliana* transgenic lines with repressed expression of the mitochondrial pyruvate dehydrogenase kinase. J Exp Bot **54:** 259–270

Marín M, Thallmair V, Ott T (2012) The intrinsically disordered N-terminal region of AtREM1.3 remorin protein mediates protein-protein interactions. J Biol Chem **287:** 39982–39991

Martin BA, Wilson RF (1983) Properties of diacylglycerol acyltransferase from spinach leaves. Lipids **18:** 1–6

Mavraganis I, Meesapyodsuk D, Vrinten P, Smith M, Qiu X (2010) Type II diacylglycerol acyltransferase from *Claviceps purpurea* with ricinoleic acid, a hydroxyl fatty acid of industrial importance, as preferred substrate. Appl Environ Microbiol **76:** 1135–1142

McFie PJ, Stone SL, Banman SL, Stone SJ (2010) Topological orientation of acyl-CoA:diacylglycerol acyltransferase-1 (DGAT1) and identification of a putative active site histidine and the role of the N-terminus in dimer/tetramer formation. J Biol Chem **285:** 37377–37387

McMichael RW, Bachmann M, Huber SC (1995) Spinach leaf sucrose-phosphate synthase and nitrate reductase are phosphorylated/inactivated by multiple protein kinases *in vitro*. Plant Physiol **108:** 1077–1082

McVetty PBE, Mietkiewska E, Omonov T, Curtis J, Taylor DC, Weselake RJ (2016) *Brassica* spp. oils. *In:Industrial Oil Crops* (eds TA McKeon, DF Hildebrand, DG Hayes, RJ Weselake) Elsevier/AOCS Press, New York/Urbana, pp. 113-156

Meegalla RL, Billheimer JT, Cheng D (2002) Concerted elevation of acyl-coenzyme A:diacylglycerol acyltransferase (DGAT) activity through independent stimulation of mRNA expression of DGAT1 and DGAT2 by carbohydrate and insulin. Biochem Biophys Res Commun **298:** 317–323

Metzger JO, Bornscheuer U (2006) Lipids as renewable resources: current state of chemical and biotechnological conversion and diversification. Appl Microbiol Biotechnol **71:** 13–22

Mhaske V, Beldjilali K, Ohlrogge J, Pollard M (2005) Isolation and characterization

of an *Arabidopsis thaliana* knockout line for phospholipid: diacylglycerol transacylase gene (At5g13640). Plant Physiol Biochem **43:** 413–417

Mietkiewska E, Siloto RM, Dewald J, Shah S, Brindley DN, Weselake RJ (2011) Lipins from plants are phosphatidate phosphatases that restore lipid synthesis in a pah1Δ mutant strain of *Saccharomyces cerevisiae*. FEBS J **278:** 764–775

Misra A, Khan K, Niranjan A, Nath P, Sane VA (2013) Over-expression of JcDGAT1 from *Jatropha curcas* increases seed oil levels and alters oil quality in transgenic *Arabidopsis thaliana*. Phytochemistry **96:** 37–45

Monod J, Wyman J, Changeux JP (1965) On the nature of allosteric transitions: a plausible model. J Mol Biol **12:** 88–118

Monreal JA, McLoughlin F, Echevarría C, García-Mauriño S, Testerink C (2010) Phosphoenolpyruvate carboxylase from C4 leaves is selectively targeted for inhibition by anionic phospholipids. Plant Physiol **152:** 634–638

Moriya H, Johnston M (2004) Glucose sensing and signaling in *Saccharomyces cerevisiae* through the Rgt2 glucose sensor and casein kinase I. Proc Natl Acad Sci U S A **101:** 1572–1577

Mosblech A, Feussner I, Heilmann I (2009) Oxylipins: structurally diverse metabolites from fatty acid oxidation. Plant Physiol Biochem **47:** 511–517

Motlagh HN, Wrabl JO, Li J, Hilser VJ (2014) The ensemble nature of allostery. Nature **508:** 331–339

Mukherjee S, Kunitake G, Alfinslater RB (1958) The esterification of cholesterol with palmitic acid by rat liver homogenates. J Biol Chem **230:** 91–96

Murphy DJ (1993) Structure, function and biogenesis of storage lipid bodies and

oleosins in plants. Prog Lipid Res **32:** 247–280

Nagy HM, Paar M, Heier C, Moustafa T, Hofer P, Haemmerle G, Lass A, Zechner R, Oberer M, Zimmermann R (2014) Adipose triglyceride lipase activity is inhibited by long-chain acyl-coenzyme A. Biochim Biophys Acta **1841:** 588–594

Nakamura Y, Yamada M (1979) The light-dependent step of de novo synthesis of long chain fatty acids in spinach chloroplasts. Plant Sci Lett **14:** 291–295

Nikolau BJ, Hawke JC (1984) Purification and characterization of maize leaf acetyl-coenzyme A carboxylase. Arch Biochem Biophys **228:** 86–96

Nukarinen E, Nägele T, Pedrotti L, Wurzinger B, Mair A, Landgraf R, Börnke F, Hanson J, Teige M, Baena-Gonzalez E, Dröge-Laser W, Weckwerth W (2016) Quantitative phosphoproteomics reveals the role of the AMPK plant ortholog SnRK1 as a metabolic master regulator under energy deprivation. Sci Rep **6:** 31697

Nunes C, Primavesi LF, Patel MK, Martinez-Barajas E, Powers SJ, Sagar R, Fevereiro PS, Davis BG, Paul MJ (2013) Inhibition of SnRK1 by metabolites: tissue-dependent effects and cooperative inhibition by glucose 1-phosphate in combination with trehalose 6-phosphate. Plant Physiol Biochem **63:** 89–98

Nykiforuk CL, Furukawa-Stoffer TL, Huff PW, Sarna M, Laroche A, Moloney MM, Weselake RJ (2002) Characterization of cDNAs encoding diacylglycerol acyltransferase from cultures of *Brassica napus* and sucrose-mediated induction of enzyme biosynthesis. Biochim Biophys Acta **1580:** 95–109

Nykiforuk CL, Laroche A, Weselake RJ (1999) Isolation and characterization of a cDNA encoding a second putative diacylglycerol acyltransferase from a

microspore-derived cell suspension culture of *Brassica napus* L. cv Jet Neuf (Accession No. AF164434) (Plant Gene Registrar 99-158). Plant Physiol **121:** 1057

Ogiso E, Takahashi Y, Sasaki T, Yano M, Izawa I (2010) The role of casein kinase II in flowering time regulation has diversified during evolution. Plant Physio **152:** 808–820

Ogiwara H, Tanabe T, Nikawa J, Numa S (1978) Inhibition of rat-liver acetyl-coenzyme-A carboxylase by palmitoyl-coenzyme A. Formation of equimolar enzyme-inhibitor complex. Eur J Biochem **89:** 33–41

Ohlrogge JB, Jaworski JG (1997) Regulation of fatty acid synthesis. Annu Rev Plant Physiol Plant Mol Biol **48:** 109–136

Pan X, Siloto RM, Wickramarathna AD, Mietkiewska E, Weselake RJ (2013) Identification of a pair of phospholipid:diacylglycerol acyltransferases from developing flax (*Linum usitatissimum* L.) seed catalyzing the selective production of trilinolenin. J Biol Chem **288:** 24173–24188

Panikashvili D, Shi JX, Schreiber L, Aharoni A (2009) The *Arabidopsis* DCR encoding a soluble BAHD acyltransferase is required for cutin polyester formation and seed hydration properties. Plant Physiol **151:** 1773–1789

Pejaver V, Hsu WL, Xin F, Dunker AK, Uversky VN, Radivojac P (2014) The structural and functional signatures of proteins that undergo multiple events of post-translational modification. Protein Sci **23:** 1077–1093

Peng D, Zhang L, Tan X, Yuan D, Liu X, Zhou B (2016) Increasing seed oil content and altering oil quality of *Brassica napus* L. by over-expression of diacylglycerol

acyltransferase 1 (SsDGAT1) from *Sapium sebiferum* (L.) Roxb. Mol Breed **36:** 136

Perry HJ, Harwood JL (1993) Radiolabelling studies of acyl lipids in developing seeds of *Brassica napus*: Use of [1-^{14}C] acetate precursor. Phytochem **33:** 329–333

Petrie JR, Vanhercke T, Shrestha P, El Tahchy A, White A, Zhou XR, Liu Q, Mansour MP, Nichols PD, Singh SP (2012) Recruiting a new substrate for triacylglycerol synthesis in plants: the monoacylglycerol acyltransferase pathway. PLoS One **7:** e35214

Piattoni CV, Bustos DM, Guerrero SA, Iglesias AÁ (2011) Nonphosphorylating glyceraldehyde-3-phosphate dehydrogenase is phosphorylated in wheat endosperm at serine-404 by an SNF1-related protein kinase allosterically inhibited by ribose-5-phosphate. Plant Physiol **156:** 1337–1350

Plaxton WC (1996) The organization and regulation of plant glycolysis. Annu Rev Plant Physiol Plant Mol Biol **47:** 185–214

Pleiss J, Fischer M, Peiker M, Thiele C, Schmid RD (2000) Lipase engineering database: understanding and exploiting sequence–structure–function relationships. J Mol Catal B: Enzym **10:** 491–508

Polge C, Thomas M (2007) SNF1/AMPK/SnRK1 kinases, global regulators at the heart of energy control. Trends Plant Sci **12:** 20–28

Polokoff MA, Bell RM (1980) Solubilization, partial purification and characterization of rat liver microsomal diacylglycerol acyltransferase. Biochim Biophys Acta **618:** 129–142

Poovaiah BW, Reddy AS (1993) Calcium and signal transduction in plants. CRC Crit

Rev Plant Sci **12:** 185–211

Pufall MA, Graves BJ (2002) Autoinhibitory domains: modular effectors of cellular regulation. Annu Rev Cell Dev Biol **18:** 421–462

Raghu P, Manifava M, Coadwell J, Ktistakis NT (2009) Emerging findings from studies of phospholipase D in model organisms (and a short update on phosphatidic acid effectors). Biochim Biophys Acta **1791:** 889–897

Rahman H, Harwood J, Weselake R (2013) Increasing seed oil content in Brassica species through breeding and biotechnology. Lipid Tech **25:** 182–185

Rani SH, Krishna TH, Saha S, Negi AS, Rajasekharan R (2010) Defective in cuticular ridges (DCR) of *Arabidopsis thaliana*, a gene associated with surface cutin formation, encodes a soluble diacylglycerol acyltransferase. J Biol Chem **285:** 38337–38347

Rao SS, Hildebrand D (2009) Changes in oil content of transgenic soybeans expressing the yeast SLC1 gene. Lipids **44:** 945–951

Reed MC, Lieb A, Nijhout HF (2010) The biological significance of substrate inhibition: a mechanism with diverse functions. Bioessays **32:** 422–429

Rubio S, Whitehead L, Larson TR, Graham IA, Rodriguez PL (2008) The coenzyme A biosynthetic enzyme phosphopantetheine adenylyltransferase plays a crucial role in plant growth, salt/osmotic stress resistance, and seed lipid storage. Plant Physiol **148:** 546–556

Reue K, Dwyer JR (2009) Lipin proteins and metabolic homeostasis. J Lipid Res **50 Suppl:** S109–114

Reynolds KB, Taylor MC, Cullern DP, Banchard CL, Wood CC, Singh S, Petrie J

(2017) A reconfigured Kennedy pathway which promotes efficient accumulation of medium-chain fatty acids in leaf oils. Plant Biotechnol J 1–12

Reynolds KB, Taylor MC, Zhou XR, Vanhercke T, Wood CC, Blanchard CL, Singh SP, Petrie JR (2015) Metabolic engineering of medium-chain fatty acid biosynthesis in *Nicotiana benthamiana* plant leaf lipids. Front Plant Sci **6:** 164

Rodrigues A, Adamo M, Crozet P, Margalha L, Confraria A, Martinho C, Elias A, Rabissi A, Lumbreras V, González-Guzmán M, Antoni R, Rodriguez PL, Baena-González E (2013) ABI1 and PP2CA phosphatases are negative regulators of SNF1-related protein kinase1 signaling in *Arabidopsis*. Plant Cell **25:** 3871–3884

Rodriguez MC, Petersen M, Mundy J (2010) Mitogen-activated protein kinase signaling in plants. Annu Rev Plant Biol **61:** 621–649

Roesler K, Shen B, Bermudez E, Li C, Hunt J, Damude HG, Ripp KG, Everard JD, Booth JR, Castaneda L, Feng L, Meyer K (2016) An improved variant of soybean type 1 diacylglycerol acyltransferase increases the oil content and decreases the soluble carbohydrate content of soybeans. Plant Physio **171:** 878–893

Roughan PG, Slack CR (1982) Cellular organization of glycerolipid metabolism. Annu Rev of Plant Physio **33:** 97–132

Routaboul, Benning, Bechtold, Caboche, Lepiniec (1999) The TAG1 locus of *Arabidopsis* encodes for a diacylglycerol acyltransferase. Plant Physiol Biochem **37:** 831–840

Runguphan W, Keasling JD (2014) Metabolic engineering of *Saccharomyces*

cerevisiae for production of fatty acid-derived biofuels and chemicals. Metab Eng **21:** 103–113

Saha S, Enugutti B, Rajakumari S, Rajasekharan R (2006) Cytosolic triacylglycerol biosynthetic pathway in oilseeds. Molecular cloning and expression of peanut cytosolic diacylglycerol acyltransferase. Plant Physiol **141:** 1533–1543

Salie MJ, Thelen JJ (2016) Regulation and structure of the heteromeric acetyl-CoA carboxylase. Biochim Biophys Acta **1861:** 1207–1213

Salie MJ, Zhang N, Lancikova V, Xu D, Thelen JJ (2016) A family of negative regulators targets the committed step of de novo fatty acid biosynthesis. Plant Cell **28:** 2312–2325.

Sampathkumar P, Mak MW, Fischer-Witholt SJ, Guigard E, Kay CM, Lemieux MJ (2012) Oligomeric state study of prokaryotic rhomboid proteases. Biochim Biophys Acta **1818:** 3090–3097

Sandager L, Gustavsson MH, Ståhl U, Dahlqvist A, Wiberg E, Banas A, Lenman M, Ronne H, Stymne S (2002) Storage lipid synthesis is non-essential in yeast. J Biol Chem **277:** 6478–6482

Sanjaya, Durrett TP, Weise SE, Benning C (2011) Increasing the energy density of vegetative tissues by diverting carbon from starch to oil biosynthesis in transgenic *Arabidopsis*. Plant Biotechnol J **9:** 874–883

Sasaki Y, Nagano Y (2004) Plant acetyl-CoA carboxylase: structure, biosynthesis, regulation, and gene manipulation for plant breeding. Biosci Biotechnol Biochem **68:** 1175–1184

Savadi S, Naresh V, Kumar V, Bhat SR (2015) Seed-specific overexpression of

Arabidopsis DGAT1 in Indian mustard (*Brassica juncea*) increases seed oil content and seed weight. Botany **94:** 177–184

Schneider CA, Rasband WS, Eliceiri KW (2012) NIH Image to ImageJ: 25 years of image analysis. Nat Methods **9:** 671–675

Schnurr JA, Shockey JM, de Boer GJ, Browse J (2002) Fatty acid export from the chloroplast. Molecular characterization of a major plastidial acyl-coenzyme A synthetase from *Arabidopsis*. Plant Physio **129:** 1700–1709

Seddon AM, Curnow P, Booth PJ (2004) Membrane proteins, lipids and detergents: not just a soap opera. Biochim Biophys Acta **1666:** 105–117

Shen W, Reyes MI, Hanley-Bowdoin L (2009) *Arabidopsis* protein kinases GRIK1 and GRIK2 specifically activate SnRK1 by phosphorylating its activation loop. Plant Physiol **150:** 996–1005

Shintani, D Shorrosh, B Roesler, K, Savage LK, PE, Ohlrogge J (1996) Alterations of tobacco leaf fatty acid metabolism using antisense-expression and reverse genetic approaches. Presented at 12th Int Symp Plant Lipids, Toronto, Canada

Shockey J, Regmi A, Cotton K, Adhikari N, Browse J, Bates PD (2016) Identification of *Arabidopsis* GPAT9 (At5g60620) as an essential gene involved in triacylglycerol biosynthesis. Plant Physiol **170:** 163–179

Shockey JM, Gidda SK, Chapital DC, Kuan JC, Dhanoa PK, Bland JM, Rothstein SJ, Mullen RT, Dyer JM (2006) Tung tree DGAT1 and DGAT2 have nonredundant functions in triacylglycerol biosynthesis and are localized to different subdomains of the endoplasmic reticulum. Plant Cell **18:** 2294–2313

Shumilin IA, Zhao C, Bauerle R, Kretsinger RH (2002) Allosteric inhibition of 3-

deoxy-D-arabino-heptulosonate-7-phosphate synthase alters the coordination of both substrates. J Mol Biol **320:** 1147–1156

Sibille N, Bernadó P (2012) Structural characterization of intrinsically disordered proteins by the combined use of NMR and SAXS. Biochem Soc Trans **40:** 955–962

Siloto RMP, Madhavji M, Wiehler WB, Burton TL, Boora PS, Laroche A, Weselake RJ (2008) An N-terminal fragment of mouse DGAT1 binds different acyl-CoAs with varying affinity. Biochem Biophys Res Commun **373:** 350–354

Siloto RMP, Truksa M, Brownfield D, Good AG, Weselake RJ (2009a) Directed evolution of acyl-CoA:diacylglycerol acyltransferase: development and characterization of *Brassica napus* DGAT1 mutagenized libraries. Plant Physiol Biochem 47: 456–461

Siloto RMP, Truksa M, He X, McKeon T, Weselake RJ (2009b) Simple methods to detect triacylglycerol biosynthesis in a yeast-based recombinant system. Lipids **44:** 963–973

Singer SD, Chen G, Mietkiewska E, Tomasi P, Jayawardhane K, Dyer JM, Weselake RJ (2016) *Arabidopsis* GPAT9 contributes to synthesis of intracellular glycerolipids but not surface lipids. J Exp Bot **67:** 4627–4638

Slack CR, Campbell LC, Browse JA, Roughan PG (1983) Some evidence for the reversibility of the cholinephosphotransferase-catalysed reaction in developing linseed cotyledons *in vivo*. Biochim Biophys Acta **754:** 10–20

Smith SJ, Cases S, Jensen DR, Chen HC, Sande E, Tow B, Sanan DA, Raber J, Eckel RH, Farese RV (2000) Obesity resistance and multiple mechanisms of

triglyceride synthesis in mice lacking Dgat. Nat Genet **25:** 87–90

Sørensen BM, Furukawa-Stoffer TL, Marshall KS, Page EK, Mir Z, Forster RJ, Weselake RJ (2005) Storage lipid accumulation and acyltransferase action in developing flaxseed. Lipids **40:** 1043–1049

Ståhl U, Carlsson AS, Lenman M, Dahlqvist A, Huang B, Banas W, Banas A, Stymne S (2004) Cloning and functional characterization of a phospholipid:diacylglycerol acyltransferase from *Arabidopsis*. Plant Physiol **135:** 1324–1335

Stone SJ, Levin MC, Farese RV (2006) Membrane topology and identification of key functional amino acid residues of murine acyl-CoA:diacylglycerol acyltransferase-2. J Biol Chem **281:** 40273–40282

Stone SJ, Myers HM, Watkins SM, Brown BE, Feingold KR, Elias PM, Farese RV (2004) Lipopenia and skin barrier abnormalities in DGAT2-deficient mice. J Biol Chem **279:** 11767–11776

Stöveken T, Kalscheuer R, Malkus U, Reichelt R, Steinbüchel A (2005) The wax ester synthase/acyl-coenzyme A:diacylglycerol acyltransferase from *Acinetobacter* sp. strain ADP1: characterization of a novel type of acyltransferase. J Bacteriol **187:** 1369–1376

Stymne S, Stobart AK (1984) Evidence for the reversibility of the acyl-CoA:lysophosphatidylcholine acyltransferase in microsomal preparations from developing safflower (*Carthamus tinctorius* L.) cotyledons and rat liver. Biochem J **223:** 305–314

Stymne S, Stobart AK (1987) Triacylglycerol biosynthesis. The biochemistry of plants

Vol 9, PK Stumpf and EE Conn, eds (New York: Academic Press) 175–214

Su JY, Storey KB (1994) Regulation of phosphofructokinase from muscle and liver of rainbow trout by protein phosphorylation. Biochem Mol Biol Int **33:** 1191–1200

Sugden C, Crawford RM, Halford NG, Hardie DG (1999) Regulation of spinach SNF1-related (SnRK1) kinases by protein kinases and phosphatases is associated with phosphorylation of the T loop and is regulated by 5'-AMP. Plant J **19:** 433–439

Sun X, Jones WT, Harvey D, Edwards PJ, Pascal SM, Kirk C, Considine T, Sheerin DJ, Rakonjac J, Oldfield CJ, Xue B, Dunker AK, Uversky VN (2010) N-terminal domains of DELLA proteins are intrinsically unstructured in the absence of interaction with GID1/gibberellic acid receptors. J Biol Chem **285:** 11557–11571

Tang M, Guschina IA, O'Hara P, Slabas AR, Quant PA, Fawcett T, Harwood JL (2012) Metabolic control analysis of developing oilseed rape (*Brassica napus* cv Westar) embryos shows that lipid assembly exerts significant control over oil accumulation. New Phytol **196:** 414–426

Tao H, Cornish VW (2002) Milestones in directed enzyme evolution. Curr Opin Chem Biol **6:** 858–864

Taylor DC, Weber N, Barton DL, Underhill EW, Hogge LR, Weselake RJ, Pomeroy MK (1991) Triacylglycerol bioassembly in microspore-derived embryos of *Brassica napus* L. cv Reston. Plant Physiol **97:** 65–79

Taylor DC, Weber N, Hogge LR, Underhill EW (1990) A simple enzymatic method for the preparation of radiolabeled erucoyl-CoA and other long-chain fatty acyl-

CoAs and their characterization by mass spectrometry. Anal Biochem **184:** 311–316

Taylor DC, Zhang Y, Kumar A, Francis T, Giblin EM, Barton DL, Ferrie JR, Laroche A, Shah S, Zhu W, Snyder CL, Hall L, Rakow G, Harwood JL, Weselake RJ (2009) Molecular modification of triacylglycerol accumulation by over-expression of DGAT1 to produce canola with increased seed oil content under field conditions. Botany **87:** 533–543

Testerink C, Munnik T (2005) Phosphatidic acid: a multifunctional stress signaling lipid in plants. Trends Plant Sci **10:** 368–375

Thompson JR, Bell JK, Bratt J, Grant GA, Banaszak LJ (2005) Vmax regulation through domain and subunit changes. The active form of phosphoglycerate dehydrogenase. Biochemistry **44:** 5763–5773

Toroser D, Plaut Z, Huber SC (2000) Regulation of a plant SNF1-related protein kinase by glucose-6-phosphate. Plant Physiol **123:** 403–412

Tovar-Méndez A, Miernyk JA, Randall DD (2003) Regulation of pyruvate dehydrogenase complex activity in plant cells. Eur J Biochem **270:** 1043–1049

Trudeau T, Nassar R, Cumberworth A, Wong ET, Woollard G, Gsponer J (2013) Structure and intrinsic disorder in protein autoinhibition. Structure **21:** 332–341

Tsay JT, Oh W, Larson TJ, Jackowski S RCO (1992) Isolation and characterization of the beta-ketoacyl-acyl carrier protein synthase III gene (fabH) from *Escherichia coli* K-12. J Bio Chem **267:** 6807–6814

Tumaney AW, Ohlrogge JB, Pollard M (2004) Acetyl-coenzyme A concentrations in plant tissues. J Plant Physiol **161:** 485–488

Turchetto-Zolet AC, Maraschin FS, de Morais GL, Cagliari A, Andrade CM, Margis-Pinheiro M, Margis R (2011) Evolutionary view of acyl-CoA diacylglycerol acyltransferase (DGAT), a key enzyme in neutral lipid biosynthesis. BMC Evol Biol **11:** 263

Úbeda-Mínguez P, García-Maroto F, Alonso DF (2017) Heterologous expression of DGAT genes in the marine microalga *Tetraselmis chui* leads to an increase in TAG content. J Appl Phycol 1–14

Uversky VN, Gillespie JR, Fink AL (2000) Why are "natively unfolded" proteins unstructured under physiologic conditions. Proteins **41:** 415–427

Vance DE, Li Z, Jacobs RL (2007) Hepatic phosphatidylethanolamine N-methyltransferase, unexpected roles in animal biochemistry and physiology. J Biol Chem **282:** 33237–33241

Valencia-Turcotte L, Rodríguez-Sotres R (2001) The treatment of purified maize oil bodies with organic solvents and exogenous diacylglycerol allows the detection and solubilization of diacylglycerol acyltransferase. Biochim Biophys Acta **1534:** 14–26

van Erp H, Bates PD, Burgal J, Shockey J, Browse J (2011) Castor phospholipid:diacylglycerol acyltransferase facilitates efficient metabolism of hydroxy fatty acids in transgenic *Arabidopsis*. Plant Physiol **155:** 683–693

Vanhercke T, El Tahchy A, Liu Q, Zhou XR, Shrestha P, Divi UK, Ral JP, Mansour MP, Nichols PD, James CN, Horn PJ, Chapman KD, Beaudoin F, Ruiz-López N, Larkin PJ, de Feyter RC, Singh SP, Petrie JR (2014) Metabolic engineering of biomass for high energy density: oilseed-like triacylglycerol yields

from plant leaves. Plant Biotechnol J **12:** 231–239

Vanhercke T, El Tahchy A, Shrestha P, Zhou XR, Singh SP, Petrie JR (2013) Synergistic effect of WRI1 and DGAT1 coexpression on triacylglycerol biosynthesis in plants. FEBS Lett **587:** 364–369

Varadi M, Kosol S, Lebrun P, Valentini E, Blackledge M, Dunker AK, Felli IC, Forman-Kay JD, Kriwacki RW, Pierattelli R, Sussman J, Svergun DI, Uversky VN, Vendruscolo M, Wishart D, Wright PE, Tompa P (2014) pE-DB: a database of structural ensembles of intrinsically disordered and of unfolded proteins. Nucleic Acids Res **42:** D326–35

Vina AD (2010) Improving the speed and accuracy of docking with a new scoring function, efficient optimization, and multithreading Trott, Oleg; Olson, Arthur J. J Comput Chem **31:** 455–461

Voelker T, Kinney AJ (2001) Variations in the biosynthesis of seed-storage lipid. Annu Rev Plant Physiol Plant Mol Biol **52:** 335–361

Wallace AC, Laskowski RA, Thornton JM (1995) LIGPLOT: a program to generate schematic diagrams of protein-ligand interactions. Protein Eng **8:** 127–134

Wang L, Shen W, Kazachkov M, Chen G, Chen Q, Carlsson AS, Stymne S, Weselake RJ, Zou J (2012) Metabolic interactions between the Lands cycle and the Kennedy pathway of glycerolipid synthesis in *Arabidopsis* developing seeds. Plant Cell **24:** 4652–4669

Wang X, Devaiah SP, Zhang W, Welti R (2006) Signaling functions of phosphatidic acid. Prog Lipid Res **45:** 250–278

Ward JJ, Sodhi JS, McGuffin LJ, Buxton BF, Jones DT (2004) Prediction and

functional analysis of native disorder in proteins from the three kingdoms of life. J Mol Biol **337:** 635–645

Wei J, Kang HW, Cohen DE (2009) Thioesterase superfamily member 2 (Them2)/acyl-CoA thioesterase 13 (Acot13): a homotetrameric hotdog fold thioesterase with selectivity for long-chain fatty acyl-CoAs. Biochem J **421:** 311–322

Weiss, S.B. and Kennedy, E.P. (1956). The enzymatic synthesis of triglycerides. J Am Chem Soc **78(14)**: 3550–3550.

Weiss SB, Kennedy EP, Kiyasu JY (1960) The enzymatic synthesis of triglycerides. J Biol Chem 235:40–44

Welti R, Li W, Li M, Sang Y, Biesiada H, Zhou HE, Rajashekar CB, Williams TD, Wang X (2002) Profiling membrane lipids in plant stress responses. Role of phospholipase D alpha in freezing-induced lipid changes in *Arabidopsis*. J Biol Chem **277:** 31994–32002

Weselake RJ (2000) Lipid biosynthesis in cultures of oilseed rape. In Vitro Cell Dev Biol Plant **36:** 338–348

Weselake RJ (2005a) Storage lipids. In: Plant Lipids: Biology, Utilization and Manipulation (ed DJ Murphy). Blackwell Publishing, Oxford 162–221

Weselake RJ (2005b) Storage product metabolism in microspore-derived cultures of Brassicaceae. In: Biotechnology in Agriculture and Forestry, Vol 56; Haploids in Crop Improvement II (eds CE Palmer, WA Keller, KJ Kasha), Springer-Verlag, Berlin 97–122

Weselake RJ, Kazala EC, Cianflone K, Boehr DD, Middleton CK, Rennie CD,

Laroche A, Recnik I (2000) Human acylation stimulating protein enhances triacylglycerol biosynthesis in plant microsomes. FEBS Lett **481:** 189–192

Weselake RJ, Madhavji M, Szarka SJ, Patterson NA, Wiehler WB, Nykiforuk CL, Burton TL, Boora PS, Mosimann SC, Foroud NA, Thibault BJ, Moloney MM, Laroche A, Furukawa-Stoffer TL (2006) Acyl-CoA-binding and self-associating properties of a recombinant 13.3 kDa N-terminal fragment of diacylglycerol acyltransferase-1 from oilseed rape. BMC Biochem **7:** 24

Weselake RJ, Pomeroy MK, Furukawa TL, Golden JL, Little DB, Laroche A (1993) Developmental profile of diacylglycerol acyltransferase in maturing seeds of oilseed rape and safflower, and microspore-derived cultures of oilseed rape. Plant Physiol **102:** 565–571

Weselake RJ, Shah S, Tang M, Quant PA, Snyder CL, Furukawa-Stoffer TL, Zhu W, Taylor DC, Zou J, Kumar A, Hall L, Laroche A, Rakow G, Raney P, Moloney MM, Harwood JL (2008) Metabolic control analysis is helpful for informed genetic manipulation of oilseed rape (*Brassica napus*) to increase seed oil content. J Exp Bot **59:** 3543–3549

Weselake RJ, Taylor DC (1999) The study of storage lipid biosynthesis using microspore-derived cultures of oilseed rape. Prog Lipid Res **38:** 1–60

Weselake RJ, Taylor DC, Pomeroy MK, Lawson SL, Underhill EW (1991) Properties of diacylglycerol acyltransferase from microspore-derived embryos of *Brassica napus*. Phytochemistry **30:** 3533–3538

Weselake RJ, Taylor DC, Rahman MH, Shah S, Laroche A, McVetty PB, Harwood JL (2009) Increasing the flow of carbon into seed oil. Biotechnol Adv **27:** 866–

878

Wickramarathna AD, Siloto RMP, Mietkiewska E, Singer SD, Pan X, Weselake RJ (2015) Heterologous expression of flax phospholipid:diacylglycerol cholinephosphotransferase (PDCT) increases polyunsaturated fatty acid in yeast and *Arabidopsis* seeds. BMC Biotechnol **15:** 63

Wider G, Macura S, Kumar A, Ernst RR, Wüthrich K (1984) Homonuclear two-dimensional 1 H NMR of proteins. Experimental procedures. J Magn Reson **56:** 207–234

Wielgat B, Kleczkowski K (1981) Gibberellic acid-enhanced phosphorylation of pea chromatin proteins. Plant Sci Lett **21:** 381–388

Winichayakul S, Scott RW, Roldan M, Hatier JH, Livingston S, Cookson R, Curran AC, Roberts NJ (2013) *In vivo* packaging of triacylglycerols enhances *Arabidopsis* leaf biomass and energy density. Plant Physiol **162:** 626–639

Winter A, Krämer W, Werner FAO, Kollers S, Kata S, Durstewitz G, Buitkamp J, Womack JE, Thaller G, Fries R (2002) Association of a lysine-232/alanine polymorphism in a bovine gene encoding acyl-CoA: diacylglycerol acyltransferase (DGAT1) with variation at a quantitative trait locus for milk fat content. Proc Natl Acad Sci U S A **99:** 9300–9305

Woodfield HK, Harwood JL, Weselake RJ (2015) Tailoring lipid synthesis in oil crops. Inform **26**: 78–83

Woods A, Munday MR, Scott J, Yang X, Carlson M, Carling D (1994) Yeast SNF1 is functionally related to mammalian AMP-activated protein kinase and regulates acetyl-CoA carboxylase *in vivo*. J Biol Chem **269:** 19509–19515

Wright PE, Dyson HJ (2015) Intrinsically disordered proteins in cellular signalling and regulation. Nat Rev Mol Cell Biol **16:** 18–29

Wu HY, Liu C, Li MC, Zhao MM, Gu D, Xu YN (2013) Effects of monogalactoglycerolipid deficiency and diacylglycerol acyltransferase overexpression on oil accumulation in transgenic tobacco. Plant Mol Bio Rep **31:** 1077–1088

Wu L, Birch RG (2010) Physiological basis for enhanced sucrose accumulation in an engineered sugarcane cell line. Funct Plant Bio **37**(12): 1161–1174

Wüthrich K (1986) NMR of proteins and nucleic acids (book) Wiley-Interscience. New York

Xu J, Francis T, Mietkiewska E, Giblin EM, Barton DL, Zhang Y, Zhang M, Taylor DC (2008) Cloning and characterization of an acyl-CoA-dependent diacylglycerol acyltransferase 1 (DGAT1) gene from *Tropaeolum majus*, and a study of the functional motifs of the DGAT protein using site-directed mutagenesis to modify enzyme activity and oil content. Plant Biotechnol J **6:** 799–818

Xu Y, Chen G, Greer MS, Caldo KMP, Ramakrishnan G, Shah S, Wu L, Lemieux MJ, Ozga J, Weselake RJ (2017) Multiple mechanisms contribute to increased neutral lipid accumulation in yeast producing recombinant variants of plant diacylglycerol acyltransferase 1. J Biol Chem Accepted.

Yeh LA, Song CS, Kim KH (1981) Coenzyme A activation of acetyl-CoA carboxylase. J Biol Chem **256:** 2289–2296

Yen CL, Monetti M, Burri BJ, Farese RV (2005) The triacylglycerol synthesis enzyme DGAT1 also catalyzes the synthesis of diacylglycerols, waxes, and retinyl

esters. J Lipid Res **46:** 1502–1511

Yen CL, Stone SJ, Koliwad S, Harris C, Farese RV (2008) Thematic review series: glycerolipids. DGAT enzymes and triacylglycerol biosynthesis. J Lipid Res **49:** 2283–2301

Yu J, Li Y, Zou F, Xu S, Liu P (2015) Phosphorylation and function of DGAT1 in skeletal muscle cells. Biophys Rep **1:** 41–50

Yu C, Kennedy NJ, Chang CC, Rothblatt JA (1996) Molecular cloning and characterization of two isoforms of *Saccharomyces cerevisiae* acyl-CoA:sterol acyltransferase. J Biol Chem **271:** 24157–24163

Yurchenko OP, Weselake RJ (2011) Involvement of low molecular mass soluble acyl-CoA-binding protein in seed oil biosynthesis. N Biotechnol **28:** 97–109

Zale J, Jung JH, Kim JY, Pathak B, Karan R, Liu H, Chen X, Wu H, Candreva J, Zhai Z, Shanklin J, Altpeter F (2016) Metabolic engineering of sugarcane to accumulate energy-dense triacylglycerols in vegetative biomass. Plant Biotechnol J **14:** 661–669

Zammit VA, Buckett LK, Turnbull AV, Wure H, Proven A (2008) Diacylglycerol acyltransferases: potential roles as pharmacological targets. Pharmacol Ther **118:** 295–302

Zancan P, Marinho-Carvalho MM, Faber-Barata J, Dellias JM, Sola-Penna M (2008) ATP and fructose-2,6-bisphosphate regulate skeletal muscle 6-phosphofructo-1-kinase by altering its quaternary structure. IUBMB Life **60:** 526–533

Zhai Z, Liu H, Shanklin J (2017) Phosphorylation of WRINKLED1 by KIN10 results

in its proteasomal degradation, providing a link between energy homeostasis and lipid biosynthesis. Plant Cell **29:** 871–889

Zhang M, Fan J, Taylor DC, Ohlrogge JB (2009a) DGAT1 and PDAT1 acyltransferases have overlapping functions in *Arabidopsis* triacylglycerol biosynthesis and are essential for normal pollen and seed development. Plant Cell **21:** 3885–3901

Zhang Y, Primavesi LF, Jhurreea D, Andralojc PJ, Mitchell RA, Powers SJ, Schluepmann H, Delatte T, Wingler A, Paul MJ (2009b) Inhibition of SNF1-related protein kinase1 activity and regulation of metabolic pathways by trehalose-6-phosphate. Plant Physiol **149:** 1860–1871

Zhang YM, Rock CO (2009) Transcriptional regulation in bacterial membrane lipid synthesis. J Lipid Res **50 Suppl:** S115–9

Zheng P, Allen WB, Roesler K, Williams ME, Zhang S, Li J, Glassman K, Ranch J, Nubel D, Solawetz W, Bhattramakki D, Llaca V, Deschamps S, Zhong GY, Tarczynski MC, Shen B (2008) A phenylalanine in DGAT is a key determinant of oil content and composition in maize. Nat Genet **40:** 367–372

Zhou XR, Shrestha P, Yin F, Petrie JR, Singh SP (2013) AtDGAT2 is a functional acyl-CoA:diacylglycerol acyltransferase and displays different acyl-CoA substrate preferences than AtDGAT1. FEBS Lett **587:** 2371–2376

Zou J, Katavic V, Giblin EM, Barton DL, MacKenzie SL, Keller WA, Hu X, Taylor DC (1997) Modification of seed oil content and acyl composition in the *brassicaceae* by expression of a yeast sn-2 acyltransferase gene. Plant Cell **9:** 909–923

Zou J, Qi Q, Katavic V, Marillia EF, Taylor DC (1999a) Effects of antisense repression of an *Arabidopsis thaliana* pyruvate dehydrogenase kinase cDNA on plant development. Plant Mol Biol **41:** 837–849

Zou J, Wei Y, Jako C, Kumar A, Selvaraj G, Taylor DC (1999b) The *Arabidopsis thaliana* TAG1 mutant has a mutation in a diacylglycerol acyltransferase gene. Plant J **19:** 645–653

APPENDIX (A) 1.

Combinatorial Engineering of *Brassica napus* Diacylglycerol Acyltransferase 1 by Combining Previously Identified Amino Acid Residue Substitutions

A.1.1. Introduction

Diacylglycerol acyltransferase 1 (DGAT1) catalyzes the acyl-CoA-dependent acylation of 1,2-diacyl-*sn*-glycerol to produce triacylglycerol (TAG), which is the predominant component of seed oil (Liu et al., 2012). In some oleaginous plants, the level of DGAT activity during seed development may have a substantial effect on the flow of carbon into TAG (Perry and Harwood, 1993; Weselake et al., 2008; 2009). Seed-specific over-expression of Arabidopsis *DGAT1* (AtDGAT1) in Arabidopsis (Jako et al., 2001) and *AtDGAT1* or *Brassica napus DGAT1* in canola-type *B. napus* resulted to increased seed oil content (Weselake et al., 2008; Taylor et al., 2009). Moreover, detailed investigation of the *B.napus* TAG biosynthetic pathway during seed development showed that TAG assembly exerts greater regulatory control than fatty acid biosynthesis in determining the extent of oil accumulation (Weselake et al., 2008; Tang et al., 2012). DGAT1 has been extensively used in numerous metabolic engineering studies to boost oil content in different oleaginous organisms (Weselake et al., 2009; Runguphan and Keasling, 2013).

Protein engineering of enzymes involves the introduction of amino acid residue substitutions in the target enzyme and subsequent selection of more active variants. A number of desired enzymatic properties have been obtained through directed evolution including higher catalytic efficiency, improved thermal stability, modified substrate specificity and even novel functionalities (Tao and Cornish, 2002). Protein engineering

of lipid metabolic enzymes have had substantial impact on the food and petrochemical alternative industries. Previously, many lipase variants have been engineered with modified properties such as increased activity and altered stereoselectivity, and these variants have found numerous applications in the biotechnology industry (Pleiss et al., 2000). Protein engineering of lipases have been easily performed using rational design as many lipase three-dimensional (3D) structures have already been reported (Anobom et al., 2014). Without a 3D structure, directed evolution provides an alternative approach, which involves the introduction of random amino acid residue substitutions in the amino acid sequence of the target enzyme. Random modifications of amino acid sequences are easily obtained using several available methods. The bottleneck in directed evolution is the selection of variants that demonstrate the desired characteristics. In this regard, our group developed a high-throughput system for screening for high performance variants of BnaDGAT1, which increase TAG content when introduced into yeast (*Saccharomyces cerevisiae*) or tobacco (*Nicotiana benthamiana*) leaves (Siloto et al., 2009a; Chen et al., 2017).

Fifty BnaDGAT1 variants were previously shown to individually increase TAG more effectively than the wild-type enzyme when introduced into *S. cerevisiae* (Chen et al., 2017). These variants include a total of 104 different mutations distributed among 81 amino acid residue positions within the polypeptide. Several single site mutants were chosen and further characterized. The best performing ones were identified as L441P and I447F. Transient expression of *I447F* or *L441P* in tobacco leaves, together with *WRINKLED1*, resulted in about a 33% or 70% increase, respectively, in leaf TAG content when compared to wild-type BnaDGAT1 (Chen et al., 2017). The current study

was aimed at further driving the directed evolution of BnaDGAT1 to the limits of yield and efficiency by combining previously identified amino acid residue substitutions shown to enhance enzyme performance.

A.1.2. Materials and methods

A.1.2.1. Construct preparation of BnaDGAT1 combinatorial library

All experiments were based on wild-type isoform BnaC.DGAT1.a (Greer et al., 2015), which is referred to as BnaDGAT1. Thirty-five beneficial amino acid residues substitutions were selected and divided into three groups (Table A.1.1). The encoding mutations in each group were combined at all possible combinations in a pYES-NTC vector and the gene library was obtained from GeneArt® Life Technologies. The three libraries were received as *E. coli* glycerol stocks, which were subjected to plasmid isolation to recover the gene library in plasmid form.

A.1.2.2. Yeast transformation, lipotoxicity selection, and screening

S. cerevisiae strain H1246 competent cells were prepared and transformed with the plasmid libraries according to the efficient method described by Gietz and Schiestl (2007). The transformants were plated on solid synthetic media lacking uracil with 2% glucose ($^{w}/_{v}$) and incubated at 30°C for 4 days. The yeast colonies were dissolved in sterile water (10 mL per plate) and pooled together in a sterile flask. The solution containing the yeast library was mixed and inoculated in 50 mL synthetic media lacking uracil with 2% glucose ($^{w}/_{v}$). After 48 h, the culture was subjected to lipotoxicity selection. The culture was inoculated in synthetic media lacking uracil with 50 mL

Table A.1.1. Each of the three libraries encodes variants with the following amino acid substitutions combined at all possible combinations.

Library 1	Library 2	Library 3
V52D	R51Q	S33T
S54T	E100D	A46P
S112R	A114P	V82E
L136F	M199T	I108T
F302I	V202I	K110N
F302L	C286Y	L164F
F302C	G332A	G290S
F308L	V336M	I314M
V341L	L438H	Y386F
N343I	L441P	M467K
F449L	L445V	F473L
	I447F	

2%($^{w}/_{v}$) galactose and 1%($^{w}/_{v}$) raffinose (induction media) with 1 mM oleic acid and 0.6%($^{w}/_{v}$) tyloxapol at a starting OD_{600} of 0.4 and incubated at 30°C. After 48 h, the culture was re-inoculated in 50 mL induction media with 1 mM oleic acid and 0.6% tyloxapol, grown at 30°C for 48 h and this cycle was repeated 5 times. For each round, 1 mL culture was harvested through centrifugation, washed twice with water, and finally resuspended in 1 mL water. The culture was then subjected to Nile red assay based on a previously optimized protocol (Siloto et al., 2009b). The cells were washed with water prior to Nile red assay since tyloxapol and oleic acid can also react with Nile red dye and affect the reading. The same set of procedures was done for positive (wild-type BnaDGAT1) and negative (LacZ) controls. After the last round of lipotoxicity selection, the cultures were plated onto solid synthetic media lacking uracil with 2% glucose ($^{w}/_{v}$) and grown for 48 h at 30°C.

About three thousand yeast colonies expressing various BnaDGAT1 combinatorial mutants were individually picked and inoculated into 200 µL of synthetic media lacking uracil with 2% glucose ($^{w}/_{v}$) in 96-well plates (autoclaved round bottom 96-well plate/Corning™ Polypropylene Plates Round). Each plate was sealed with Thermo Scientific™ Easy Peel Heat Sealing Foil. The yeast library was incubated at 30°C. After 72 h, 10 µL of the initial culture was inoculated into 190 µL induction media in 96-well plates and incubated at 30°C. After 72 h without shaking, 100 µL of each culture was subjected to Nile red assay. Nile red assay was done based on the procedure established previously by Siloto et al. (2009a; 2009b). Briefly, 100 µL of yeast culture were incubated with 5 µL of 0.1 mg/mL Nile red solution in methanol. The change in fluorescent emission was measured before and after 5 minutes of adding Nile

red solution using a Synergy H4 hybrid reader (Biotek). The total neutral lipid content was measured as change in fluorescence for TAG over change in fluorescence for phospholipid (PL).

For the second rounds of screening, the top 5.6% of yeast colonies expressing various BnaDGAT1 combinatorial mutants were selected and inoculated into 96-well plates again. Ten µL of stationary culture were inoculated into 190 µL of induction media and the cultures were incubated at 30°C with shaking. After 24 h, 20 µL of the overnight culture were inoculated into 450 µL of induction media in 96-deep-well plates (Costar™ 96-Well Assay Blocks/07-200-700, sealed with permeable film (AeraSeal™, Excel Scientific Polyester Sealing Film, Sterile/ESCBS-25) and incubated at 30°C with shaking. After 72 h, the cultures were subjected to the Nile red assay.

The top 10% of yeast cultures during the second round were re-inoculated in 10 mL induction media in 50 mL Falcon™ conical tubes and screened again using the Nile red assay. The best performing mutants were subjected to plasmid miniprep. The isolated plasmids were subjected to DNA sequencing to establish their identities and determine the combinations that produced the best results

A.1.3. Results and discussion

A yeast library of BnaDGAT1 with the different combinations of beneficial mutations was prepared using strain H1246 as a host, which is deficient of enzymes with DGAT activity (Sandager et al., 2002). The library was first subjected to the lipotoxicity selection assay through repeated incubation in media with oleic acid. Oleic acid is toxic to yeast cells that cannot store fatty acids as TAG (Siloto et al., 2009b). This selection step enriched the culture with cells producing highly active BnaDGAT1 variants, and impeded the growth of cells with inactive ones. Thereafter, the library was subjected to three rounds of screening.

During the first round of screening, about three thousand yeast colonies were picked and grown first in media with glucose as the carbon source, and then transferred to an induction media wherein glucose was replaced by galactose and raffinose. The *BnaDGAT1* cDNAs were placed under the control of a galactose-inducible promoter. After 72 h, the cultures were subjected to Nile red assay based on a previously optimized protocol (Siloto et al., 2009b). The changes in fluorescence (ΔF TAG/ΔF PL) values for each culture were determined. Of the colonies screened, only 12.73% exhibited similar or higher ΔTAG/ΔPL than the wild-type enzyme, indicating that majority of the multiple combinations resulted in less active enzymes (Fig. A.1.1).

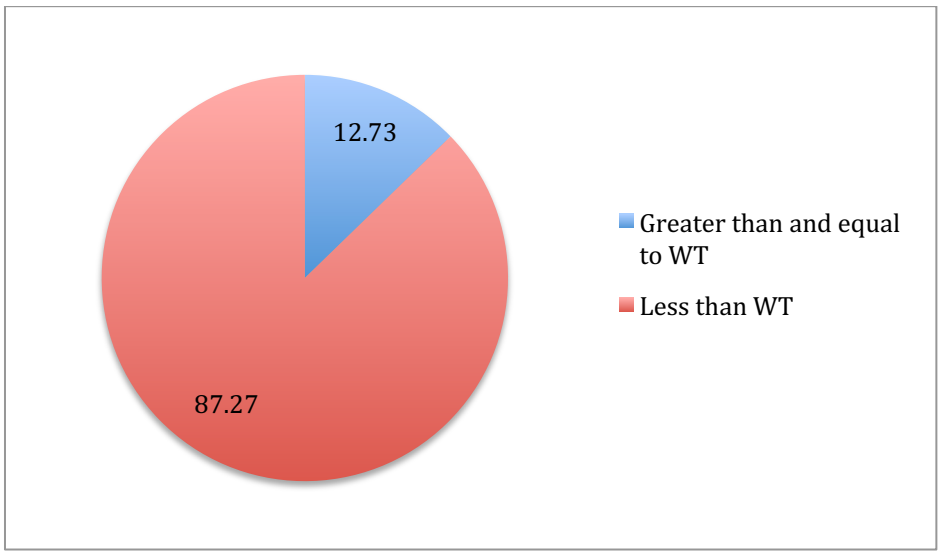

Figure A.1.1. Results of the first screening of the BnaDGAT1 combinatorial library. About 3000 colonies were picked and inoculated in 96-well plates. Each culture was subjected to the Nile red assay where neutral lipid content is represented by the change in fluorescence (ΔF) for triacylglycerol (TAG) divided by (ΔF phospholipid (PL). ΔF PL is proportional to the amount of cells present. The pie chart shows the performance of the BnaDGAT1 variants in terms of percentage relative to wild-type (WT) BnaDGAT1 (WT).

The top 5.6 percent of yeast cultures expressing the BnaDGAT1 combinatorial variants were selected for the second round of screening, which involved culture growth in 1 mL media in deep-well plates with aerated cover. The cultures were incubated at 30°C and subjected to Nile red assay after 72 h. The results of the second screening are summarized in Figure A.1.2, which shows that more than 90% of the colonies screened exhibited similar or higher oil content when compared to the wild-type enzyme.

The top 30 yeast cultures expressing the BnaDGAT1 combinatorial variants were further analyzed in a third round of screening. The average ΔF TAG/ΔF PL are shown in Figure A.1.3. All variants chosen resulted in higher cellular neutral lipid content than the wild-type enzyme. The top 5 colonies were subjected to plasmid miniprep and the plasmids were sent for DNA sequencing. These colonies were all found to have the same sequence, having the same set of mutations. This indicated that the yeast expressing this BnaDGAT1 variant predominated the culture during the lipotoxicity selection assay.

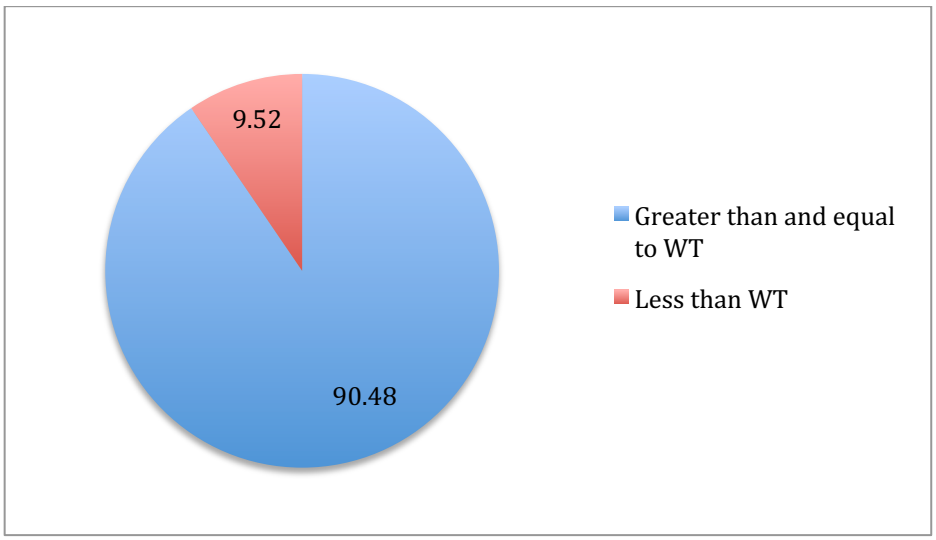

Figure A.1.2. Results of the second screening of the BnaDGAT1 combinatorial library. Each culture was subjected to the Nile red assay for determination of neutral lipid content. The pie chart shows the performance of the BnaDGAT1 variants in terms of percentage relative to wild-type (WT) BnaDGAT1.

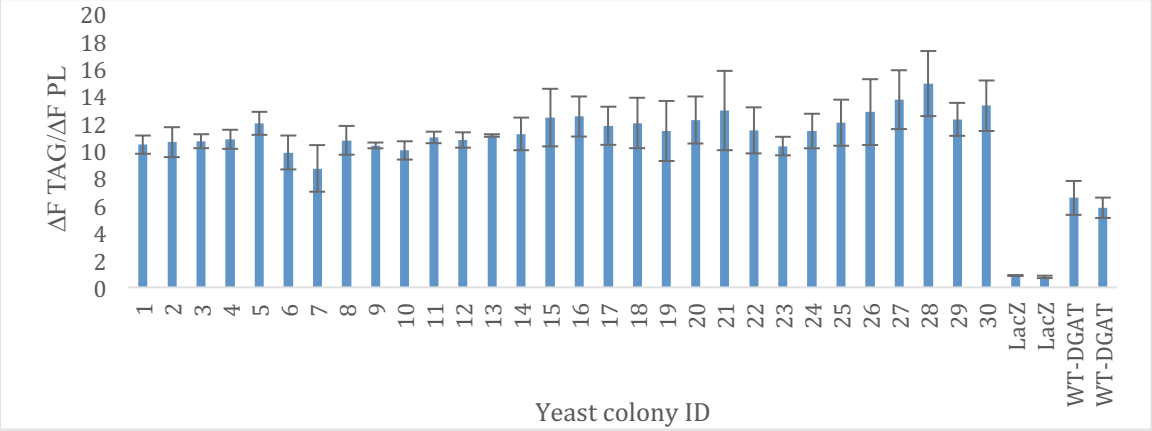

Figure A.1.3. Results of the third screening of the BnaDGAT1 combinatorial library. Each culture was subjected to the Nile red assay for determination of neutral lipid content. Change in fluorescence (ΔF) for triacylglycerol (TAG) is proportional to the amount of TAG accumulated by the yeast culture while ΔF phospholipid (PL) is proportional to the amount of cells present.

The best combination was found to have the following amino acid substitutions: V52D, S54T, F302L, F309L, N343I and F449L. The predicted topology of BnaDGAT1 shows the locations of these mutations within the polypeptide (Fig. A.1.4). The first amino acid substitutions are located within the hydrophilic N-terminal region, which was previously identified as the regulatory domain of BnaDGAT1 (Chapter 4). These amino acid residue substitutions sites are specifically located within the IDR, which facilitates dimerization and has an autoinhibitory function. It would be interesting to probe further the short segment spanning the two amino acid residue substitutions since this segment may house an important regulatory motif. The other amino acid substitutions identified are found in the membrane-bound regions surrounding the predicted substrate binding sites and catalytic histidine. One of the mutations is within the 9th predicted transmembrane domain, which was recently found to contain several amino acid residue substitutions identified during directed evolution (Chen et al., 2017).

The best combinatorial variant was then compared with L441P, which is identified as the best single site variant. When subjected to Nile red assay, however, the combinatorial variant was not superior to variant L441P (Fig. A.1.5). A recent kinetic study demonstrated that L441P was less sensitive to substrate (acyl-CoA) inhibition than wild-type BnaDGAT1 (Xu et al., unpublished data).

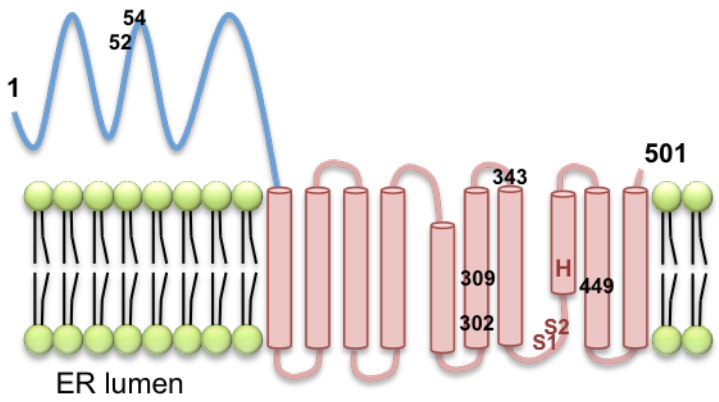

Figure A.1.4. Topology diagram of BnaDGAT1 as predicted by TMHMM Server V2.0. The positions of the amino acid residue substitutions present in the best combinatorial variant (V52D, S54T, F302L, F309L, N343I and F449L) are indicated. The predicted substrate binding sites for acyl-CoA and 1,2-diacyl-*sn*-glycerol are indicated as S1 and S2, respectively. The predicted catalytic histidine is also shown in the topology.

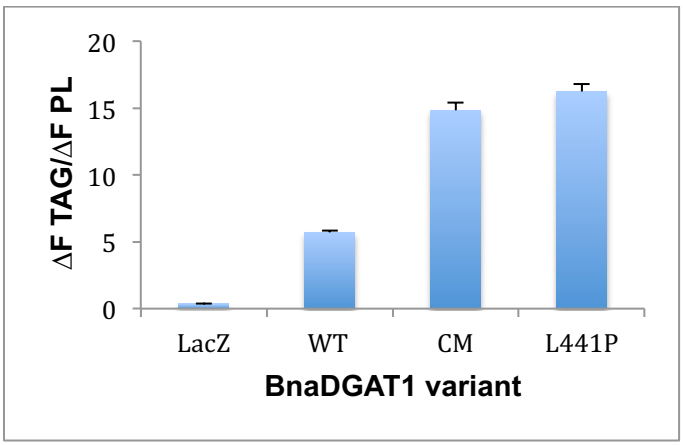

Figure A.1.5. Nile red assay result of yeast H1246 producing the best BnaDGAT1 combinatorial library mutant (CM) compared to wild-type enzyme (WT) and the best single site variant (L441P). Change in fluorescence (ΔF) for triacylglycerol (TAG) is proportional to the amount of TAG in the yeast culture while ΔF phospholipid (PL) is proportional to the amount of cells present.

Previous work on *C. americana* and *G. max* identified DGAT1 variants with higher affinity for oleoyl-CoA (Roesler et al., 2016). These variants were able to boost the accumulation of oil in soybean somatic embryos to higher levels than the wild-type enzyme. The best soybean variant with 14 amino acid substitutions also increased the oil levels in soybean seeds by 16% higher relative to the wild-type enzyme. Recently, two selected high performance BnaDGAT1 variants were transiently introduced into a tobacco leaf expression system in combination with the transcription factor, WRINKLED1 (Chen et al., 2017). Transformation of tobacco leaves with each of the variant cDNA resulted in a substantial increase in TAG content compared to what could be achieved with transformation with cDNA encoding wild-type enzyme. WRINKLED1 has previously been shown to enhance TAG accumulation in leaf tissue (Sanjaya et al., 2011) and exerts a synergistic effect when introduced in combination with a DGAT (Vanhercke et al., 2013). Future studies on the combinatorial BnaDGAT1 mutant may involve the expression of this variant in a transient leaf expression assay to assess its performance in a plant-based system.

APPENDIX 2.

Partial Characterization of *Brassica napus* Diacylglycerol Acyltransferase 2

A.2.1. Introduction

Type 1 and 2 diacylglycerol acyltransferases (DGATs) are membrane-bound enzymes catalyzing the acyl-CoA-dependent biosynthesis of triacylglycerol (TAG). DGAT2 is smaller in size and has less transmembrane regions than DGAT1 (Liu et al., 2012). In Arabidopsis, DGAT1 appears to be the key player in the acyl-CoA-dependent TAG biosynthesis. Arabidopsis mutant lines with inactivated DGAT1 exhibited a substantial reduction in oil content whereas *DGAT2* knockout plant did not exhibit any change in oil levels (Katavic et al., 1995; Routaboul et al., 1999; Zhang et al., 2009a). Furthermore, when DGAT2 was knocked out in Arabidopsis with inactivated DGAT1, no further reduction in oil content was observed (Zhang et al., 2009a). Determining the relative contributions of acyl-CoA-dependent and acyl-CoA-independent TAG biosynthesis to seed oil accumulation in Arabidopsis is in need of further investigation. The case seems to be different for mammals as *DGAT1* knockout mice resulted in reduced accumulation of TAG, whereas *DGAT2* knockout mice succumbed to premature death (Smith et al., 2000; Stone et al., 2004). In *Saccharomyces cerevisiae*, DGAT2 (Dga1p) and a PDAT (LRO1) enzyme are the main enzyme responsible for TAG biosynthesis whereas DGAT1 is absent in this yeast (Lardizabal et al., 2001; Sandager et al., 2002).

Plant DGAT2 has been suggested to play a major role in some species accumulating fatty acids modified on PC. In castor (*Ricinus communis*), *DGAT2* (*RcDGAT2*) was highly expressed in seeds during active oil accumulation (Kroon et al., 2006).

RcDGAT2 also actively utilized ricinoleoyl-CoA and diricinolein as substrates *in vitro*. It was also found that RcDGAT2 exhibited enhanced acyl acceptor preference for diricinolein over diolein and dilinolein (Burgal et al., 2008). Furthermore, *RcDGAT1* was found to have similar expression levels in seeds and leaves, and its seed expression pattern did not correlate with oil accumulation (Kroon et al., 2006), although *in vitro* assay also showed that RcDGAT1 can also use diricinolein as acyl acceptor (Xe et al., 2004). Similarly, tung tree (*Vernicia fordii*) DGAT2 also exhibited preference for forming trieleostearin, which is the most abundant molecular species of TAG in this source (Shockey et al., 2006). The *in vivo* functionality of Arabidopsis DGAT2 (AtDGAT2) was confirmed upon transient expression in *N. benthamiana* leaves (Zhou et al., 2013) and through the use of a codon-optimized *AtDGAT2* in *S. cerevisiae* strain H1246, (Ayme et al., 2014). H1246 is a strain of *S. cerevisiae* which is devoid of functional TAG-biosynthetic enzymes (Sandager et al., 2002).

This study aimed to characterize *B. napus* DGAT2 (BnaDGAT2) recombinantly-produced in strain H1246 and to attempt purify the recombinant enzyme using the protocol optimized for BnaDGAT1. This study involves the use of a codon-optimized cDNA, as previously reported for *AtDGAT2* (Ayme et al., 2014). Previous investigation in our laboratory showed that non-codon optimized *BnaDGAT2* could not be be functionally expressed in H1246 (Liu et al., 2012).

A.2.2. Materials and methods

A.2.2.1. Identification of BnaDGAT2 isoforms

A BLAST search was done using Arabidopsis DGAT2 protein sequence as query to identify possible BnaDGAT2 genes. Two cDNAs were selected and codon-optimized for expression in *S. cerevisiae* H1246 The codon-optimized cDNAs were ordered from BioBasic Inc. (Ontario) and cloned into the pYES-NTA vector (Invitrogen).

A.2.2.2. Expression in yeast H1246, fatty acid feeding experiments and Nile red assay

Yeast H1246 was transformed with pYES-NTA-BnaDGAT2 vectors using the S.c. EasyComp Transformation Kit (Thermo Fisher Scientific) and grown on solid synthetic media lacking uracil with 2% glucose ($^{w}/_{v}$). Colonies were grown in synthetic media lacking uracil with 2% glucose ($^{w}/_{v}$) for 24 h and then transferred into synthetic media lacking uracil with 2%($^{w}/_{v}$) galactose and 1%($^{w}/_{v}$) raffinose (induction media). The colonies were also inoculated in three induction media supplemented with different types of fatty acids (oleic acid/18:1, linoleic acid/18:2, and α- linolenic acid/18:3). The fatty acids were prepared as 0.5 M stock solutions in ethanol and added into the media to a final concentration of 100 μM. The media was also supplemented with 0.1% ($^{v}/_{v}$) tyloxapol to facilitate the dissolution of the fatty acids. After 96 h, cell cultures were harvested (1 mL) and washed five times with 1 mL water to remove tyloxapol and fatty acids. The final cell pellet was resuspended in 1 mL water and subjected to the Nile red assay. The Nile red assay was done in a similar to Siloto et al. (2009a; 2009b). Briefly, 100 μL of yeast culture was placed in black 96-well plates and added with 5 μL of 0.1 mg/mL Nile red solution in methanol. The change in fluorescent emission was measured

before and after 5 minutes of adding Nile red solution using a Synergy H4 hybrid reader (Biotek). The total neutral lipid content is measured as change in fluorescence for TAG over change in fluorescence for phospholipid.

A.2.2.3. Preparation of microsomes and BnaDGAT2 activity assays

Yeast cells grown using the above conditions were harvested at an OD_{600} of 6.0. The cell pellet was resuspended in lysis buffer (50 mM Tris–HCl buffer, pH 8.0, containing 300 mM NaCl, 10% ($^{v}/_{v}$) glycerol, 10 mM imidazole, 2 μg/mL pepstatin, 2 μg/mL leupeptin and 2 mM phenylmethylsulfonyl fluoride) and lysed through bead beating. The cell lysate was recovered after spinning at 10,000 x g for 30 min and then subjected to ultracentrifugation at 105,000 x g for 1 h. The 10,000-105,000 x g microsomal pellet was recovered, resuspended in lysis buffer, and stored at -80°C. The protein content of microsomes was determined using the Bradford assay using BSA as a standard (Bradford, 1976).

For the DGAT assay, the reaction was performed at 30°C for 30 s to 1 min (10 min for $BnaDGAT1_{114\text{-}501}$) in a 60-μL reaction mixture containing 100 μM *sn*-1,2-diolein (pre-dispersed in 0.2% [$^{v}/_{v}$]) Tween 20), 0.1-15 μM [^{14}C] oleoyl-CoA (60 mCi/mmol) or [^{14}C] palmitoyl-CoA (60 mCi/mmol), 200 mM HEPES-NaOH pH 7.4, 4.6 mM $MgCl_2$ and 1–10 μg protein. The enzyme reaction was initiated by addition of the acyl-CoA and quenched with 10 μL of 10% (w/v) SDS. The final reaction mixture was spotted onto a preparative TLC plate (0.25 mm Silica gel, DC-Fertigplatten) with a separate lane for [^{14}C]-triolein standard. The plate was placed in a chamber with hexane:diethyl ether:acetic acid (80:20:1, v/v/v), dried and visualized by phosphorimaging (Typhoon Trio Variable Mode Imager, GE Healthcare). The TAG

spots were obtained, mixed with scintillant and placed in a Beckman-Coulter LS6500 to quantify radioactivity

A.2.2.4. Western blotting, solubilization and chromatography of BnaA.DGAT2.b

Yeast H1246 cells expressing *BnaA.DGAT2.b* were inoculated in 5 mL synthetic liquid media lacking uracil with 2% ($^{w}/_{v}$) raffinose and grown at 30°C. The culture was transferred into 250 mL of the same media and grown for another 24 h. This pre-culture was used to inoculate synthetic media containing 2% ($^{w}/_{v}$) galactose and 1% ($^{w}/_{v}$) raffinose at a starting OD_{600} value of 0.40. The cells were pelleted through centrifugation at 6000 x g for 10 min when an OD_{600} value of 8 was reached.

To confirm expression and location of BnaDGAT2 in SDS-PAGE, microsomal BnaDGAT2 was subjected to Western blotting. 15 and 10 µg protein were resolved through SDS–PAGE followed by electroblotting onto polyvinylidene fluoride membrane. The recombinant enzyme was probed with anti-HisG-HRP conjugated antibody (Invitrogen) and detected through incubation with ECL Advance Western Blotting Detection Kit (Amersham) for 5 min. The blot was scanned using a variable mode imager (Typhoon Trio+, GE Healthcare) and the protein bands were semi-quantified using ImageJ software (Schneider et al., 2012).

Purification of BnaDGAT2 was then attempted using the protocol established for purification of Bna.C.DGAT1.a (Chapter 3). The cell pellets were resuspended in Buffer A (50 mM Tris-HCl pH 8.0, 300 mM NaCl, 10%($^{v}/_{v}$) glycerol, 10 mM imidazole, 2 µg/mL pepstatin, 2 µg/mL leupeptin and 2 mM phenylmethylsulfonyl fluoride), and lysed by passing through a Benchtop homogenizer (Constant Systems) at 35 kpsi twice. The microsomal fraction was recovered by centrifugation at 10,000 x g for 20 min and

subsequent ultracentrifugation of the supernatant at 105,000 x g for 1 h at 4°C. The microsomes were resuspended in 100 mL Buffer A with 1% DDM for 1 h with stirring and centrifuged for 30 min at 30,000 x g. The supernantant containing the detergent-solubilized proteins was mixed with 2 mL TALON® Metal Affinity Resin (Clontech) for 2 h with rocking at 4°C. The resin was placed in a glass-fritted column and washed with 20 column volumes of Buffer A with 15 mM imidazole. BnaDGAT2 was eluted in Buffer A with 500 mM imidazole. BnaDGAT2 was concentrated using Amicon Ultra-4 centrifugal filter units with 30,000 NMWL (EMD Millipore), and injected onto an FPLC-Superdex 200 13/30 (GE Healthcare Life Sciences) size-exclusion column. The column was pre-equilibrated with three column volumes of size-exclusion buffer (25 mM Tris-HCl at pH 8 containing 150 mM NaCl, 5% (v/v) glycerol, 1 mM EDTA and 0.05% DDM). SDS-PAGE was used to analyze purified fractions.

A.2.3. Results and discussion

A.2.3.1. Identification of BnaDGAT2 isoforms and *in silico* analysis

Four BnaDGAT2 isoforms were identified from the database using AtDGAT2 as driver sequence. Multiple sequence alignment revealed that the four isoforms are highly conserved all throughout the polypeptide (Fig. A.2.1). The protein is mainly hydrophobic (shaded blue). Phylogenetic analysis showed that the DGAT2 family forms a distinct clade from DGAT1 (Fig. A.2.2). The phylogenetic tree further showed that the four BnaDGAT2 isoforms can be grouped into two clades, wherein one clade is more closely related to AtDGAT2. Previously, a similar grouping was observed for BnaDGAT1 where it was shown that the two clades exhibited different substrate preference for α-linoleoyl-CoA (Greer et al., 2015; 2016).

All four proteins are predicted to have two transmembrane segments, with small and large cytosolic N- and C-terminal regions, respectively (Fig. A.2.3). Previous studies on tung tree DGAT2 showed that it is targeted to the ER(Shockey et al., 2006). Previously, *S. cerevisiae* DGAT2 was shown to have four transmembrane segments through cysteine-scanning mutagenesis (Liu et al., 2011). Murine DGAT2, on the other hand, was found to have two transmembrane segments near the N-terminus through introduction of epitopes, for immunchemical detection, throughout the polypeptide (Stone et al., 2006). For both topology models, the N- and C- termini were both oriented towards the cytosolic side of the ER.

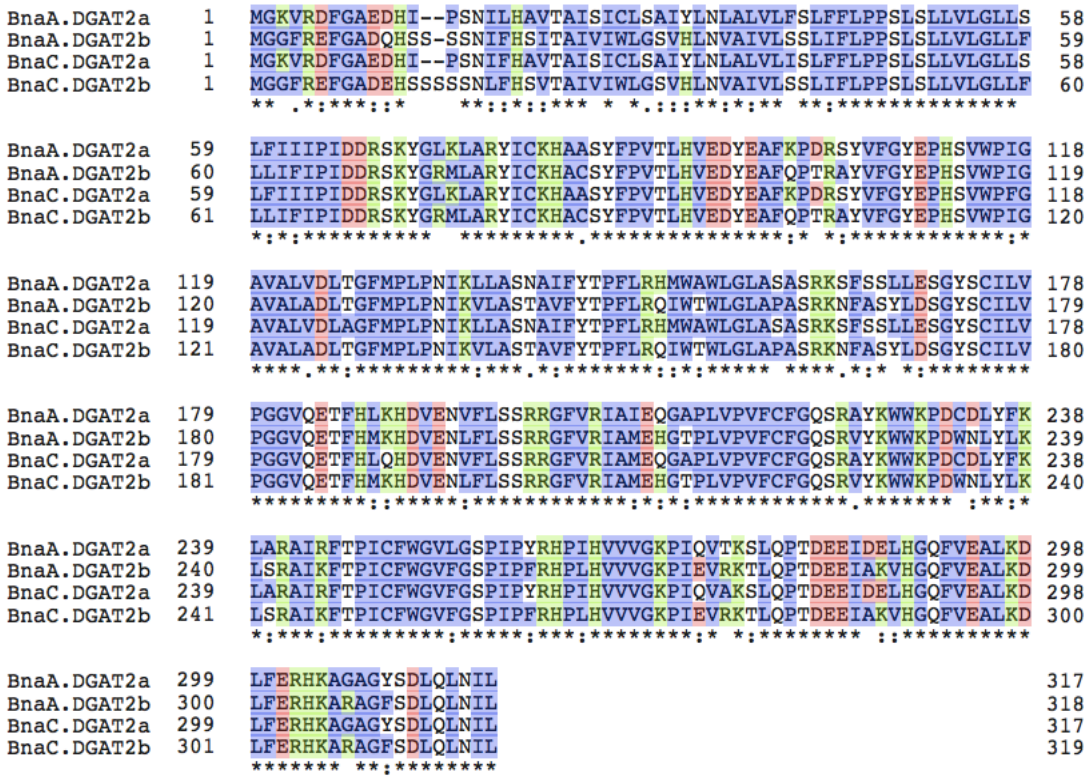

Figure A.2.1. Multiple sequence alignment of BnaDGAT2 isoforms. Four isoforms of BnaDGAT2 where identified from BLAST using AtDGAT2 as query.

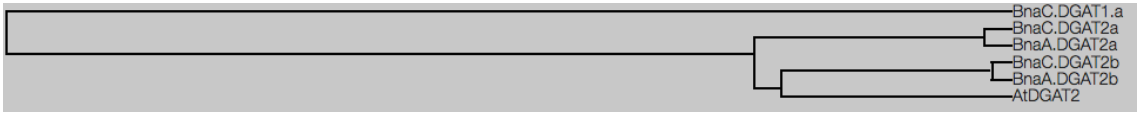

Figure A.2.2. Phylogenetic analysis of BnaDGAT2 isoforms and AtDGAT2 using BnaC.DGAT1.a as outgroup. BnaDGAT2 constitutes a distinct group from BnaDGAT1 and can be further classified into two clades.

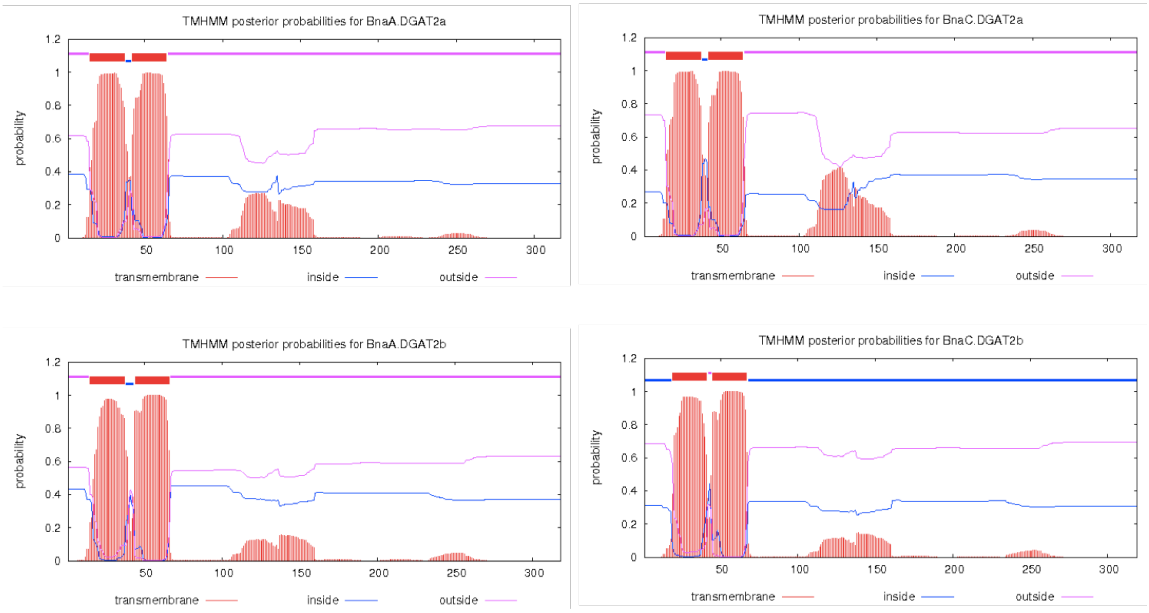

Figure A.2.3. TMTMM prediction for transmembrane helices for the four BnaDGAT2 isoforms. Two transmembrane helices near the N-terminus were predicted for all the isoforms.

A.2.3.2. Recombinant BnaA.DGAT2.b is active when produced in H1246 yeast

BnaA.DGAT2.a and *BnaA.DGAT2.b* were selected for further investigation, and were codon-optimized and purchased from a gene-synthesizer company. Each cDNA was cloned into pYES-NTA and the resulting vector together with LacZ as negative control was transformed into strain H1246. The transformed yeasts were grown in induction media supplemented with different types of fatty acids and subjected to Nile red assay (Fig. A.2.4). Introduction of BnaA.DGAT2.b significantly enhanced neutral lipid content in H1246 yeast with or without feeding of exogenous fatty acid. Furthermore, the measured TAG content for BnaA.DGAT2.b was significantly different than the negative control (data not shown). In contrast, introduction of BnaA.DGAT2.a did not result in enhanced neutral lipid content when compared to the LacZ control (Fig. A.2.4). Insight into the substrate preference of BnaA.DGAT2.b could not be reliably inferred though due to the small differences in neutral lipid content.

Microsomes were prepared from yeast producing the two recombinant BnaDGAT2 isoforms and then subjected to *in vitro* assay with [1-^{14}C] oleoyl-CoA as acyl donor and 1,2-dioleoyl-*sn*-glycerol as acyl acceptor. BnaA.DGAT2.a did not exhibit any activity when compared to the negative control (Fig. A.2.5). On the other hand, BnaA.DGAT2.b was active, consistent with the results of the Nile red assay. This isoform exhibited a specific activity of 10.70 ± 0.67 pmol TAG/min/mg protein. The reported microsomal BnaDGAT1 specific activity, however, is more than 300-fold greater than that obtained for BnaA.DGAT2.b (Caldo et al., 2015; Greer et al., 2015).

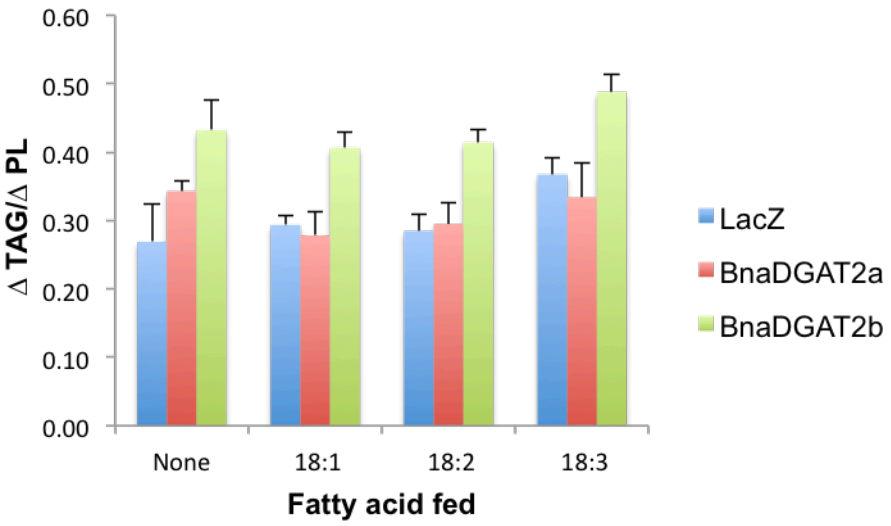

Figure A.2.4. Nile red assay of yeast H1246 expressing cDNAs encoding two BnaDGAT2 isoforms. Cultures were supplemented with oleic acid (18:1), linoleic acid (18:2) or α-linolenic (18:3). The change in fluorescence (ΔF) for triacylglycerol (TAG)/ΔF for phospholipid (PL) was determined. In essence, this represents neutral lipid content normalized based on cell density.

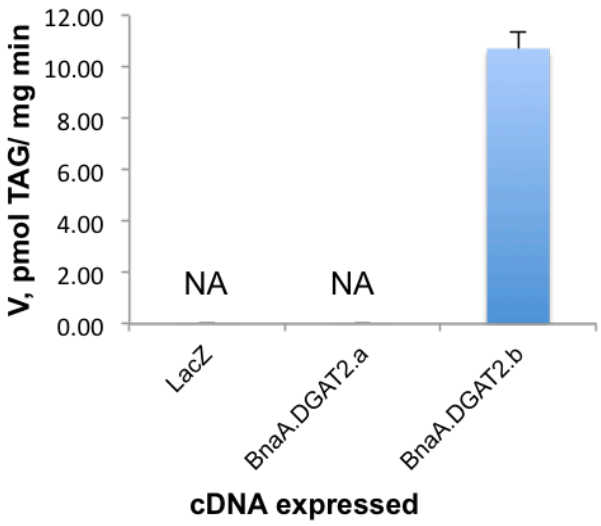

Figure A.2.5. ***In vitro*** **assay of microsomal BnaDGAT2 isoforms using [^{14}C] oleoyl-CoA as acyl donor and sn-1,2-dioleoylglycerol as acyl acceptor.** LacZ was used a negative control. Abbreviations: NA, no activity detected; TAG, triacylglycerol.

In vitro assays of microsomal or purified BnaDGAT1 have shown that the enzyme can effectively use acyl-CoAs representing all major fatty acids found in canola seed oil (i.e., 16:0, 18:0, 18:1, 18:2 or □-18:3) (Greer et al., 2016; Chapter 3). The ability of active forms of BnaDGAT1 or BnaDGAT2 to utilize substrates containing erucic acid (22:1), however, would also be interesting to explore. Canola-type *B. napus* was developed from erucic acid-enriched *B. napus* by selecting for naturally occurring mutations which result in a seed oil with low erucic acid content (McVetty et al., 2016). Elongation of oleoyl-CoA to 22:1-CoA on the ER is inactivated in canola due to a mutation in the gene encoding fatty acid elongase (Katavic et al., 2002). Microsomes from microspore-derived embryos of *B. napus* was shown to effectively utilize 22:1-CoA (Weselake et al., 1991) but this analysis has not been performed with isolated DGAT isoforms of the enzyme. In addition, microsomal enzymes from *B. napus* seeds also showed preference for 22:1-CoA over oleoyl-CoA when assayed at low concentration (Cao and Huang, 1987). Another study also found that the *sn*-3 position of TAG in seeds of high erucic acid *B. napus* lines contained high proportion of 22:1, possibly due to enhanced selectivity of DGATs for 22:1-CoA (Bernerth and Frentzen, 1990).

A.2.3.3. Solubilized BnaA.DGAT2.b aggregates during column chromatography

Attempted purification of BnaA.DGAT2.b was performed based on a previously optimized protocol for BnaDGAT1 (Chapter 3). Microsomal proteins were first solubilized using DDM and the solubilized proteins were subjected to Co affinity chromatography and size-exclusion chromatography. The size-exclusion chromatography profile as assessed by absorbance at 280 nm and SDS-PAGE analysis

of column fractions suggested that BnaA.DGAT2.b aggregated during chromatography (Fig. A.2.6). The predominant protein band in the gel corresponded to the molecular mass of the band obtained during western blotting. The activity was not determined as the enzyme appeared not to exist in optimal form. The enzyme was eluted starting from the void volume and up to a monomer peak suggesting that the BnaDGAT2 isoform was forming different states of oligomerization, which may have arisen from non-specific aggregation of the protein. These results suggest that the protocol optimized for BnaDGAT1 has to be modified for effective purification of BnaA.DGAT2.b

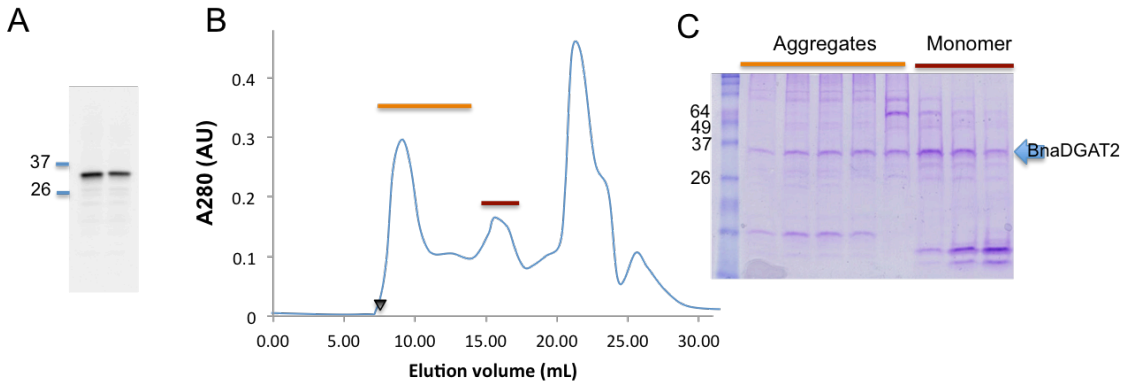

Figure A.2.6. Attempted purification of BnaA.DGAT2.b using FPLC-size exclusion chromatography. A, Western blot analysis of microsomal BnaDGAT2 using anti-HisG-HRP/ECL chemiluminescence detection system. B, SEC profile of the protein C, SDS-PAGE of the peaks where BnaDGAT2 are found. BnaDGAT2 forms a monomeric peak indicated by brown line and multiple higher order oligomers, which may be due to non-specific aggregation. The void volume is indicated by a black triangle.

In summary, four isoforms of BnaDGAT2 were identified and predicted to have two transmembrane segments near the N-terminus. The activities of two selected recombinant isoforms, encoded by clade I and II genes of the A genome of *B. napus*, were characterized using the Nile red assay and *in vitro* assay for DGAT activity. BnaA.DGAT2.b was found to be active while BnaA.DGAT2.a did not show any activity. Although the production level of recombinant BnaA.DGAT2.b appears to be amenable for protein purification, the protein aggregated during size-exclusion chromatography.

Additional information:

Amino acid sequence of BnaDGAT2 isoforms:

>BnaA.DGAT2.a (Uniprot ID: A0A078DN07)
MGKVRDFGAEDHIPSNILHAVTAISICLSAIYLNLALVLFSLFFLPPSLSLLVLGLLSLFIIIPIDDRSKYGLKLARYICKHAASYFP
VTLHVEDYEAFKPDRSYVFGYEPHSVWPIGAVALVDLTGFMPLPNIKLLASNAIFYTPFLRHMWAWLGLASASRKSFSSL
LESGYSCILVPGGVQETFHLKHDVENVFLSSRRGFVRIAIEQGAPLVPVFCFGQSRAYKWWKPDCDLYFKLARAIRFTPIC
FWGVLGSPIPYRHPIHVVVGKPIQVTKSLQPTDEEIDELHGQFVEALKDLF ERHKAGAGYSDLQLNIL

>BnaA.DGAT2b (Uniprot ID: A0A078H779)
MGGFREFGADQHSSSSNIFHSITAIVIWLGSVHLNVAIVLSSLIFLPPSLSLLVLGLLFLLIFIPIDDRSKYGRMLARYICKHAC
SYFPVTLHVEDYEAFQPTRAYVFGYEPHSVWPIGAVALADLTGFMPLPNIKVLASTAVFYTPFLRQIWTWLGLAPASRKN
FASYLDSGYSCILVPGGVQETFHMKHDVENLFLSSRRGFVRIAMEHGTPLVPVFCFGQSRVYKWWKPDWNLYLKLSRAI
KFTPICFWGVFGSPIPFRHPLHVVVGKPIEVRKTLQPTDEEIAKVHGQFVEALKDL FERHKARAGFSDLQLNIL

>BnaC.DGAT2a (Uniprot ID: A0A078GU55)
MGKVRDFGAEDHIPSNIFHAVTAISICLSAIYLNLALVLISLFFLPPSLSLLVLGLLSLFIIIPIDDRSKYGLKLARYICKHAASYFP
VTLHVEDYEAFKPDRSYVFGYEPHSVWPFGAVALVDLAGFMPLPNIKLLASNAIFYTPFLRHMWAWLGLASASRKSFSS
LLESGYSCILVPGGVQETFHLQHDVENVFLSSRRGFVRIAMEQGAPLVPVFCFGQSRAYKWWKPDCDLYFKLARAIRFTP
ICFWGVFGSPIPYRHPIHVVVGKPIQVAKSLQPTDEEIDELHGQFVEALKDLFERHKAGAGYSDLQLNIL

>BnaC.DGAT2b (Uniprot ID: A0A078FPB3)
MGGFREFGADEHSSSSSNLFHSVTAIVIWLGSVHLNVAIVLSSLIFLPPSLSLLVLGLLFLLIFIPIDDRSKYGRMLARYICKHA
CSYFPVTLHVEDYEAFQPTRAYVFGYEPHSVWPIGAVALADLTGFMPLPNIKVLASTAVFYTPFLRQIWTWLGLAPASRK
NFASYLDSGYSCILVPGGVQETFHMKHDVENLFLSSRRGFVRIAMEHGTPLVPVFCFGQSRVYKWWKPDWNLYLKLSR
AIKFTPICFWGVFGSPIPFRHPLHVVVGKPIEVRKTLQPTDEEIAKVHGQFVEALKD LFERHKARAGFSDLQLNIL

Nucleotide sequence of codon-optimized BnaDGAT2:

>BnaA.DGAT2a

ATGGGTAAGGTTCGTGATTTCGGTGCTGAAGACCACATTCCATCTAACATCTTGCATGCTGTTACCGCTATCTCCATT
TGTTTATCCGCTATCTACTTGAACTTGGCCTTAGTCTTATTCTCCTTGTTCTTTTTGCCACCATCTTTGTCTTTGTTGGT
TTTAGGTTTGTTGTCTTTGTTCATTATCATCCCTATCGACGATAGATCTAAATACGGTTTGAAATTGGCTAGATACAT
CTGTAAGCACGCTGCTTCCTACTTTCCAGTTACTTTGCATGTCGAAGACTACGAAGCCTTCAAGCCTGATAGATCTTA
CGTTTTCGGTTACGAACCACATTCCGTTTGGCCAATTGGTGCTGTTGCTTTGGTTGATTTGACTGGTTTTATGCCATT
GCCAAACATCAAGTTGTTAGCTTCTAACGCCATTTTCTACACTCCATTCTTAAGACACATGTGGGCCTGGTTGGGTTT
GGCTTCTGCTTCCAGAAAGTCCTTCTCTTCCTTGTTGGAATCTGGTTACTCTTGTATCTTGGTTCCAGGTGGTGTTCA
AGAGACTTTCCATTTGAAGCACGACGTCGAAAACGTTTTCTTATCCTCTAGAAGAGGTTTCGTTCGTATTGCCATTG
AACAAGGTGCCCCATTGGTCCCAGTTTTcTGTTTTGGTCAATCTAGAGCCTATAAGTGGTGGAAGCCTGATTGTGAT
TTGTACTTCAAGTTAGCTCGTGCTATTAGATTCACTCCAATTTGCTTCTGGGGTGTTTTGGGTTCCCCTATTCCATACC
GTCACCCAATCCACGTTGTTGTCGGTAAGCCAATCCAAGTTACCAAGTCCTTGCAACCAACCGATGAAGAAATTGAT
GAATTGCATGGTCAATTCGTCGAGGCTTTGAAGGATTTGTTCGAAAGACACAAGGCTGGTGCTGGTTACTCCGATT
TGCAATTGAACATCTTATAA

>BnaA.DGAT2b

ATGGGTGGTTTTAGGGAATTTGGAGCTGATCAACATTCCTCTTCTTCGAACATTTTCCACTCCATTACAGCAATCGTT
ATTTGGTTAGGTTCTGTGCACTTGAATGTGGCGATTGTGTTGAGTTCGCTGATTTTCCTTCCGCCATCATTGTCCTTG
CTAGTGCTTGGATTGCTATTCTTGTTGATTTTCATTCCCATAGATGACAGATCAAAGTATGGGAGGATGTTAGCAAG
GTACATTTGCAAACATGCATGTAGTTATTTTCCGGTCACTTTGCATGTAGAGGATTACGAAGCATTCCAACCCACAA
GAGCCTATGTCTTTGGCTATGAACCTCATTCCGTATGGCCTATAGGTGCTGTTGCCTTAGCGGACTTGACTGGCTTT
ATGCCTCTGCCAAACATCAAAGTTCTGGCATCAACCGCTGTTTTCTATACACCGTTCTTACGTCAAATTTGGACGTGG
TTAGGTTTGGCACCAGCTTCAAGAAAGAATTTTGCCTCATATCTAGATAGTGGATACAGTTGTATCCTAGTACCAGG
TGGTGTTCAAGAAACGTTTCACATGAAGCATGATGTCGAGAATCTATTCCTGTCTAGCAGAAGAGGGTTTGTCAGA
ATCGCTATGGAACATGGCACTCCTTTGGTTCCAGTCTTTTGTTTTGGTCAATCTAGAGTGTACAAATGGTGGAAACC
AGATTGGAACTTATACTTGAAATTAAGCAGAGCTATAAAATTCACCCCAATATGCTTTTGGGGTGTATTTGGATCTC
CTATACCCTTTAGACACCCATTACATGTTGTTGTTGGCAAGCCAATAGAGGTACGTAAGACTCTTCAACCTACAGAT
GAAGAGATTGCCAAAGTTCATGGTCAGTTTGTCGAAGCCTTAAAGGACCTTTTCGAAAGACACAAAGCTAGAGCTG
GATTTAGCGACTTACAGTTGAATATCCTTTAA

APPENDIX 3.

Contributions to Other Manuscripts and a Patent Application

Pan X, Chen G, Kazachkov M, Greer MS, Caldo KM, Zou J, Weselake RJ (2015) *In vivo* and *in vitro* evidence for biochemical coupling of reactions catalyzed by lysophosphatidylcholine acyltransferase and diacyglycerol acyltransferase. J Biol Chem **290**: 18068-18078

Contributions: I redesigned the lysophosphatidylcholine acyltransferase clone with a protease site and a His10 affinity tag and performed preliminary studies on the purification and solubilization of lysophosphatidylcholine acyltransferase.

Chen G, Xu Y, Siloto R, Caldo KMP, Vanhercke T, El Tahchy A, Niesner N, Chen Y, Mietkiewska E, Weselake RJ (2017) High performance variants of plant diacylglycerol acyltransferase 1 generated by directed evolution provide insights into structure-function. Plant J *Accepted*

Contributions: I characterized BnaDGAT1 single mutants through Nile red assay and western blotting and reviewed the manuscript.

Xu Y, Chen G, Greer MS, Caldo KMP, Ramakrishnan G, Shah S, Wu L , Lemieux MJ, Ozga J, Weselake RJ Different factors contribute to increased neutral lipid content in yeast producing variants of plant diacylglycerol acyltransferase 1. J Biol Chem. *Accepted*

Contributions: I provide insights in kinetic data analysis and reviewed the manuscript.

Weselake RJ, Chen G, Siloto R, Truksa M, Yang X, Caldo KMP. Plant DGAT-1 Variants. US Provisional Patent Application Serial No. 62/443,102. Filed on 6 January 2017.

Contributions: I characterized BnaDGAT1 single mutants through Nile red assay and western blotting.